PC-BASED VISUAL SIMULATION OF HIGH PRESSURE ARC PLASMA

A THESIS SUBMITTED TO THE UNIVERSITY OF LIVERPOOL FOR THE DEGREE OF DOCTOR OF PHILOSOPHY IN THE FACULTY OF SCIENCE AND ENGINEERING

By

Yiyi ZHAN

BSc (Guangdong), MSc (Liverpool), AMInstP

Plasma and Complex Systems Research Group

Department of Electrical Engineering and Electronics

University of Liverpool

First Supervisor – **Dr Joseph D. YAN**

Second Supervisor – **Professor Joseph W. SPENCER**

January 2011

ABSTRACT

The work in this thesis is concerned with the visual simulation of high pressure arc plasmas in two different applications. The first one is an arc maintained in water for the formation of nano-structures such as nanotubes and fullerenes. The second application is high power switching using puffer circuit breakers. The fundamental behaviour of both arc plasmas was computationally studied.

The structure of the thesis starts with an introduction to the background and objectives of the present work, the arc models used for the two applications are described in Chapter 2 together with a consideration of the radiation and turbulence models, material properties initial and boundary conditions, and issues relating to solution procedures. Chapter 3 is devoted to the modelling of the carbon plasma in water taking into account size of gas bubble growth, water evaporation and chemical reactions in the gas. Chapter 4 presents the computational simulation of the whole arcing process of a high voltage puffer circuit breaker where predicted arc voltage and pressure evolution in the storage volume are compared with the test results. Modelling of the current zero period and the calculation of the critical RRRV is also included. The proposed method for object based visual simulation is described in Chapter 5. Finally conclusions are drawn in Chapter 6 together with a discussion of the future work.

For the arc in water case, it is the first time that an arc model is applied to study the carbon arc confined in water considering chemical reactions of water vapour and carbon vapour. The arc is generated between two carbon electrodes which are immersed in water with a gap length of 1 *mm*. The anode has a conical shape with a rod diameter of 8.2 *mm* and a tip diameter of 2 *mm* with a full conical angle of 60^o. The anode has a cylindrical shape with a diameter of 12 *mm*. A local thermal equilibrium arc model was used to tackle the problem based without considering the sheath layer in front of the electrodes. The loss of carbon vapour due to formation of solid carbon structures is represented by a negative volumetric source. The erosion rate of the anode is derived from experimental result.

Results show that the strong influx of carbon vapour displaced the original water vapour in the gap in a few microseconds, typically 5 μs. By 4 *ms* the arc burns in a carbon dominated environment with about 25% of water vapour in the region near the cathode. Our results thus suggest that for most of the time the arc can be regarded as burning in a carbon vapour dominated environment.

Reaction rate coefficient between carbon vapour and water vapour was derived from that at low temperature (300 *K*) using the well known Arrhenius expression. The value of this coefficient is 1.054×10^6. It has been found that the mass concentration of H_2 and CO peaks in a layer surrounding the arc column. The maximum concentration is only 0.2% and 2.8% respectively, in a region near the cathode surface. Although typically 30% of the

$\frac{m^3}{mol\cdot s}$

carbon vapour is consumed by chemical reaction, water vapour still dominates the arc surrounding gaseous environment since the erosion rate of carbon anode (6×10^{-7} *kg/s*) is still much lower than the water evaporation rate (6×10^{-5} *kg/s*).

The predicted voltage of the arc column at 30 *A* is 7 *V* while the measured arc voltage including the sheaths is 17 – 20 *V*. The difference is attributed mainly to the exclusion of the electrode sheath model in the present work. Considering that the first ionisation energy of carbon vapour at ground state which is 11.26 *eV*, the predicted voltage of the arc column is well placed in the expected range.

A numerical scheme has been established in the present work to simulate the growth of gas bubble confined in water. The position change of the interface of the bubble-water is controlled by the pressure difference between that inside the bubble and the atmospheric pressure. The inertia of the water surrounding the bubble is taken into account in the construction of the dynamic response. Our results show that the growth of the bubble is dominated in the first half millisecond by the retreat of the water surface as a result of evaporation. Further on in the arcing process, the pressure difference makes a dominant contribution in the growth of the bubble.

For the switching arc case, the arcing process for four test duties of a 252 *kV* puffer circuit breaker has been simulated. A novel method was proposed to improve the arc voltage prediction by mitigating the effect of Lorentz force near the tips of hollow contacts and their filling transparent contacts. The proposal of this method is based on consideration of the most probable practical scenario in reality. Results present in the thesis show that this method is effective and gives satisfactory arc voltage prediction for all four test cases at different current levels and arc durations. As an example the arc voltage in the 47 *kA* case at 16.8 *ms* with an instantaneous current of 55 *kA* is 220 *V*, almost the same as that of the measurement while without using the method the prediction is 340 *V*.

Turbulence is important in the interruption process of high voltage SF_6 circuit breakers. It has been found that Prandtl mixing length model with a constant turbulence parameter is not able to predict the important extinction peak in the puffer circuit breaker. In the present work this turbulence parameter is made variable, as a function of instantaneous current that is an indirect measure of the presence of cold SF_6 flow around the arc column. The modified turbulence model was then applied to simulated the current zero period (from 15 *kA* before final current zero onwards to the current zero point) of a 47 *kA* case and a 10 *kA* case. The predicted arc voltage using the modified turbulence model starts to increase rapidly shortly before the final current zero point, qualitatively agree with the measurement. A detailed comparison is not sensible since the accuracy of the measurement is not known.

The present work covers the simulation of the cold flow period, the high current, current zero and the post arc periods. The predicted pressure variation in the puffer cylinder and another three points including the middle of the flat nozzle surface all agrees reasonably

well with the corresponding measurement. Detailed results on the high current phase were represented and discussed.

The thermal interruption capability of a circuit breaker is represented by the critical RRRV, a value of the rate of rise of recovery voltage that the circuit breaker can with stands. Procedures were set up and some example results reported in the thesis. Accurate prediction of the critical RRRV is not possible at present. Nevertheless, the established procedure for the calculation of the post arc current under the influence of system recovery voltage can be of help in studying the behaviour response of a circuit breaker when a design parameter is changed. The shift of the critical RRRV in response to a design parameter change gives an indication of the effectiveness of the change in design.

Computer simulation of electric arcs for industrial devices proves a difficult job in the sense that much coding and setting is required to implement the arc in a chosen software package. An approach has proposed to use Object oriented programming to change the model setup from manually to automatic. The feasibility of the approach has been demonstrated in the present work by a component builder and a Visual Analyser and Monitor (VCM). Information exchange between ISEE and the CFD solver is through memory sharing. Typical results for visual simulation are given in Chapter 2, demonstrating a range of useful functionalities it provides and the benefits for arc modellers.

A number of aspects of the present work that require further work were identified. The importance of obtaining experimental results was discussed. This include the mass spectroscopic measurement of gases generated in the arc in water case, the more accurate arc voltage measurement just before current zero, and the post arc current measurement.

ACKNOWLEDGEMENTS

Firstly, I would like to give an enormous thanks and dedication to Dr Joseph D. Yan for always being a truly enlightening and encouraging supervisor. I am deeply honored to have been his research student. I must also give the same appreciation and kind respect to Professor M. T. C. Fang for working closely with me and the research group and for his valuable guidance during my study. Moreover, another special thanks goes to Dr. J. L. Zhang for being there to provide me with much appreciated comfort and friendship. And finally, I want to declare my deepest and warmest thanks to my loving husband Paul Harvey and our dearest families.

TABLE OF CONTENTS

Chapter 1 - Introduction

1.1 Atmospheric Arc Plasmas

An ionised gas is known as plasma if its Debye length is much smaller than the characteristic length of the system. For such a system charge quasi-neutrality holds. Plasma is commonly known as the fourth state of matter.

Plasma in general consists of electrons, positive and negative ions, atoms and molecules. Depending on the discharge conditions, plasmas can be broadly classified as those in local thermal equilibrium (also known as thermal plasmas or plasma in LTE [Bou94]) and non-equilibrium plasmas. Under certain discharge conditions, usually for pressure at atmospheric or above, the constituent species of the plasma attain the same temperature. When this condition is satisfied the plasma is in LTE.

Arc discharges usually refer to those discharges at atmospheric pressure or above, which are maintained by a current between two electrodes. Arc discharge is characterised by low voltage drop in the cathode region and large current density at the cathode. The plasma column between cathode and anode regions is usually in LTE and is often simply referred as arc. In common with all LTE plasmas the properties of an arc are determined by two thermodynamic quantities (e.g. temperature and pressure) and the distribution of particles among available energy levels obeys Boltzmann's distribution. The behaviour of an LTE plasma can be described by conservation of mass, momentum and energy together with the equation of state, the laws governing electromagnetic fields, charge transport (Ohm's law) and supplementary relations for transport properties (i.e. electrical conductivity, viscosity etc.).

The present work is aimed at the establishment of appropriate mathematical models and obtaining detailed computational results for the plasma environment in two systems under investigation, one is concerned with an arc discharge with carbon electrodes

(hereafter referred to as carbon arc) surrounded by water and the other an arc in a high voltage circuit breaker. The two topics represent the two areas for which Liverpool University has expertise. Both applications involve moving boundary and the processes are transient.

In this chapter, a brief history of plasma research is given in Section 1.2 which is followed by a review of literature on switching arc modelling. In section 1.4 we discuss the important aspects of carbon arc and its application related to nanotechnology and finally the scope of investigation and organisation of the thesis will be given.

1.2 Brief history of plasma research and applications with particular reference to arc plasmas

1.2.1 Background of arc plasma applications

The discovery of arc discharges at the turn of the 19th century can be regarded as the beginning of the study of man-made plasmas. Up to the Second World War, little was known about the fundamental processes occurring in plasmas. The discovery of nuclear fusion and the subsequent realisation of the potential of controlled thermal nuclear fusion promoted intense research activities in basic plasma physics during and immediately after the war [Sim59]. The basic equations describing the behaviour of plasmas ranging from collisionless to collision dominated plasmas were formulated. In parallel with the development of basic plasma theory, diagnostic techniques, especially after the invention of the lasers, have been developed to such an extent that the measurement of basic plasma parameters has become common.

Arc plasmas are characterised by their high temperature and high energy density/flux, which is ideal for certain technical applications such as light sources, material welding and cutting and surface spraying. More recently arc plasmas have been used for decomposition (waste disposal), deposition (thermal plasma chemical vapour deposition) and synthesis of new materials (in the nanometer scale range) through plasma densification [Pfe99].

1.2.2 The motivation of the proposed research work on arc in water

In these systems, the plasma is often generated and maintained either in high frequency electromagnetic fields or between two electrodes with a DC or AC voltage applied. The efficiency and stability of such systems critically depends on the plasma behaviour under specified working conditions and the interaction between the plasma and work piece or the material being processed. For the carbon arc in water, diagnosis of the plasma parameters is extremely difficult because of the small electrode gap surrounded by a volume of water. However to correlate the working conditions with the yield of the system and to subsequently improve the design, fundamental knowledge of plasma behaviour is essential. This inevitably requires the establishment of good physical models and simulation of the arcing process for detailed information within the plasma environment because of the complexity and difficulties involved. There have not been many publications that simulate the plasma environment in a water plasma system because of the complexity and difficulties involved. The problem is multi-disciplinary in that processes at microscopic atomic and molecular level are closely coupled with plasma motion under the influence pressure field and electromagnetic fields. Intense interaction between plasma and its surroundings causes additional difficulty in gaining an understanding of such discharges. The production the nanostructures is not the main concern in the present work. The focus is on the fundamental characteristics of the electric arcs and its interaction with the gaseous and liquid water.

The arc model for arc in water can also be applied to other applications such as arc in oil. This is because the gaseous environment in both cases is formed as a result of vaporisation of liquid, whether water or not. However the material properties of the arcing gas are different. So the thermodynamic and transport properties of the vapour supporting the arc must be used to obtain correct results. Different materials of the electrodes will have different erosion characteristics when they interact with the arc. The difference will be reflected in model parameters such as the total energy required to erode a unit mass of electrode material.

1.3 Switching arcs and their modelling

1.3.1 SF_6 based circuit breakers

Circuit breakers are used for normal switching operations and for interrupt a fault current in a power system. Upon the separation of two contacts in a breaker an electrical arc is drawn between two contacts. The design of a breaker ensures that the arc is extinguished after passing a current zero. The presence of an arc in a breaker is desirable in that excessive over voltage can be avoided as the fault current is interrupted around current zero. Modern circuit breakers are of two types: vacuum circuit breakers where the arc burns in the metal vapour supplied by the electrodes and gas filled circuit breakers. For the latter SF6 is exclusively used due to its superior insulation and arc quenching ability. This thesis is concerned with high voltage. Part of the thesis is concerned with gas filled high voltage circuit breakers at transmission voltage level, which is of gas blast type.

SF_6 puffer circuit breakers have almost exclusively been used in extra high voltage (EHV) power systems nowadays for their excellent performance and their well established technology [Yan09]. The principle of this type of circuit breaker is illustrated in Figure 1.1. The puffer is used to generate high speed gas flow that imposed strong cooling on the arc column when the current passes through its zero point to extinguish the arc thus disconnecting the circuit.

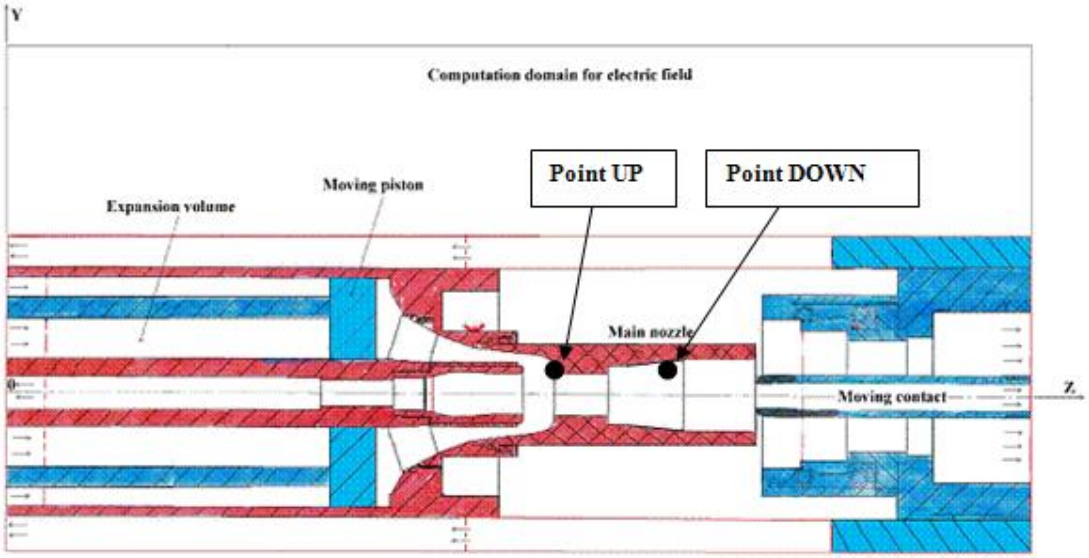

Figure 1.1 *Schematic diagram of PingGao's 252 kV circuit breaker under investigation. This diagram is produced from the original circuit breaker drawing, indicating the shape of major components and the overall geometry of the arcing chamber.*

The interruption of a current in a puffer circuit breaker requires a powerful operating mechanism which is able to compress the gas in the cylinder to produce the necessary gas flow at current zero. It must overcome the high pressure in the puffer cylinder during the high current phase. The driving mechanism needs also to drive the moving contact sufficiently fast so that the gap length between the two contacts after current zero can withstand the high recovery voltage imposed by the power system. The combination of these two requirements demands a powerful operating mechanism which is very costly. Despite the costliness of this type of circuit breaker, it is still exclusively used for voltage ratings higher than 252 *kV*. A typical example is the puffer circuit breakers used in the GIS of a 1000 *kV* transmission line under trial operation in China since 2009 [Yan09].

Recent development on high voltage circuit breakers has also been in the direction of reducing the operating energy by advantageously exploiting part of the arc energy to establish a gas flow in the nozzle for current interruption [Yan99]. This is the basic principle of an auto-expansion circuit breaker, a new generation of circuit breaker.

It is certainly not a new idea to extinguish an arc by exploiting part of its energy. In an early design of oil circuit breakers, an explosion pot system had been used to force the

gas which is generated by the dissociation of oil flowing through a hole in the pot so that the switching arc running in the hole could be efficiently blown out [Lyt72]. Extension of the principle of the explosion pot system to SF_6 circuit breakers was, to the author's knowledge, first carried out by Reyrolle Switchgear [Rey75] in 1973. Renewed interest in the auto-expansion principle was first reported in 1981 by Ueda et al [Ued81]. The Japanese group studied the self-flow generation phenomenon in a puffer circuit breaker with the help of pressure and arc voltage measurement and optical observation [Ued81, Ushi81, Mur82, Sas82, Ued82, Oom83, Sas90]. A compact 7.2 *kV*, 63 *kA* circuit breaker with reduced volume of the puffer cylinder and low energy driving mechanism was then developed in 1982 [Ued82]. To help the interruption of small current without any puffer action, a ring-shaped permanent magnet attached coaxially to the nozzle was used to rotate the arc over the surface of the hollow contact. In 1990, they developed a magnet-assisted auto-expansion circuit breaker rated at 24 *kV*, 25 *kA*. In Europe, Bernard et al at Merlin Gerin (France) and at the University of Liege (Belgium) [Ber88, ber90, Sca92] reported in 1988 the development of a similar magnet-assisted auto-expansion circuit breaker rated at 15 *kV*, 25 *kA*. Recent developmental work on auto-expansion circuit breakers with voltage ratings of 45 *kV* and above have been reported by ABB [Hof94], AEG [Sch90] and Alsthom [Duf91]. Alsthom had been actively involved in the research and development of auto-expansion circuit breakers in the voltage range from 52 to 245 *kV* without any magnet-assistance [Duf91]. Products (FXT range) operated by BLRXE spring control mechanism have been available for voltage ratings of 52, 72.5, 100 and 123 *kV*. Auto-expansion circuit breakers fitted with a device called a "back-piston" to accelerate the contact separation were tested in 1991, having a voltage rating between 145 *kV* and 245 *kV* [Duf91]. Products from several international switchgear manufacturers at 252 *kV* commercially available (for example GL 314P from Areva T&D).

Despite the differences in the operation principles of generating the high speed gad flow for arc cooling between these two types of circuit breakers, they share most of the fundamental physical processes decisive to their interruption performance. Despite the very high voltage ratings of puffer circuit breakers, there are still many challenges faced by the design engineers and researchers, such as reducing the size, operating energy, cost of the breaker, and to exploit new concept of switching that is environmentally

friendly. An understanding of the arcing process, arc behaviour, and performance factors is still essential.

1.3.2 Electric arcs as switching medium and the necessity of arc modelling

An electric arc, for example burring in SF6 at a current 1*kA* or above, has a temperature in its electrically conducting core no less than 20,000 *K*. Electrical conductivity of SF6 at such a temperature is approximately 1000^{th} of that of copper. Thus, the arc is a very good conductor. The fulfilment of switching duty requires the breaker to convert the arc from a good conductor to an insulator within tens of microseconds near an a.c. current zero. The arc's behaviour during the current zero period is therefore critical in determining the performance of a breaker. In modern ultra high voltage gas filled breakers, which are of puffer or self-blast type, the arcing conditions in current zero period depend on the whole arcing history after the separation of contacts. For such breakers the effects of changing a design parameter are not easily known [Tay91, Fang92, Fang94]. Development of circuit breaker relying upon short-circuit test will be too costly.

The rapid development of computer technology during the last 30 years has made possible to simulate the detailed operation of a gas filled circuit breaker on a PC [Yan 99] using commercially available computational fluid dynamics (CFD) package such a PHOENICS. Computer simulation of circuit breaker operations has become a useful design tool for breaker development. Such simulation is based on the well-known Navier-Stokes equations modified to take into account of the effects of electromagnetic fields, radiation transport and turbulent mixing for momentum and energy transfer. For the study of dynamics of electrical power system especially the influence of switching operation on power system stability it is not practical to use an arc model based on Navier- Stokes equations as it is computationally too time consuming. Black box arc models are still used for power network simulation. In the following section the literature on arc modelling will be reviewed.

1.4 Review of arc models

1.4.1 The Black Box Model

Although the discovery of electrical arcs can be dated back to the beginning of the 19th century, investigation of the underlying physical processes in an electric arc have only started in the 20th century. Slepian [Sle28] was probably the first person to propose a theory for arc interruption: the race between the reapplication of voltage across the contacts of a circuit breaker and the recovery of dielectric strength of the contact gap determines the arc behaviour.

The first mathematical description of a dynamic arc was given in 1939 by Cassie [Cas39], who assumed constant and uniform temperature in the arc column. This is virtually an approximation for a radiation controlled, optically thin arc at very high current. The diameter of the arc responds proportionally to the variation of the electric current. Since the energy loss is proportional to the arc's volume zero optical thickness, this can be expressed as:

$$\begin{aligned} P_{loss} &= \frac{energy\ loss \text{ at steady state}}{\text{volume at steady state}} \times (volume \text{ at transient state}) \\ &= \frac{E_0 I_0}{(1/\mathrm{R}_0)}(1/R) = \frac{E_0^2}{R} \end{aligned} \tag{1-1}$$

where P_{loss} is the energy loss in a transient arc, E the electric field strength, I the current and R the resistance per unit length. The subscript 0 refers to a steady state at the same temperature. Based on the overall energy balance in the arc column, Cassie arrived at the following equation:

$$R\frac{d}{dt}(\frac{1}{R}) = \frac{1}{\tau}\left[(\frac{E}{E_0})^2 - 1\right] \tag{1-2}$$

where $\tau = Q_0 R_0 / E_0^2$ is a time constant with Q_0 being the heat content at a steady state.

Four years later in 1943, Mayr [May43] proposed a model for low current arcs. He assumed that the arc radius and the energy loss per unit length remain constant. By relating the resistance of the arc, R, to its heat content, Q, in the form $\mathrm{R} \propto \exp(-\mathrm{Q}/\mathrm{Q}_0)$

with Q_0 being the heat content at a steady state, Mayr expressed the energy conservation equation in a differential form:

$$R\frac{d}{dt}(\frac{1}{R}) = \frac{1}{\tau}\left[\frac{EI}{P_0} - 1\right] \tag{1-3}$$

where P_0 is the energy loss at a steady state and $\tau = Q_0/P_0$ is again a time constant.

The models of Cassie and Mayr are only for extreme cases in circuit interruption. Although Browne [Bro48] in 1948 combined these two models by using Cassie's equation before current zero and that of Mayr for the post zero period, the performance of these "black box" models depends on the availability of test results since the fundamental physical processes inside the arc were not represented at all.

Elenbaas [Ele46] in 1946 first started the work to describe the arc's behaviour in terms of its thermal and electrical properties from the view of conservation of energy:

$$\frac{1}{r}\frac{d}{dr}(rk\frac{dT}{dr}) + \sigma E^2 = 0 \tag{1-4}$$

where T is the temperature, k the thermal conductivity, Equation (1-4) is obviously oversimplified in that some of the important processes such as radiation and convection are excluded from the energy balance. Subsequent applications of Elenbaas' equation by Frind [Fri65] and Phillips [Phi64] to transient wall stabilised arcs established for the first time how the arc's time constant is related to the gas properties and the system dimensions.

1.4.2 The Integral Model

In high voltage circuit breakers arcs usually burn in strongly accelerating flow. Thus the effect of convection had to be considered. However due to the relatively high computational cost in comparison with that of short-circuit test in the nineteen seventies of the last century simplifications of arc conservation equations were necessary. It was

assumed that the arcs are axisymmetrical. Arc conservation equations were radially integrated. The result radially integrated conservation equations are known as the integral arc conservation equations. The closure of the integral arc conservation equations requires the knowledge of the radial temperature and velocity profiles. The differences between various arc integral models lie with the different assumptions on the temperature and velocity profiles. A series of seven papers on arc modelling were published by Swanson and Roidt [S&R70-77] between 1970 and 1977, which, together with the work of Topham [Top71], marked a turning point in gas blast arc modelling. The similarity between an arc in an axial flow and a hot boundary layer was clearly recognised and used to simplify the arc conservation equations. However, their starting conservation equation for energy [S&R70] is in general not correct, as pointed out by Fang [Fang83]. The treatment of the terms in the radially integrated energy equation was not physically justified.

In 1975, Lowke and Ludwig [L&L75] developed a simple arc model for convection stabilised arcs that is only applicable to a certain current range. The current must first be large enough so that thermal conduction and turbulent loss do not influence the central arc temperature. The current must not cause blocking in the nozzle. Tuma and Lowke [T&L75] applied this model to analyse the data of Hermann et al [Her72]. El-Akari and Tuma [E&T77] later extended this channel model to transient arcs.

At the same time, extensive investigations on arcs in gas flow were undertaken by BBC (Brown Boveri) [Her71-77]. Their work on arc radiation and turbulence has greatly enhanced our understanding. A two-zone model including turbulent momentum and heat transfer was successfully employed in elucidating the physics of a 2 *kA* nitrogen nozzle arc [Her74]. A similar arc model neglecting the axial variation of thermodynamic quantities was used to study the arc behaviour during the current zero period [Her76]. In spite of the drastic simplifications introduced, the model has achieved remarkable success when compared with test results. However, the application of this arc model requires the input of six parameters, the value of which cannot be determined by a consideration of physics or system dimension.

Following the same lines as those of Hermann and Ragaller [her72], Tuma and his co-workers [Ric80, Tum80] studied the free recovery and current zero behaviour of a gas

blast arc. Parameters, which control the turbulence strength and the radial profiles of temperature and axial velocity component, have to be adjusted so that the interruption capability agrees with experiment.

An important step in the development of a simplified method of arc analysis, the boundary layer integral method, was taken in 1974 by Cowley [Cow74] in that the arc conservation equations in general form, together with the external flow equations, were rigorously formulated. In a later paper [Cow76] Chan et al extended Cowley's formulation to include an energy integral equation for the arc conducting zone. Thus, the models discussed above are all special cases of this general formulation. The Liverpool-Cambridge arc model has achieved considerable success in elucidating experimental [Mal77, Bot74, C&J78] and computer simulated arcs [Cha78, Fang76]. Recently, this method has been used to investigate the effects of nozzle ablation [Bu90, Fang91, Fang83].

1.4.3 Two and Three Dimensional Full Differential Models

Integral method of arc analysis had served its historical purpose by the middle of nineteen eighties. From that time, the rapid increase in computing power and the availability of reliable numerical method for solving the partial differential flow conservation equations [Pan84] have made arc modelling in full differential form practical. The basic idea of the differential approach is to solve the conservation equations of mass, momentum and energy with appropriate initial and boundary conditions of the physical domain. Since some of the important physical mechanisms in switching arcs, such as radiation transfer, turbulent mixing and electrode sheath interaction, are still too complex, simplifications and approximations must be made. This gives rise to various models devised for different arcing situations.

Ragaller et al [Rag82II] at BBC proposed a model in 1982 for predicting the dielectric recovery of a gas blast arc after current zero. Viscous dissipation and axial heat conduction are neglected in the energy equation. To simplify the problem, the radial momentum equation is reduced to a uniform radial pressure distribution. Thus the surrounding cold flow solely determines the axial pressure distribution. Their

numerical solution involves an isothermal transformation of the differential equations. Strong turbulent energy exchange needs to be introduced in their model in order to bring the numerical prediction close to the measured dielectric recovery characteristics [Rag82I]. Turbulence starts to play an important role in the cooling of the residual hot gas at the stagnation point from about 30 μs after current zero. Flow downstream of the nozzle throat becomes turbulent before current zero.

Mitchell et al [Mit85] investigated the dielectric behaviour after current zero assuming laminar flow. Radiation from the high temperature core is assumed to be fully absorbed in a single layer of one-cell thickness at the arc edge. Adaptive grids are used in the solution because of the very high radial temperature gradient. The solution at the stagnation point is first obtained. The conservation equations are then solved in the downstream region. The boundary condition for the energy equation at the upstream stagnation point is obtained by solving the mass and energy conservation equations at z=0, with the axial gradient of the axial velocity extrapolated from the cell downstream. Although Mitchell et al [Mit85] argued that the energy loss by convection and laminar thermal conduction is sufficient to cool the residual plasma under the same conditions as in [Rag82II], their results of radial temperature profiles (figure 8 in [Mit85]) are clearly similar to those of Hermann and Ragaller based on laminar flow (figure 2 in [Rag82II]) for the period up to 200 μs after current zero. The results given by Mitchell et al [Mit85] of a steady state SF_6 arc at 1200 *A* and 3.6 *bar* indicated that the net emission coefficient given by Liebermann and Lowke [L&L76] should be increased by a factor of 4.

Lowke and Lee [L&L85] investigated the thermal recovery process of a gas blast circuit breaker. They start the transient simulation from a steady state at 2 *kA* before current zero. However, their laminar flow results showed that the predicted critical RRRV for both nitrogen and SF_6 is more than one order of magnitude lower than that given by Hermann and Ragaller [Her77].

Since the middle of the 1980's Fang and his co-workers [Fang94, Fang92, Fang90] at the University of Liverpool have been at the forefront of gas blast arc modelling. They have shown that for nitrogen arcs theory based on laminar flow can give a reasonable prediction of the thermal interruption capability [Fang90] but not for SF_6

[Fang94,Fang92]. Introduction of turbulence has been found necessary for SF_6 arcs. Shock waves are unavoidable during the operation of gas-blast circuit breakers. The behaviour of SF_6 arcs under shock conditions has been investigated by Fang et al [Fang 83].

Extensive investigation into free burning arcs in the last thirty years has been focus on several aspects of the generation of arc plasma. Models differ from each other mainly in two aspects: the arc rooting (current density distribution over the cathode surface) and the calculation of radiation transfer. Prediction based on laminar flow theory and the assumption of optical thin arc column agreed well with measured temperature field for argon arc at 200 *A* [K&L85-Fang05] for 200 *A* steady state argon arcs.

Arc rooting is a complex phenomenon that involves the interaction between plasma and electrode surface, resulting in non-equilibrium sheath layer. Most of the models for free burning arcs neglect this sheath layer and assume a distribution of current density over the cathode surface. The current density over the axisymmetrical cathode is usually described by an exponentially decaying function of the distance from the axis of the cathode surface [Hsu83, Kov86] or of the square of the distance from the centre [Kad95]. There are also models assuming uniform current density in a circular spot on the cathode surface [Kov85]. The current density distribution and heat conduction at the cathode surface had also been calculated by introducing one dimension conservation equations of electron number density and energy and generalised Ohm's law in the cathode sheath layer [Low92, Zhu92]. More recently, there has been considerable effort [Bie99-Ben05] to develop models for the cathode and anode layers by considering mass balance for electrons, ions, neutrals and the change of ions velocity distribution function from Maxwellian to a profile fulfilling the so called Bohm criteria [Ret96].

Commercial computational fluid dynamic software per se is not normally tailored for arc modelling, which requires provision for specific phenomena such as electrical conduction. However, such software can be adapted for this purpose on generic computer hardware with reasonably reliable simulation results.

1.5 Carbon arc for Formation of Nanostructures

As mentioned in section 1.2, the second part of the present work is to model carbon arcs generated in water. This type of plasma system is used in the formation of carbon structures such as nanotubes and fullerenes [San02, San01]. The present work is not concerned with the morphology or functionalities of the nanostructures. The focus is on the fundamental characteristics of the electric arcs and its interaction with the gaseous and liquid water environment because the efficiency and quality of the nanostructures depends heavily on the arc parameters and its environment. Therefore only a very brief review on nanotechnology is provided, which is followed by a review on the experimental arrangement, conditions and results of carbon arcs interesting to the present work.

1.5.1 Nanotechnology and Formation of Nanostructures

The properties of materials begin to be dominated by the physics of atoms and molecules on the surfaces when ordered atomic arrangements are made at nanometre level [Fos05]. Nanotechnology (NT) is the production and use of materials with purposely engineered features at atomic or molecular level. It provides the ability to create materials, devices and systems with fundamentally new functions and properties.

Nanomaterials can comprise of a range of different morphologies including nanotubes, nanowires, and a range of spherical structures [Hsi01]. The use of carbon nanotubes (CNTs) as a material is an important branch in NT.

A nanometer-scale structure named C_{60} fullerenes were first discovered in 1985 by Kroto et al [Kro85]. In the 1980s and early 1990s extensive research was carried out on fullerene theory, synthesis, and characterization [Ebb92]. Iijima [Iij91] first reported in 1991 his observations on elongated and concentric layered microtubules made of carbon atoms using transmission electron microscopy (TEM). This is in fact what we call nowadays the CNTs. This propelled the research of one of the most actively investigated structures of the last century: the CNTs. Since then there has been substantial research effort in the formation of CNTs using various methods. Apart from

plasma chemical vapour deposition CVD [Li96, Ter97, Ren98] and laser vaporisation [Guo95], carbon arc in gaseous and liquid environment has been regarded as a unique way of nanoparticle formation. The arcing environment includes helium [Iij91, Jou97, Nis04], argon [Che03], nitrogen [Ish00], sodium chloride solution [Wan05], and water [San02, Lan03, San01, Ant03, San03, Zhu02, Bir03, Ale04, Wan05].

1.5.2 Carbon arcs in Liquid and Gaseous environment

In the past 15 years, the carbon arc discharge method has been increasingly used for the formation of CNTs and other nanostructures. In fact, mass production of fullerenes was first achieved using an arc discharge with the Kratschmer-Huffman method [Kra90]. This method is probably one of the simplest methods for synthesising nanotubes on a large scale. In this method, an arc is ignited between two graphite electrodes in a gaseous background (usually argon/hydrogen) [Gam95, Bar99, Lan99]. The arc evaporates the carbon material and meanwhile it cools and condenses in a way that some of the product forms as filamentous carbon on the cathode. The simultaneous production of a multi-morphology soot demands several purification steps.

Among all the methods mentioned here, the plasma in water environment is very promising since it has several distinct advantages. Firstly, it does not require a vacuum environment that is needed for plasma based CVD and the purity of the product is usually high [San02]. Secondly, the production rate can be high as a result of efficient cooling of the reaction region near the cathode and arc edge by water and water vapour [Lan03]. For example two 6 mm graphitic rod electrodes immersed in 3 *litres* of water can produce 1 *mg* of nanotubes and onions per minute at a current of 50 *A*. This production rate is far higher than the other methods.

Thirdly, this method does not need any special method to remove the nano-materials from the reaction surface since the particles can automatically detach from the electrode surface and float to the water surface or sink to the bottom of the container for collection.

Most of the research has so far focused on the examination of the structure of product from arc discharge using TEM or Scanning Electron Microscopy (SEM) under different experimental conditions [Shi07, Sai93, Aki00, Jos93, Hsi01], which is not directly relevant to the present work. Quantitative experimental study on the plasma parameters and formation rate is rather limited.

The formation of nanostructures using carbon arc relies on the heating and erosion of the electrode materials. The erosion rate of a tipped carbon anode in the case of water confined arc discharge was measured to be 117 *mg* per minute with a direct current of 30 *A* and an electrode gap of 1 *mm* long [San02]. The average arc voltage is approximately 20 *V*, corresponding to 600*W* power dissipation. Only a fraction of the evaporated electrode material, about 15%, forms separable nanostructures. Radiation and heat from the arc column causes the confining water to evaporate.

Limited spectroscopic diagnosis of the emission characteristics of the water based arc and its plasma parameters is available but the results were obtained on an average sense because the line intensities were not spatially resolved. Lange et al [Lan99] used a CCD camera to identify the lines and bands emitted from a water plasma. The Swan band from the C_2 radicals were then used to derive the column density (standard density integrated over electrode gap length, thus having a unit of $1/m^2$) of C_2 and the temperature. Because of the fluctuations of the plasma zone associated with bubble dispersion and motion of arc root over the electrode surface, the results can only be interpreted on an average sense. At a current of 40 *A* and arc voltage of 21 *V*, the temperature is estimated to be in the range of 5500 K to 6500 K in the electrode gap [San02]. It was noted that the same discharge condition in helium results in a plasma temperature that is 1500 *K* lower than that in the water plasma [Lan99].

The C_2 number density is strongly affected by the material of the electrodes. The measured column density (number density multiplied by the electrode gap) with pure carbon (graphite) electrodes is lower ($1x10^{19}/m^2$) than that with C+0.8% Gd [electrode ($1.4x10^{19}/m^2$) It was proposed by Lang [Lan99] that the lower density is a consequence of the low erosion rate of pure carbon in comparison with doped electrode material.

The formation and growth of CNTs and fullerenes requires the existence of a region having a temperature below the boiling point of carbon which is 4203 *K* [San02]. The possible regions that meet this temperature requirement are the water cooled cathode surface and at the edge of the arc column where a steep temperature gradient exists. It is therefore not surprising that water plasma systems for nanostructure formation employ a very short electrode gap between 0.7 to 1.5 *mm* and a current below 100 *A* to create such cooled regions [San02]. Although these parameters are obtained from experience by examining the production rate and morphology of carbon structures, it nevertheless has its physical reasons. The use of a small anode tip assures a high and uniform energy flux from the arc column to the electrode surface, thus maintaining stable electrode erosion. On the other hand, a small anode attachment results in a stronger magnetic pinch effect which produces gas flow away from the anode surface. This convective flux helps transport the carbon species towards the cathode surface.

The reasons for the use of a small gap length are not well explained in the literature. There could be two possibilities. One possibility is that with a larger gap length, there will be excessive Ohmic heating from within the arc column and more energy will be lost through radiation, increasing the system instability and reducing efficiency of the system. Another possibility is that with a longer electrode gap, carbon vapour produced at the anode surface may be more easily transported outside the arc column by diffusion and convection, resulting in less carbon species reaching the cathode surface and reduce the production rate of carbon structures.

There has been little knowledge on the mechanisms of formation of carbon structures, which is partly because an understanding of the formation of plasma environment and the pattern of transport of carbon particles (ions and atoms) from the erosion surface to the cathode surface and arc edge, where nanostructures are formed, is not available.

It has been proposed by Gamaly [Gam95] that the growth of nanotubes is a result of direct motion of carbon ions from the anode surface under the action of the electric field. However, this view is not shared by some of the other researchers since it has also been demonstrated that nanotubes can also grow in an environment with isotropic velocity distribution of carbon atoms or ions [Guo95]. However, it is commonly accepted that the concurrent presence of a high concentration of carbon particles (ions or atoms) and a

suitable temperature environment for nucleation and growth of the carbon structures is critical to the production rate of the nanostructures.

Given the difficulties encountered in diagnostics of the plasma parameters in a hostile environment where the surrounding water is easily contaminated by the carbon soot and optical access to the plasma column must pass through the liquid water, a detailed understanding of the plasma environment and the transport of carbon species can only be obtained by appropriately modelling the arcing process. This forms one of the mean objectives of the present work. Since the formation of carbon structures are both beyond the scope of a fluid dynamics simulation and also far too complicated to be included in such a simulation, the main concerns are of establishing a model to simulate the effect of carbon vapour from the anode, the transport of carbon species in the arcing environment and the dynamics of gas bubbles. It is hoped that such a model will serve as a platform upon which further advanced investigation into the formation of carbon nanostructure is based.

1.6 The Objectives of Research and Organization of Thesis

1.6.1 Water plasma

The first part of this thesis is aimed at developing realistic arc models for the simulation of atmospheric arc plasma environments which are encountered in applications for the production of nanometer scale carbonstructures. In consideration of the complexity of the process involved, most of the effort is focussed on modelling the arc and its surrounding environment. There is experimental suggestion that the bubble is not in a stable state. It is thus necessary to study the bubble growing process and to identify the characteristic time of this growing process. Numerical schemes have been developed to represent vaporising and moving water surfaces with a spherical shape. Conservation of mass, momentum and energy are considered to include the transport of carbon vapours from the anode surface to the reaction zone where nanotubes or fullerenes are formed. The arcing process is intrinsically transient and results at different instances of the simulation are presented and discussed. Since our focus is on the arc region,

experimental results on anode erosion, water evaporation, and formation rate of nanomaterials were used to set the boundary conditions or volumetric sources representing the generation and loss of carbon species. The formation of carbon particles is not directly simulated in the present work for the reasons stated in section 1.5. However the loss of carbon particles as a result of the formation of carbon structures is taken into account. The chemical reactions between carbon vapour and water vapour are also considered to investigate the concentration distribution of the relevant species.

1.6.2 Switching arcs

For the issues associated with computer simulation of high voltage puffer circuit breakers, arcs burning between two hollow contacts are discussed and several test cases are modelled with a two dimensional axisymmetric arc model. The unrealistic influence of the Lorentz force associated with the uncertainties in arc rooting on the shape of the arc column and the arc voltage is demonstrated and its cause is argued based on arc voltage measurement. The concept of a transparent arc root was introduced to suppress the unwanted arc column contraction. Reasonable agreement between the predicted and measured arc voltages is obtained for high current arcs. Effort is also made to simulate the extinction peak shortly before the final current zero.

1.6.3 Object based visual simulation

Interactions with switchgear manufacturers in the past years have show that the effective use of computer simulation by design engineers has been hindered by the complexity of domain and grid generation, model setup, relaxation control and analysis of the results. For academic research, there is often a need to study the performance of a newly developed arc model by inspecting the distribution of relevant physical quantities during a modelling process and their sensitivity to model parameters in an efficient and convenient approach.

In this thesis key issues in developing an integrated simulation and evaluation environment (ISEE) have been discussed and a model structure for object based visual simulation of thermal plasma systems proposed. This simulation method is based on the requirement from design engineers and also the experience accumulated in the past 15 years. It allows the design engineers to visually manufacture (define) all important components of a thermal plasma system in terms of visual objects and assign physical and simulation properties to the objects. The components can then be assembled using user friendly graphical user interface (GUI) into a product such as a circuit breaker. Once this has been done, the ISEE will automatically translate the visual product into a computer model to simulate the arcing process. Furthermore, the ISEE will allow the user to visually inspect all important physical quantities during or immediately after the simulation process to conveniently retrieve information directly relevant to product design or system performance enhancement.

The feasibility of the ideas is demonstrated by a purposely developed Windows based software package that works seamlessly with a commercial computational fluid dynamics (CFD) package, PHOENICS [Phoe], for the simulation of circuit breaker arcs.

1.7 Reference

[Bou94] Boulos M. I., "Thermal Plasma – Fundamentals and Applications (Volume 1)", Plenum Press, New York, 1994

[Sim59] Simon A., "An Introduction to Thermonuclear Research", Pergamon Press, 1959

[Pfe99] Pfender E., "Thermal Plasma Technology: Where Do We Stand and Where Are We Going?", Plasma Chemistry and Plasma Processing, Vol. 19, No.1, 1999

[Yan09] Yan JD, Han SM, Zhan YY, Zhao HF and Fang MTC, "Computer simulation of the arcing process in high voltage puffer circuit breakers with hollow contacts", Proceedings of XVIII Symposium on Physics of Switching Arc, Brno Czech Republic, pp 99-108, 2009

[Lyt72] R.T. Lythall, The J&P Switchgear Book (7th Edition), Newnes-Butterworths, Londn, 1972

[REY75] Reyrolle Research Report, RD&C/TL/75/9/R, 1975

[Ued81] Y. Ueda, H.Sasso, Y.Murai, K. Yoshinaga, T.Miyamoto and S.Tominaga, "Self-flow generation in a gas circuit breaker without puffer action", IEEE Trans. on power Apparatus and Systems, Vol.PAS-100, Vol.PAS-100, Pp.3888-3898, 1981

[Ush81] T.Ushio, S. Tominaga, H. Kuwahara, T.Miyamoto, Y. Ueda and H.Sasao, "SLF interruption by a gas circuit breaker without puffer action", IEEE Trans. on Power Apparatus and Systems, Vol. PAS-100, Pp. 3801-3810, 1981

[Mur82] Y. Murai, S. Yamaji, T. Miyamoto, H.Sasao and Y.Ueda, "An improvement of low current interrupting capability in self-interruption GCB", IEEE Trans. on Power Apparatus and Systems, Vol. PAS-101, Pp.448-453,1982

[Sas82] H.Sasao, S.Hamano, T.Oomori, Y.Ueda and Y. Murai, "mixing process of arced gas with cold gas in the cylinder of gas circuit breaker", IEEE Trans. on Power Apparatus and Systems, Vol. PAS-101, Pp. 1115-1121, 1982

[Ued82] Y.Ueda, Y.Murai, A.Ohno and T.Tsutsumi, "Development of 7.2 KV- 63KA advanced puffer gas circuit breaker", IEEE Trans. on Power Apparatus and Systems, Vol. PAS-101, Pp. 1504-1510, 1982

[Oom83] T.Oomori, S.Hamano, H. Sasao, Y.Ueda and Y. Murai, "Optical observation of self-gas-flow in GCB", IEEE Trans.on Power Apparatus and Systems, Vol. PAS-102, Pp. 1408-1413,1983

[Sas90] H.Sasao, S.Hamano, Y.Wada, H.Hasegawa and N.Kobayashi, "Development of a magnet-assisted autopuffer GCB", IEEE Trans.on Power Delivery, Vol.5, Pp. 1355-1361, 1990

[Ber88] G.Bernard, P. Malkin and W.Legros, “An SF6 circuit breaker using auto-expansion principle”, IEEE Trans. on Power Delivery, Vol. 3, Pp. 1739-1744, 1988

[Ber90] G.Bernard, A. Girard, P. Malkin and P.Scarpa, “An SF6 circuit breaker using auto-expansion principle”, IEEE Trans. on Power Delivery, Vol. 3, Pp. 1739-1744, 1988

[Sca92] P.Scarpa, B. Dauby, J.M.Defise, M.Barrault, and G. Bernard, “SF6 auto-expansion circuit breaker design: numerical and experimental investigations of arc-gas interactions”, IEEE Trans. on Power Deleivery, Vol.7, Pp.339-349, 1992

[Hof94] W.Hofbauer and J.Stechbarth, “Strategic tools-application for the development of a 300kV/50kA GIS self-blast circuit breaker”, GIGRE 94, 13-110, Paris, 1994

[Sch90] Dipl.-ing. Andreas Schiemann, “Third-generation SF6 circuit breakers”, Electricity International, Pp. 18-24, September 1990

[Duf91] D.Dufournet, “Evolution of the SF6 thermal blast interruption in high voltage up to 245kV”, GEC Alsthom Technical Review, No.6, Pp. 47-58, 1991

[Tay91]Taylor, S., Fang, M.T.C., Jones, G.R., and Shimmin, D.W. "Current zero flow conditions in a circuit breaker-nozzle" Proc. IEE Pt.A., Vol. 138, pp. 259-264, 1991

[Fang92] Fang, M.T.C. and Zhuang, Q. "Current Zero Behaviour of an SF_6 Gas Blast Arc, Pt.I: Laminar Flow" J.Phys.D.: Appl. Phys., Vol.25, pp. 1197-1204, 1992

[Fang94] Fang, M.T.C., Zhuang, Q. and Guo, X. "Current Zero Behaviour of an SF_6 Gas Blast Arc, pt II. Turbulent Flow", J. Phys. D: Appl. Phys., Vol. 27, pp 74-83, 1994

[Yan99] Yan J D, Fang, M.T.C. and Hall, W., “The development of PC based CAD tools for auto-expansion circuit breaker design”, IEEE Transactions on Power Delivery, Vol. 14, pp.176-181, 1999,

[Sle28] J.Slepian, “Extinction of an a.c. arc”, AIEE Trans. Vol.47, Pp. 1398-1402, 1928

[Cas39] Cassie A. M., "Arc rupture and circuit severity: a new theory", CIGRE, Paper 102, pp. 1-14, 1939

[May43] Mayr O., "Beitrage zur theorie des statischen und des dynamischen lichtbogens (contribution to the theory of static and dynamic arcs)", Arch. Elect., 37, pp. 588-608, 1943

[Bro48] Browne Jnr T. E., "A study of ac arc behaviour near current zero by means of mathematical models", AIEE Trans., Vol. 67, Pt. 1, pp. 147-153, 1948

[Ele46] Elenbaas W., Phillips Research Report, Vol. 1, No. 5, 1946

[Fri65] Frind G., "Time constant of flat arcs cooled by thermal conduction", IEEE Trans. on Power Apparatus and Systems, Vol. 84, pp. 1125-1131, 1965

[Phi64] Phillips R. L., "The behaviour of dynamic electric arcs", ARL Report 64-150, 1964

[S&R70] Swanson B. W. and Roidt R. M., "Boundary layer analysis of an SF6 circuit breaker arc", IEEE Trans., PAS-90, pp. 1086-1903, 1970

[S&R70] Swanson B. W, Roidt R. M. and Browne T. E., "Arc cooling and short line fault interruption", IEEE Trans. PAS-90, pp. 1094-1102, 1970

[S&R72] Swanson B. W. and Roidt R. M., "Thermal analysis of an SF6 circuit breaker arc", IEEE Trans. PAS-91, pp. 381-389, 1972

[S&R71] Swanson B.W. and Roidt R.M., "Some numerical solutions of the boundary layer equations for an SF6 arc", Proc. IEEE., Vol. 59, pp. 493-501, 1971

[S&R72] Swanson B.W. Roidt R.M, and Browne T.E., "A thermal arc model for short line fault interruption", ET-Z-A, Bd.93, pp. 375-380, 1972

[Swa74] Swanson B.W., "A thermal analysis of short line fault interruption", IEE Winter Power Meeting, Paper C-47, 1974

[Swa77] Swanson B.W., "Nozzle arc interruption in supersonic flow", IEEE Trans., PAS-96, 1977

[Top71] Topham D.T., "The electric arc in a constant pressure axial gas flow", J. Phys. D.,Vol. 4, pp. 114-1125, 1971

[Fang83] Fang M.T.C., "A review of gas-blast circuit breaker arc modelling", ULAP-T75, Dept. of Ele. Eng. And Electronics, University of Liverpool, 1983

[L&L75] J.J.Lowke and H.C.Ludwig, "A simple model for high current arcs stabilised by forced convection", J.Appl.Phys., Vol.46,Pp.3361-3367,1975

[T&L75]D.T.Tuma and J.J.Lowke, "Prediction of properties of arcs stabilised by forced convection", J.Appl.Phys., Vol.46,Pp.3352-3360, 1975

[Her72] W.Hermann and E.Schade, "Radiation energy balance in cylindrical nitrogen arc", JQSRT, Vol.12, Pp, 1257-1263, 1972

[E&T77] F.R.EI-Akkari and D.T.Tuma, "Simulation of transient and zero current behavior of arcs stabilised by forced convection", IEEE Trans., PAS, Vol. PAS-96, Pp. 1784-1788,1977

[Her74]W.Hermann, U.Kogelschatz, L.Niemeyer, K.Ragaler and E.Schade, "Experimental and theoretical study of a stationary high current arc in a supersonic nozzle flow", J.Phys.D., Vol.7, Pp.1703-1722, 1974

[Her76]W.Hermann, U.Kogelschatz, L.Niemeyer, K.Ragaler and E.Schade, "Investigation of the physical phenomena around current zero in HV gas blast breakers", IEEE Trans.PAS, Vol.PAS-95, Pp.1165-1176, 1976

[Her77] W.Hermann, K.Ragaller, "Theoretical description of the current interruption in high voltage gas blast circuit breakers", IEEE Trans.PAS, Vol.PAS-96mPp.1546-1555, 1977

[Her71] W.Hermann, K.Ragaller and W.Schneider, "Theory of high pressure arc in a strong axial gas flowProc.10th Int.Conf.on Phenomena in Ionised Gases,Pp.199-201, 1971

[Ric80] E.Richley and D.Tuma, "Free recovery of the gas blast arc column", IEEE Trans.on plasma Science, Vol.PS-8, Pp.405-410, 1980

[Tum80]D.T.Tuma, "A comparison of the behavior of SF6 and N2 gas blast arcs around current zero", IEE Trans., PAS, Vol. PAS-99, pp.2129-2137, 1980

[Mal77]V.R.Malghan, M.T.C.Fang, and G.R.Jones, "Investigation of quasi-steady state high current arcs in an orifice air flow", J.Appl. Phys., Vol.48, Pp. 2331-2337, 1977

[Bot74] I.R. Bothwell, M.D.Cowley and b. Grycz, IEE Conf.Publication, no. 118,Pp. 474-477, 1974

[C&J78] A. Chapman and G.R. Jones, "The local electrical properties of gas blast arc near current zero", IEEE Trans. Plasma Science, vol. PS-6, Pp. 300-313, 1978

[Cha78] Chan, S.K., Fang, M.T.C. and Cowley, M.D., "The DC arc in a Supersonic Flow", IEEE Trans., Plasma Science, Vol.PS-6 pp. 394-405, 1978

[Fang76] M.T.C. Fang, S.K. Chan and M.D. Cowley, "Transient behavior of interrupted arcs in laminar flow", J.Phys. D, vol. 9, Pp. 1757-1770, 1976

[Bu90] W.H.Bu, M.T.C. Fang and Z.Y. Guo, "The behavior of ablation-dominated DC nozzle arcs", J.Phys.D: Appl. Phys.23, Pp. 175-183, 1990

[Fang91] M.T.C.fang and W.H.Bu, "Investigation of ablation dominated AC nozzle arcs", IEE Proc.-A, Vol. 138, Pp. 71-77,1991

[Fang83] M.T.C.fang and D.B.new land, “DC nozzle arcs with mild wall ablation”, J.Phys.,D: Appl. Phys. 16, Pp. 793-810, 1983

[Pan84] Pantankar S.V., “Numerical Heat Transfer and Fluid Flow”, Hemisphere, New York, 1984

[Rag82II] Ragaller K., Egli W. and Brand K.P., “Dielectric recovery of an axially blown SF6-arc after current zero, Part II theoretical investigation”, IEEE Trans. On Plasma Science, Vol. PS-10, pp. 154-162, 1982

[Mit85]R.R.Mitchell, D.T.Tuma and J.F.Osterle, “Transient two dimensional calculations of properties of forced convection stabilized electric arcs”, IEEE Trans. On Plasma Science, Vol.PS-13, Pp. 207-213, 1985

[L&L76]R.W. Liebermann and J.J.Lowke, “Radiation emission coefficients for sulphur hexafluoride arc plasmas”, JQSRT, Vol.17, Pp.253-264, 1976

[L&L85] J.J. Lowke and H.E. Lee, “A numerical study of a two dimensional circuit breaker arc during current interruption”, Proc. of gas discharge and their applications, Oxford, Pp. 54-56, 1985

[Fang92] Fang, M.T.C. and W. Y. Lin. "Current Zero Behaviour of an SF_6 Gas Blast Arc, Pt.I: nitrogen " IEE Proc., Vol.137, Pt.A, No.1, Pp.85-86, 1996

[K&L85] Kovitya P. and Lowke J. J., “Two-dimensional analysis of free-burning arcs in argon”, J. Phys. D: Appl. Phys., 18, pp. 53-70, 1985

[Hsu83] Hsu K.C., Etemadi K. and Pfender K., “Study of the free-burning high-intensity argon arc”, Appl J., Phys. 54 (3), pp. 1293-1301, 1983

[Kov86] Kovitya J. and Cram L.E., “A two-dimensional model of gas-tungsten welding arcs”, Welding Journal, pp. 34-39, 1986

[Low92] Lowke J.J., Kovitya P. and Schmidt H.P., "Theory of free-burning arc columns including the influence of the cathode", J. Phys. D: Appl. Phys. 25, pp. 1600-1606, 1992

[Zhu92] Zhu P. Y., Lowke J.J. and Morrow R., "A unified theory of free burning arcs, cathode sheaths and cathodes", J. Phys. D: Appl. Phys. 25, pp. 1221-1230, 1992

[Kad95] Kaddani A., Zahrai S., Delalondre C. and Simonin O., "Three-dimensional modelling of unsteady high-pressure arcs in argon", J. Phys. D: Appl. Phys. 28, pp. 2294-2305, 1995

[Fang05] Fang M. T. C., Zhang J. L. and Yan J. D., "On the Use of Langmuir Probes for the Diagnosis of Atmospheric Thermal Plasmas", IEEE Transaction on Plasma Science, Vol. 33, No. 4, pp. 1431-1442, 2005

[Bie99] Biehler S., Ecker G. and Riemann K. U., "Theory of the presheath in a weakly ionized plasma with hot neutrals", Phys. Fluids, Vol. 31, Issue 7, 1999

[Li07] Li H. P. and Benilov M. S., "Effec of near-cathode sheath on heat transfer in highpressure arc plasmas", J. Phys. D: Appl. Phys., Vol. 40, pp. 2010-2017, 2007

[Ben97] Benilov M. S., "Analysis of thermal non-equilibrium in the near-cathode regioin of atmospheric-pressure arcs", J. Phys D: Appl. Phys., Vol. 30, pp3353-3359, 1997

[Sch02] Schmitz H. and Riemann K. U., "Analysis of the cathodic region of atmospheric pressure discharges", J. Phys. D: Appl. Phys., Vol. 35, pp. 1727-1735, 2002

[Ben02] Benilov M. S., "Theory and modelling of arc cathodes", Plasma Sources Sci. Technol., Vol. 11, 2002

[Ben03] Benilov M. S. and Cunha M. D., "Heating of refractory cathodes by high-presure arc plasmas:II", J. Phys. D: Appl. Phys., Vol. 36, pp. 603-614, 2003

[Ben05] Benilov M. S., Cunha M. D. and Naidis G. V., "Modelling interaction of multispecies plasmas with thermionic cathodes", Plasma Sources Sci. Technol.,Vol. 14, pp. 517-524, 2005

[Ret96] Rethfeld B., Wendelstorf J., Klein T. and Simon G., "A self-consistent model for the cathode fall region of an electric arc", J. Phys. D: Appl. Phys., Vol. 29, pp. 121-128, 1996

[Fos05] Foster L. E., "Nanotechnology: Science, Innovation, and Opportunity", Prentice Hall, 2005

[Hsi01] Hsin Y. L., Hwang K. C., Chen F. R. and Kai J. J., "Production and in -situ Metal Filling of Carbon Nanotubes in Water", Adv. Mater. Vol. 13, No. 11, 2001

[Kro85] Kroto H. W., Heath J. R., O'Brien S. C., Curl R. F. and Smalley R. E., "C_{60}: Buckminsterfullerene, Nature, Vol. 318, pp. 162, 1985

[Ebb92] Ebbesen, T. W., Ajayan, P. M., "Large-scale synthesis of carbon nanotubes". Nature, Vol. 358, pp. 220-222, 1992

[Iij91] Iijima S., "Helical microtubules of graphitic carbon", Nature, Vol. 354, pp. 56-58, 1991

[Guo95] Guo T., Nikolaev P., Rinzler A. G., Tomanek D., Colbert D. T. and Smalley R. E, "Self-Assembly of Tubulear Fullerenes", J. Phys. Chem., Vol. 99, pp. 10694-10697, 1995

[Li96] Li W. Z., Xie S. S., Qian L. X., Chang B. H., Zou B. S., Zhou W. Y. Zhao R. A. and Wang G., "Large-Scale Synthesis of Aligned Carbon Nanotubes", Science, Vol. 274, pp. 1701-1703, 1996

[Ter97] Terrones M., Grobert N., Olivares J., Zhang J. P., Terrones H., Kordatos K., Hsu W. K., Hare J. P., Townsend P. D., Prassides K., Cheetham A. K., Kroto H. W. and Walton D. R. M., "Controlled production of aligned-nanotubes bundles", Nature, Vol. 388, Issue 6637, pp. 52-55, 1997

[Ren98] Ren Z. F., Huang Z. P., Zu J. W., Wang J. H., Bush P., Siegal M. P. and Provencio P. N., "Synthesis of Large Arrays of Well-Aligned Carbon Nanotubes on Glass", Science, Vol. 282, No. 5391, pp. 1105-1107, 1998

[Jou97] Journet C., Maser W. K., Bernier P., Loiseau A., Lamy de la Chapelle M., Lefrant S., Deniard P., Lee R. and Fischer J. E., "Large-scale production of single-walled carbon nanotubes by the electric-arc technique", Nature, Vol. 388, 756-758, 1997

[Nis04] Nishio M., Akita S., Nakayama Y., "Cooling effect on the growth of carbon nanotubes and optical emission spectroscopy in short-period arc-discharge", Thin Solid Films, 464-465, pp 304-307, 2004

[Che03] Chen C. K., Perry W. L., Xu H., Jiang Y., Phillips J., "Plasma torch production of macroscopic carbon nanotubes structures", Carbon, Vol. 41, pp. 2555-2560, 2003

[Ish00] Ishigami M., Cumings J., Zettl A. and Chen S., "A simple method for the continuous production of carbon nanotubes", Chem. Phys. Lett., Vol. 319, pp. 457-459, 2000

[Wan05] Wang S. D., Chang M. H., Lan K. M. D., Wu C. C., Cheng J. J. and Chang H. K., "Synthesis of carbon nanotubes by arc discharge in sodium chloride solution", Carbon, Vol. 43, 1778-1814, 2005

[San02] Sano N., Wang H., Alexandrou I., Chhowalla M., Teo K. B. K. and Amaratunga G. A. J., "Properties of carbon onions produced by an arc discharge in water", Journal of Applied Physics, Vol. 92, No. 5, pp. 2783-2788, 2002

[Lan03] Lange H., Sioda M., Huczko A., Zhu Y. Q., Kroto H. W. and Walton D. R. M., "Nanocarbon production by arc discharge in water", Carbon, Vol. 41, pp. 1617-1623, 2003

[San01] Sano N., Wang H., Chhowalla M., Alexandrou I., Amaratunga G. A. J., "Synthesis of carbon 'onions' in water", Nature, Vol. 414, pp. 506, 2001

[Ant03] Antisari M. V., Marazzi R., Krsmanovic R., "Synthesis of multiwall carbon nanotubes by electric arc discharge in liquid environments", Carbon, Vol. 41, pp. 2393-2401, 2003

[San03] Sano N., Wang H., Chhowalla M., Alexandrou I., Amaratunga G. A. J., Naito M. and Kanki T., "Fabrication of inorganic molybdenum disulfide fullerenes by arc in water", Chem. Phys. Lett., 368, pp. 331-337, 2003

[Zhu02] Zhu H. W., Li X. S., Jiang B., Xu C. L., Zhu Y. F., Wu D. H. and Chen X. H., "Formation of carbon nanotubes in water by the electric-arc technique", Chem. Phys. Lett., 366, pp. 664-669, 2002

[Bir03] Biro L. P., Horvath Z. E., Szalmas L., Kertesz K., Weber F., Juhasz G., Radnoczi G. and Gyulai J., "Continuous carbon nanotube production in underwater AC electric arc", Chemical Physics Letters 372, pp. 399-402, 2003

[Ale04] Alexandrou I., Wang H., Sano N., Amaratunga G. A. J., "Structure of carbon onions and nanotubes formed by arc in liquids", Journal of Chemical Physics, Vol. 120, pp. 1055-1058, 2004

[Wan05] Wang S. D., Chang M. H., Cheng J. J., Chang H. K., Lan K. M. D., "Unusual morphologies of carbon nanoparticles obtained by arc discharges in deionized water", Carbon, Vol. 43, pp. 1317-1339, 2005

[Lan99] Lange H., Saidane K., Razafinimanana M. and Gleizes A., "Temperatures and C_2 column densities in a carbon arc plasma", J. Phys. D: Appl. Phys., 32, pp. 1024-1030, 1999

[Kra90] W. Kratschmer, Lowell D. Lamb, K. Fostiropoulos &Donald R. Huffman., "Solid C_{60}: a new form of carbon" , Nature 347, 354 - 358 1990

[Bar99] Baronnet J.-M, Ershov-Pavlov E.A., Megy S., "Plasma parameters of an argon DC arc with graphite electrodes", J.Phys. D: 32; pp2552-2559, 1999

[Shi07] S. Sawaya, S. Akita, and Y. Nakayama, "Correlation between the mechanical and electrical properties of carbon nanotubes", Nanotechnology 18, 2007

[Sai93] Y. Saito, M.Inagaki, "Optical Emission Studies on Chemical Species in an Arc Flame of Fullerene/Metallofullerene Generator", Jpn. J. Appl. Phys. 32 pp. L954-L957, 1993

[Aki00] S.Akita, H.Ashi, Y.Nakayama, "Optical Emission Spectroscopy of Arc Flame Plasma for Generation of Carbon Nanotubes", Jpn. J. Appl. Phys. 9 pp. 4939-4944, 1993

[Jos93] Jose-Yacaman, M., Miki-Yoshida, M., Rendon, L., Santiesteban, J. G., "Catalytic growth of carbon microtubules with fullerene structure", Appl.Phys.Lett. 62(2), pp202-204, 1993

[Hsi01] Y.L.Hsin, K.C.Hwang, F.R.Chen, J.J.Kai, "Production and in-situ Metal Filling of Carbon Nanotubes in Water", Adv.Mater.12, No.11, pp830-833, 2001

[Gam95] Gamaly E. G., "Mechanism of carbon nanotube formation in the arc discharge", Physical Review B, Vol. 52, No. 3, pp. 2083-2089, 1995

[Phoe] PHOENICS is the name of a commercial CFD package supplied by CHAM which is based at Bakery House, 40 High Street, Wimbledon Village, London, SW19 5AU, UK.

Chapter 2 The Arc Models and the simulation method

2.1 Introduction

A mathematical model is always required for the simulation of any physical processes. It should be a correct mathematical representation of all important mechanisms determining the behaviour of the system. Assumptions are often necessary in the establishment of a mathematical model because of the complexity of the system under investigation. An example in the present work is the assumption of local thermodynamic equilibrium (LTE) for the state of the plasma in the interrupter of a circuit breaker and for the water confined carbon arc. In this chapter the arc models for two different applications will be developed with a careful consideration of the important issues affecting the validity of the mathematical description.

2.2 Governing Equations for High Pressure Arc Plasma

2.2.1 SF_6 Circuit breaker arcs

The concept of complete thermodynamic equilibrium (CTE) greatly simplifies the mathematical description of the behaviour of a gas or a plasma. For a system under CTE, the random motion of constituent particles can be statistically described by the Maxwellian velocity distribution and all species attain the same temperature, the population density of energy levels in an atom, a molecule or an ion obeys Boltzmann distribution, ionisation is described by Saha's Equation, radiation field by Planck's law and the principle of detailed balancing is valid. However not all conditions of detailed balancing under which CTE is established can be met in industrial devices such as a circuit breaker. Deviations from CTE can be caused by many factors. In the case of atmospheric arc particles collide with each other frequently. However, due to finite

dimension of the system radiation inevitably escapes from the plasma to the surroundings, thus radiation field in a practical plasma is no longer blackbody. Thus, reactions or ionisation related to photons are no longer balanced. To ensure the validity of Boltzmann's distribution and Saha's equation we require that electron number density is above a minimum value. As a rule of thumb, electron number density needs to be above $10^{21}/m^3$ although to ensure Boltzmann distribution the threshold electron number density depends on plasma temperature and the energy difference between two energy levels. Non-uniformity and time variation always exist in laboratory and industrial plasmas. As the plasma under investigation will be treated as a continuous medium this requires that the characteristic length for spatial variation of a physical quantity, for example, temperature, should be much bigger than the typical mean free path of the plasma:

$$\left|\frac{T}{\nabla T}\right| \gg \lambda$$

As plasmas are usually maintained by an electrical power input, to ensure that excessive electron energy gained from electrical field can be transferred to heavy particles through collisions the following is required

$$\frac{T_e - T}{T} = \frac{2}{9} \cdot \frac{1}{\delta} \cdot (\frac{eE\lambda}{kT})^2 \ll 1$$

Where E is the electrical field, T_e and T are respectively electron and heavy particle temperature, k the Boltzmann constant and δ is the mass ratio of electron mass to that of heavy particle.

For SF_6 arcs at 5 bar, the dominant species is F at temperatures below 20,000 K and electron and F^+ above 20,000 K. The elastic collision cross section between F and electron is approximately 2.5×10^{-20} m^2 and that between electron and F^+ is much larger due to the long range nature of electric interaction. The main free path for elastic collision between electron and heavy particles is smaller than 10^{-6} m. On the other hand the characteristic length of system parameter variation is in the order of millimetre. Thus the plasma can be treated as continuum medium. Using $\lambda = 10^{-6}$ m and T = 20,000

K, a value of 0.02 was obtained for $(T_e - T)/T$. Thus, a single temperature can be used for electrons and heavy particles.

If a plasma is in a transient state an additional condition for LTE needs to be imposed. That is the slowest reaction time should be much smaller than the characteristic time of the transient process. This condition is normally fulfilled for high pressure arcs at power frequency.

An arc plasma in a modern high voltage (HV) circuit breaker is at atmospheric and above. It satisfies the conditions for LTE. The behaviour of such an arc plasma is fully described by Navier-Stokes equations modified to take into account the effects of electromagnetic fields and radiation transport. These equations are supplemented by equation of state, transport properties as a function of two thermodynamic quantities, Maxwell's equations for the calculation of electric and magnetic fields, radiation transport equations and Ohm's law.

Conservation equations of mass, momentum and energy can be written in the following general form

$$\frac{\partial(\rho\emptyset)}{\partial t} = \nabla \cdot \left(\rho\vec{V}\emptyset - \Gamma\nabla\emptyset\right) = S_\emptyset \qquad (2\text{-}1)$$

where ϕ , Γ_ϕ and S_ϕ are the dependent variable to be solved , diffusion coefficient and source terms, respectively. For circuit breaker arcs, Table 2.1 gives details on the governing differential equations with a breakdown of the contribution by laminar and turbulent processes in momentum and energy transfer.

Table 2.1: Mass, Momentum and Energy Conservation Equations for circuit breaker arcs

	ϕ	Γ_ϕ	S_ϕ
Continuity	*1*	0	0
Radial momentum	*v*	$\mu_l + \mu_t$	$-\frac{\partial P}{\partial r} + j_z \times B_\theta + viscous\_term$

Axial momentum	w	$\mu_l + \mu_t$	$-\frac{\partial P}{\partial z} - j_r B_\theta + viscous\_terms$
Enthalpy	h	$(k_l + k_t)/c_p$	$\sigma E^2 - q + \frac{dP}{dt} + viscous\_terms$
Potential	φ	σ	0

Radiation transfer is the most efficient way of transporting energy inside and around the arc column. For SF_6, the use of net emission coefficient (NEC) has proven reasonable. Radiation transport leads to a volumetric energy source, q in Table 2.1, which can be positive (loss of energy through net emission) and negative (radiation absorption). q depends on the temperature and pressure fields and the gas composition. Details of the radiation model will be described in section 2.4.1.1. Lorentz force, $\vec{J} \times \vec{B}$, accounts for the interaction between the current and the magnetic field. It is a volumetric source to the momentum equations. The calculation of *J* and *B* will be given in section 2.3. The transport properties and the equation of state for SF_6 are given in [Low92]. For completeness, the relevant variables and quantities are listed below together with their meanings:

ρ : gas density – mass per unit volume

h : static enthalpy – the sum of the internal energy *e* plus the product of the pressure *p* and specific volume *V*

P : pressure - force per unit area

v : *y*-direction velocity component

z : *z*-direction velocity component

μ_l and μ_t: the laminar and turbulent viscosity

k_l and k_t : the laminar and turbulent molecular thermal conductivity.

ρD_l *and* ρD_t*:* the laminar and turbulent diffusion coefficient

c_p : specific heat at constant pressure – heat energy in unit volume

σ : electrical conductivity

j_r : *r*-direction current density component

j_z : *z*-direction current density component

B_r : *r*-direction magnetic field component – a vector field surrounding moving

electric charges and magnetic dipoles

B_z : *z*-direction magnetic field component

q :net radiation loss per unit volume and time.

In the case of SF_6 circuit breakers, the arc at high current emits strong radiation which results in ablation of the PTFE nozzle. The PTFE vapour enters the flow domain and forms of a mixture of SF_6 and PTFE vapour. Previous study [Yan99I] has shown that the thermodynamic properties of PTFE vapour is similar to those of SF_6 with a maximum difference of 20% within the temperature range of interest because of the dominant presence of fluorine atoms in both gases at high temperature. For the present work on puffer circuit breaker, SF_6 is not distinguished from PTFE to save computation time (avoiding solution of PTFE vapour concentration equation and interpolation of transport properties of mixture). This means that ablation from PTFE nozzle is treated as a source for SF_6. Details on the calculation of the ablation rate are given in section 2.4.2.

2.2.2 Arc in Water

As to be shown in chapter 3, the arc confined by water burns in fact in an environment dominated by carbon vapour as a result of strong erosion of the carbon anode. The arc column is surrounded by a mixture of water vapour and other gaseous species. Saidane et al. [Lan99] performed spectroscopic diagnosis on a carbon arc burning in helium at a pressure of 13 *kPa* and with a gag length of 1*mm*. The arc current is 65 *A*. The electron number density in the arc centre is in the range of 10^{19} to 10^{20} m^{-3} and the arc temperature is in the range of 4,600 *K* to 5,400 *K* on the axis. Lange et al. [Lan99] measured the temperature of a 40 *A* d.c. arc in water and obtained a temperature of 6,000 *K* to 7,000 *K*. It seems that the arc temperature is too low for the assumption of LTE. It however must be noted that the spectroscopic measurement performed in the arc in water case is subject to potentially large uncertainties due to contamination of the water by formed nano-particles and optical deformation in water. Simulation results in [Gleizes] and from the present work indicate that the temperature at the arc centre can reach 10,000 *K*. LTE is used in the work in [Gleizes] at a pressure of 13 *kPa*. In the present case, the pressure is atmospheric and the arc plasma state is expected to be

closer to LTE. By assuming LTE state, the arc in water system can also be described by the governing equations in the form of equation (2-1). Gas flow inside and around the arc column is laminar because of the rather limited arcing space.

Up to now the exact gas environment surrounding the arc is not known. The most probable chemical reaction suggested by experiment is the production of hydrogen (H_2) and carbon monoxide (CO) [San02]. Although the concentration of H_2 and CO is low in the region well away from the arc, but it is substantial in the region close to the electrode surface and at the arc edge where CNT and fullerenes are formed so the chemical reaction should be considered.
The reaction can be described as

$$C + H_2O => CO + H_2 \qquad (2\text{-}2)$$

It is to be noted that the mass concentration of the four species does not follow the stochastic relationship controlled by (2-2) since the reaction is regarded as unidirectional. In addition, carbon vapour can be lost through formation of carbon nano-structures. It is therefore necessary to solve the mass concentration equation for C (C_1), H_2 (C_3), and CO (C_5) and derive the concentration for water vapour by

$$C_w = 1 - C_1 - C_3 - C_5 \qquad (2\text{-}3)$$

The concentration equation for the gaseous species takes the following form:

$$\frac{\partial \rho C_x}{\partial t} + \nabla \cdot \left(\rho \vec{V} C_x\right) - \nabla \cdot \left(\rho D \nabla C_x\right) = S_x \qquad (2\text{-}4)$$

where x takes the value of 1, 3 and 5. While the mass concentration is a dimensionless variable, the source term S_x has a unit of $kg/(m^3 s)$. In solving (2.4) the diffusion coefficients of the species and the mass source terms as a result of reaction are needed.
The loss of carbon vapour due to chemical reaction can be expressed as:

$$S_1 = -A^*[C_1][C_w]\exp\left(\frac{-E_a}{RT}\right) \qquad (2\text{-}5)$$

where A is a prefactor, E_a the reaction activation energy and R the gas constant. The determination of the transport properties and further details on the reaction will be given in Chapter 3. The material properties for the arcing gas will be given in Chapter 3.

2.3 Calculation of the Electric and Magnetic Fields

The calculation of Ohmic heating in the energy equation and the Lorentz force in the momentum equation requires knowledge of the electrical conductivity, the current density and the magnetic flux density. Circuit breakers operate at 50 or 60 *Hz* and the arc in water is sustained by a direct current. The displacement current is negligible compared with conduction current. In addition the induced electric field due to arc motion in its own magnetic field is also much smaller than that externally imposed through the two contacts. Under these conditions, Ohms Law in its simplest form becomes:

$$\vec{j} = \sigma\vec{E} \qquad (2\text{-}6)$$

where σ is the electrical conductivity and E= -∇φ with φ being the electrostatic potential. The potential can be calculated from the current continuity equation

$$\nabla \cdot (\sigma\nabla\varphi) = 0 \qquad (2\text{-}7)$$

Equation (2-7) is solved in both gaseous and solid part of the domain. It becomes invalid when σ is zero. To avoid the invalidation the electrical conductivity is limited to a minimum threshold value of $10^{-3}\ \Omega^1 m^{-1}$ for gas at low temperature. This is a common practice used in arc simulation.

Two transparent contacts filling the holes of the two hollow contacts are used since in the two dimensional axisymmetric model the arc always sits on the axis and its root radius can become smaller than the inner diameter of the contact hole. The transparent

contacts are virtual since they do not cause any block to the gas flow, as shown in Figure 2.1. The electrical conductivity in the real and transparent contacts is given a value of 10^6 $\Omega^{-1}m^{-1}$.

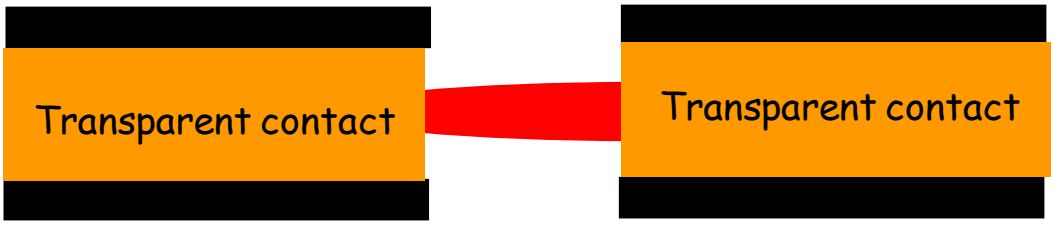

Figure 2.1 Diagram illustrating the use of transparent contacts to support current continuity in circuit breaker arc simulation.

For current below 15 *kA* in high voltage circuit breakers, the length of the arc column is normally much larger than its radial size and the radial electric field component can be neglected. With this assumption, the axial electric field is calculated by the following equation:

$$I = E_z \int_0^{R_c} \sigma 2\pi r dr \qquad (2\text{-}8)$$

where R_c is the radius of the conducting column, normally taken as the radial distance from the axis to the point of T = 3,000 *K*. Inside the nozzle the gas temperature may be above 3,000 *K*. In this case R_c will be taken as the nozzle radius. The current density is then σE_z.

The magnetic field induced by the arc current has only an azimuthal component because of the axisymmetric feature of the arc column. Assuming a permeability of the arcing medium as that of the vacuum μ_0, to be homogenous, the magnetic field can be calculated by

$$B_\theta = \frac{\mu_0 \int_0^r J_Z 2\pi\xi \, d\xi}{2\pi r} \qquad (2\text{-}9)$$

where $\mu_0 = 4\pi \times 10^{-7}$ *H/m* is the permeability of free space and J_z the current density in the axial direction.

2.4 Subsidiary Models

2.4.1 Radiation Model

Radiation transport is an important mechanism to redistribute energy in the arcing space. In puffer circuit breakers, radiation transport in SF_6 arcs is dominated by a few hundred lines, which are neither optically thin nor thick [Bin06]. Even with the computing power of the present day computers, the computational cost for such a 3-D or 2-D radiation transport calculation is still prohibitively high. In practice, such a detailed radiation transport computation also encounters difficulties because the spectra data required for such calculation is not complete. In addition, SF_6 arcs in circuit breakers are often contaminated by the ablated vapour of the nozzle wall and contact materials. This makes such an approach impractical as the spectra data for a contaminated arc is often not available. Thus, an approximate method for calculating q needs to be found, which avoids the detailed calculation of radiation transport.

2.4.1.1 Radiation Model for Puffer Circuit Breaker

For cylindrical wall stabilized arcs Lowke [Low92] demonstrated that the use of NEC, which is a function of arc radius, temperature and pressure, can predict satisfactorily the temperature distribution. NEC is the difference between emission and absorption. Lowke [Low92] derived the net emission coefficient at the centre of an infinitely long tube assuming that the radial temperature profile is a top hat. The results of the calculation are tabulated as a function of tube radius, pressure and temperature.

$$\varepsilon_{N=}\varepsilon_N(T,P,R) \qquad (2\text{-}10)$$

Typical results of NEC are shown in Figure 2.2. In order to use NEC for the account of radiation transport in SF_6 switching arcs an equivalent tube radius needs to be defined.

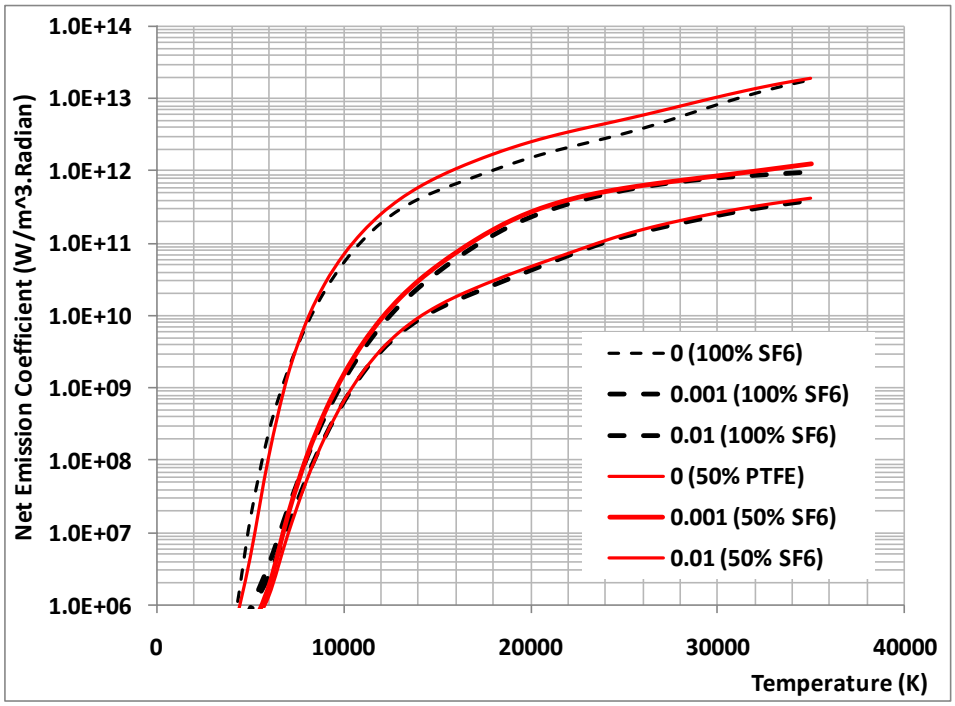

Figure 2.2 Comparison of net emission coefficient of pure SF6 and 50% SF6 – 50% PTFE vapour at 40 bar which is the typical pressure in the nozzle during high current phase. Unit of emission radius is in metre.

The NEC method was modified by Zhang et al [Zha87] to calculate the radiation transport of a nitrogen arc burning in a supersonic nozzle with much success. Their modification includes a region where a large proportion of the radiation escaping from the edge of the arc core (defined below) is reabsorbed. However, their method assumes a radial monotonically decreasing temperature profile. For puffer circuit breakers the complexity of the flow often results in the maximum temperature off the axis of symmetry. In order to ensure a converging solution of the arc equations, the radiation model has to be improved to accommodate any hot spot away from the symmetric axis in the radial temperature profile, as described below.

In Figure 2.3, the maximum temperature is T_m which is off the axis, which is considered to be equivalent to the maximum temperature, T_0 of a monotonically decreasing temperature profile. The arc core is defined as the region from the axis to the radial position of the $0.83T_m$ isotherm. In the arc core, q is a function of temperature, pressure, and arc radius which is defined as the radial distance from the axis to $0.83T_{max}$ isotherm in the high current phase. This choice of the definition for arc radius in the high current phase (the period from arc initiation to the 15 *kA* point before the final current zero) is because in modern circuit breakers the contact gap has usually a large space and the gas

is hot. Using T = 4000 *K* will result in an excessively large arc radius. When the current is very low the use of $0.83T_{max}$ to define the radiation radius often results in large fluctuations of the latter. Therefore for current less than 15 *kA* where the arc is normally burning in axially dominant flow, the radiation radius is defined as the average of the two radii corresponding to $0.83T_m$ and 5000 *K*. The net emission coefficient is given in [Yan09] but multiplied by a factor of 1.5.

In calculating the NEC it is assumed that the plasma is isothermal with a clear boundary defining the radius. Therefore the NEC is most accurate if the plasma temperature is close to isothermal. In a circuit breaker arc, it is possible that the maximum temperature is off the axis. The above method of defining an equivalent arc radius is likely to be an over-estimate in which case *q* will be smaller than the actual radiation loss. In order to compensate this net emission coefficient is increased by a factor of 1.5. It has been found by numerical experiments that a value of 1.5 gives satisfactory prediction when compared with test results.

Radiation from the arc core is partly absorbed in the region between the core edge and the 5,000 *K* isotherm. This region is also called the re-absorption region. It has been found that 80% of the radiation flux at the core edge is absorbed in this region [Zha87]. The net radiation loss in this region follows an exponential profile and its exact value is calculated from the requirement that 80% of the radiation flux at the core edge is absorbed.

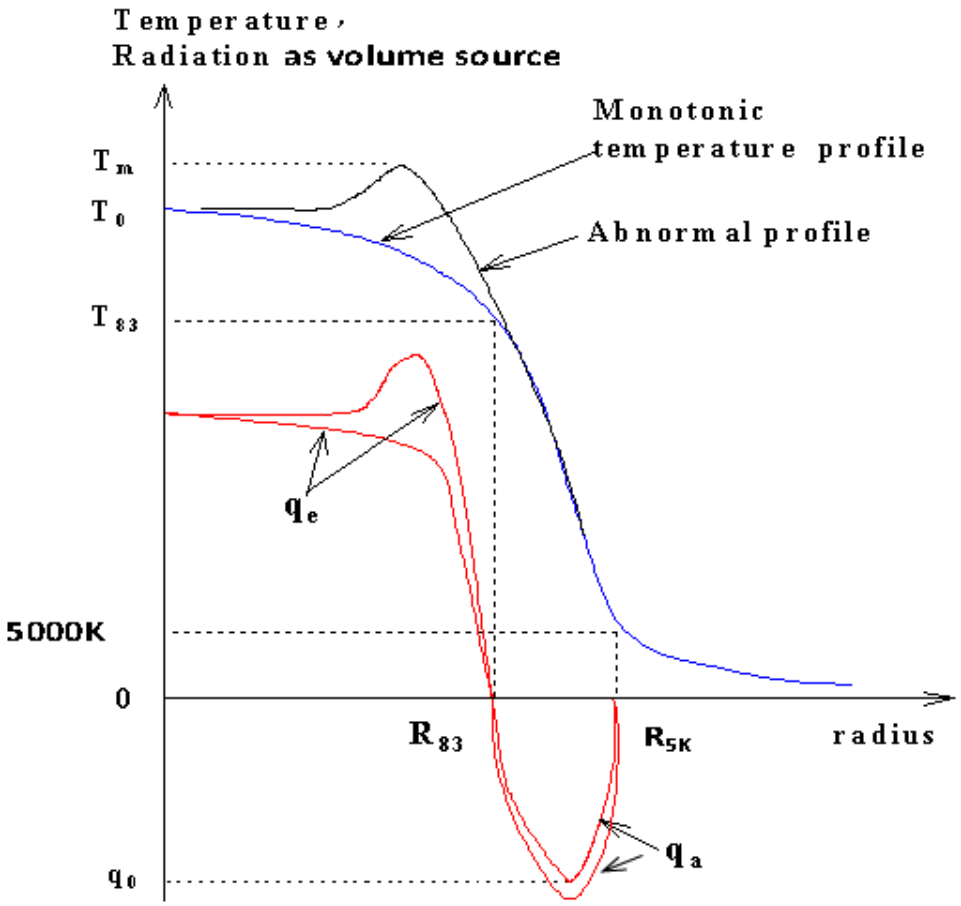

Figure 2.3 Diagram showing the approximate one dimensional model for calculating radiation transfer in puffer circuit breakers.

2.4.1.2 Radiation Model for Arc in Water

In the water confined carbon arc case, the arc initially burns in water vapour before the carbon vapour produced from anode erosion dominates the arc column. At a late stage, although the arc is burning in carbon environment with carbon concentration close to 100%, radiation from the arc core can still be absorbed by gas surrounding the arc. Thus, the radiation characteristics of the arcing gas need to be known. Similar to the circuit breaker arcs, a net emission coefficient (NEC) is used to obtain the locally emitted radiation in the arcing space. However, there is a lack of the radiation characteristics of the gas mixture present in the arc surrounding region. Riad et al [Ria03] calculated the NEC of carbon and water vapour separately, which are shown respectively in Figure 2.4. It can be seen that carbon has stronger radiation in the range of temperature interesting to us, 5000 *K* to 10,000 *K*. The carbon concentration is very

high in the arc core. The NEC of the mixture is therefore calculated by interpolation with the mass concentration of carbon as a parameter.

In a water vapour dominated environment, that is the environment surrounding the arc column, it is found necessary to consider radiation re-absorption [Jen03]. Thus to calculate the radiation as an energy source in the governing equation, we need to first calculate the emission from the arc core which is basically carbon and the re-absorption in the surrounding region which is mostly water vapor.

An approach similar to that for circuit breaker arcs is followed for the arc in water plasma. However, there is an important difference in the flow field in comparison with the switching arc case. Because the arc is enclosed in a bubble, flow outside of the arc column is rather stagnant. Basically two aspects in the radiation model need to be considered. The first one is the determination of the radiation radius for the NEC. The temperature range inside the arc column is 6000 *K* – 7000 *K* based on experiment [Lan99] while the simulation results produced in the present work is reaches 10,000 *K*. The radial extent from the axis to the 5000 *K* isotherm is around 1 *mm*. It has been found that the definition of the NEC radius using the method for circuit breaker arcs leads to numerical oscillation in the results because of the fluctuations in the calculated NEC radius. A constant radius of 1 *mm* is therefore used. As shown in Figures 2.4, most of the radiation-absorption takes place in the first 1 *mm* for both water and carbon vapor. For radius larger than 1 *mm*, the difference in NEC is very small in the temperature range below 10,000 *K*. The use of 1 *mm* for calculating the radiation emission in the arc core is thus justified.

Radiation absorption depends on the temperature field. It is however difficult to determine the thickness of the radiation re-absorption region. It is assumed that radiation re-absorption takes place in the whole surrounding region, i.e. the thickness of the re-absorption region is R_B - R_{83} with R_{83} being the radius corresponding to 83% of T_0 (maximum temperature) and R_B the bubble radius.

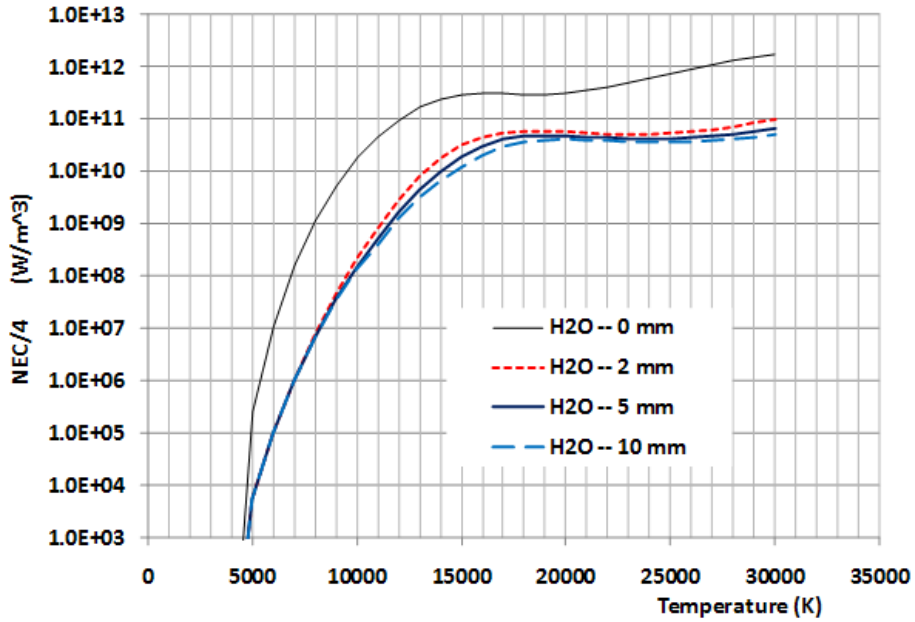

(a)

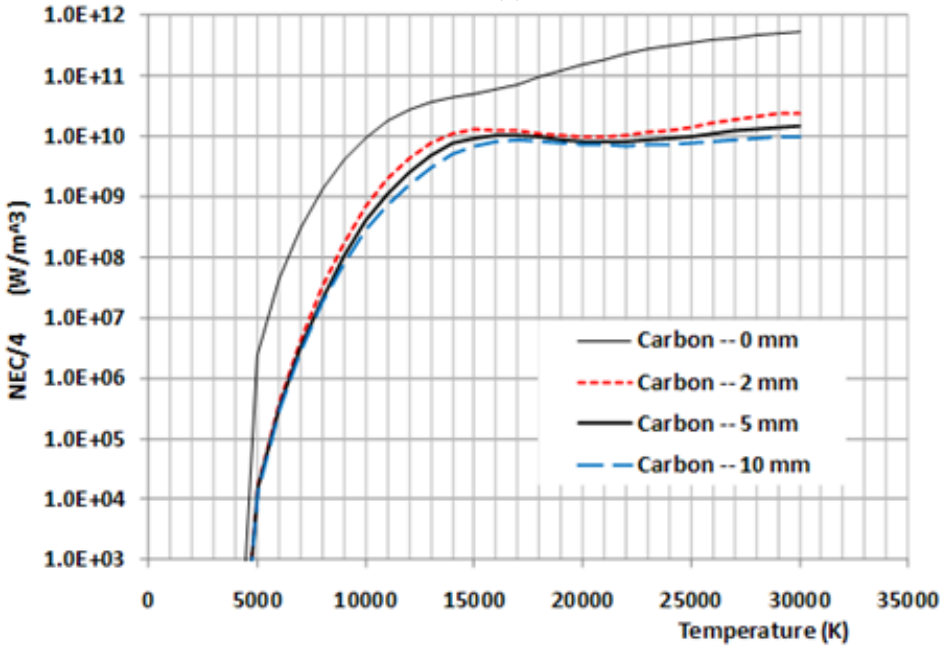

(b)

Figure 2.4 Net emission coefficient of water vapor (a) and carbon vapor (b).

2.4.2 PTFE ablation Models for Puffer Circuit Breaker

For the PTFE nozzle used in the investigation, the rate of ablation is determined by:

$$(1-\alpha)Q = mh_a \qquad (2\text{-}11)$$

where Q is the total radiation flux per unit length from the arc core, α = 0.8 the percentage of radiation absorbed at the arc edge and $\dot{m}$ the rate of ablation per unit length. h_a is the total energy required to break up the chain of PTFE molecules (depolymerisation) and to raise a unit mass of ablated PTFE vapour from room temperature to 3,400 *K*, which is equal to 1.19×10^7 *J/kg* [Zhang00]. Because the thermal dynamic properties and radiation emission coefficient of SF_6 and PTFE are very similar, a species concentration is not solved in the present work. The vapour is injected into the computational domain as SF_6. The uncertainties caused in the results are expected to be small (10%).

It must be made clear that the percentage of radiation from the arc centre which is re-absorbed at the arc edge has no university value. For arcs burning in supersonic nozzle with normal flow, about 80% of the radiation from the arc centre is re-absorbed at the arc edge. A value of 80% is used in the present work for puffer circuit breakers.

2.5 Turbulence Models

In switching applications turbulent enhanced momentum and energy transfer has a significant influence on the arc characteristics in the low current regime before the final current zero, as shown in theoretic work [Fang92, Fang94] and experiment [Her76, Bra78]. For arcs in axially dominant flow, the interaction between the arc and its surrounding flow results in turbulent eddies of different scales. The eddies across the arc edge, where steep temperature gradient exists, contribute most to arc cooling. Although there has been significant success in using the simple Prandtl mixing length model to predict the thermal recovery behaviour of nozzle arcs [Fang04, Zhang00], the value of the turbulence parameter, c, which is a proportional coefficient relating the turbulence length scale to the arc's thermal radius, has to be varied for different nozzle geometry and dimensions [Fang92, Zhang00]. To simulate the whole arcing process, especially the current zero period of puffer circuit breakers (<15 *kA* for a 30 *mm* diameter nozzle), more study is required on the value of c to be used and the validity of using a constant value of it. In addition, the definition of the arc's thermal radius also require a more careful examination since the temperature field changes its pattern in the period from high current towards current zero. This will be one of the objectives of this

section.

The standard *k*-epsilon model is based on the incompressible flow assumption. Fluctuation in density is not taken into account. In arc related applications flow is highly compressible and there is always steep density gradient at the arc edge, especially in the radial direction in nozzle arcs. It was shown that convective instability is originated in the region of steep density gradients [Blun97] In a previous study [Yan99II], it was found that the *k*-epsilon model is not able to produce agreement between predicted and measured radial temperature profile for a steady state nozzle arc in the current range from 100 *A* to 1800 *A*. Its validity for transient switching arcs has never been proved. In a recent work, the standard *k*-epsilon model is modified to take into account the effect of radial temperature (density) gradient and its behaviour assessed for both steady state and transient cases.

2.5.1 Modification to Prandtl mixing length model

2.5.1.1 Prandtl mixing length model

In analogy with shear layer or high-velocity fluid jet, the mixing length is related to the jet radius which is representative of the size of the typical turbulent eddies. For nozzle arc, this is related, for convenience, to the high-temperature arc core as the gas in this region attains very high speed due to its low density. Thus, the mixing length for turbulence-enhanced momentum transfer is given by

$$l_{\mathrm{m}} = cR \qquad (2\text{-}12)$$

where R is the arc thermal radius and c the so-called turbulence parameter. The turbulence eddy viscosity is related to the flow field by the following equation:

$$\mu_t = \rho(cR)^2 \left(\left|\frac{\partial v}{\partial z}\right| + \left|\frac{\partial w}{\partial y}\right|\right) \qquad (2\text{-}13)$$

The turbulence enhanced energy transfer, which is defined by a quantity k_{t} as a counterpart of the laminar thermal conductivity, is related to the turbulent eddy viscosity through the turbulent Prandtl number:

$$Pr_t = \frac{\mu_t}{k_t/C_p} \qquad (2\text{-}14)$$

The value is P_{rt} is set to unity following [Fang04]. Similarly, the turbulent diffusion coefficient of nozzle vapour is related to the turbulent eddy viscosity through a turbulent Schmidt number Sc_t by

$$D_t = \frac{\mu_t}{\rho Sc_t} \qquad (2\text{-}15)$$

with Sc_t being given a value of 1.0. Thus the accuracy and applicability of the Prandtl mixing length model depends on the choice of the turbulence parameter, *c*.

2.5.1.2 The modification to the turbulence parameter

Preliminary results for a 252 *kV* puffer circuit breaker showed that using a constant value for c is not able to predict the fast rising extinction peak. Thus improvement to the Prandtl mixing length model in the present work is based on the argument that different values of c may need to be used when the size of the arc column experiences significant change from the high current phase to the current zero point. In the high current phase, the arc column occupies almost the whole nozzle hole and there is insufficient cold gas flow around it to promote the development of instability into fully developed turbulence in the high density gradient region and in the clod flow, thus inhibiting turbulent momentum and energy exchange between cold flow and hot arc core. When the current decreases towards current zero, typical for current less than 15 *kA* in a circuit breaker nozzle with a throat diameter of 30 *mm*, the arc column only takes a proportion of the nozzle diameter and a sizeable layer of cold flow is formed. This allows space for the development of turbulent eddies that subsequently enhances energy transfer. In addition, an arc column with a small diameter can also be easily deformed, increasing the arc's instability. Turbulence in arc has not been fully understood. Arc instability due to other mechanisms also contributes. The turbulence model for arc modelling is thus intended to account for the combined enhancement in momentum and energy transfer. Following these arguments, the turbulence parameter *c* in equation (2-12) should increase when the current decreases in a transient case. The turbulence parameter

as a function of arcing conditions is given below:

$$c = c_h + (1 - \frac{|i|}{i_0})(c_0 - c_h) \quad (2\text{-}16)$$

where c_h is the turbulence parameter for high current phase and c_0 that for current zero and post arc period. i_0 is a threshold value dividing the high current and current zero period and for the 252 *kV* puffer circuit breakers i_0 = 15 *kA*, c_h = 0.1 and C_0 is given a value of 0.5. These values are determined by fitting the predicted arc voltage with measurement results for a calibration case because at present there are no universal turbulence parameters applicable to switching arcs.

2.5.1.3 The definition of thermal radius

The thermal radius of the arc column is used to represent the size of the high speed arc column. It is defined as the radial extent for the axis to the isotherm of a threshold temperature. In the high current phase this threshold temperature is set as 5000 *K*. The choice of 5000 *K* is based on the observation that a large portion of the space between the hollow contact and the main nozzle can sometimes be filled with hot gas (3000 *K* to 5000 *K*) as a result of nozzle ablation, as shown in Figure 2.5. The use of a lower temperature could lead to erroneous over-estimated values for the thermal radius *R*.

For current zero and post arc current simulation, the use of 5000 *K* will lead to an underestimate of the radial size of the high speed plasma column. The arc column at current zero is usually very thin, in the range of 1 – 3 *mm* (Figure 2.6). R is then defined as the radius corresponding to 3000 *K*. It is to be noted that *R* is naturally affected by the choice of the threshold temperature. It in turn has an influence on the value of c_0 that should be used in the simulation.

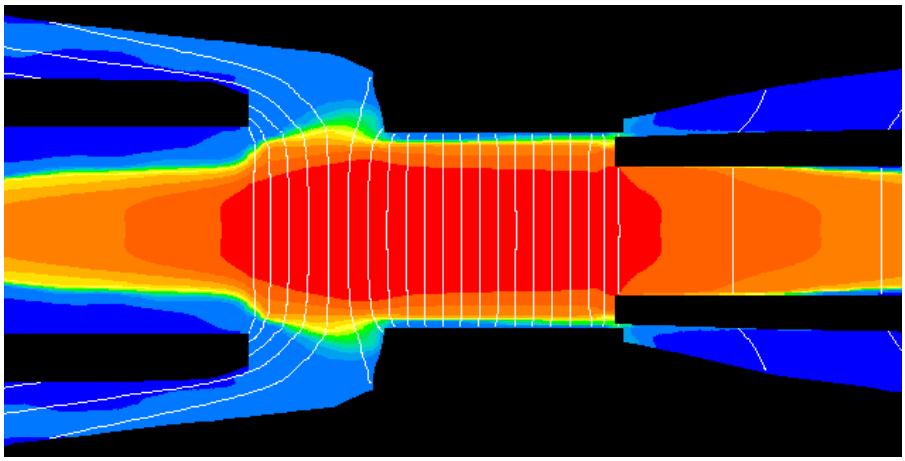

Figure 2.5 The temperature field of a transient arc with an instantaneous current of 61kA in a 252 kV puffer circuit breaker.

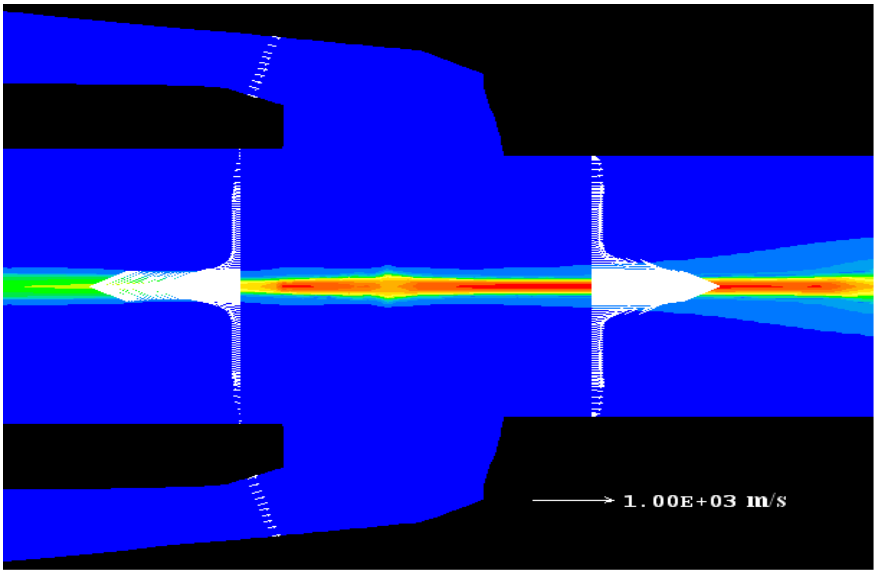

Figure 2.6 Velocity profile and shape of arc column at 1 kA before the final current zero for a 47 kA (rms) transient case. for refernece the arc radius is 15 mm.

A number of simulations were performed to study the influence of the threshold temperature on the arc behaviour at low current to support the choice of 3,000 *K* for the threshold temperature. The circuit breaker used is a 252 *kV* puffer circuit breaker with a filling pressure of 7 bar. The simulations ran from 15 *kA* to current zero with the turbulence parameter being determined by equation (2-16). Details of the arcing conditions will be given in Chapter 4 since here we are only concerned with the relative change in arc temperature field.

The radial temperature profiles at three axial locations in the arcing chamber were

compared, which gave a full picture of the situation because at different axial locations the arc size can be different. The three locations are shown in Figure 2.7. Because the current and the arc size changes rapidly near current zero, six current levels are chosen to study the radial temperature profiles.

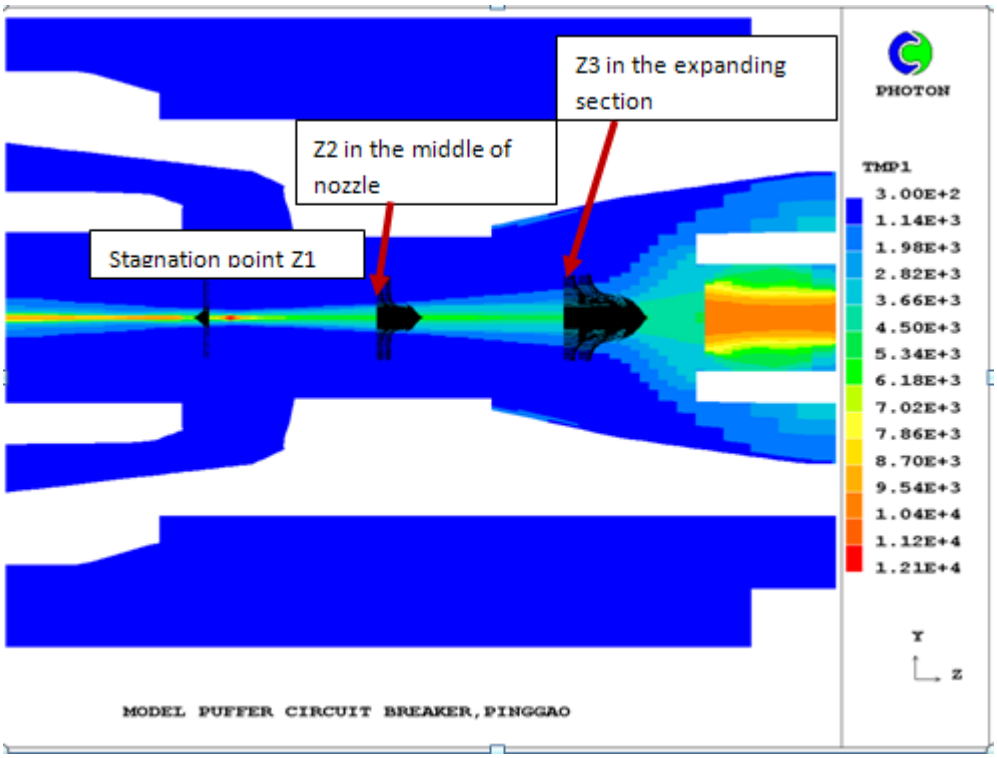

Figure.2.7 Diagram showing the three axial locations, from left to right the stagnant position (z = 130), the middle of the nozzle (z = 160) and the expanding section (z = 180 mm), where the radial temperature profiles are studied for the purpose of turbulence modelling at low current.

A typical radial temperature profile at current zero is given in Figure 2.8. The results were obtained with the thermal radius defined at the 3000 *K* point. As can be seen, there are three distinctive zones. Each zone starts with a steeper and ends up with a lower temperature gradient. The boundary between the first and second zones is at 3000 *K*. The temperature profile can be explained by our turbulence model. The turbulence length scale for the arc region is the radius at 3000 *K* multiplied by the turbulence parameter c given in equation (2-12). It is assumed that turbulence in relation to the high speed arc flow only exists in the region of $r < R$. Further towards the nozzle surface, convection takes over for energy transport. Therefore for gas outside the arc (represented by *R*), the turbulence parameter c is set to a very small value ($c = 0.0001$).

This means that inside the arc column turbulence enhanced energy exchange is much stronger and in the arc surrounding region turbulence is much weaker. This is clearly shown in Figure 2.9. The peak value at the arc edge indicate that in a particular cell at the arc edge there exists a very high velocity gradient as a result of a sudden change in velocity. There needs to be a steep temperature gradient in zone 2 just away from the 3000 *K* position to carry away the energy flux from zone 1. This can be estimated by using a continuity of the radial thermal flux at the arc edge by the following relationship:

$$-\frac{k_{t1}}{Cp_1}\left(\frac{\partial h}{\partial r}\right)_1 = -\frac{k_{t2}}{Cp_2}\left(\frac{\partial h}{\partial r}\right)_2 \qquad (2\text{-}17)$$

where the subscript 1 represent value on the zone 1 side and 2 that on the zone 2 side. k_{t1}/C_{p1} inside the arc column is much stronger than that in the surrounding flow so the temperature (enthalpy) gradient on the zone 2 side is higher.

The local temperature peak at $r = 0.02$ in Figure 2.8 is due to a patch of stagnant hot gas near the nozzle wall as a result of flow circulation. An important feature of the results with R_{3K} (R is defined at 3,000 *K* point) is that the axial velocity starts to rapidly decrease from R_{3K} at current zero, therefore R_{3K} is a good representation of the boundary of the high speed plasma jet.

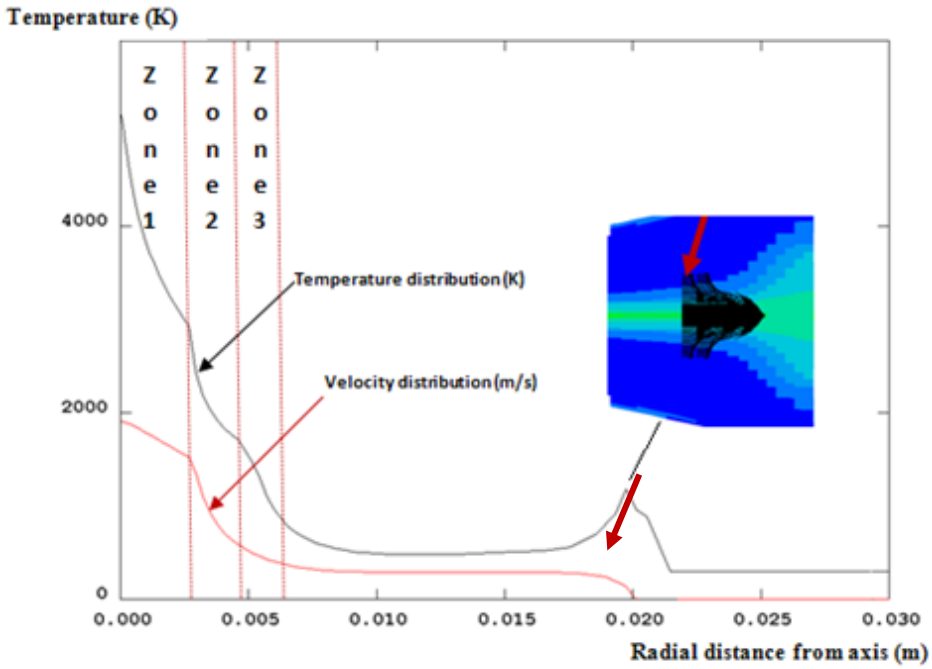

Figure 2.8 Diagram showing the radial temperature profile at current zero at Z3 which is calculated using a threshold temperature of 3000 K for the thermal radius.

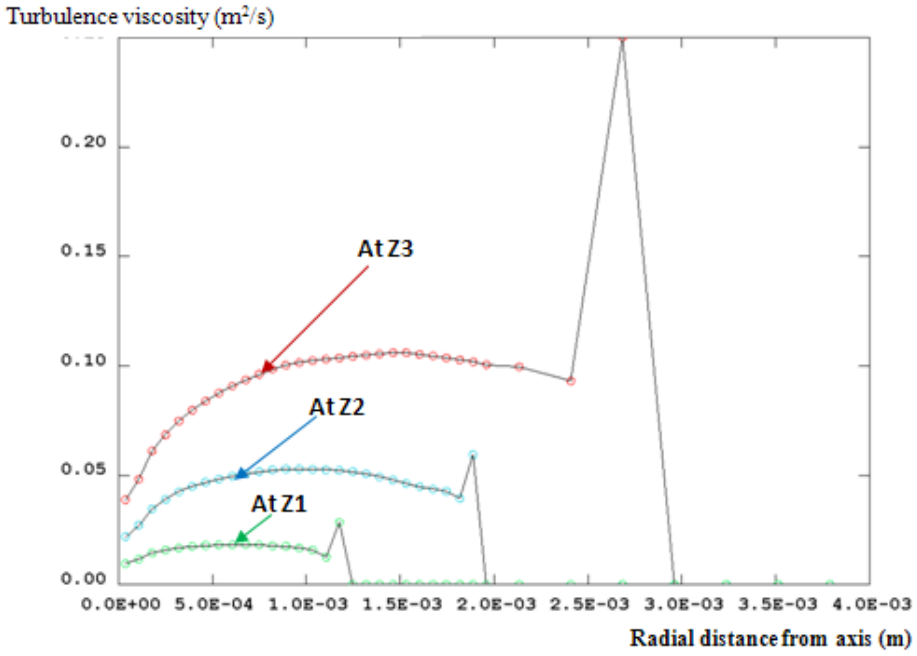

Figure 2.9 Diagram showing the radial turbulence viscosity profile at current zero.

To have a clear picture of the radial temperature profiles at different current in a transient case are plotted in Figures 2.10 to 2.12 for three locations in the arcing chamber, as given in Figure 2.7.

Another interesting point to observe is that the difference of the positions of 3,000 *K* (R_{3K}) and 5,000 *K* (R_{5K}) at different current levels, as given in Table 2.2. At 10 *kA*, the difference is only 16% to 30% of R_{5K}. However, when the current decreases, R_{5K} tends to be zero (Figure 2.8), computationally resulting in virtually no turbulence. In contrast, R_{3K} remains in a comfortable range (>1 *mm*). From experiment [Her76, Bra78] it is well known that turbulence does exist at current zero. So the use of R_{3K} is more reasonable for low current simulation.

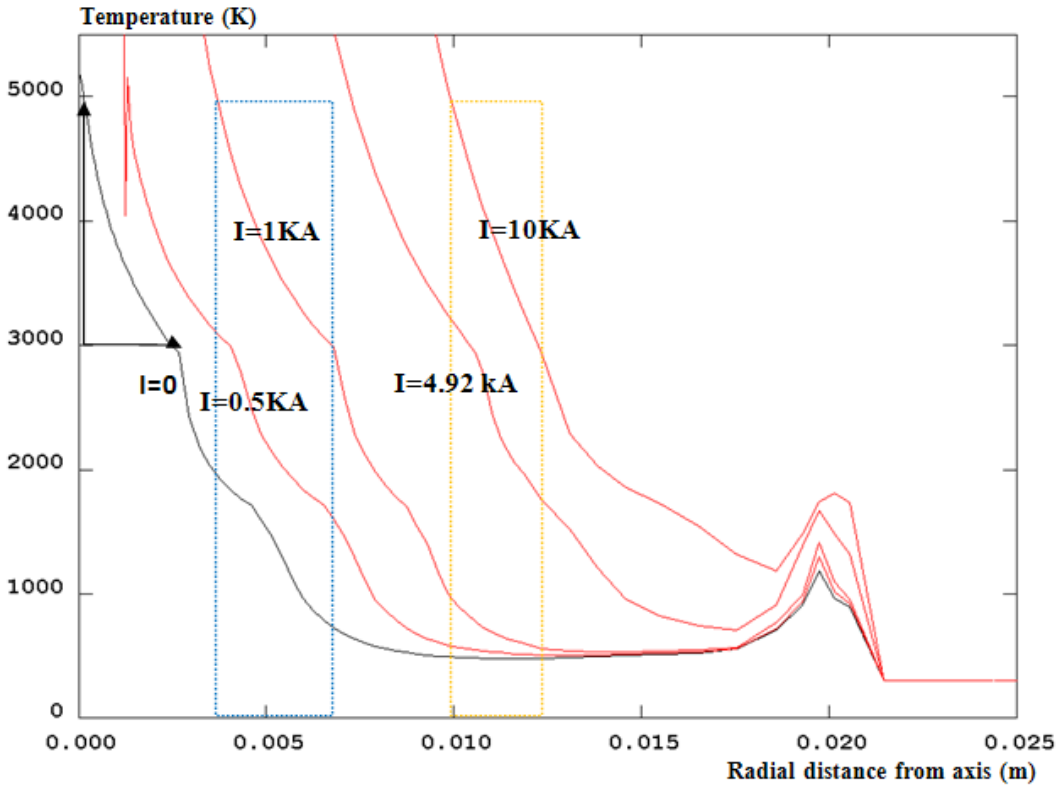

Figure 2.10 Radial temperature distribution at the axis of the nozzle (Z = 180 mm) at different time (current) before the current zero for the case of 47 kA case.

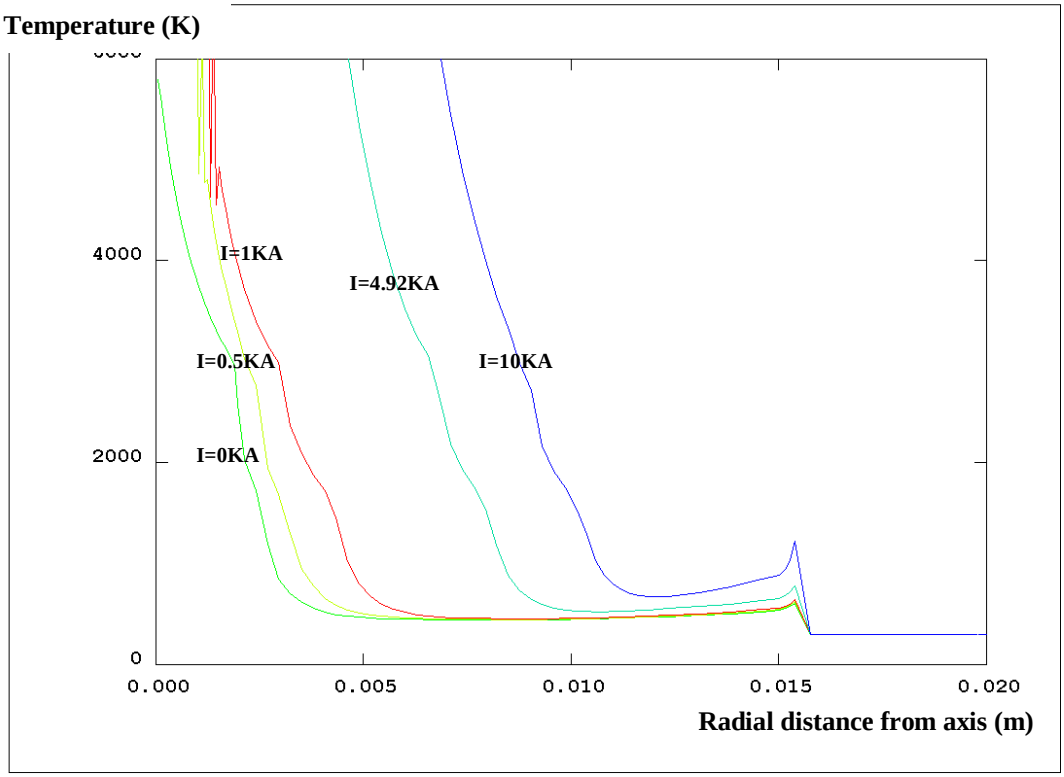

Figure 2.11 Radial temperature distribution at the axis of the nozzle (Z = 160 mm, middle of nozzle) at different time (current) before the current zero for the case of 47 kA current zero case.

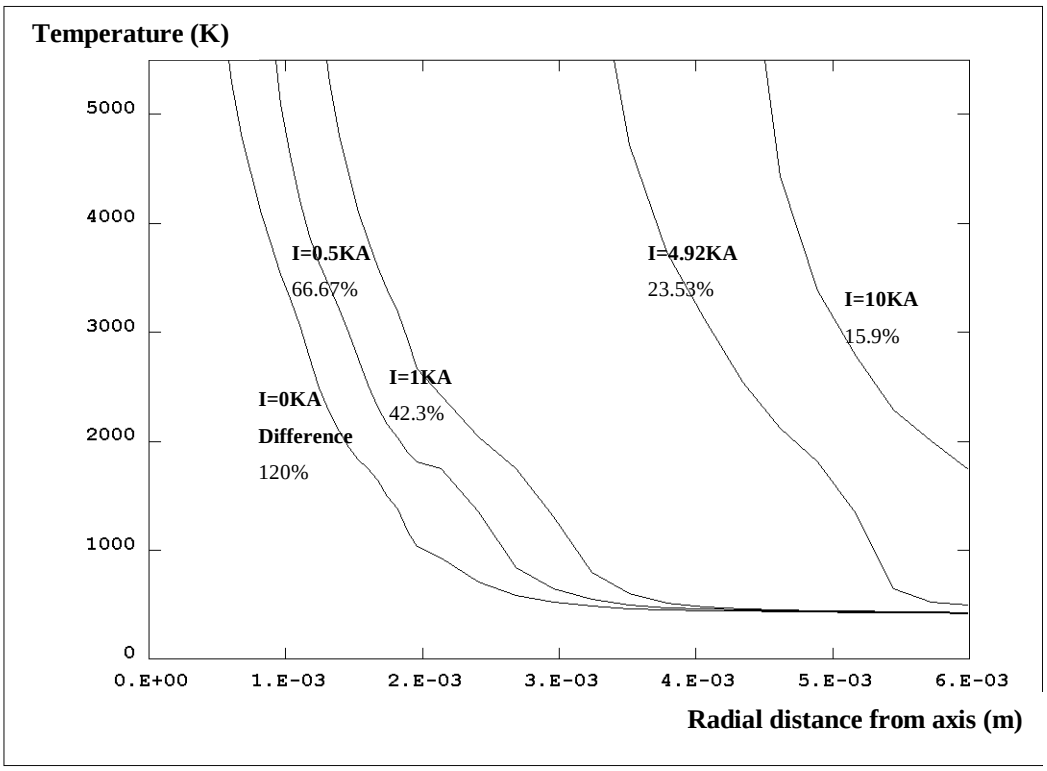

Figure 2.12 Radial temperature distribution at the axis of the nozzle (Z = 130 mm, stagnation point) at different time (current) before the current zero for the case of 47 kA

current zero case.

Table 2.2 Quantitative description of the difference between R_{5K} and R_{3K}

Z=180	**I=10 *kA***	**I=4.92 *kA***	**I=1 *kA***	**I=0.5 *kA***	**I=0**
R_{5K}	9.5e-3	7.0e-3	3.8e-3	1.4e-3	3e-5
R_{3K}	12.3e-3	10.05e-3	6.5e-3	4.3e-3	2.5e-3
Absolute and Percentage difference $\frac{\lvert R_{5k} - R_{3k} \rvert}{\mathrm{R_{5k}}}$	-2.8e-3 29.47%	-3.05e-3 43.57%	-2.7e-3 71%	-2.9e-3 207%	-2.47e-3 8233%
Z=160	**I=10 *kA***	**I=4.92 *kA***	**I=1 *kA***	**I=0.5 *kA***	**I=0**
R_{5K}	7.1e-3	5e-3	1.4e-3	1.1e-3	1e-4
R_{3K}	8.7e-3	6.4e-3	2.8e-3	2.1e-3	1.7e-3
Absolute and Percentage difference $\frac{\lvert R_{5k} - R_{3k} \rvert}{\mathrm{R_{5k}}}$	-1.6e-3 22.54%	-1.4e-3 28%	-1.4e-3 100%	-1.0e-3 90.9%	-1.6e-3 1600%
Z=130 (stagnation point)	**I=10 *kA***	**I=4.92 *kA***	**I=1 *kA***	**I=0.5 *kA***	**I=0**
R_{5K}	4.4e-3	3.4e-3	1.3e-3	9e-4	5e-4
R_{3K}	5.1e-3	4.2e-3	1.85e-3	1.5e-3	1.1e-3
Absolute and Percentage difference $\frac{\lvert R_{5k} - R_{3k} \rvert}{\mathrm{R_{5k}}}$	-0.7e-3 15.9%	-0.8e-3 23.53%	-0.55e-3 42.3%	-0.6e-3 66.67%	0.6e-3 120%

As can be seen in Figure 2.13, further decreasing the threshold value for thermal radius produces excessively strong turbulence and results in a lower axis temperature of just above 4000 *K*. The axial velocity no longer experiences a sharp decrease at R_{2K}, indicating that turbulence is unreasonably strong. A comparison of the resultant radial temperature profile using R_{3K} and R_{2K} is given in Figure 2.14. The radial extent corresponding to 2000 *K* has changed by 5.5 *mm*. The viscosity with R_{2K} is given in Figure 2.15.

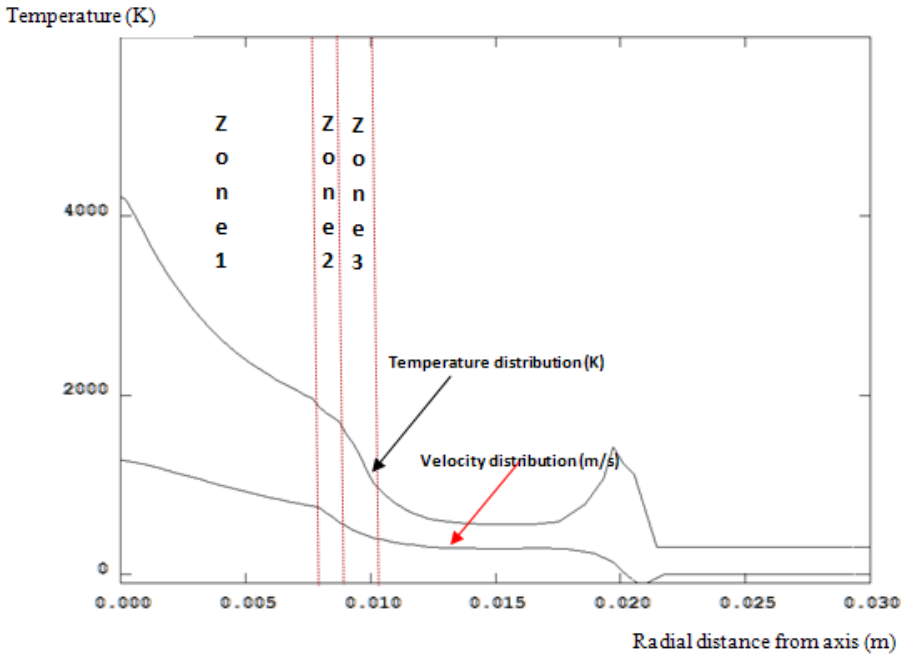

Figure 2.13 Radial temperature profile at current zero which is calculated using a threshold temperature of 2000 K for the turbulence length scale at Z3 (downstream of flat nozzle throat).

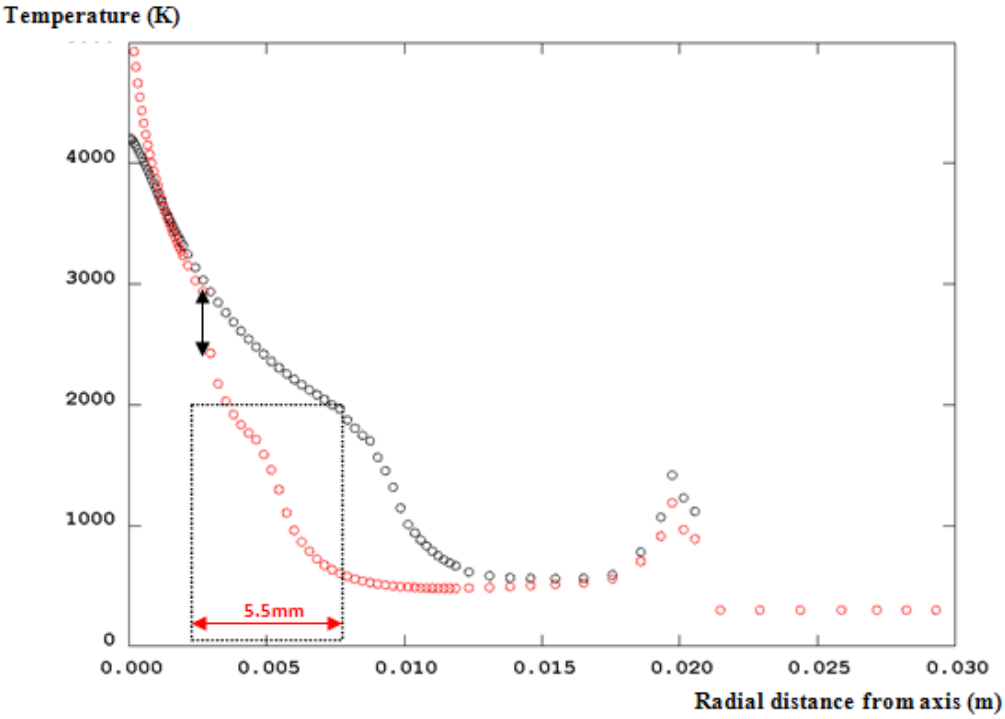

Figure 2.14 Diagram showing temperature distribution using R_{3K} (red) and R_{2K} (black) at current zero at the stagnation point as shown in Figure 2.6.

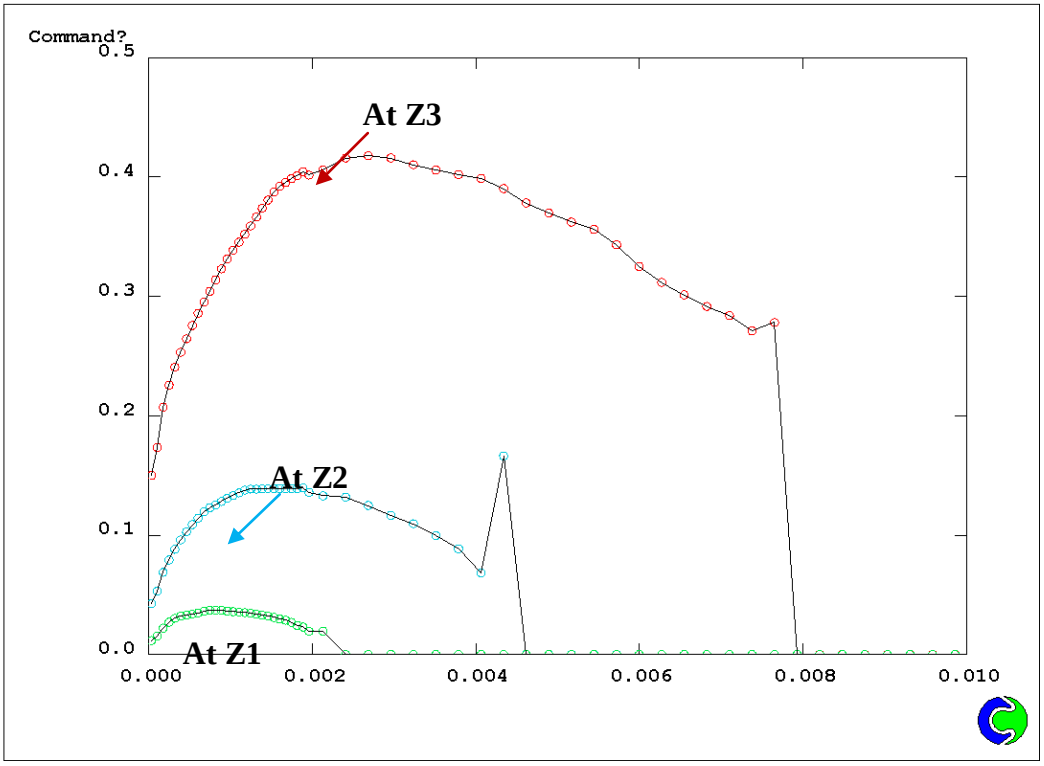

Figure 2.15 Diagram showing the radial turbulence viscosity profile at current zero at Z3.

2.5.1.4 Result for puffer circuit breakers

The modified Prandtl mixing length model has been used to predict the arc voltage for a lower current case (10 *kA*, peak current in final loop is 3 *kA*) and three high current cases (24 *kA*, 46 *kA* and 47 *kA*, all rms value) of a 252 *kV* puffer circuit breaker with dual hollow contacts.

As discussed earlier in this section, turbulence is most important in the low current period just before the final current zero. It directly affects the temperature and size of the arc column, thus the arc resistance. Given the current change as a known function of time, the arc voltage should be most sensitive to turbulence enhanced energy transfer. The predicted arc voltage for the 10 *kA* case is shown in Figure 2.16. It can be seen that c = 0.1 is not able to produce an extinction peak and the arc voltage is lower than the measurement. Using a constant value of c = 0.3 increases the arc voltage and produces a small extinction peak, but it is still remarkably lower than the measurement. A value of

0.3 for C_0 in equation (2-6) predicts not only satisfactory agreement for the major part of the second loop, but also for the sharply increasing extinction peak.

Using the same turbulence parameter settings, the current zero period for the 47 *kA* case was simulation starting from 15 *kA* before the final current zero. A comparison given in Figure 2.17 shows a qualitative agreement between the predicted and measured arc voltage in the extinction peak.

It must however be noted that the accuracy of the measurement used in this section for the 10 *kA* and 47 *kA* cases is not known since the measurement circuit was intended only for the arc voltage measurement in the region around the peak values. Despite this, we can conclude that

- The use of a variable turbulence parameter (*c*) for the Prandtl mixing length model is preferred for low current transient switching arcs sustained in a nozzle;
- Relating the value of *c* to the instantaneous arc current results in an extinction peak that follows closely the measurement;
- Since the arc diameter is dependent on the instantaneous current, further research is needed to gain clearer understanding of the influencing parameters for *c*, such as the nozzle diameter, the arc diameter, the temperature profile and the surrounding flow field.

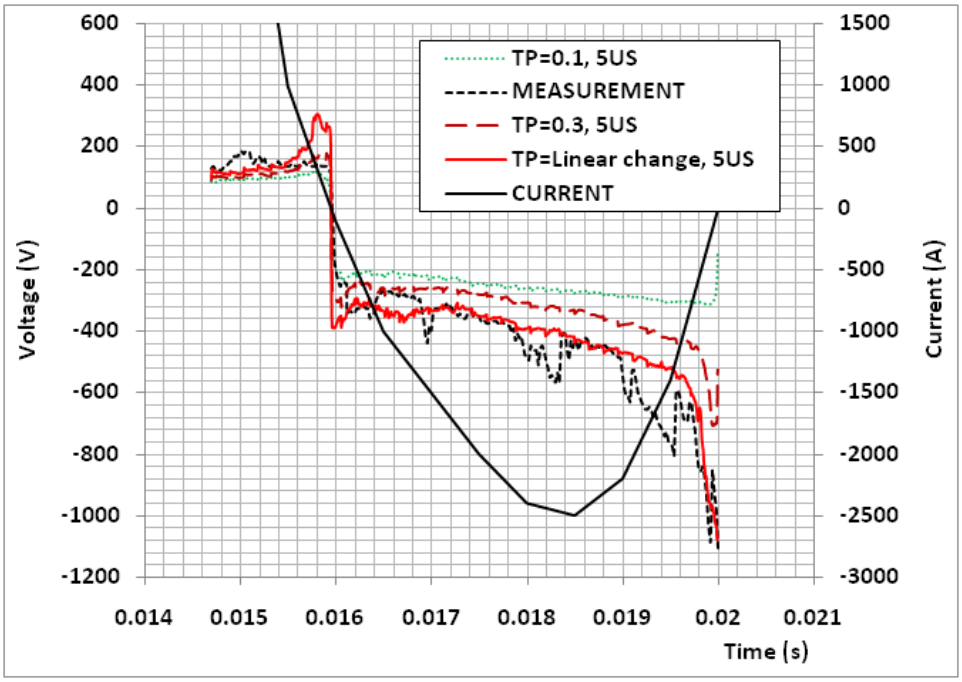

Figure 2.16 Predicted arc voltage with different settngs for the turbulence parameter(TP) for the 10 kA case

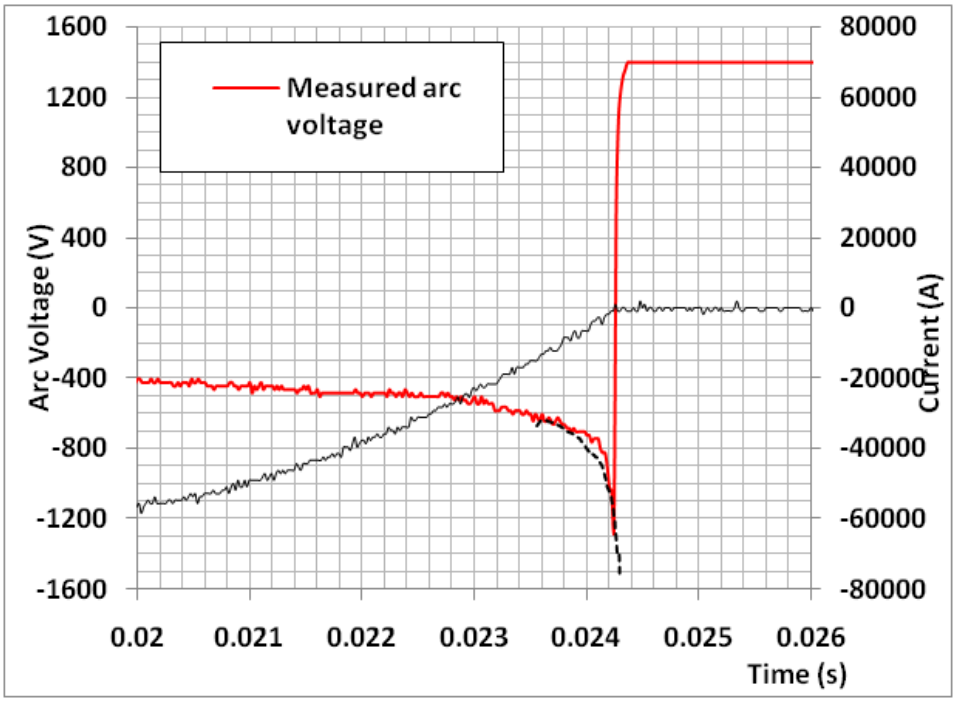

Figure 2.17 Measurement for the 47 kA case. (a) Current, travel, arc voltage, and (b) the measued and predicted extinction peak.

2.5.2 Modification to the k-epsilon Model

In a previous research it was found that the *k*-epsilon model has no advantages over the simple Prandtl mixing length model for nozzle arcs since the turbulence parameters in both models need to be adjusted in order to reach agreement between predicted and measured radial temperature profile [Yan99II]. It was however claimed in a recent publication that modification to the *k*-epsilon model with temperature correction leads to better agreement for hot gas jet. The applicability of this approach for nozzle arcs was thus studied in the present work with the attention to obtain a turbulence model with no adjustable parameters that is applicable to circuit breaker arcs.

2.5.2.1 The standard k-Epsilon model

The standard *k*-epsilon model is described by the following differential equations for turbulent kinetic energy, *k*, and turbulent energy dissipation rate, ε:

$$\frac{\partial(\rho k)}{\partial t} + \nabla \cdot \left(\rho \vec{V} k - \frac{\rho \nu_t}{\sigma_k} \nabla k\right) = \rho(G - \varepsilon) \tag{2-18}$$

$$\frac{\partial(\rho \varepsilon)}{\partial t} + \nabla \cdot \left(\rho \vec{V} \varepsilon - \frac{\rho \nu_t}{\sigma_\varepsilon} \nabla \varepsilon\right) = \rho \frac{\varepsilon}{k}(c_{1e} G - c_{2e} \varepsilon) \tag{2-19}$$

where ρ is the density of the main flow, V the velocity vector, and ν_t the turbulent viscosity. The two parameters C_{1e} and C_{2e} have the default values of 1.44 and 1.92. The Prandtl number for k and ε, σ_k and σ_ε have respectively the default values of 1.0 and 1.3.

The turbulence generation function, G, is the main source responsible for maintaining the turbulence. It is related to the density, turbulent viscosity and velocity gradient:

$$G = \rho v_t \left[2\left(\frac{\partial w}{\partial z}\right)^2 + 2\left(\frac{\partial v}{\partial r}\right)^2 + 2\left(\frac{v}{r}\right)^2 + \left(\frac{\partial w}{\partial r} + \frac{\partial v}{\partial z}\right)^2 \right] \tag{2-20}$$

The turbulence length scale is defined as

$$l = C_D k^{1.5}/\varepsilon \tag{2-21}$$

where C_D has a default value of 0.1643. Thus the turbulent kinematic viscosity ν_t is related to k and ε by the following equation:

$$v_t = C_v l\sqrt{k} = C_\mu k^2/\varepsilon \tag{2-22}$$

where C_ν has a value of 0.5478 so C_μ is equal to 0.09.

2.5.2.2 Approach I: Modification to C_μ

Abdol-Hamid et al [Abd04] proposed a modification to the standard k-epsilon model based on qualitative consideration to account for the effect of temperature gradient in a hot gas jet. The supersonic jet with a mach number of 2 was produced from a supersonic nozzle with an outlet diameter of 91.44 *mm*. The stagnation temperature of the gas emerging from the nozzle varies from 313 *K* to 1116 *K* in three supersonic cases and from 294 *K* to 831 *K* in three subsonic cases.

Without providing an argument, it was proposed in [Abd04] that C_μ be modified to consider the effect of temperature gradient. The formula that relates C_μ to the temperature field was however determined by the best match to measured total temperature for a supersonic case and a subsonic case. The default constant C_μ is multiplied by a term representing the temperature gradient effect:

$$C_\mu = 0.09\left[1 + \frac{(\nabla T_t \cdot (k^{3/2}/\varepsilon)T_t)^3}{0.041 + f(M_\tau)}\right] \tag{2-23}$$

where ∇T_t represents the magnitude of the gradient of total temperature T_t which is defined as

$$\nabla T_t = \sqrt{\left(\frac{\partial T_t}{\partial x_i}\right)^2} \tag{2-24}$$

and $f(M_T)$ is introduced to extend the model for high speed flow:

$$f(M_\tau) = \left({M_\tau}^2 - {M_{\tau 0}}^2\right) H(M_\tau - M_{\tau 0}) \tag{2-25}$$

where

$$M_\tau = \frac{\sqrt{2k}}{a} \tag{2-26}$$

is the turbulence Mach number with a being the local sound speed. *H (x)* is the Heaviside step function. M_τ = 0.1 is selected as a threshold value to indicate incompressible flow.

2.5.2.3 Approach II: Direct modification to G

A study on the instability of arcs in nozzle flow [Blun97] indicated that flow can become unstable when there is large density gradient. Therefore we argue qualitatively that the existence of steep density gradient at the arc edge should contribute to the generation of turbulent eddies and a modification to the turbulence generation term, *G*, should be made. It is therefore proposed in the present work that the generation function given in equation (2-20) is modified by multiplying a term that represents the effect of density gradient. Since density is a function of pressure and temperature under LTE

conditions, for nozzle arcs commonly used in switching applications density gradient at the arc edge is mainly caused by temperature gradient, thus the modification is represented by a dimensionless temperature gradient T_g.

$$T_g = |\nabla T| \cdot r/T \tag{2-27}$$

where T is the local gas temperature, $|\nabla T|$ the magnitude of the local radial temperature gradient and r the radial distance from the symmetric axis of a nozzle. The present modification is intended for arcs burning in axisymmetric nozzles. A fundamental difference between equation (2-27) and the definition of T_g in [Yan99II] is the use of r instead of the local turbulence length scale in equation (2-23) to make T_g dimensionless. This is based on the consideration that in turbulent nozzle arcs at low current (the arc must be surrounded by a cold gas flow layer) the steepest temperature gradient occurs at the arc edge and the size of the turbulent eddies is comparable to the radial size of the arc column. So T_g represents the relative change of temperature over the stretch of typical turbulence eddies. The modification takes the following form:

$$G_T = G(1 + T_g) \tag{2-28}$$

which recovers to the standard expression when T_g disappears. There is no further adjustable parameters introduced.

2.5.2.4. A comparison of the effectiveness of the modifications

The approach I as proposed in [Abd04] produced good agreement for hot gas jet with large diameter (91.44 *mm*) and low stagnation temperature (below 1116 *K*). However when it is used to simulate the steady state arcs in nozzle, it was found that the turbulence generated for the 1800 *A* case in Aachen nozzle is far too low and the predicted radial temperature at the nozzle throat is similar to the standard k-epsilon model. For completeness, the results for three current levels are given in Figures 2.18 to 2.20.

The approach II of modification, which is proposed in the present work, exhibits much improvement when compared with the measured temperature profile but is still poorer than mixing length model.

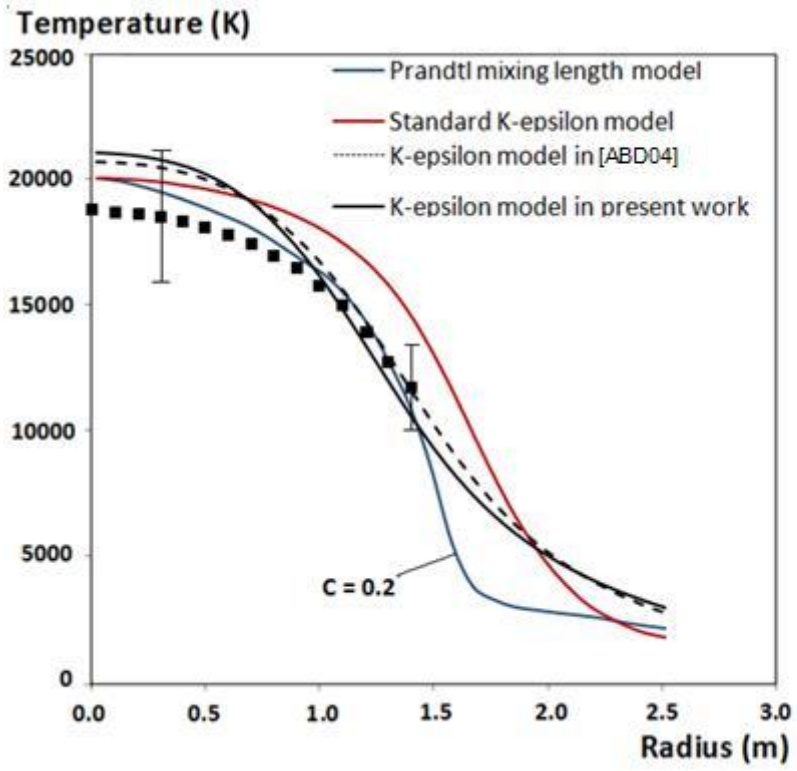

Figure 2.18 Radial temperature distributions at the nozzle throat of the 100 A SF_6 arc with different models.

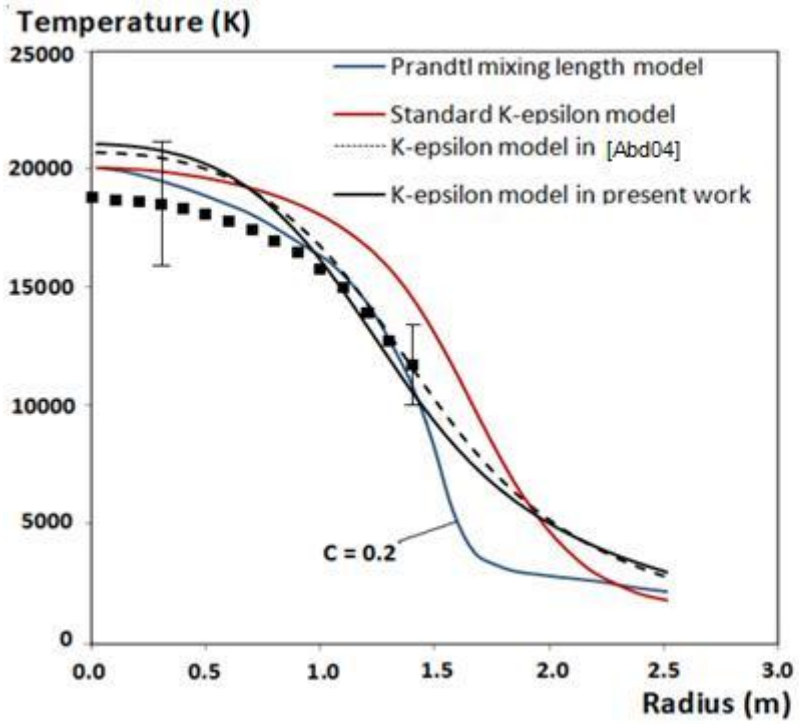

Figure 2.19 Radial temperature distributions at the nozzle throat of the 600 A SF_6 arc with different models

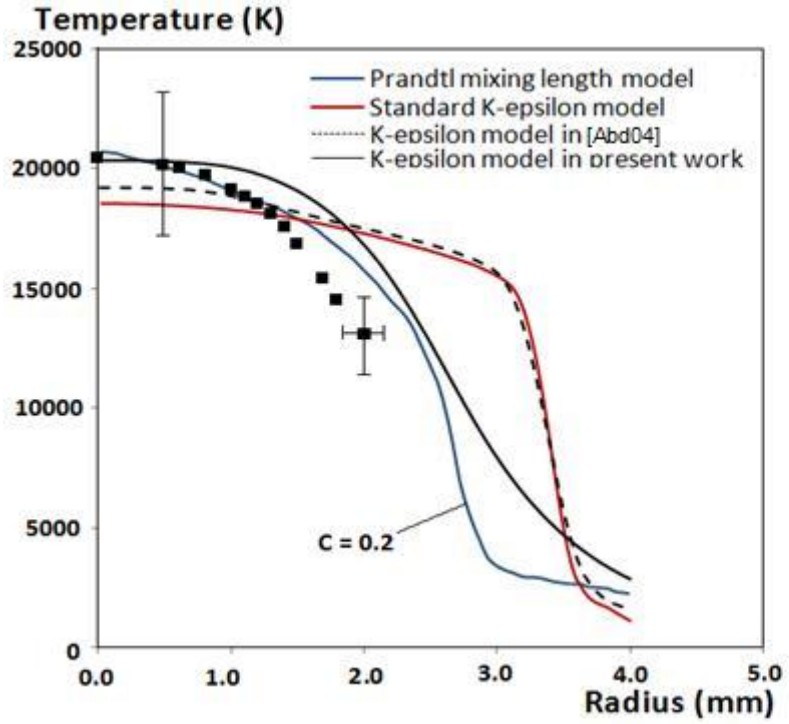

Figure 2.20 Radial temperature distributions at the nozzle throat of the 1800 A SF6 arc with different models.

The same model is also applied to the current zero period of the 10 *kA* case of the 252*kV* puffer circuit breaker. The predicted arc voltage is given in Figure 2.21. It is clear that the standard *k*-epsilon model and that modified by Abdol-Hamis et al [Abd04] produces close agreement around the rising side of the second half loop, but it does not predict any extinction peak. On the other hand, the proposed change in the present work produces a much lower voltage around the peak current but predicts an extinction peak. If we look into the results given in Figures 2.18 and 2.19, it becomes apparent that the proposed modification in the present work tends to under-represent the effect of turbulence when current is higher than 1800 *A*. This explains the large voltage difference for the 10 *kA* case between 17 *ms* to 19.5 *ms*. Once the instantaneous current is lower than 1500 *A*, the difference in predicted and measured arc voltage starts to decrease (for period >19.5 *ms* in Figure 2.21). Thus the present modification needs further refinement. Computer simulation of the puffer circuit breakers in Chapter 4 will be based on the modified Prandtl mixing length model as described in equation (2-16).

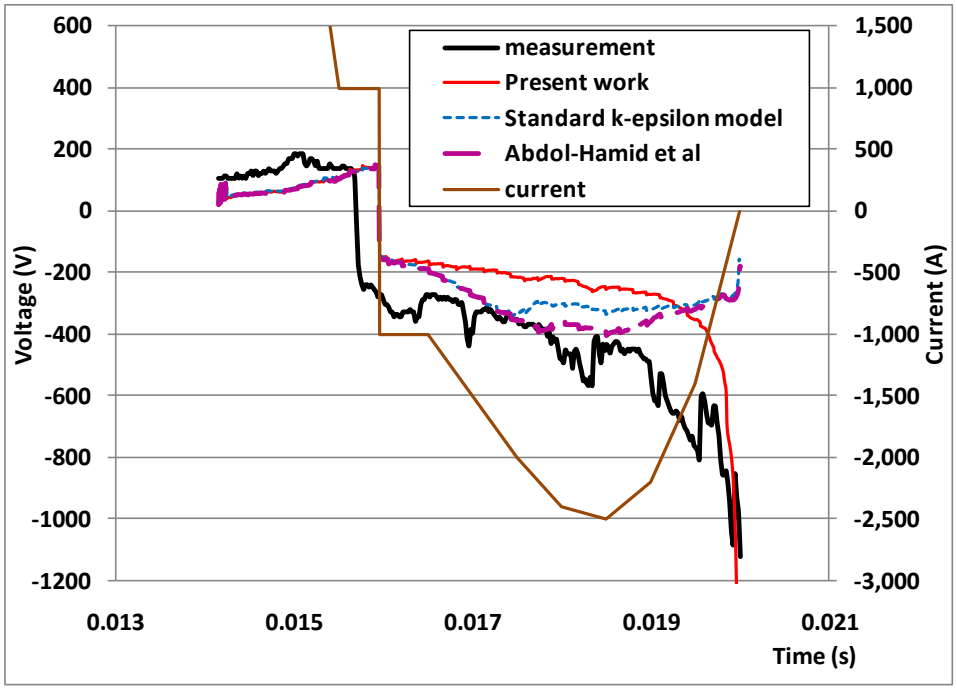

Figure 2.21 Predicted arc voltage of the 10 kA case with different turbulence models.

2.6 Initial/Boundary Conditions and Special Sources

Due to the volume of this chapter and the unique nature of switching arc and arc in water, the initial and boundary conditions for each case will be described in each of the following two chapters before results are presented and discussed. The loss of carbon vapour as a result of formation of carbon nano-structures will be discussed deferred until Chapter 3.

2.7 An Integrated Simulation and Evaluation Environment for Switching Arcs

An Integrated Simulation and Evaluation Environment (ISEE) is configured to work with a commercial CFD package, PHOENICS for the realization of visual simulation. It can be defined as a virtual environment serves as a platform on which the specification of the problem, definition of the mathematic model, implementation of the model in CFD software, and the analysis of the results can all be carried out in a visually interactive manner. The ultimate users of the simulation tools are R&D engineers, who should be knowledgeable with all the relevant mathematical models in CFD software packages, have a good ability to extract information. It is complex and time costly to build and test a product, even defining a component needs several hundreds of codes. Therefore, there is a strong need to simulation an easier job. ISEE, as an advanced simulation technique, provides all features for virtually building and testing high voltage circuit breaker. Arc simulation is conventionally centred at the implementation of mathematic models directly into a CFD package. It could take up to 6 months or even longer to simply learn how to use CFD software and correctly set up an arc model. However, with ISEE, design engineers those come from a background with little or no knowledge in CFD are also able to become a good designer.

2.7.1 Overall Structure of ISEE

The proposed environment ISEE has three constituting components, i.e. the Visual Model Builder (VMB), the solver, and the Visual Controller and Analyser (VCA). The relation and data transmission among them are illustrated in Figure 2.22.

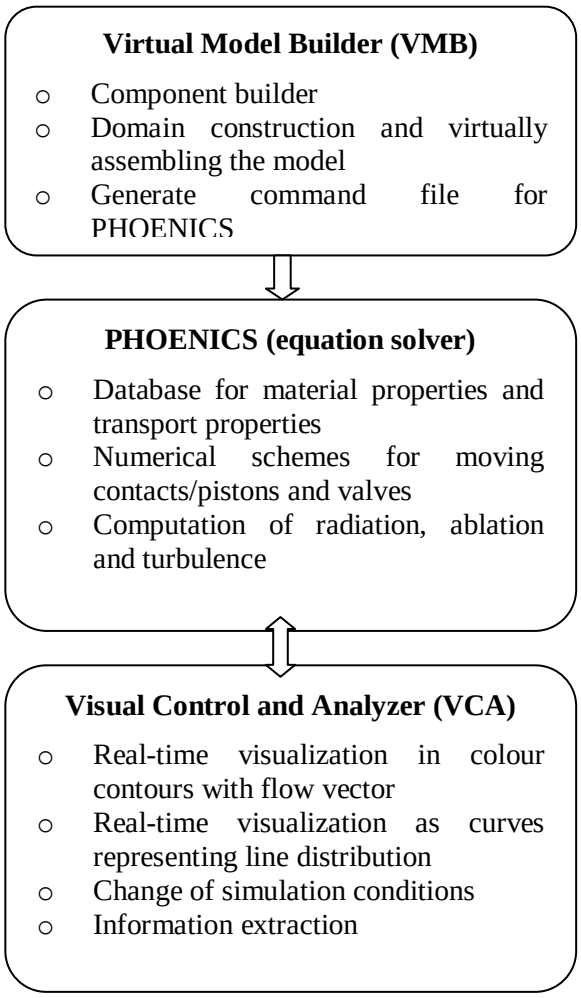

Figure 2.22 Diagram showing the roles of each of the constituting components of the integrated simulation environment

Virtual model builder is used to define each component of a product to the corresponding object with appropriate properties and behaviours. The whole product can be virtually built up in a user-friendly interface by assembling the existing objects. Then the virtually built product can be automatically translated into correctly defined grid system, initial and boundary conditions and other necessary settings for surface ablation, moving contact and so on for PHONICS Input Language (PIL) in Q1 and Fortran commands of the ground.for file.

The CFD software is regarded as merely an equation solver, which solves the governing differential equations according to the specified initial and boundary condition, and does not interact with users directly. That is the reason why ISEE are capable to make arc simulation be an easier job.

The simulation process of CFD software can be extracted by the control of VCA and displayed in the interface. Designers are also able to check how the arc changes in response to the parameter change.

2.7.2 Visual Model Builder

A component is constructed using Object-Oriented Programming (OOP). It represents a hardware part of the circuit breaker such as a contact and nozzle. All hardware parts of a circuit breaker are mapped into the simulation domain with appropriate properties and behaviours defined in the corresponding objects. An object is a collection of a group of hardware components with identical or similar physical behaviour and motion characteristics in reality. Using OOP as the programming method allow programmers define not only the type of a data structure (properties), but also the types of operations (behaviour) that can be applied to an object. In addition, objects are capable to communicate with each other but relatively independent. It means that programmer can simply create a new object without influencing other modules so that object oriented program is easier to modify. In one word, the approach OOP offers the capability of parallel computation, implementation of new functionality, and easy software maintenance.

2.7.2.1 An object example

Since an object represents a hardware part of a circuit breaker, a nozzle is used as an example as shown below. This object is regards as a quadrilateral in 2-Dimention. The four corners, which are highlighted using blue circle in Figure 2.23, are named as physical corners with three coordinate values for each, for instance, C_NL means low north corner while C_SH means high south corner. The four sides including south, high, north, low sides are starts from one corner point and end up with another. To define each curve, a number of intermediate points are needed. There are two methods available for defining these points. One is picking up the boundary point of a component in a CAD plot. The other is manually entering the points by VMB users.

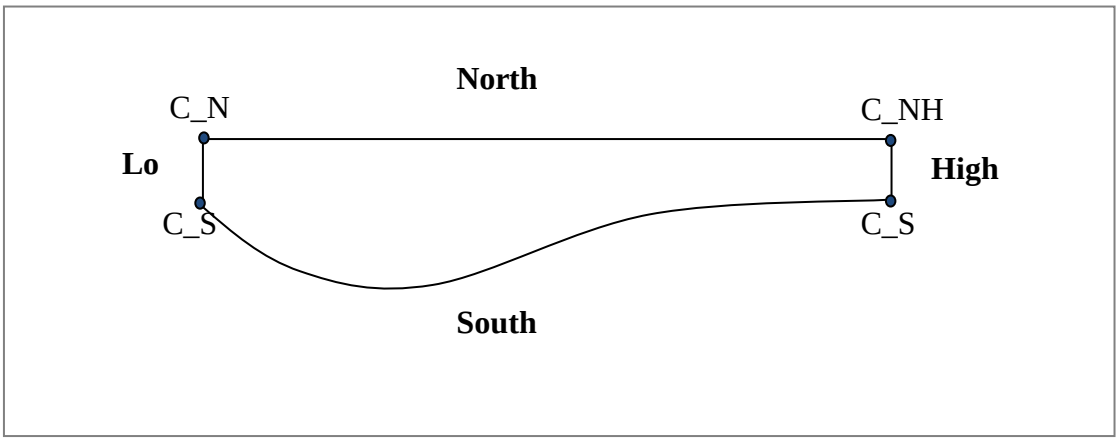

Figure 2.23 a nozzle object as an example of common quadrilateral object

The structure of each type of object is defined as a class. The structure contains the required information for components properties in arc modelling. The following properties are contained in an object.

- Geometry and boundary information
  Use a group of points to define each curve for the sharp of component.

- Material properties
  Specify thermal conductivity, electrical conductivity, density, ablation energy of a kind of material.

- Motion properties
  Specify the velocity displacement and maximum distance that each component can move.

- Simulation properties
  Give the number of cells in both *z* and *y*-directions, flow inlet and outlet condition, or surface ablation properties.

- Scaling
  When the component is displayed, a scale factor will need to be used to scale the objects to the required resolution. It has a unit of pixel per meter

- Modification

  Change the position of object in domain according to the movement of a component such as a piston in reality.

2.7.2.2 Visual studio C++ Implementation

In software design using Microsoft .NET the graphical user interface (GUI) is implemented through a Form control. A Form is basically a drawing surface where you can plot curves or 2-D shapes. It is also a container control in the sense that can be placed other controls in it. A control in visual studio is a visual object in GUI that allows the user to interact with the user application. Such an object is made available to the user who can then possibly click it, move it, resize it, type characters in it or retrieve something from it. A snapshot of VMB is given in Figure 2.24.

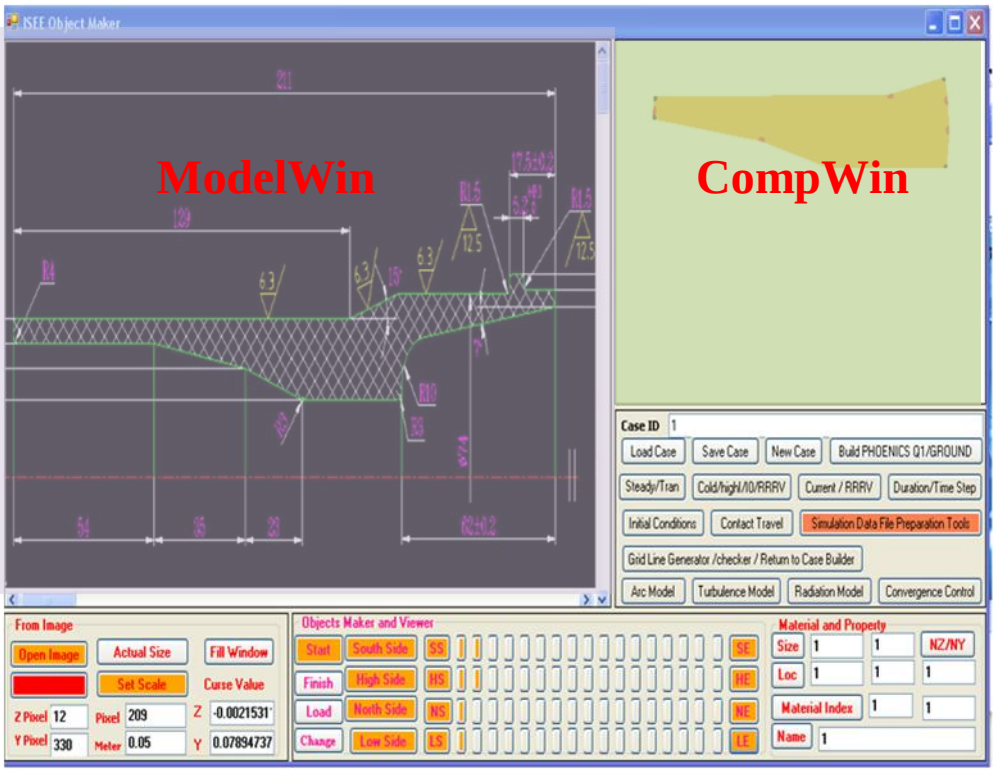

Figure 2.24 Snapshot of VMB in the process of making an object (right window) from a circuit drawing

Figure 2.24 shows the graphic user interface of VMB. It mainly contains two windows. The first one is a Model Window (ModelWin) for displaying the circuit breaker plot,

selecting component defining points from the plot, and displaying the built model. The second is a Component Window (CompWin) to display a constructed component or making settings to the component. Grouped buttons will be used to operate the software with consideration to the requirement

The main functionality of VMB includes:

- Import an image file representing the drawing of a circuit breaker and view it with its original resolution (pixel per unit length) or in a scaled mode.
- When the image is larger than the view window (ModelWin) on the GUI, different part of the image can be viewed by clicking and dragging the mouse.
- A group of components with similar shape and modelling properties can be represented by an object class in a pre-defined library and its exact dimensions can be set conveniently by either clicking defining points on the circuit breaker plot or entering the coordinate values though the GUI. With respect to this requirement, the structure of the object class has to be carefully developed.
- The component under construction can be graphically displayed in the CompWin and simulation properties, such as number of cells in both z- and y-directions, flow inlet and outlet conditions, or surface ablation properties, be set in a visual manner.
- All objects can be visually assembled in the ModelWin and the overall grid system generated and displayed for grid checking including the orthogonality.
- The package keeps a register of all objects, the first one being the container domain, so that a component can be deleted if necessary.
- The movement of the contacts can be visually checked when the contact travel is given and the important instants corresponding to strategically important positions of the contact can be easily found out. The time step in a transient simulation can be optimised using ISEE and appropriate settings made in Q1.
- When an object is added or deleted, or when the properties of an object is changed in ISEE, the package can locate the corresponding part of the code in the Q1 and ground for files and make correct settings .

2.7.2.3 Equation solver

The CFD software could be commercial or in-house packages as long as there is interface for data communication with VMB and VCA. Parallel processing is increasingly used for computation intensive simulations. Most of the parallel algorithms are based on domain division. For arc simulation, much CPU time is devoted to the calculation of nonlinear material properties of gases and their mixtures and radiation transfer in part of the domain (the arc region). A suitably constructed, object-based parallel algorithm may prove advantageous for arc simulation. For example, a group of objects with large volumes but mild CPU usage, such as solid blocks in the domain, can be designated to a single CPU, while the arc region which is more computation intensive can be divided into more than one objects and each assigned to a CPU. The object based modelling approach commonly used for geosimulation [3] may provide ideas of developing an object-based parallel algorithm for arc simulation.

In the present work, the non-parallel version of PHOENICS is used as the equation solver. The Q1 and ground.for files of PHOENICS serve as an interface with VMB and VCA. These two files are generated by a translator object in VMB. The VCA interacts with PHOENICS through memory sharing. Different channels are used for data transfer and synchronisation control between PHOENICS and VCA.

2.7.2.4 Virtual Controller and Analyser

Once simulation starts, control is passed to VCA. Except the grid system, all other simulation parameters can be changed in VCM (**Virtual Control Monitor**). Figure 2.25 is a snapshot of VCA for a nozzle arc. The software was developed using OOP in Microsoft Visual Studio and its event-driven nature makes the implementation of different functionalities easily achievable. For example, visualisation of the simulation results is implemented in an event handler while the synchronisation with PHOENICS is achieved through a different event handler. The code for plotting the results is executed in response to an event which is generated when data from PHOENICS is read.

Information exchange between PHOENICS and VCM is a key issue since it has to be sufficiently rapid. This is realised through a memory sharing method. There are several groups of data to be exchanged and their sequence is critical. Through careful consideration and test, a method is developed which is shown in Figure 2.26. The user interface provided by PHOENICS is listed as groups on the left hand side column. Since VCM is designed in an OOP approach, its interface for information exchange is in the form of event handlers. An event handler is a special C++ function in response to a user action such as a click of button or on reaching the end of a time interval set to a timer. The middle column in Figure 2.26 lists all the data in the form of memory files. The coordinated operation of reading and writing of the memory files by PHOENICS and VCM allows the realisation of information exchange.

The main functionality of VCA includes:

- Attach to and detach from PHOENICS operation, providing maximum flexibility. PHOENICS can still carry on with the simulation even when VCA is detached from it and shut down. The connection status with PHOENICS is indicated by a status button.

- Colour contour mode. For design engineers and researchers in general, qualitative review of the distribution of physical quantities can be important. This requires colour visualisation of the field quantities such as pressure, temperature, velocity of arcing gas. VCA thus provides a colour contour mode for this purpose. Figure 2.27 shows the temperature distribution of a 100 *A* d.c. SF_6 arc in a supersonic nozzle. All field quantities can be displayed in VCA by simply clicking on the variable name located on the right hand side of the VCA window in Figure 2.27. The size and location of the portion of the domain to be visualised can be chosen conveniently. This region can be enlarged if necessary.

- Line visualisation mode. There are occasions when the distribution of a quantity along a line needs to be carefully inspected. For nozzle arcs this can be the radial and axial distribution of quantities such as temperature, electric field, velocity etc. In the example shown in Figure 2.28, the radial distribution of arc temperature at the nozzle throat is visualised together with experimental data for comparison. The axial or radial location where the distribution of a quantity to be drawn in “real time” can be

chosen by the user. This mode and the colour contour mode can be switched by a mouse click.

- Change of simulation conditions. VCA provides convenience to assess the influence of simulation conditions on the arc behaviour. For example, now it is possible to instantly change the arc current and upstream pressures to perform simulations under different conditions without stop and re-start the simulation. Some typical results are given in Figures 2.29 and 2.30.

- Relaxation control. An important issue in computer simulation is the control of the solution process so results are fully converged. For circuit breaker arcs, strong radiation and Ohmic heating creates steep density gradient at the arc edge that makes convergence difficult in some cases. Often it is not easy to identify the exact course or location of divergence/oscillation due to the coupling of a number of operating mechanisms in more than one governing equations. For example it was found previously that at certain current level (e.g.1800 *A*), solution could start to oscillate without any obvious reason and it was not possible to locate the oscillation among the huge number of cells in the computational domain. With the present simulation environment, this becomes a much easier task. It has been found that oscillation of the solution occurs at the arc edge near the exit of the nozzle (Figure 2.30(a)). With adjustment of the relaxation parameters, solution starts to converge quickly, as shown in Figure 2.3(b).

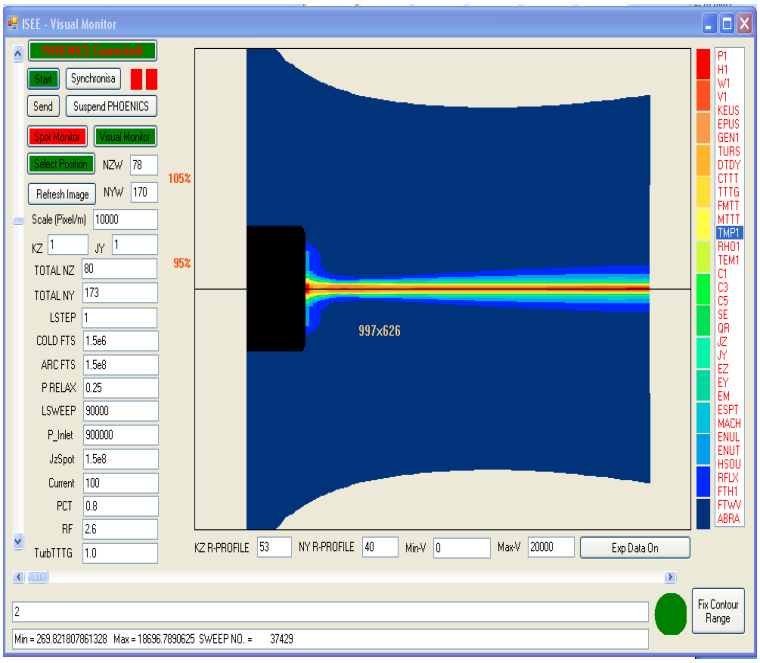

Figure 2.25 Snapshot of VCA in colour contour mode showing a 100 A SF_6 arc with an inlet stagnation pressure of 9bar and exit pressure of 2.5 bar.

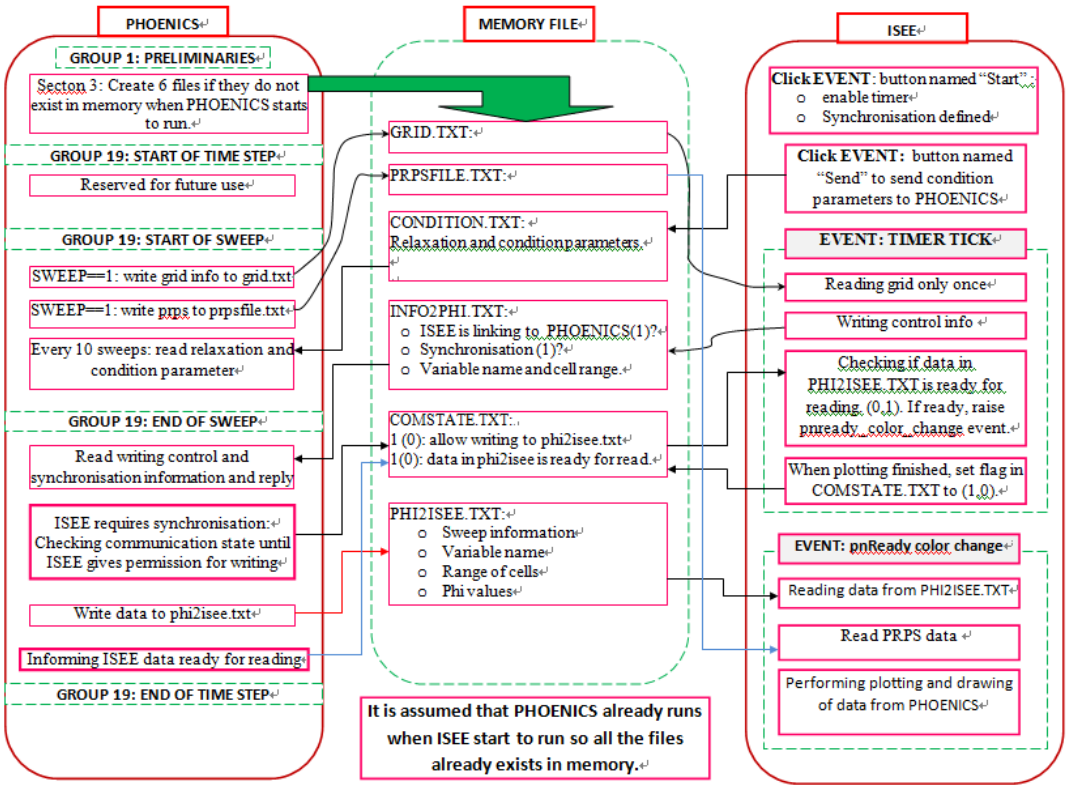

Figure 2.26 Diagram shows how PHOENICS interact with ISEE through memory sharing

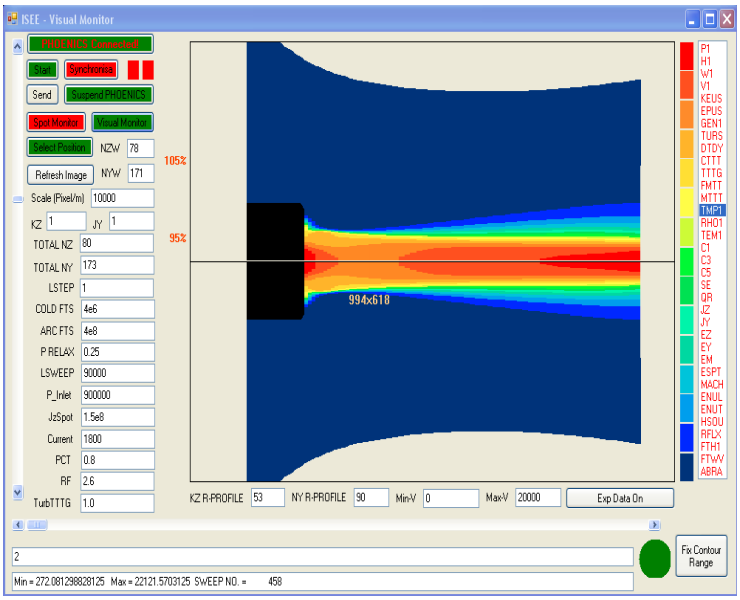

Figure 2.27 Increase of arc column size and temperature in response to current change from 100 A as shown in Figure 2.25 to 1800 A in this figure.

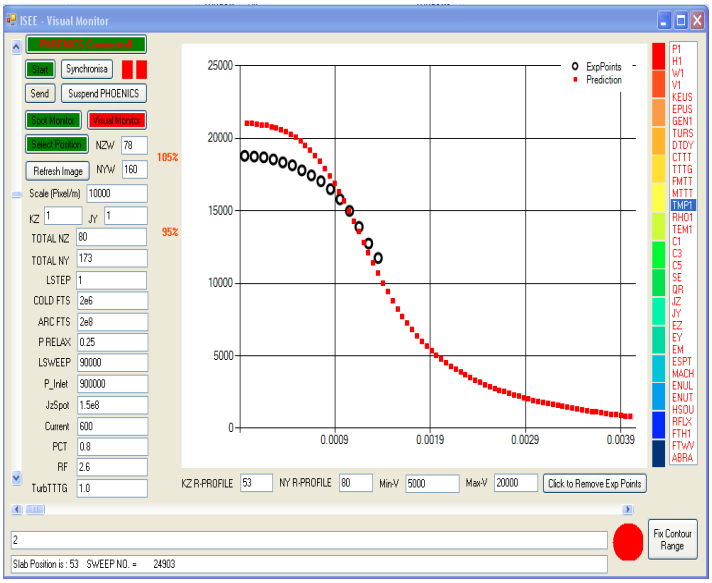

Figure 2.28 Snapshot of VCA in Line Visualisation mode. Circles – Experimental data read from a text file. Squares – Predicted radial temperature distribution at nozzle throat.

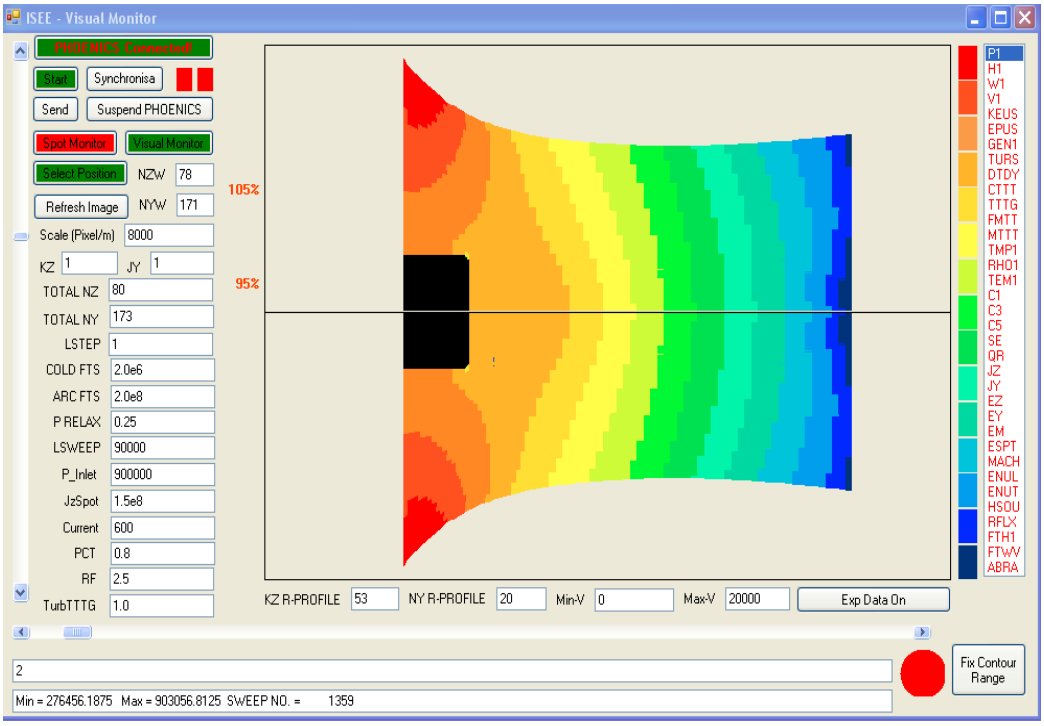

(a)

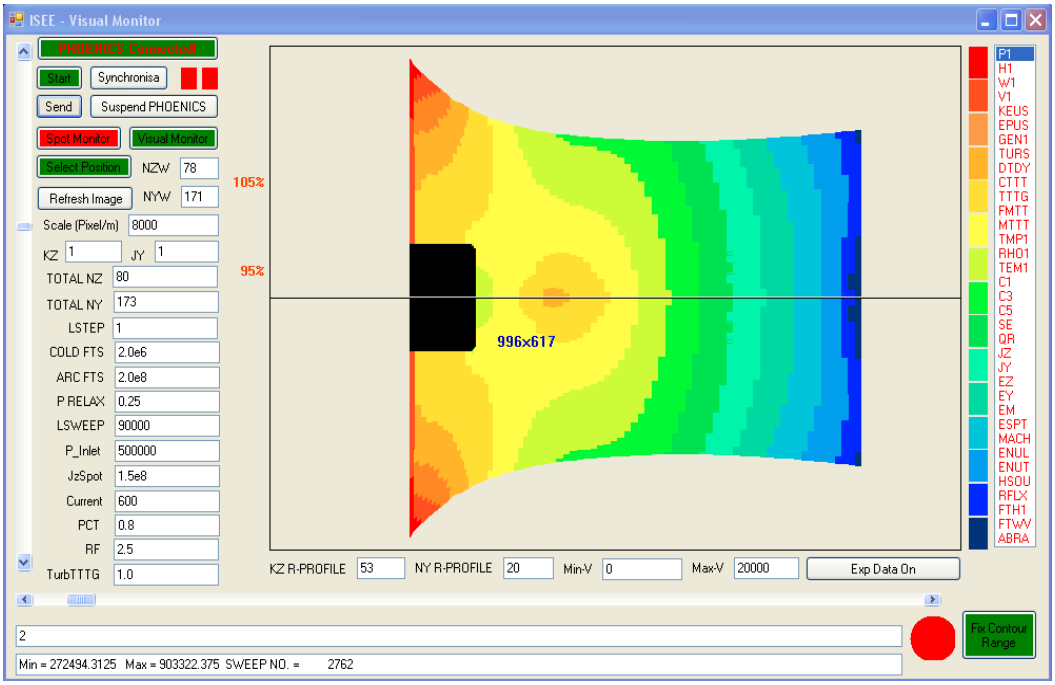

(b)

Figure 2.29 Diagram showing the pressure distribution inside the nozzle when the inlet pressure is changed from 9 bar in (a) to 5 bar in (b)

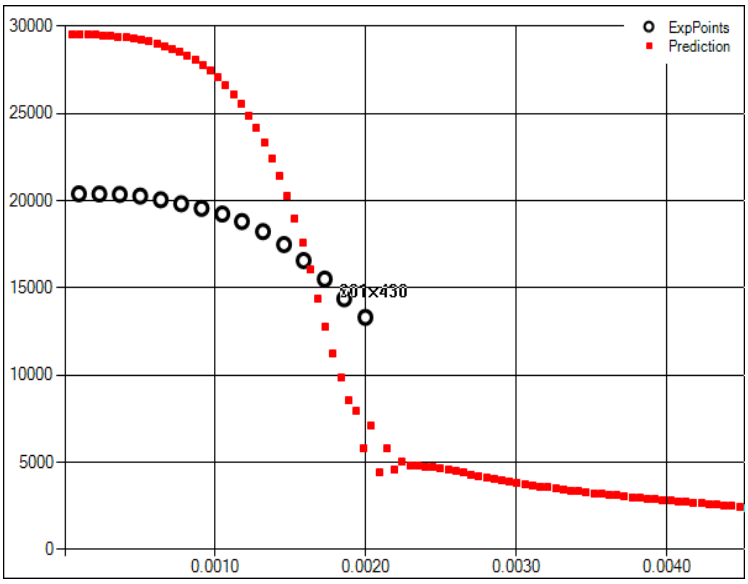

(a)

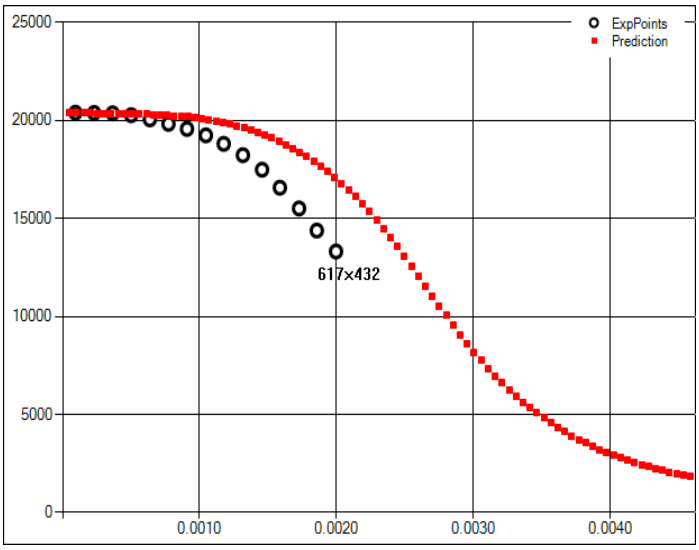

(b)

Figure 2.30 Diagram showing oscillation of solution under certain current and relaxation conditions. Vertical axis is temperature in K and horizontal axis is radius in metre. (a) Oscillation of solution at arc edge, (b) fully converged solution. Arc current = 1800 A under same conditions as in Figure 2.25.

2.8 Summary

The mathematic models to describe the switch and arc-in-water cases were first presented in this chapter. While the two cases share the same set of governing equations, the arc in water case has additional complexity in the sense that chemical reaction has to be taken into account in the model in terms of sources for energy and species concentration equations. The chemical reaction rate coefficient is calculated using the Arrhenius equation. The calculation of magnetic field and current density is also presented.

Turbulence is important for switching arcs. The Prandtl mixing length model and the *k*-epsilon model were modified to improve their accuracy and applicability for puffer circuit breakers. Results in this chapter show that using a varying turbulence parameter *c* in the Prandtl mixing length model produces improved agreement between the predicted and measured temperature profiles for steady state arcs and also arc voltage for puffer circuit breakers. the simulation of the circuit breaker arc in Chapter 4 will thus be based on the modified Prandtl mixing length model.

Two forms of modification to the *k*-epsilon model were also assessed using experimental results for steady state nozzle arcs and transient circuit breaker arcs. Results show that they also produce moderate improvement in comparison with the standard *k*-epsilon model. Further work is thus needed to improve the *k*-epsilon.

The benefit of ISEE to circuit breaker design engineers is obvious, as has been demonstrated by the VCA working with PHOENICS. The success is based on a well developed memory sharing method as described in section 2.7.2.4. However there are limitations to the present tools since the user interface provided by the commercial CFD package PHOENICS is rather limited in its functionality. A model for the development of VMB was proposed and the software in this present form allows objects construction and display. However automatic generation of Q1 and ground.for files needs to be realised in future work due to the limited time available for this project.

2.9 References

[Low92] Lowke J. J., Kovitya P. and Schmidt H. P., "Theory of free-burning arc columns including the influence of the cathode", J. Phys. D: Appl. Phys., Vol. 25, pp. 1600-1606, 1992

[Lew85] E. Lewis, N Prasad and G R Jones. "Current zero spec&scopy of a high power SF6 circuit breaker arc"; Proc. Int. Con$ on Gas Discharges and Their Applications (Oxford) (Leeds: Leeds University Press) Pp 314, 1985

[Gle90] A. Gleizes, A.A. M. Habib, M. Razafinimanana, M. Sabsabi and S. Vacquie, "Departures from Saha equilibrium in SF6 arc plasmas", Spactrochemic Acta, Vol.45B, No. 7, Pp 789-797, 1990

[Jon80] G.R.Jones and M.T.C Fang, "The physics of high power arcs", Rep. Prog.Phys., Vol.43, Pp. 1415-1465, 1980

[Sch85] E.Schade, "Recovery of switching arcs", Proc. XVIIth Int. Conf. Phenomena Ionised Gases, Pp. 277-297, 1985

[Yan01] J. D. Yan, M.T.C Fang, and Q. S. Liu "Dielectric recovery of a residual SF6 plasma between two parallel electrodes", IEEE Transactions on Dielectrics and Electrical Insulation, Vol. 8, pp.129-136, 2001

[Zha02] J. L. Zhang, J. D. Yan, A.B. Murphy, W. Hall, and M.T.C Fang. "Computational investigation of arc behaviour in an auto-expansion circuit breaker contaminated by ablated nozzle vapour", IEEE Trans.on Plasma Science, 30: 706-719, 2002

[Pat80] S.V.Patankar, "Numerical Heat Transfer and Fluid Flow", McGraw-Hill, New York (1980).

[Jen03] Jenista J., "Water-vortex-stabilized electric arc: III. Radial energy transport, determination of water-vapour-boundary and arc performance", J. Phys. D: Appl. Phys. 36, pp. 2995-3006, 2003

[Lan99] H Lange, K Saidane, M Razafinimanana and A Gleizes, "Temperatures and C2 column densities in a carbon plasma"

[San02] Sano N., Wang H., Alexandrou I., Chhowalla M., Teo K. B. K. and Amaratunga G. A. J., "Properties of carbon onions produced by an arc discharge in water", Journal of Applied Physics, Vol. 92, No. 5, pp. 2783-2788, 2002

[Low74] Lowke J J , J. Quanr. Spectrosc. Radial. Transfer 14 I1I, 1974

[Yan99I]Yan J D, Fang M T C and Hall W, "The development of PC based CAD tools for auto-expansion circuit breaker design", *IEEE Transactions on Power Delivery*, Vol. 14, pp. 176-181. 1999

[Yan99II]Yan JD, Nuttall KI and Fang MTC, "A comparative study of turbulence models for SF6 arcs in a supersonic nozzle" J. of Physics D: Applied Physics, Vol. 32, 1401-1406, 1999

[Bin06] Bini R., Monno M. and Boulos M. I., "Numerical and experimental study of transferred arcs in argon", J. Phys. D: Appl. Phys., Vol. 39, pp. 3253-3266, 2006

[Fang92] Fang, M.T.C. and Zhuang, Q. "Current Zero Behaviour of an SF_6 Gas Blast Arc, Pt.I: Laminar Flow" J.Phys.D.: Appl. Phys., Vol.25, pp. 1197-1204, 1992

[Fang94] Fang, M.T.C., Zhuang, Q. and Guo, X. "Current Zero Behaviour of an SF_6 Gas Blast Arc, pt II. Turbulent Flow", J. Phys. D: Appl. Phys., Vol. 27, pp 74-83, 1994

[Zha87] Zhang J. F., Fang M. T. C. and Newland D. B., "Theoretical investigation of a 2kA arc in a supersonic nozzle", J. Phys. D: Appl. Phys., Vol. 20, pp. 368-379, 1987

[Her76] Hermann W, Kogelschatz U, Niemeyer L, Ragaller K and Schade E, “Investigation on the physical phenomena around current zero in HV gas blast breakers”, IEEE Trans. On Power Appratus and systems, Vol. PAS 95, 1165-1176, 1976

[Bra78] Brand KP and Kopainsky J, "Particle densities in a decaying SF_6 plasma", Appl. Phys., Vol. 16, 425-432, 1978.

[Blun97] Blundell R E, Fang M T C and Vourdas A Stability of a DC SF6 arc in accelerating flow IEEE Trans. Plasma Sci. 25 852-9, 1997

[Abd04]Abdol-Hamid KS, Paul Pao S, Massey SJ, “Temperature corrected turbulence model for high temperature jet flow”, Transactions of the ASME, Vol. 126, 844-850, 2004

[Zhang00] J. L. Zhang, J. D. Yan, and M T. C. Fang, Investigation of the Effects of Pressure Ratios on Arc behaviour in a Supersonic Nozzle, IEEE TRANSACTIONS ON PLASMA SCIENCE, VOL. 28, NO. 5, OCT 2000

[Ria03] Riad H., Gonzalez J. J. and Gleizes A., “Net emission coefficient for thermal plasmas in H2, O2, H2O, CF4 and CH4”, 12th Int. Symp. On Plasma Chem. (ISPC16), 2003

[Yan09] Yan JD, Han SM, Zhan YY, Zhao HF and Fang MTC Computer simulation of the arcing process in high voltage puffer circuit breakers with hollow contacts. In: eds. *Proceedings of XVIII Symposium on Physics of Switching Arcs*.FSO2009, Brno Czech Republic:Local Organisation Committee,pp.99-108, 2009

[Phoe] PHOENICS is the name of a commercial CFD package supplied by CHAM which is based at Bakery House, 40 High Street, Wimbledon Village, London, SW19 5AU, UK.

[Tang08] K. M. Tang, "Computer Simulation of Atmospheric Technological Plasmas", PhD Thesis, 2008

[Low92] Lowke J. J., Kovitya P. and Schmidt H. P., “Theory of free-burning arc columns including the influence of the cathode”, J. Phys. D: Appl. Phys., Vol. 25, pp. 1600-1606, 1992

Chapter 3 Computer Simulation of a Carbon Arc Confined in Water

3.1 Introduction

The electrode gap length commonly used in the arc in water experiments is 0.7 to 1 *mm* for efficient production of nano-structures. A conical anode and a cylindrical cathode are commonly used. Images of the arc suggest that the gaseous environment has approximately the shape of a gas bubble (figure 3.1) and the size of the gas environment undergoes rapid fluctuation in a cycle of growth-collapse. The collapsed gaseous region forms bubbles floating towards the water surface. The actual process is much more complex due to the irregular shape of the contact tips as a result of carbon erosion.

To make the problem manageable simplifications have to be made. Firstly, we will assume that the arc is initiated using new electrodes so the shape of the electrodes is "ideal". Secondly, electrode erosion does not cause noticeable change to its geometry for the period of arcing to be simulated. Thirdly, the electrodes are arranged vertically and the gaseous environment is close to rotational symmetry. With these simplifications, the work in this chapter aims at a study of the dynamics of the gaseous environment and the plasma behaviour in one repeating cycle, namely the growth of the bubble shaped gaseous environment, its composition, and the characteristics of the arc in this dynamic environment.

The governing equations for arc in water have been introduced in Chapter 2 with a brief description of the chemical reaction to be considered. The equation of state and the transport properties will be given in section 3.2 together with the determination of chemical reaction rate. This is followed by a description of the numerical scheme for simulating the growth of bubbles in section 3.3 together with the initial and boundary conditions, and the grid system. Results will be discussed in section 3.4 and a summary is given in section 3.5.

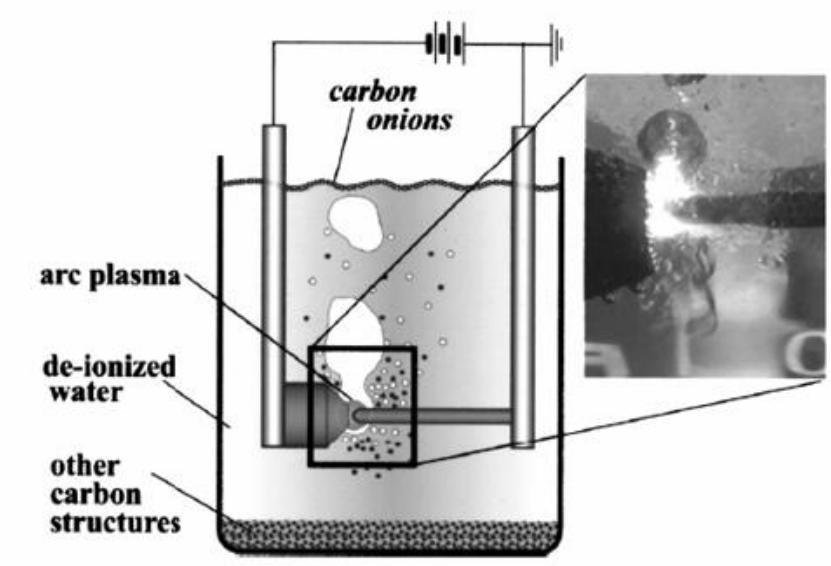

Figure 3.1 Image from a real carbon arc confined in liquid water [Hsi01] fitted with the spherical bubble model that is to be used in this chapter. In experiment the electrodes were positioned horizontally.

3.2 Material Properties and Chemical Reaction Rate

The thermodynamic and transport properties of the mixture of water vapour, carbon vapour, H_2 and CO are not available. Thus approximation will need to be used to obtain the data for the mixture. In performing the simulation conversion between temperature and enthalpy is first required. Since the enthalpy equation is used for energy transport, the temperature of the gas mixture needs to be derived. Figure 3.2 shows that over the temperature range of 3,000 *K* to 10,000 *K*, the specific enthalpy of carbon vapour and water vapour is close to each other [Gleizes]. As mentioned in Chapter 2, inside the arc column, carbon vapour is the dominant species (>95%) with a small amount of water vapour for most of the arcing time when the bubble grows. The temperature inside the arc can thus be obtained by interpolation using the enthalpy of the gas mixture and the mass concentration of carbon vapour.

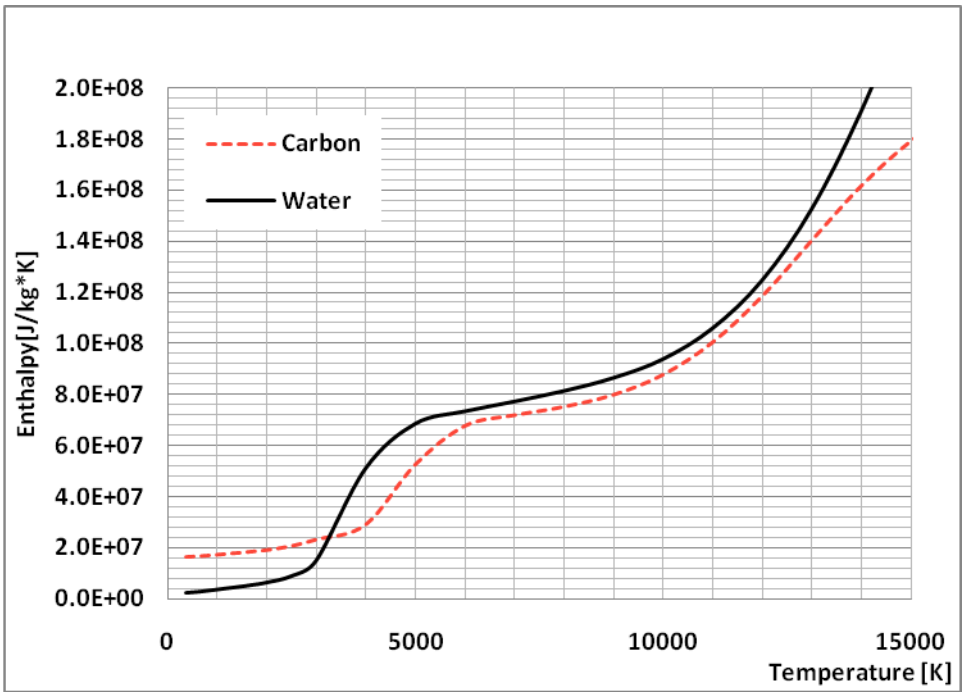

Figure 3.2 Enthalpy of 4 gases at 1atm as a function of temperature (300 to 25,000 K).

It is also expected that the arc characteristics is largely controlled by the material properties of pure carbon because of its dominant presence in the arc region. The equations of state of the gaseous species are expressed as data tables. The relationship between density and temperature at 1 bar are shown in figure 3.3 [Gleizes]. The viscosity and thermal conductivity of the two pure gases are given in figures 3.4 and 3.5, respectively and that of the mixture is obtained based on interpolation. It must be noted that the method of interpolation may not be accurate when the concentration of the two constituting species is comparable. In our case however the mixture in the arc region is dominated by carbon species and the material properties obtained by interpolation of the pure gases are expected to be reasonably accurate. The electrical conductivity of carbon and water vapour at high temperatures is given in figure 3.6.

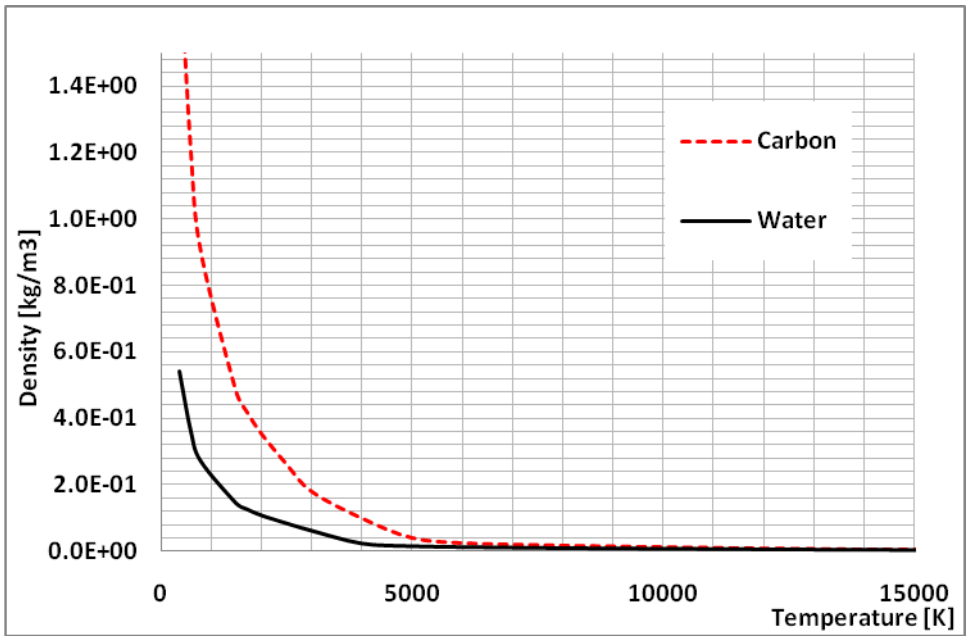

Figure 3.3 Density of carbon and water vapour as function of temperature at 1 bar.

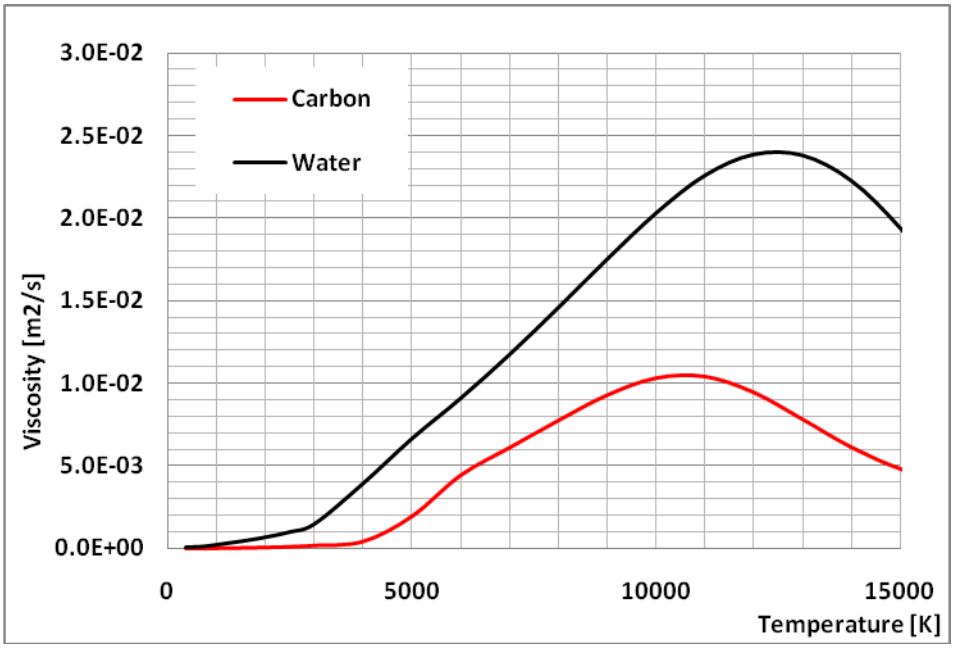

Figure 3.4 Viscosity of pure gas species in the temperature range of 300 K to 15,000 K.

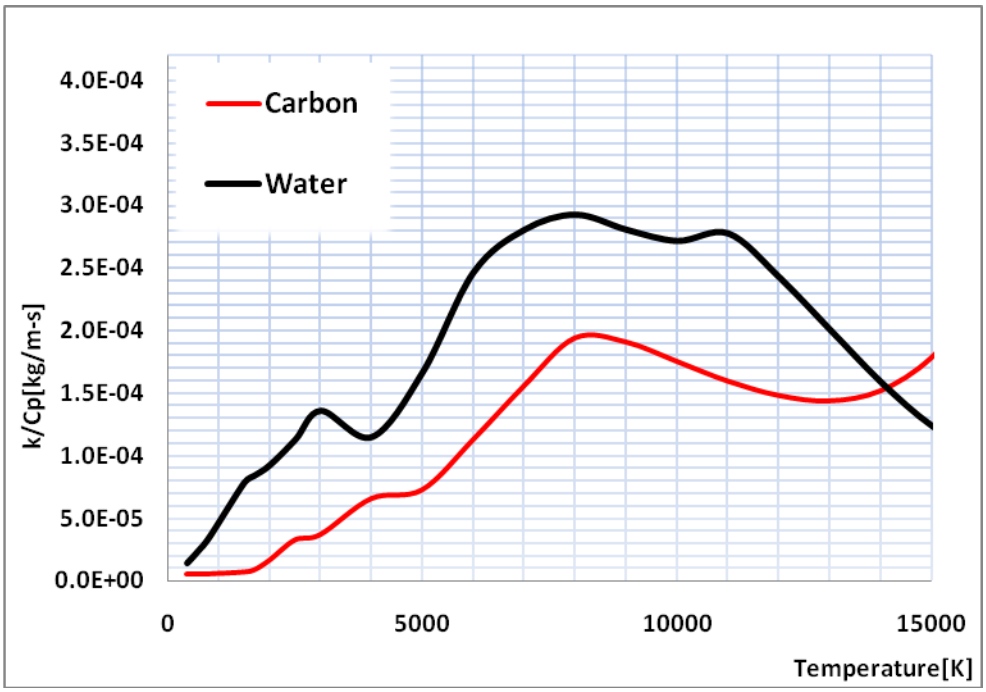

Figure 3.5 Ratio of thermal conductivity over specific heat of two pure gases over the temperature range of 3,000 K to 15,000 K.

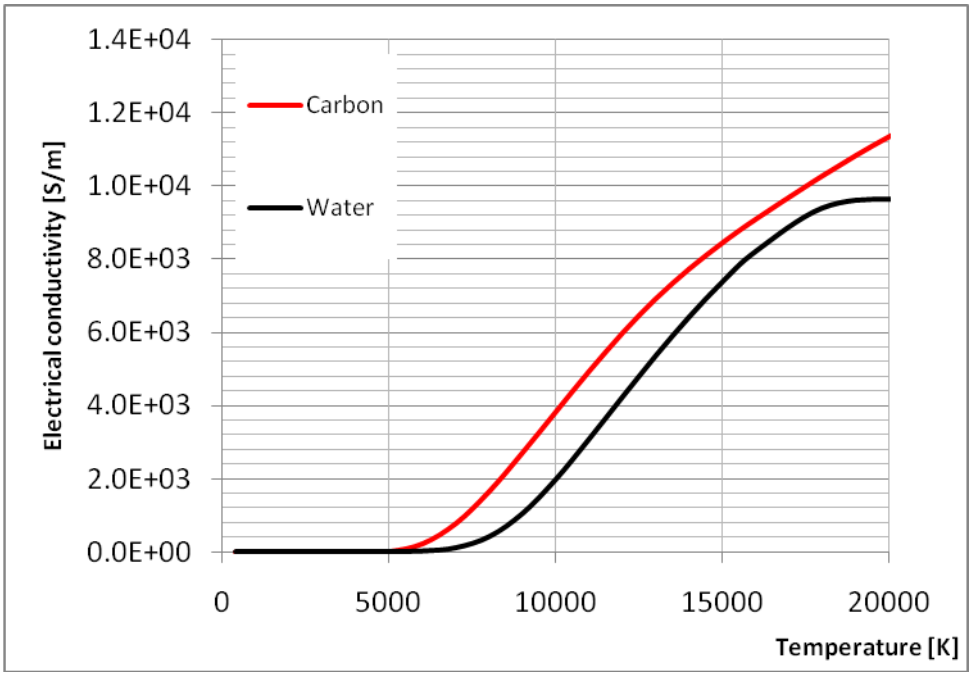

Figure 3.6 Electrical conductivity of carbon and water vapour.

Outside the arc column, the gas temperature drops significantly and is mostly below 4,000 *K*. The concentration of H_2 and CO is higher than that inside the arc column but is still much lower than that of the water vapour and carbon vapour, typically less than 1% of the mixture. With such a concentration, the presence of H_2 and CO does not change

the material properties other than the enthalpy of the mixture. As shown in figure 3.7, the enthalpy of H_2 at 4,000 *K* is 4 times that of the water vapour. Given an upper limit of 0.2% for H_2 concentration, the uncertainty caused by the omission of H_2 and CO in the material properties is less than 8%.

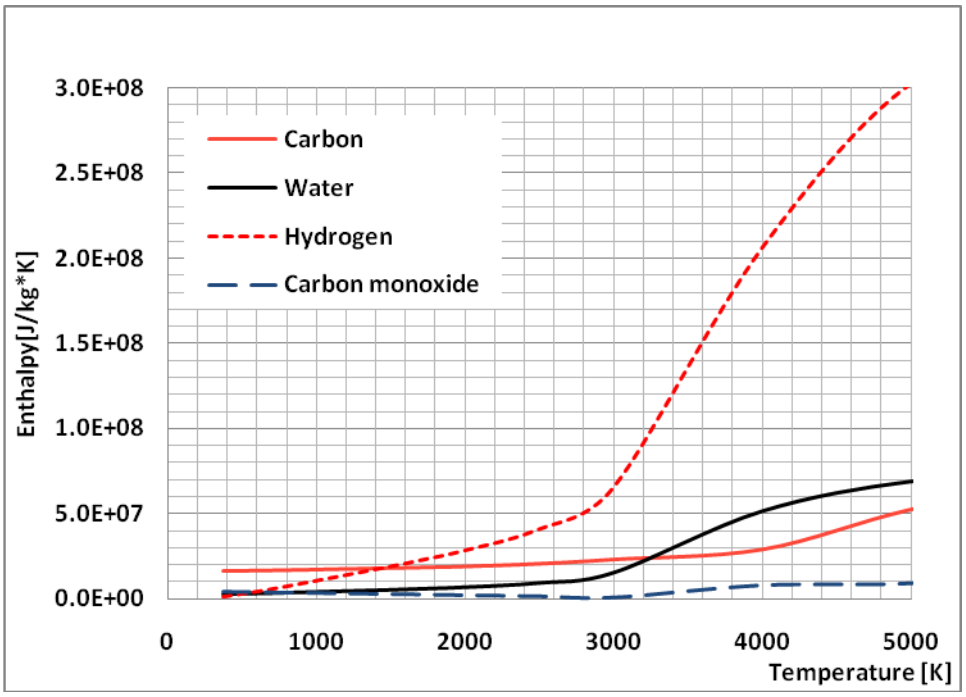

Figure 3.7 Enthalpy of pure gases in the temperature range of 300 K to 5,000 K.

Solution of the concentration equations for carbon vapour, H_2 and CO requires knowledge of the diffusion coefficient of each species in the mixture. So far these data are not available. An estimation has been done to obtain the order of magnitude for each species using information given in [Gleizes], the results from the estimation are given in figure 3.8 for carbon vapour and water vapour. The diffusion coefficient for H_2 and CO is given a constant value of $10^{-3}\ m^2/s$.

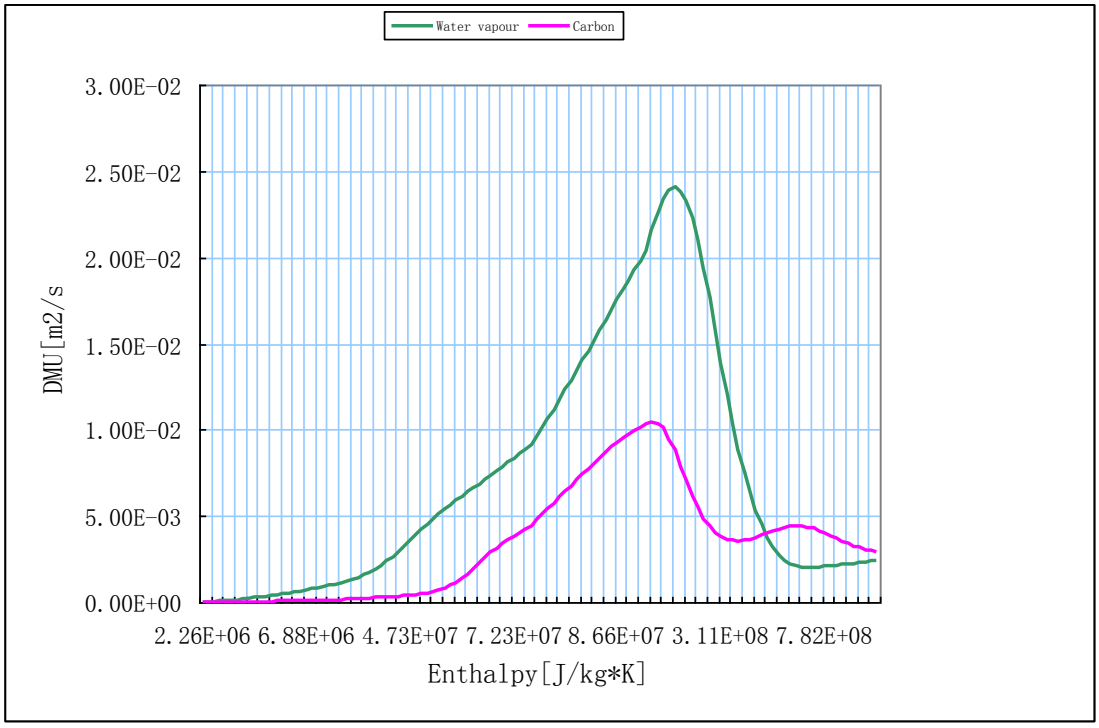

Figure 3.8 Diffusion coefficient estimated using information provided in [Slattery and Bird]

This is a remarkably accurate formula for calculating the reaction rate coefficient. It takes the form of

$$K = Ae^{-\frac{E_a}{RT}} \qquad (3\text{-}1)$$

where A is a pre-factor and R the gas constant. E_a is the activation energy that means the minimum kinetic energy that reactants must have in order to form products. Both A and E_a only depend on the type of reaction, not the concentrations of the reactants. Therefore K is the rate constant which is independent of the concentrations of the species taking part in the reaction. However it depends on the temperature T which determines the distribution of energy of the reactant particles.

Most of the data on reaction rate reported in literature is for solid carbon and water vapour. In the present work, carbon vapour reacts with water vapour to produce H_2 and CO. The reaction rate coefficient, especially at higher temperatures, is not readily available. The rate at 300 K was given as 1.0×10^{12} [$cm^3/(mol\ s)$.] by Hussain and Young [Hus75].

Using the concentration of the reactants, the rate coefficient at 300 *K* was calculated as $1\times10^{6}\ m^{3}/(mol\ s)$. With the value of E_a =131.33 *KJ/mol* and *R*=8.314472 $J\cdot K^{-1}\cdot mol^{-1}$, A value of $1.054\times10^{6}\frac{m^{3}}{mol\cdot s}$ was obtained. Reaction of carbon vapour with water vapour is expected to take place outside the arc column where the water vapour concentration starts to dominate. However in this region, the gas temperature is already low (<5,000 *K*) in comparison with the arc column. The value of $1.054\times10^{-6}\frac{m^{3}}{mol\cdot s}$ is used in the present work. The unit of *A* calculated here is not in standard form and care has been taken in the calculation to use a single unit system.

3.3 Initial and Boundary Conditions and Loss of Carbon due to Formation of Carbon Nano-structures

An arc has to be burnt in a gaseous environment. The breakdown in water is not considered here. It is assumed that the arc is initiated in a small gaseous cavity whose dimension is comparable to the tip of the anode (the upper electrode). Since we have no knowledge of the arc temperature at the start of the process a hot column is simply used to form a current conducting channel, as shown in figure 3.9. The radius of this hot column is 0.2 *mm* and its temperature is 24000 *K* on the axis. It has been checked that the arc behaviour at later stage is not sensitive to the initial condition because shortly after the arc initiation, strong carbon vapour flux from the anode starts to control the arc behaviour. The initial pressure is 1 bar and the gaseous environment is pure water.

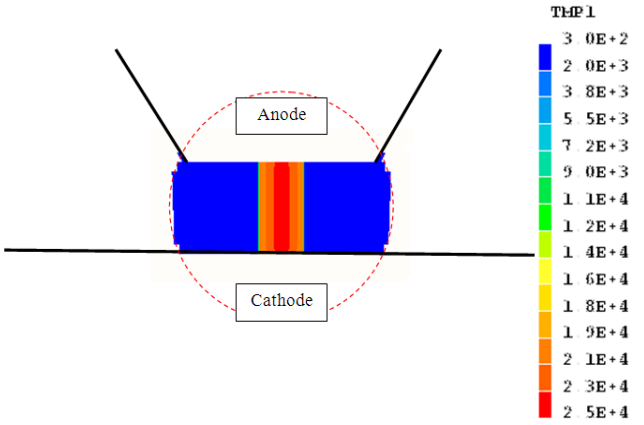

Figure 3.9 Initial state of arc and bubble environment. The bubble at time zero is filled with water vapour at 1 bar and 300 K.

Because of the very low flow in the bubble, friction between gas and solid surface is not considered. Thus there is no source for the momentum equations as a result of surface friction. The arcing time in the present work is only several milliseconds. There is no thermal conduction between the bubble gas and the liquid water. On the anode surface, an axial influx of carbon vapour into the computational domain is imposed. Since the arc-electrode interaction via the thin non-LTE layer is not considered, apart from the vapour flux, the arc does not transfer energy with the anode. An erosion rate of 117 *mg/min* is used in the simulation following the measurement in [Hsi01] whose experimental conditions are close to those used in the present work. The measurement in was derived from the mass change of carbon electrode over the whole arcing process. In the model, we assume the erosion rate is a constant of 2.0×10^{-6} *kg/s*. Since the size of the anode arc root changes with time, we have assumed that the erosion only takes place over the anode attachment where the gas temperature is higher than 4500 *K*, the boiling temperature of carbon. The mass flux is then calculated by

$$\dot{m}_{carbon} = \frac{2\times10^{-6}}{\int_0^{r_{4500}} 2\pi r dr} \qquad (3\text{-}2)$$

where r_{4500K} is the radius over the anode surface where the gas temperature is 4500 *K*. The carbon vapour enters the domain with a temperature of 4500 *K* which is the boiling temperature of carbon. On the cathode surface, the thermal conduction between the plasma gas and the electrode is approximately considered by adding a volumetric energy loss source of

$$\dot{h} = -\frac{T_{gas}-6000}{10^{-4}\cdot\Delta z^2}\cdot k_{ave} \qquad (3\text{-}3)$$

where k_{ave} = 0.7 *J/(m.s.K)* and $\Delta z = 1.0\times10^{-4}$ *m* which is chosen as the typical dimension over which the gas temperature drops rapidly. The use of 6000 *K* as the low temperature end is based on the consideration that in the cathode sheath layer CNTs are formed in the deposit of the cathode surface and the temperature near the CNTs should be slightly

higher than the boiling temperature of carbon which can be as high as 5800 *K* depending on the carbon form.

In practice the bubble will detach form the discharge region when its size is over a limit. This is simulated in the present model by attaching a channel around the anode body to allow for gas loss, as shown in figure 3.10. The escape channel is only operating when the bubble boundary connects to the end of the channel in figure 3.10.

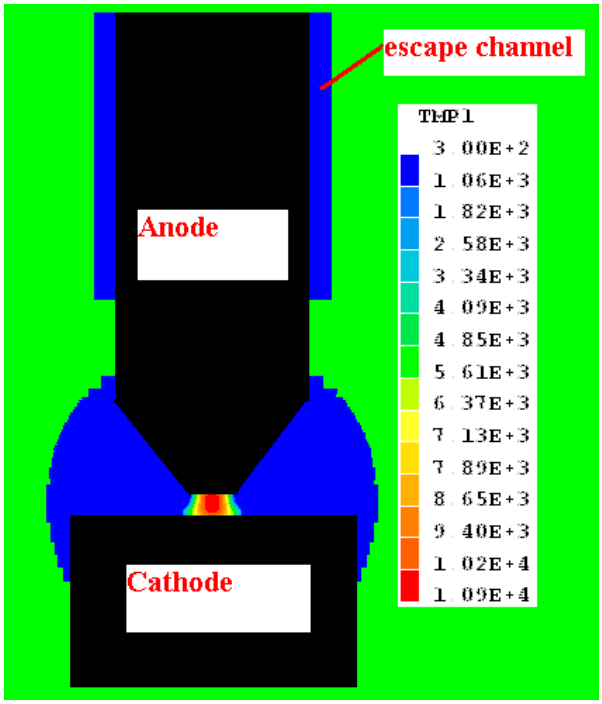

Figure 3.10 The addition of a escape channel for gas to escape from the arcing environment when the bubble radius is greater than 15mm. The upper end of the channel is maintained at a pressure of 1bar.

Carbon vapour is lost from the arc column through several mechanisms. The first mechanism is the carbon vapour loss near the cathode surface where CNTs are formed and also solid carbon deposits are formed. The second mechanism for carbon vapour loss is by the arc edge (figure 3.11) according to [Hsi01] where the steep temperature gradient turns carbon vapour into fullerene-like structures. For an anode evaporation rate of 117.0 *mg/min*, 19.5 *mg/min* is collected as solid matters. This gives a carbon vapour loss percentage of about 15%. Other experiment produces similar results [Zhu02]. Because the mechanisms for the formation of carbon structures and the

relationship between production rate and plasma environment are poorly understood so far, a flux controlled model is adopted in considering the carbon vapour loss. The axial velocity at 0.1 *mm* away from the cathode surface is used to calculate the carbon vapour flux towards the cathode surface.

This flux Γ_{cc} is

$$\Gamma_{cc} = \rho_c wc \qquad (3\text{-}4)$$

where ρ_c is the density of carbon vapour, w is the axial velocity and c is the carbon concentration. 15% of this carbon flux is assumed to be lost from the computational domain in the cells immediately adjacent to the cathode surface. A similar approach is taken at the arc edge. Starting from the axis marching in the radial direction, in the first cell with a local temperature of lower than 4500 *K*, 15% of the positive flux in the radial direction is lost from the domain. The flux can be expressed as

$$\Gamma_{ce} = \rho_c vc \qquad (3\text{-}5)$$

where v is the radial velocity.

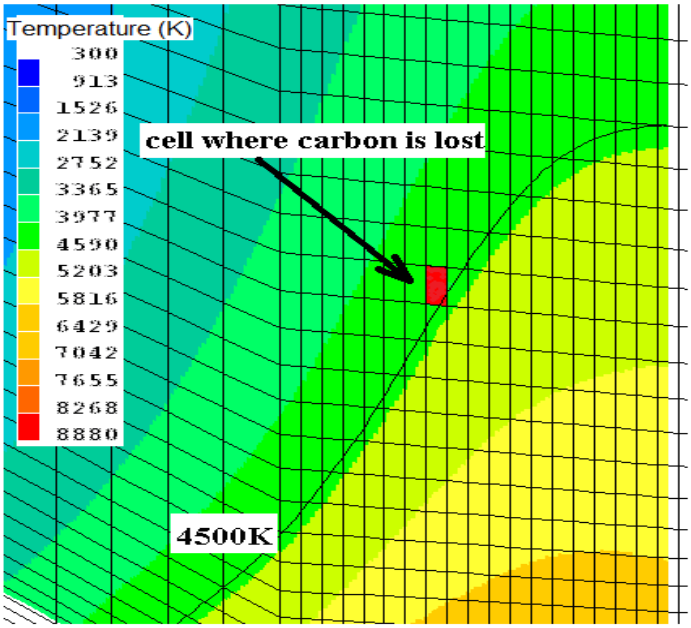

Figure 3.11 Diagram showing carbon vapour is lost from the domain at the arc edge

The provision of an escape channel is to simulate the effect of gas exhaustion into the atmosphere when the bubble size grows to a certain size. Once the bubble connects to

the channel, gas will flow out into the atmosphere. The pressure at the outlet of the channel is fixed to a constant pressure of 1 *bar* and diffusion of mass, momentum and energy is ignored because of the negligible gradient along the length of the channel.

.

3.4 Grid System and numerical Scheme for Bubble Growth

3.4.1 The grid system

The number of grids in the present simulation is 110 cells in axial direction and 130 cells in radial direction, giving sufficient spatial resolution. The electrode gap (1 *mm*) is axially divided into 20 cells. The typical radial width of the cells in the arc region is 25 *μm* and that in the arc surrounding region is typically 0.5 *mm* since the physical quantities in this region has low gradient. Body fitting coordinates (BFC) are used to simulate flow around curved bodies, as shown in figure 3.12.

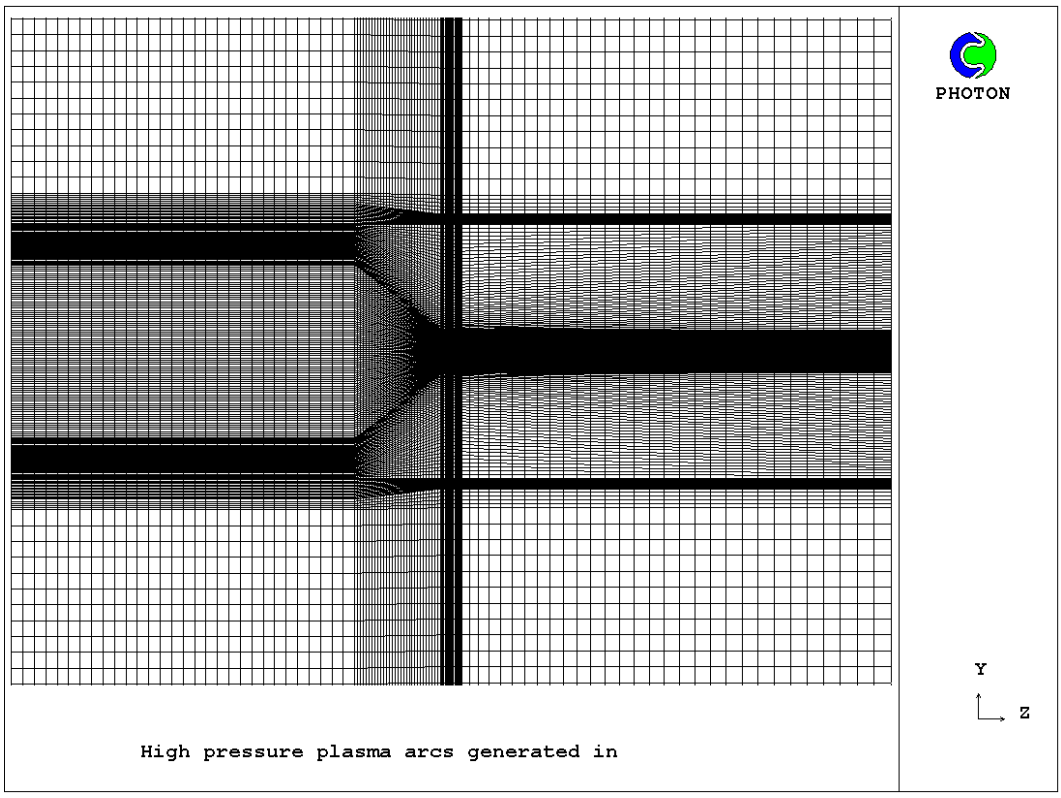

Figure 3.12. Grid system used for simulation

3.4.2 Water displacement due to pressure difference

The growth of the bubble is governed by a number of processes which will be described blow. The first factor that contributes to the growth of the bubble is the pressure acting on the bubble surface. In the present work, we used a conic anode and a cylindrical cathode, as shown in figure 3.13. Shortly after the arc is initiated, strong Ohmic heating will heat up the gas in the discharge zone and thus increase it pressure. A force is thus acted on the bubble surface. For fixed discharge geometry and dimensions of the electrode assembly, the area of the bubble surface is a function of the bubble radius. Mathematically this area can be calculated using an integral method. For our case, the ratio of the actual area to the whole area of the sphere as a function of bubble radius is given in figure 3.14 for the geometry shown in figure 3.13.

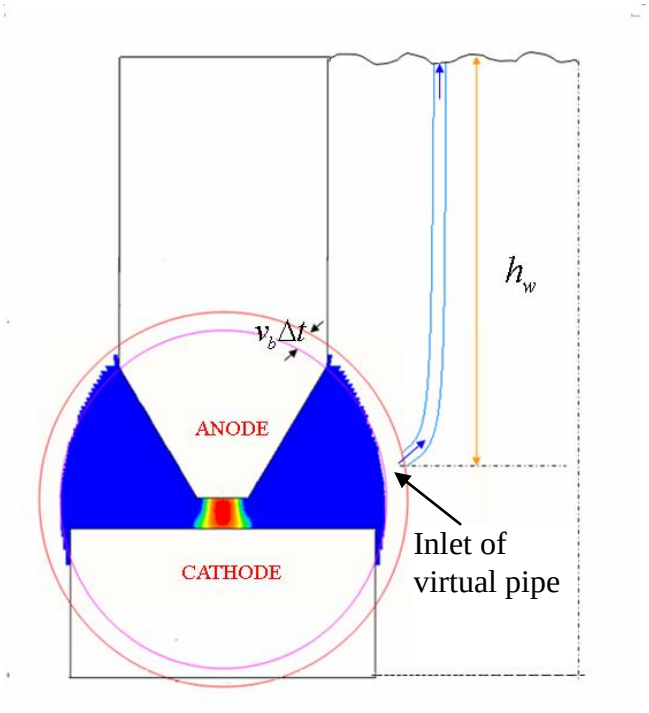

Figure 3.13 Diagram showing calculation of water displacement due to pressure difference.

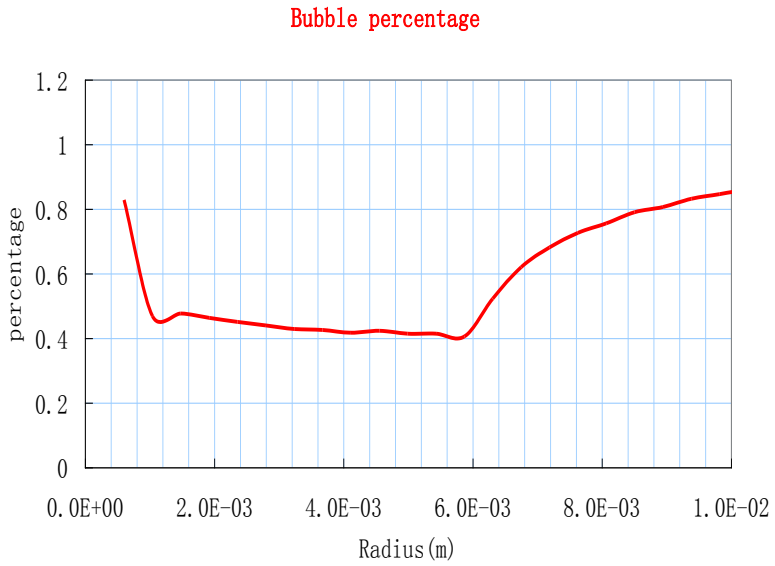

Figure 3.14 Actual bubble surface area as percentage of sphere surface area as a function of bubble radius.

Flow in the bubble is generally stagnant except the strong gas flow near anode due to electrode erosion. Thus the pressure inside the bubble is expected to by uniform. Using P_A as the average pressure near the bubble surface, the force acting in the normal direction of a mall area of the bubble surface is

$$F_{\delta A} = P_A \cdot \delta_A \qquad (3\text{-}6)$$

where δ_A is the surface element. The displacement of water in the beaker by bubble growth is a complex fluid dynamics phenomenon and is out of the scope of the present research. A simple one dimensional model is thus employed to simulate the dynamic of the bubble. As shown in figure 3.13, we assume that the water adjacent to the bubble surface will be displaced in a virtual pipe (similar to a streamline pipe) with a length equal to the water level h_w as indicated in the diagram. With this assumption, we can then sum up the total normal force acting on the inlet of the virtual pipe by

$$F_A = P_A \cdot A(r_b) \qquad (3\text{-}7)$$

On the other end of the virtual pipe the total force acting by the atmosphere on the water in the virtual pipe is

$$F_{air} = 10^5 A(r_b) \tag{3-8}$$

where we have assumed that the virtual pipe has a constant cross section across its length. Neglecting the pressure due to the height of the water (20 *mm* to 100 *mm* in practice), the net force acting on the water that is to be displaced is

$$F = (P_A - 10^5) \cdot A(r_b) \tag{3-9}$$

With the mass of water in the virtual pipe being $\rho_w A\ (r_b)\ h_w$ where ρ_w is density of water, the instantaneous displacement speed of the water due to pressure difference is

$$V_{bp} = V_{bpo} + \int_0^t \frac{(P_A - 10^5) A(r_b)}{\rho_w A(r_b) \cdot h_w} dt = V_{bo} + \int_0^t \frac{(P_A - 10^5)}{\rho_w h_w} dt \tag{3-10}$$

where the bubble area has been cancelled. V_{bp0} is the initial speed of the bubble. It is assumed to be zero in the simulation.

Equation (3-10) is a simple and ideal representation of the bubble displacement process. It has been noticed in the simulation results to be presented in this chapter that once the water is accelerated at the initial stage of arcing with a high pressure in the bubble, the dimension of the bubble will continue to grow at a relatively high speed due to the inertia of the water in the virtual pipe, leading to a very low pressure in the bubble. In practice there is viscous effect in the body of water which will help prevent this type of overshot of the bubble size. To take this factor into account, we simply reset the bubble displacement speed due to pressure difference to zero when the pressure in the bubble is lower than the atmospheric pressure. The effect of this setting will be discussed in the result section.

3.4.3 Bubble Growth Due To Water Evaporation

The growth of the bubble size is also affected by the evaporation of water at the bubble surface. In the absence of force on the bubble surface due to pressure difference, the bubble can still expand according to the evaporation rate. Since in the present model we use a spherical shape for the bubble, this implies that the amount of water evaporated is uniformly taken from the whole bubble surface. The amount of vapour produced is assumed to be proportional to the amount of radiation reaching the bubble surface. Evaporation due to heat transfer between the gas and the water is not considered. Assuming the total amount of radiation emitted from the arc core for a unit length of arc column (a hot region where net radiation is emitted out) is Q_e, the amount of radiation re-absorption in the cold surrounding is Q_a, then the amount of radiation reaching the bubble surface is

$$Q_s = Q_e - Q_a \qquad (3\text{-}11)$$

The ratio of Q_a/Q_e is discussed in the radiation model. The energy required to evaporate unit mass of liquid water to vapour at its boiling point is designated by h_{ev}, which includes the enthalpy change from room temperature to the boiling temperature of water and the latent energy of water which is 2.27×10^6 *J/kg*, the amount of water evaporated is then

$$\dot{m} = \frac{Q_s}{h_{ev}} \qquad (3\text{-}12)$$

This amount of water divided by its density will give the volume of liquid water that is evaporated:

$$\dot{v} = \frac{\dot{m}}{\rho_w} \qquad (3\text{-}13)$$

Equating the total evaporation rate of water to the volume of liquid water contained in the layer between the two spheres shown in figure 3.14, then

$$\int \dot{m} dz = A(r) \cdot V_{bs} \qquad (3\text{-}14)$$

where V_{bp} is the speed of bubble surface movement due to evaporation. The combined speed of bubble growth is therefore

$$V_b = V_{bp} + V_{be} \tag{3-15}$$

3.4.4 Numerical scheme for bubble movement

In the simulation the movement of bubble surface is implemented by changing the liquid cells immediately outside of the bubble into gas according to the bubble radius. The criterion is that all cells whose distance (from the cell centre) to the origin of the bubble is smaller than the bubble radius will be set as gas cells at the beginning of each time step in a transient simulation. However, simply changing a cell form liquid into gas does not guarantee the conservation of mass, momentum and energy, therefore is incorrect.

In reality, the flow of gas just by the bubble surface is determined by two processes. Firstly, for an evaporating surface, the water vapour generated from the bubble surface adds mass, momentum and energy to the cells by the bubble surface. These sources tend to force the gas to flow towards the interior of the bubble. At the same time, the continuous expansion of the bubble has the effect of taking gas away from the cells by the bubble surface. With small size of cells, the conservation of mass requires that the reduction of mass per unit time in the boundary gas cells as a result of bubble expansion should be equal to the total volume of cells that are changed from liquid to gas in unit time. Mathematically this can be expressed by

$$\delta A S_s dt = -\delta A V_b dt \rho_{gas} \tag{3-16}$$

which can be further simplified as

$$S_s = -V_b \rho_{gas} \tag{3-17}$$

To simplify the numerical scheme, it is necessary to convert the negative surface mass source given by equation (3-17) into a volume source. This is achieved by decomposing the bubble growth speed into two velocity components as shown in figure 3.16 for a grid system that is close to orthogonal. The negative volume source obtained for the boundary cells is

$$S_{bv} = \frac{S_{sr}}{\Delta V} + \frac{S_{sz}}{\Delta V} = \frac{-2\pi r \Delta z \rho_{gas} V_{br}}{2\pi r \Delta r \Delta z} - \frac{-2\pi r \Delta r \rho_{gas} |V_{bz}|}{2\pi r \Delta r \Delta z} = \frac{-\rho_{gas} V_{br}}{\Delta r} - \frac{-\rho_{gas} |V_{bz}|}{\Delta z} \quad (3\text{-}18)$$

where *Ssr* and *Ssz* represent the decomposed surface mass source given in (equation 3-19 and 3-20). It is found that, due to the solution process of PHOENICS, the density in the liquid cells needs to be set in a particular manner to make sure the computed results are correct. Since this is package dependent, the details will be neglected despite it required much substantial coding effort.

$$V_{br} = \frac{(y-y_0)V_b}{\sqrt{(z-z_0)^2+(y+y_0)2}} \quad (3\text{-}19)$$

$$V_{br} = \frac{(y-y_0)V_b}{\sqrt{(z-z_0)^2+(y-y_0)2}} \quad (3\text{-}20)$$

Where x and y are the coordinates of the cell centre.

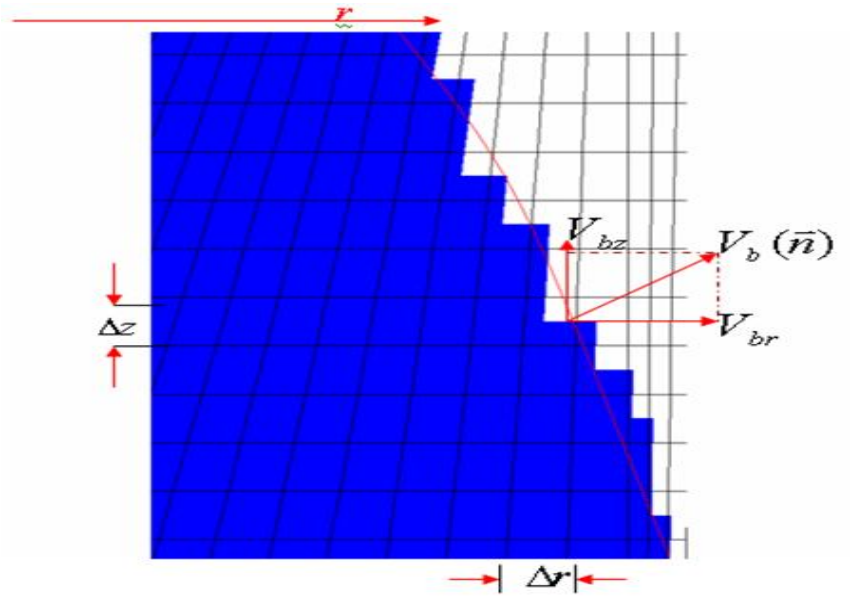

Figure 3-15 Implementation of bubble growth in BFC grids.

3.5 Results and Discussion

3.5.1 The formation of a proper arc column

In the present work the arc is initiated with a hot column in water vapour as shown in figure 3.9 with a current of 30 *A*. The maximum temperature in the arc is initially set to 24,000 *K*, which is very much higher than the real arc temperature. Since the anode vapour comes into the domain at a high speed (200 *m/s*), carbon species is rapidly convected towards the cathode. At 5us, most of the arc column is filled with carbon (figure 3.16c). The arc column at this time is also expanded with an adjusted temperature distribution (figure 3.16b). The maximum temperature goes rapidly down to 12,000 *K*. The axial velocity reduces at the cathode surface and the impingement of the carbon jet results in reverse flow also near the cathode. At the same time, water vapour is evaporated at the bubble surface and generates an inwards flow. Reaction between carbon and water vapour produces a small amount of H_2 and CO in the transition region between carbon vapour and water vapour. A swirling flow pattern is

formed around and the anode root (figure 3.16b). Results suggest that the influence of initial arc temperature and size is restricted to the first 5 μs.

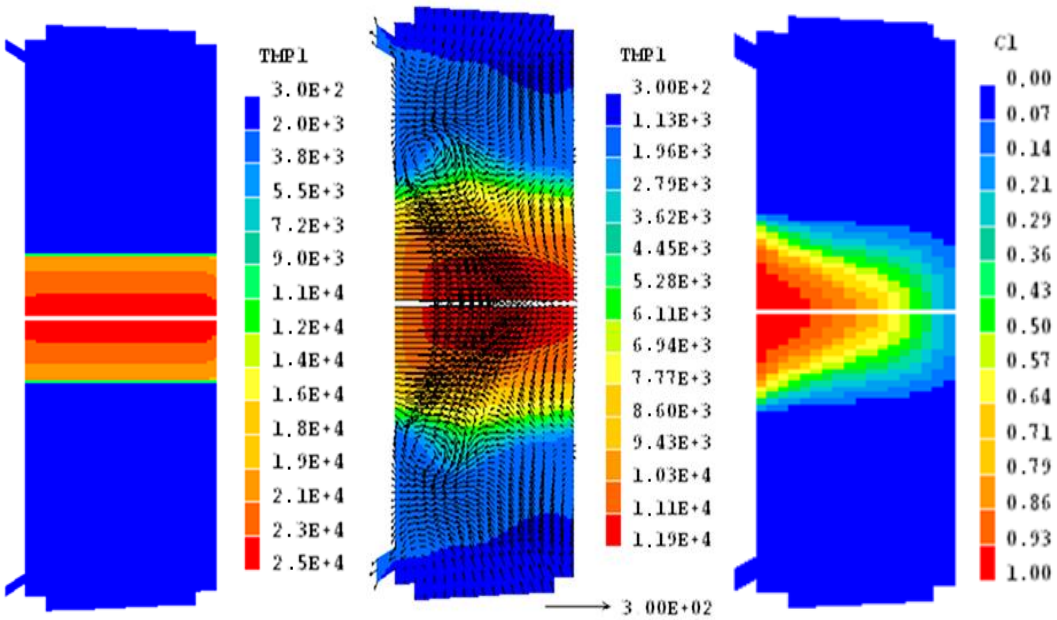

Figure 3.16 Comparison of arc temperature and carbon concentration at initiation and at 5 μs.

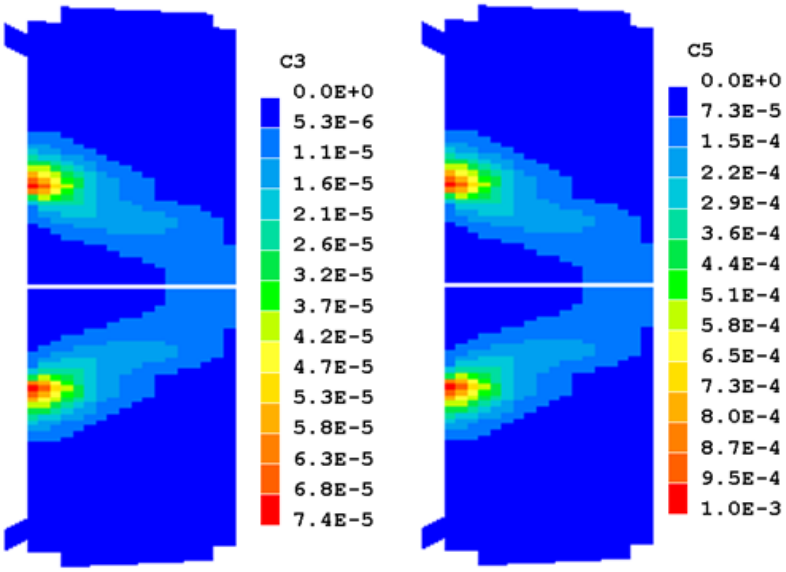

Figure 3.17 Distribution of H2 and CO at 5 us from arc initiation

3.5.2 Development of arc column and transport of carbon species

With time going on, the arc column adjusted its shape and size when the bubble grows. By 4 *ms*, the bubble has grown to a size that connects itself to the escape channel (figure

3.18). The growth speed of the bubble is given in figure 3.18. At the very beginning the bubble has a mall size and the growth of the bubble is mainly due to the retreat of the water surface as a result of evaporation of water by arc radiation. Displacement of water surface by pressure difference is negligible because of the inertia of the water surrounding the bubble. The peak at 30 *μs* is a result of the joint action of pressure increase and temperature decrease inside the arc. The pressure increases as given in figure 3.19 while the temperature decreases rapidly (figure 3.20). The total amount of radiation is relatively stable after the initial arcing stage while the size of the bubble increases steadily. Thus the role played by radiation in bubble growth rapidly diminishes. On the other hand, the injection of carbon species and the heating of the arc surrounding gas by radiation absorption tend to pressurise the bubble and accelerates its growth. At 0.2 *ms*, bubble growth speed due to pressure difference already overtakes that due to water evaporation. The sudden collapse of the bubble growth is a result of a restriction imposed on the pressure difference. At 0.48 *ms* the pressure inside the bubble already drops to the atmospheric pressure due to rapid expansion of the bubble (figure 3.19). As proposed in section 3.4.2, the bubble displacement velocity is set to zero once the pressure inside the bubble is lower than atmospheric. This can be clearly seen in figure 3.21. Resetting the bubble growth velocity to zero stops the pressure drop inside the bubble and it slowly builds up as more carbon vapour is injected into the bubble and more evaporation of water due to arc radiation. This explains the sudden change in growth speed at 0.4 *ms* and 3 *ms*.

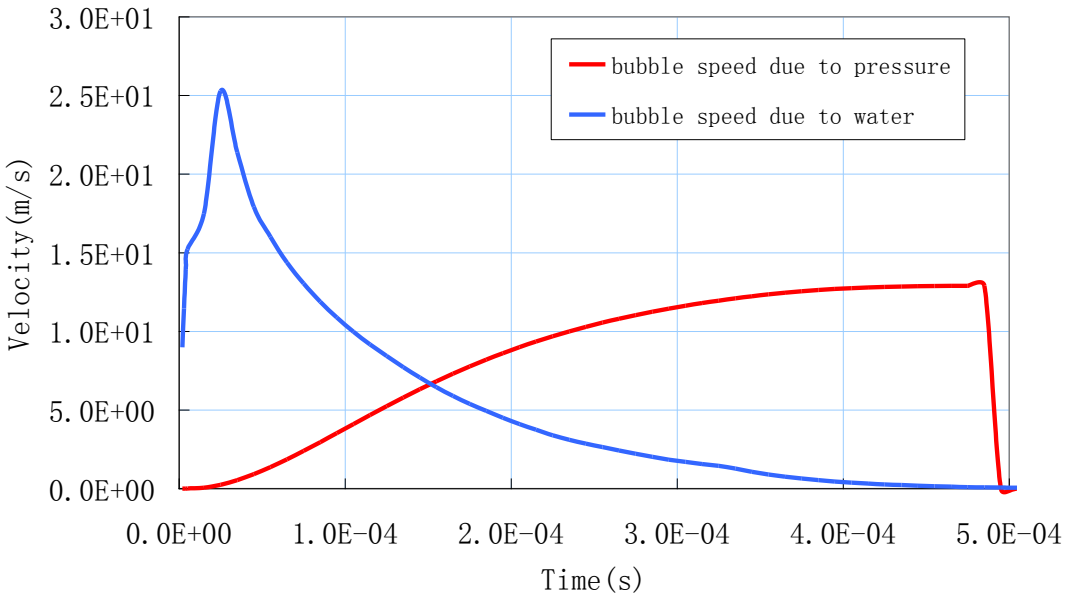

Figure 3.18 Speed of bubble growth as a function of time.

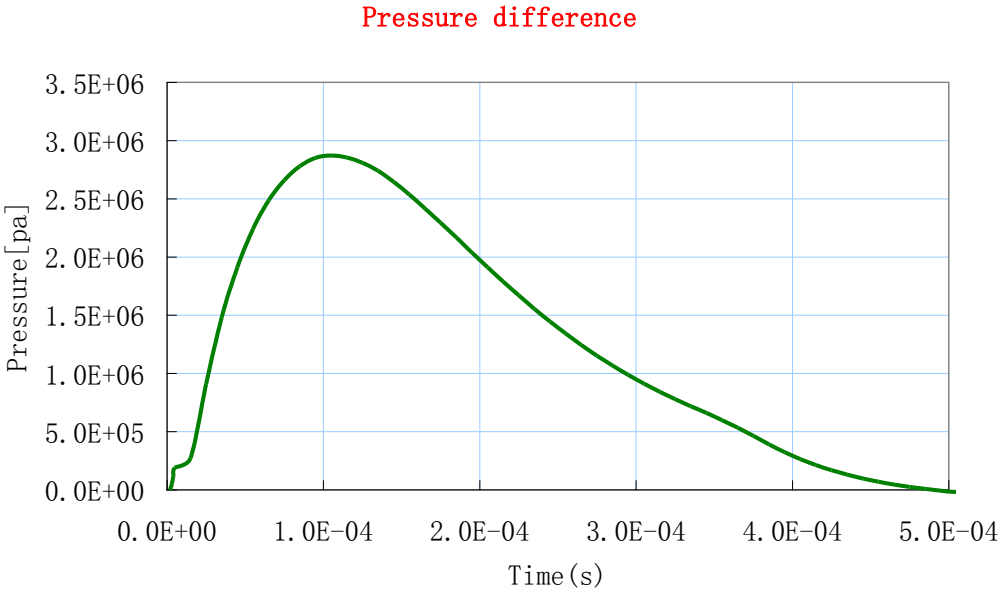

Figure 3.19 Pressure on the axis at the centre of the electrode gap as a function of time.

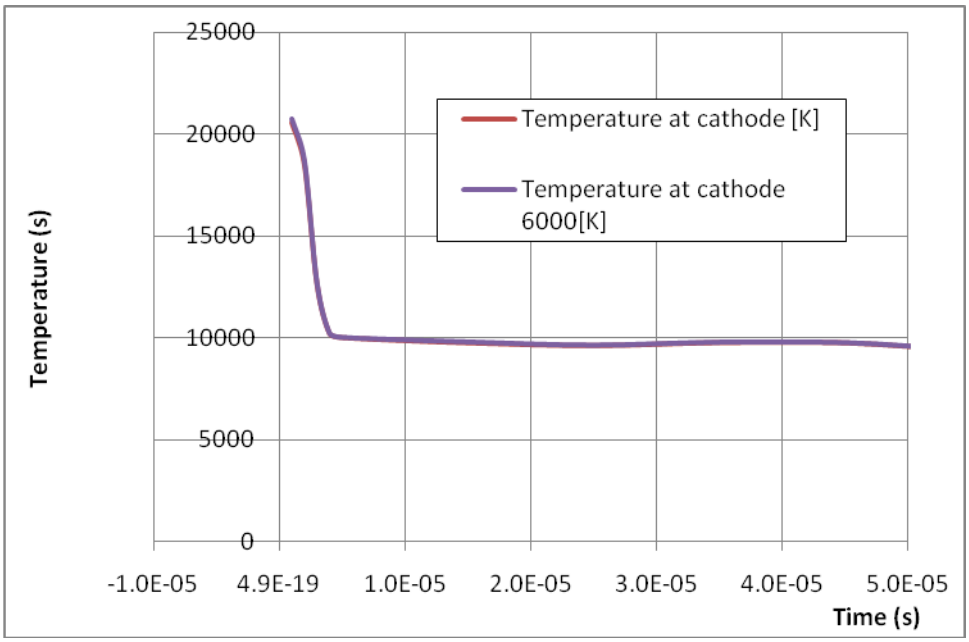

Figure 3.20 Variation of temperature on the axis at the middle of the electrode gap at the beginning of the arcing process.

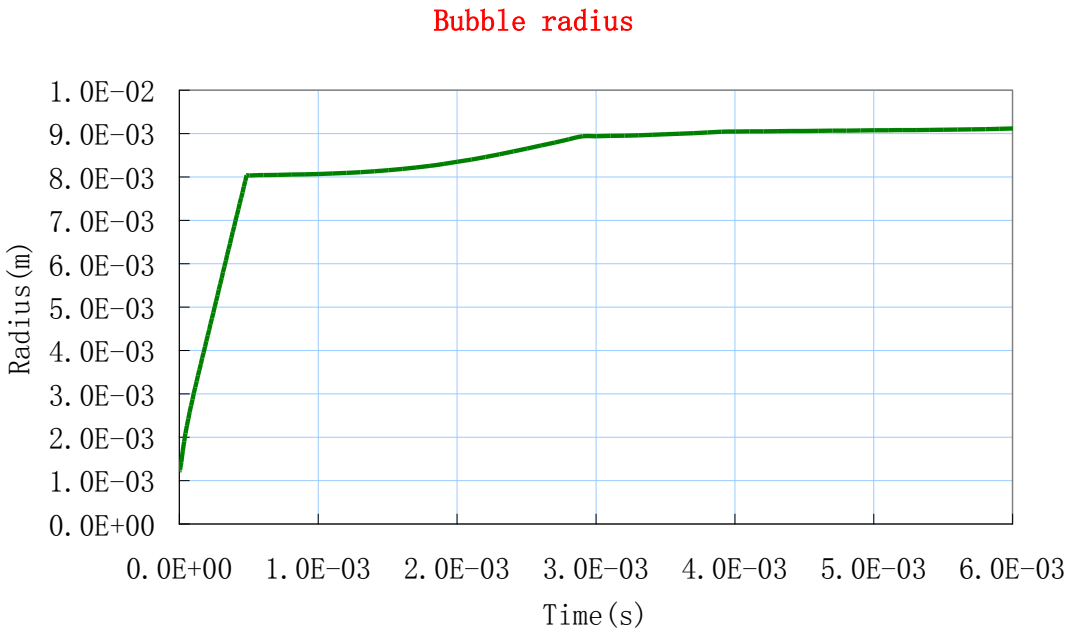

Figure 3.21 Variation of bubble radius as a function of time.

The carbon vapour has been convected and diffused into a much larger region (figure 3.22) at 4ms. Near the anode, the arc burns in pure carbon vapour while near the cathode the carbon vapour concentration drops to 0.85. Our results show that H_2 and CO concentration is low, with their maximum being only 2% and 2.8% respectively (figures 3.23 and 3.24). The maxima for H_2 and CO form a skirt for the arc column at this time. This is understandable since to have maximum reaction rate the product of the concentrations of carbon and water vapour have to be maximum and the temperature as high as possible. The most favourite place for this is the location of 0.5 for carbon concentration (figure 3.23). The outgoing flow field however transports the generated H_2 and CO in the positive radial direction and shapes the maxima of H_2 and CO as illustrated in figure 3.24 and 3.25.

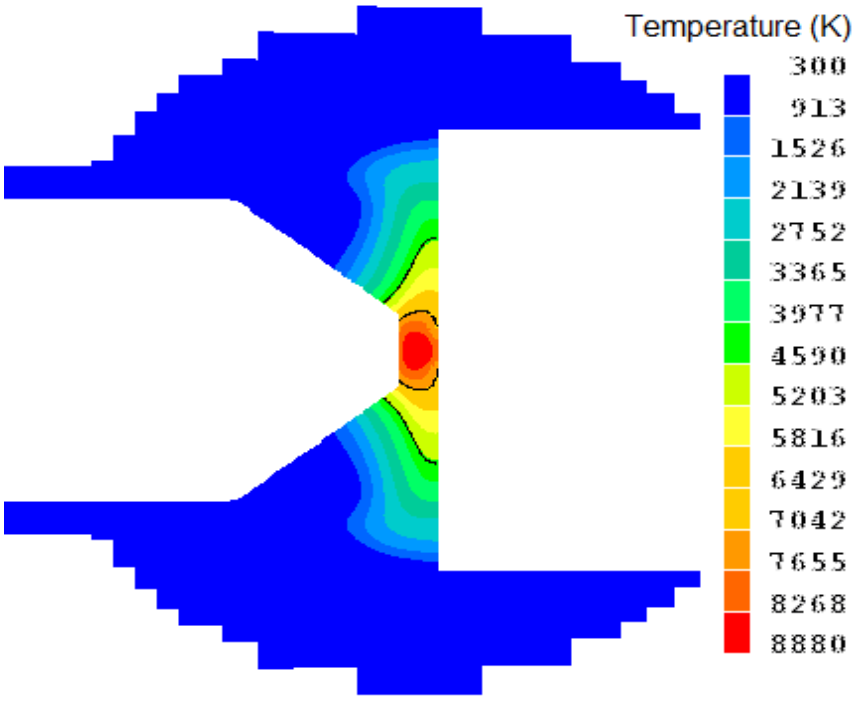

Figure 3.22 Temperature contour with lines indicating temperature of 4500 K and 7000 K.

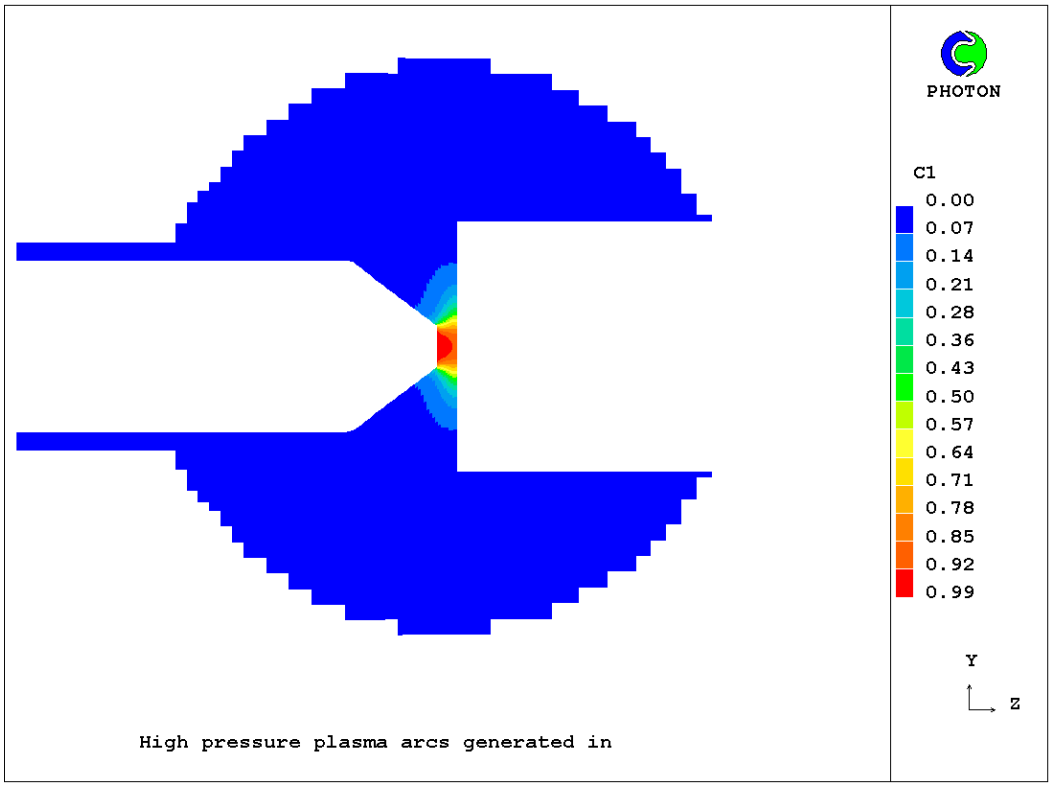

Figure 3.23 Carbon concentration at 4 ms

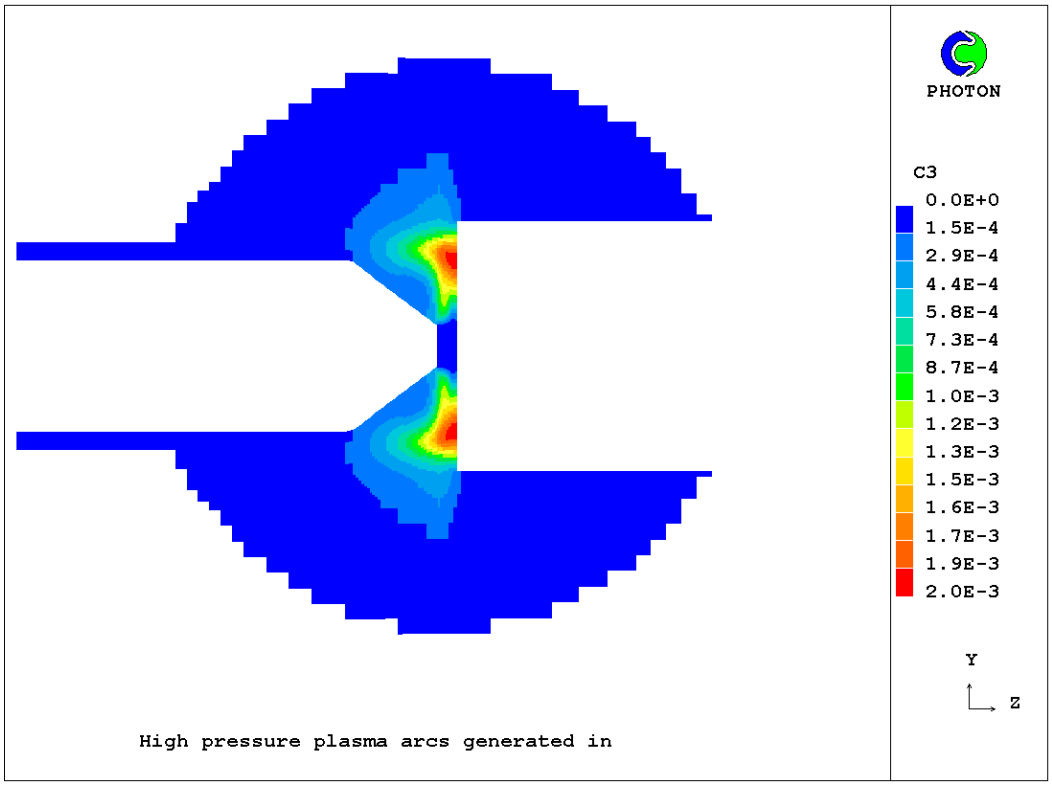

Figure 3.24 Concentration of H_2 at 4 ms

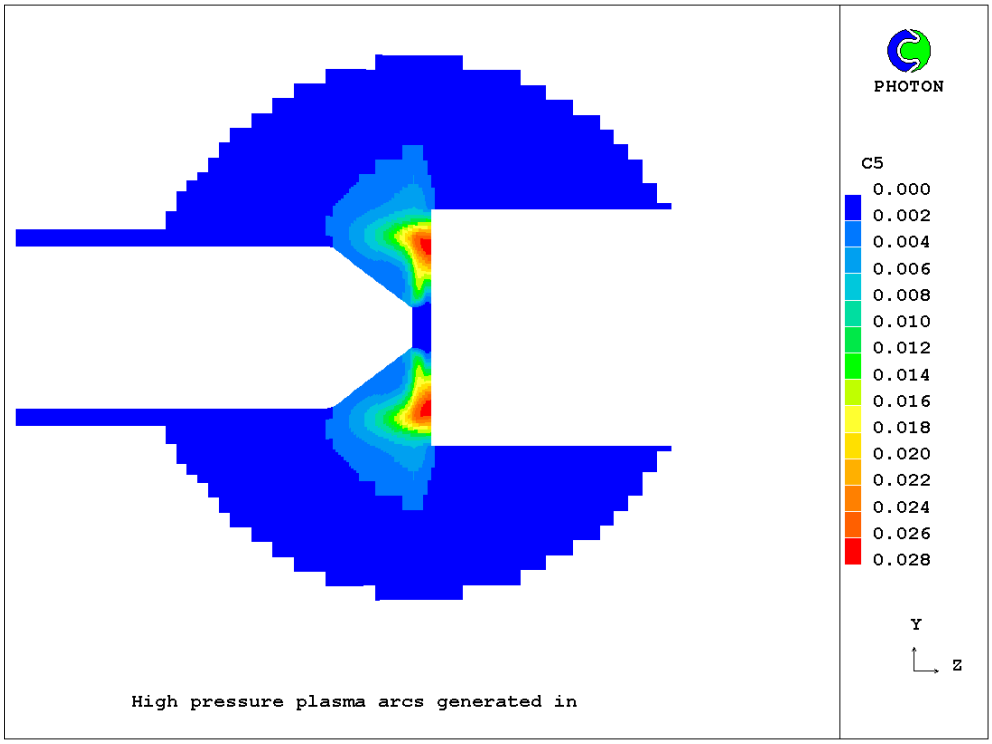

Figure 3.25 Concentration of CO at 4 ms

3.5.3 Characteristics of the arc

As the arc changes its shape and composition, the arc voltage also undergoes a rapid change at the beginning of the arcing process (figure 3.26). The sudden increase in the first 5 μs can be explained by the rapid drop of arc temperature (figure 3.20). The arc voltage then starts to drop. This voltage drop is associated with a number of factors, including pressure, arcing gas composition and arc size. By comparing figures 3.16 and 3.23 it can be seen that there is a significant change of gaseous composition at soon after the arc initiation. The water vapour concentration decreases while the carbon vapour increases. From figure 3.6 it is clear that the electrical conductivity of carbon vapour is much higher than that of the water vapour in the temperature range from 5000 *K* to 10,000 *K*. With an increased electrical conductivity the arc voltage decreases. It then settles down with a value of 7 *V*.

In the arc in water case, the electrodes are cooled by the surrounding water. The conduction energy loss to the cathode surface is calculated using an effective surface temperature of 6,000 *K* (equation (3-3)). The sensitivity of the arc voltage to this temperature has been studied by using a value of 4,000 *K*. An arc voltage of 7.9 *V* was obtained, representing a change of 12.8%. The arc voltage is increased as a result of arc cooling leading to a lower electrical conductivity near the cathode.

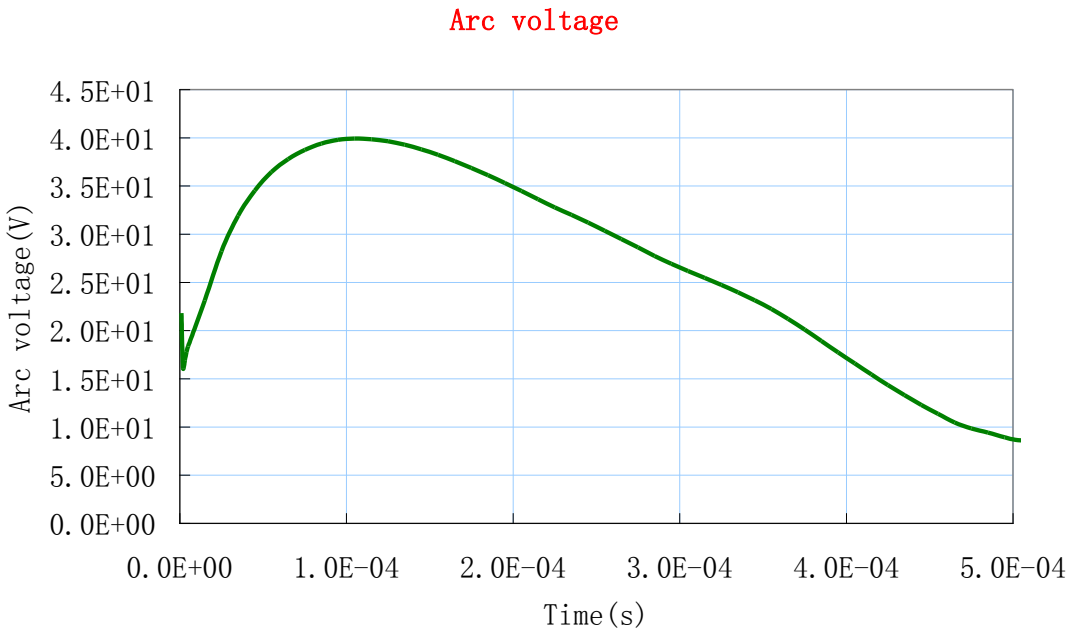

Figure 3.26Variation of arc voltage during the arcing process.

The measured arc voltage for a current of 30 *A* is 17 - 19 *V* [San02]. Our prediction gives a voltage of only 7 *V*. There is a difference of 13 *V*. This difference is mainly because in the present work we only simulates the arc column and the non-LTE electrode layer is not considered. The voltage drop near the cathode corresponds approximately to the first ionisation energy of the atomic species at the arc root, which is 11.26 *eV* for carbon. This explains the major difference. The inclusion of a sheath model for the cathode and anode should therefore be part of the improvement in future.

An accurate comparison of the predicted and measured arc temperature is not possible because the experimental uncertainty is not known, especially in the presence of water surrounding the arc. The axis temperature given in [Lange] is 6500 *K* which is lower than the predicted value of 10,000 *K* in the current work.

An overall mass balance for carbon vapour was carried out, as shown in figure 3.27. The vertical axis represents the rate of each process as a percentage of the total injected carbon vapour mass (kg) at the anode. The curve labelled DIFF (broken red) reflects the overall numerical accuracy of the mass balance calculation. It is generally better than 10%. It can be seen that in the first half millisecond most of the injected carbon vapour is consumed by chemical reaction. This high rate is a result of the carbon vapour encountering the water vapour species inside the arc column at the beginning of the arcing period. After 0.5 *ms*, the arc burns in a carbon vapour dominated environment and the reaction yields decreases. About 60% of the carbon vapour is dumped in the bubble and only 30% is used in the reaction. Despite this, the concentration of H_2 and CO is low, only 0.2% and 2.8% for their maxima as shown in figure 3.24 and 3.25. Carbon loss at the arc edge and near the cathode is low, only 2% of the injected carbon. The dominant water environment in the arc surrounding region can be explained by figure 3.28 which shows that the water evaporation rate (4×10^{-5} *kg/s*) I much higher than the carbon vapour injection rate at the anode (2×10^{-6} *kg/s*).

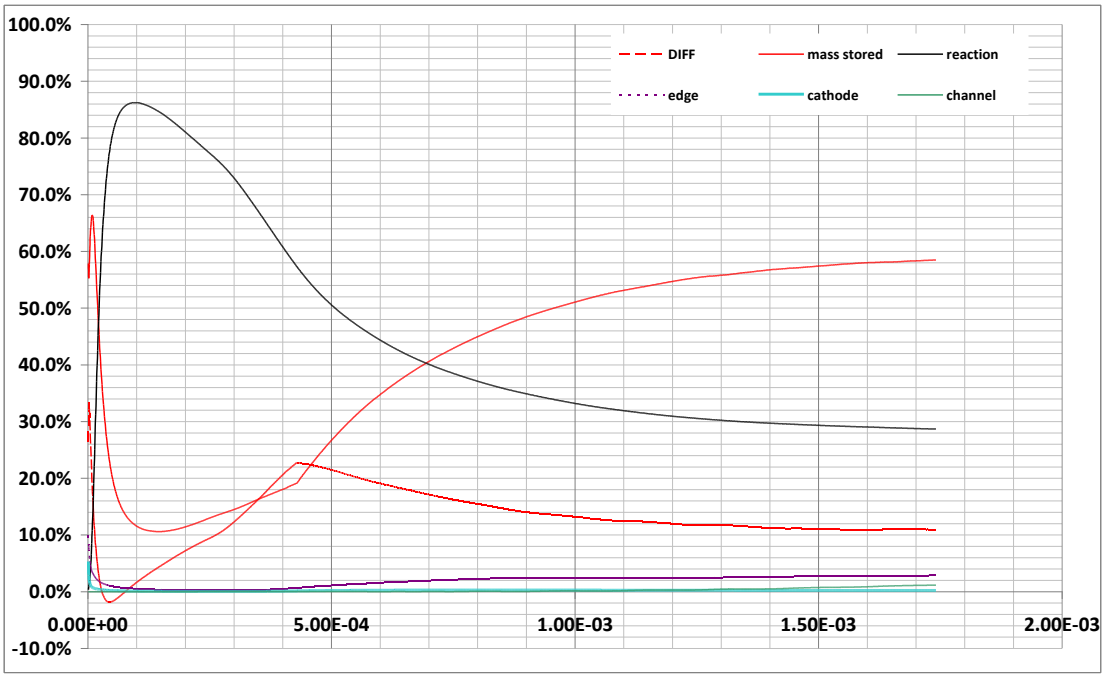

Figure 3.27 Overall mass balance for carbon vapour in terms of percentage of injected mass from the anode. The horizontal axis is time (s).

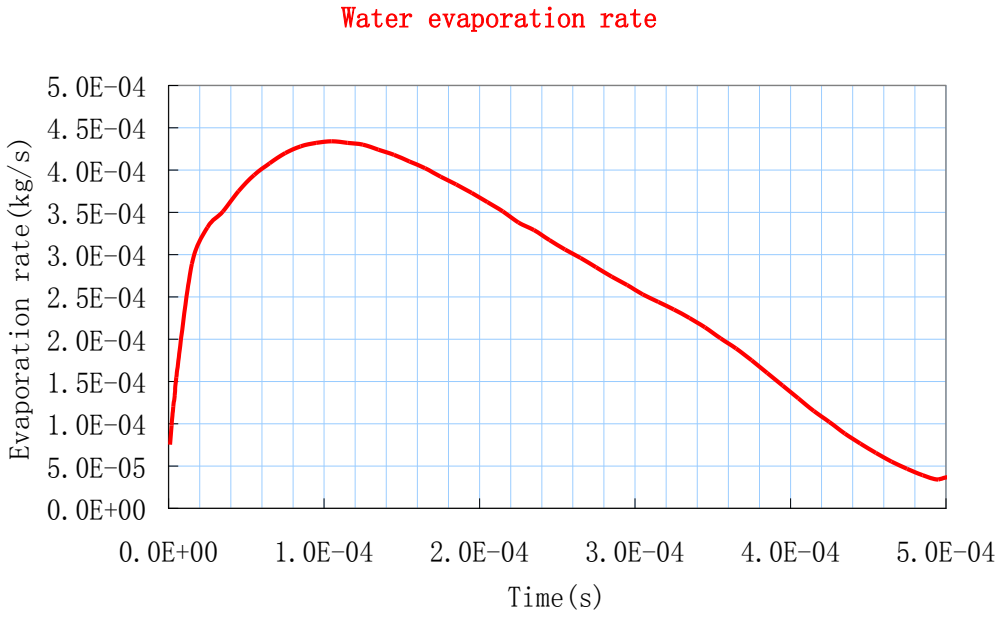

Figure 3.28 Water evaporation rate as function of time

3.6 Summary

The arc in water case is simulated in this chapter. The transport properties were calculated based on interpolation between those of the pure carbon vapour and water vapour. The reason for doing this was also given. The reaction rate coefficient was estimated to be $1.054\times10^{6}\frac{m^3}{mol\cdot s}$ based on published data at 300 *K*. Results have shown that the growth time for the bubble is in the order of millisecond and the electrode gap is rapidly filled by carbon vapour from the anode surface. The growth of the bubble is mainly due to the pressurisation of the bubble by carbon vapour injection. Although about 30% of the injected carbon vapour is consumed by chemical reaction, the concentration of H_2 and CO is rather low, less than 2% and 2.8% respectively. The predicted arc voltage is within a reasonable range if the voltage drop in the cathode sheath layer is considered. An improved model for the arc in water case must include the sheath layer in future.

3.7 References

[Hsi01] Hsin Y. L., Hwang K. C., Chen F. R. and Kai J. J., "Production and in-situ Metal Filling of Carbon Nanotubes in Water", Adv. Mater. Vol. 13, No. 11, 2001

[Gleizes] Gleizes, A., Private communication.

[Zhu02] Zhu H. W., Li X. S., Jiang B., Xu C. L., Zhu Y. F., Wu D. H. and Chen X. H., "Formation of carbon nanotubes in water by the electric-arc technique", Chem. Phys. Lett., 366, pp. 664-669, 2002

[Hus75] Husain, D., and A. N. Young , Kinetic investigation of ground state carbon atoms C(2 3*Pj*), *J. Chem. Soc., Faraday Trans. 2*, *71*, 525–531. 1975

[San02] Sano N., Wang H., Alexandrou I., Chhowalla M., Teo K. B. K. and Amaratunga G. A. J., "Properties of carbon onions produced by an arc discharge in water", Journal of Applied Physics, Vol. 92, No. 5, pp. 2783-2788, 2002

Chapter 4 Computer Simulation of the Arcing Process in a Puffer Circuit Breaker

4.1 Introduction

As discussed in Chapter1, SF_6 based puffer circuit breakers are still exclusively used in the EHV and UHV range up to 1000 *KV*. The design of puffer circuit breakers at such a voltage rating, in terms of its interruption and insulation capacity, still relies heavily on experience and test, and the safety margin is normally larger than the lower voltage-rating circuit breakers. Major international circuit breaker manufacturers are investing heavily in developing the technologies to increase the voltage rating, interruption capacity and reduce the overall size and manufacturing cost. The development effort can be seen in a recent renewed interest in the understanding and modelling of the whole arcing process in puffer type circuit breakers [Ior08, Lia07, San06] with the aim of guiding product design and reducing development cost.

For puffer circuit breakers, there are still large discrepancies between measurement and prediction, especially of arc voltage. The objective of the work in this Chapter is to review the specific features of the arcing process associated with puffer circuit breakers with hollow contacts, and to develop an arc model that can be used to simulate the arcing process in high voltage puffer circuit breakers and is able to produce realistic results that agree reasonably well with available test results. It can then be used to simulate different arcing situations to help optimising product design.

The test conditions and available results are introduced firstly in Section 4.2. The issues relevant to the modelling of arc root are discussed in Section 4.3. The Grid system, initial and boundary conditions are summarised in Section 4.4. Results are then presented in four successive sub-sections of Section 4.5, corresponding to the No-Load phase of the puffer circuit breaker operation (Section 4.5.1), the high current phase (Section 4.5.2), the current zero period (Section 4.5.3), and the post arc period (Section 4.5.4). A summary of the work in this chapter is given in Section 4.6.

4.2 Test Conditions and Available Results

4.2.1 Calibration and synchronisation of measurement

The test results used in this chapter for the verification of the arc model were provided by Henan Pinggao Electric Co Ltd as part of a collaborative project. Before these test results are used for comparison with the simulation results, their accuracy has to be checked. In addition, translation of the time scales in the oscilloscopic records needs to be performed since synchronisation between the pressure and arc voltage records using two different oscilloscopes is maintained by the current waveform. Thus it is necessary to check the agreement of electric current records from two different current probes (each oscilloscope uses a separate current probe). The use of two oscilloscopes is based on safety considerations.

The electric current can be obtained from the oscilloscope data by applying a calibration scheme represented by the following equation

$$I_{real} = C(V_i - V_{ref}) \tag{4-1}$$

where I_{real} is the current in Amps, V_i the recorded voltage by the oscilloscope in volts (from the current probe), V_{ref} the base voltage with zero current, and C is a conversion coefficient. For the oscilloscope DL750 (Yokogawa), C= 160000 *A/V* is provided by the manufacturer and V_{ref} = -0.0493 *V* by inspecting the raw data from the record using Microsoft Excel. The time base for different oscilloscopes is different. For DL750 the starting time is -30 *ms* while for Tektronix oscilloscope it is -5 *ms*. The electric current obtained from the record of DL750 is shown in figure 4.1 as the broken curve. The peak current in the first half cycle is 65600 *A* corresponding to 46.4 *kA* (rms) and 60600 *A* in the second half cycle. The duration of current is only 19.3 *ms*. This case is therefore referred to as the 47 *kA* case in this Chapter.

Data from the Tektronix oscilloscope is matched to the DL750 current waveform by shifting the time base using

$$t_1 = t_2 - 0.0193 \tag{4-2}$$

where t_1 is the time base for DL750 and t_2 the time base used in the Tektronix oscilloscope. A different calibration is applied to the Tektronix record with C= 11800 *A/V* given by the manufacturer and V_{ref} set to 0.4 *V* in equation (4.1). The results are given in figure 4.1. The two records match well in the first half cycle. The peak from Tektronix in the second half cycle is 57600 *A*, 5% lower than that from the DL750. The peak current in the second half cycle is 5 *kA* lower than that in the first half cycle.

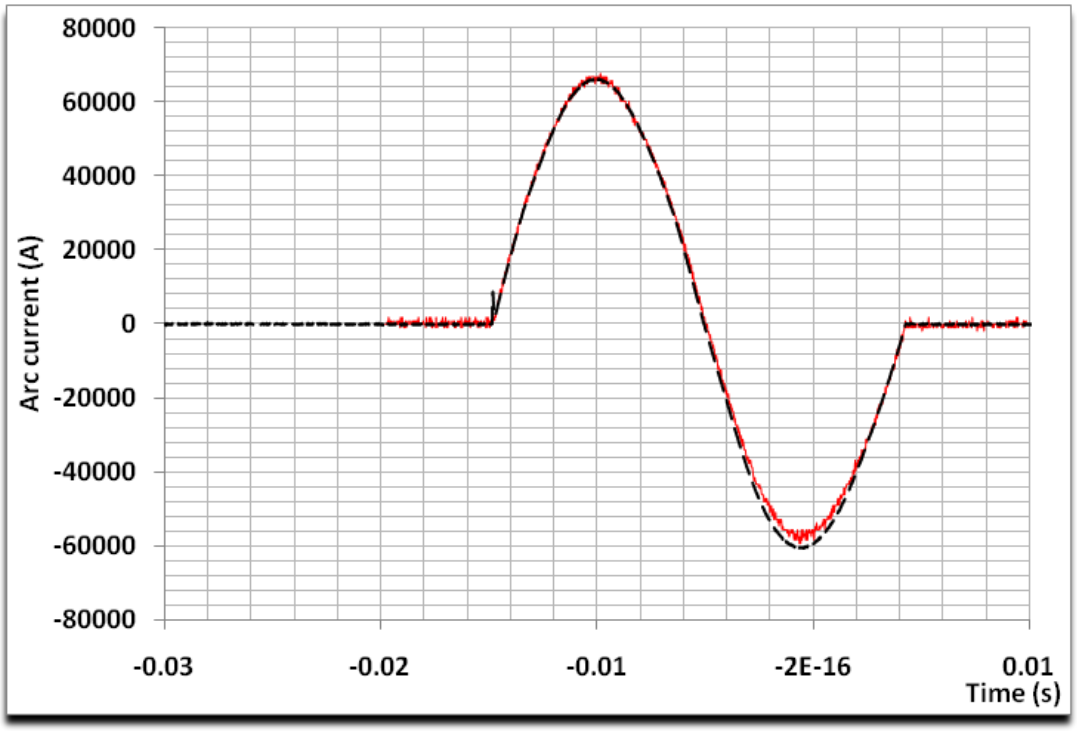

Figure.4. 1 Comparison of the current waveforms recorded by DL750 (broken line, black) and Tektronix (solid line, red) for the 47kA case.

There is a mismatch for the 10 *kA* case between the two current measurements, as shown in figure 4.2. Clearly DL750 produces a longer second half cycle (solid black curve) that does not synchronise with the arc voltage measurement. On the other hand, the current measurement recoded by the Tektronix oscilloscope (green) has very large

noise but is synchronised with voltage. The current for this 10 *kA* case is therefore smoothed before used in the simulation, as shown in figure 4.3 (orange circles). The data for the other cases (24 *kA*, 46 *kA*) are checked and processed in a similar approach to that of the 47 *kA* case.

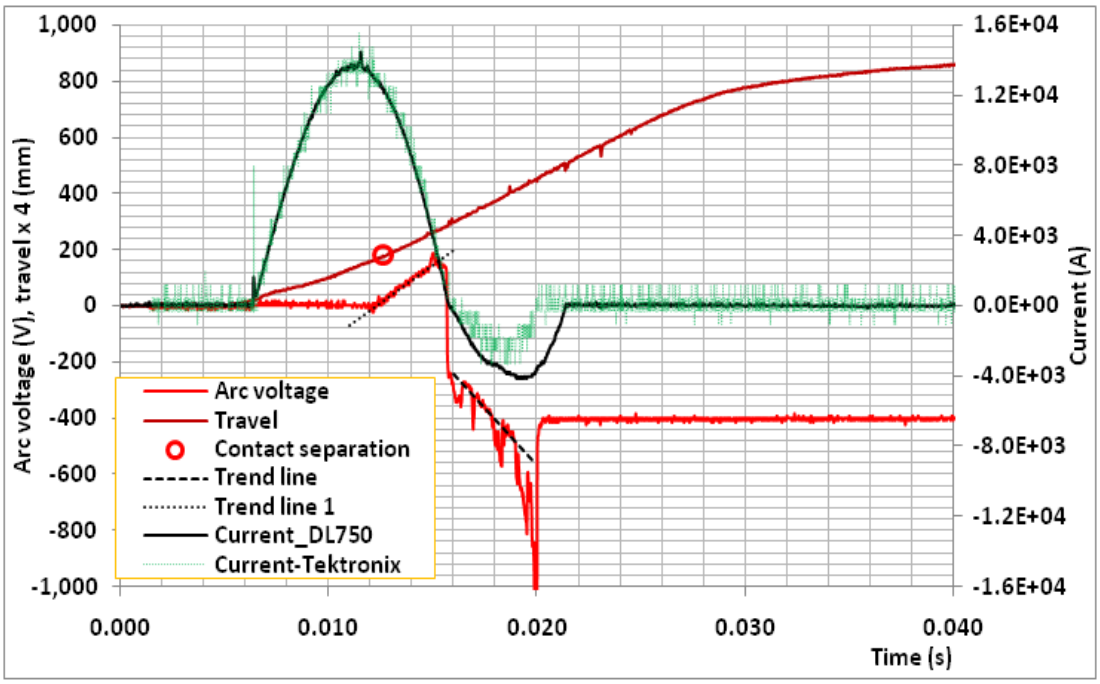

Figure.4. 2 Contact travel, current and arc voltage measurement for the 10kA case.

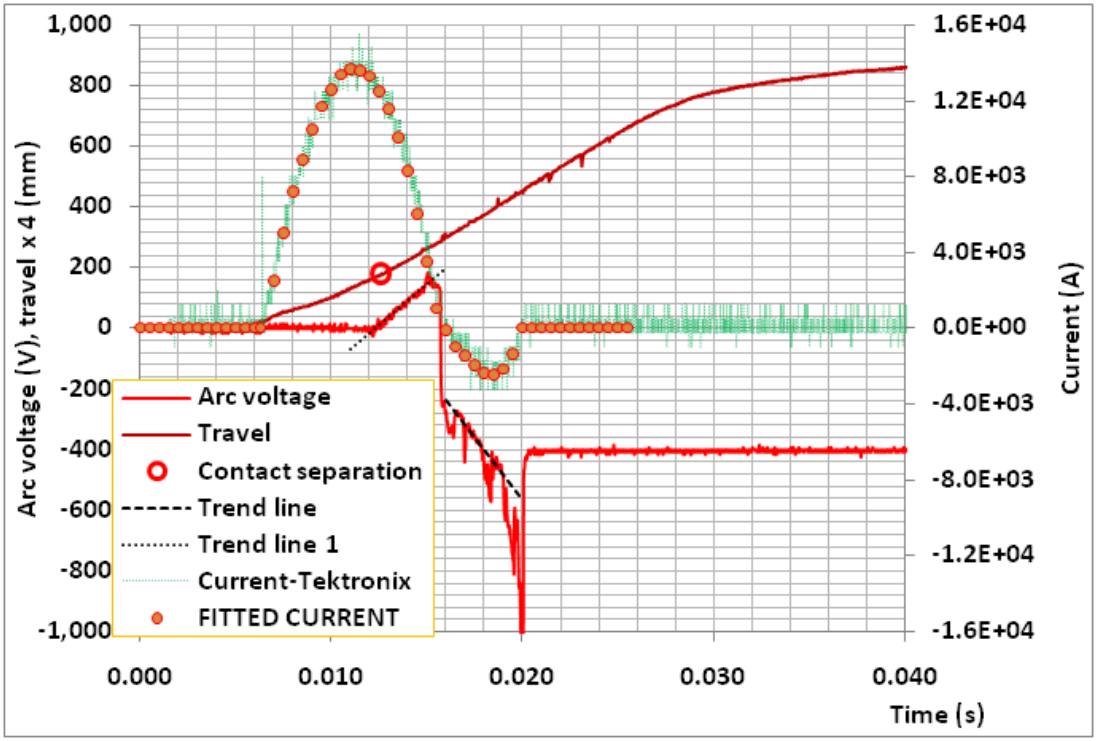

Figure.4. 3 Contact travel, smoothened current and arc voltage measurement for the 10kA case.

Tests at different current levels using a prototype 252 *kV* puffer circuit breaker were carried out to provide valuable information for verifying the arc model. Pressure inside the puffer cylinder, contact travel, arc voltage and current waveforms were measured. The four cases are summarised in Table 4.1.

Table 4. 1

Test ID	**Arcing duration (*ms*)**	**Maximum contact speed (*m/s*)**	**Peak current in last loop (*kA*)**
10 kA	7	9.6	2.5
24 kA	11.5	9.2	30
46 kA	6	9.2	65
47 kA	11	9.6	57.6

4.2.2 Basic features of measurement: average electric field inside arc column

For verifying the arc model, arc voltage measurement is extremely important. It directly reflects how satisfactorily the arc column is modelled. On one hand, the arc voltage determines the power dumped inside the arc, which affects the gas temperature and pressure distribution in the arcing chamber including the puffer not only in the high current phase, but also indirectly in the period around current zero. One the other hand, the temperature at the arc centre is largely determined by the balance of radiation and Ohmic heating and the arc voltage is sensitive to the size and shape of the arc column. Therefore accurate arc voltage prediction is a key aspect of the model. The pressure comparison will be of second importance in the verification of the simulation model for puffer circuit breakers.

At high current levels, such as the case shown in figure 4.4 (47 *kA)*, the measured arc voltage is relatively smooth, indicating that the change of the shape of the arc column is rather gradual because fluctuation in arc voltage is normally associated with sudden

change in the shape or size of the arc column. The average contact speed for period from 14.2 *ms* to 22.45 *ms*, corresponding to the linearly varying arc voltage segment in the second half cycle, is 9.45 *m/s* (figure 4.5) and contact separation takes place near the end of the first half cycle (3.1 *ms* before the first current zero). Using a trend line, the average rate of change of arc voltage with time is estimated to be 47 *kV/s*. With the above contact speed an average axial electric field of 4.97 *kV/m* is obtained. A sharp extinction peak is present in the experimental record, as shown in figure 4.4b. Unfortunately there is a lack of information regarding the dynamic response and accuracy of the measurement of the extinction peak. Caution therefore needs to be exercised on drawing conclusions from a comparison of the predicted and measured extinction peaks of the puffer circuit breakers.

At lower currents, such as that in the 10 *kA* case (figure 4.3), the arc voltage is no longer smooth, exhibiting strong fluctuations and the current amplitude is below 3 *kA* in the second half cycle. The fluctuation in the measured arc voltage is possibly associated with arc instability (including movement of arc root on the surface of hollow contacts) and deformation of arc column. Shortly after contact separation at 12.6 *ms*, the arc voltage increases linearly up to 15.2 *ms* corresponding to a contact gap of 22.5 *mm*. The arc in this period is stable and the arc voltage increases smoothly. The contact speed between 12 *ms* and 15 *ms* is approximately 8.33 *m/s*. The rate of change of the arc voltage in this period is 54 *kV/s*. Using the average contact speed, we obtain an axial electric field strength of 6.48 *kV/m*. In the second half loop, the rate of change of arc voltage between 15.74 *ms* and 20 *ms* is 81.6 *kV/s*, and the average contact speed is 8.9 *m/s*. So the order of magnitude of the axial electric field in the second half cycle is estimated as 9.17 *kV/m*. This suggests that arc at relatively low current is subject to more severe cooling as a result of arc instability (including turbulence) and deformation of the arc column and the axial electric field is thus stronger than that in the higher current cases.

4.2.3 Basic features of measurement: extinction peak

An extinction peak was observed in all four cases and for the three cases of 24 *kA*, 46 *kA* and 47 *kA* (all are in RMS values) the arc voltage starts to rapidly increase at approximately the instantaneous current of 15 *kA* before the final current zero (figure 4.4b, red curve).

The nozzle throat radius of the 252 *kV* puffer circuit breaker is 15.5 *mm*. The development of the extinction peaks from 15 *kA* in all three cases is an important feature. Arc cooling by turbulence can only occur if there is a significant layer of cold flow where turbulent eddies can exist. It implies that at 15 *kA* cold gas from the puffer is able to isolate the arc column from the nozzle and build up a normal nozzle flow. In this sense, the end of the high current phase is defined as the point when the current reaches 15 *kA* before the final current zero for the three higher current cases.

For the 10 *kA* case, the rapid rise in arc voltage starts at 1500 *A* before the final current zero. The record of the extinction peak together with the arc voltage measurement in the 10 *kA* case provides also valuable information for studying the turbulence effect at low current. Different from the 47 *kA* case, the current when the arc is on is low (<2.5 *kA*) and around the peak current arc parameters changes slowly. This low current case should have some of the features of a steady state arc.

The pressure variation in the cylinder remains smooth in the 10 *kA* case as shown in figure 4.6. The arc does not significantly alter the pressure variation in the cylinder in comparison with the no-load case (the latter is not shown). The pressure measured on the inner surface at the middle of the flat nozzle throat exhibits a large pulse that cannot be explained in straightforward manner because it is well above the pressure in the cylinder. Because of the uncertainties in this pressure measurement, the measurement taken in the puffer cylinder will only be used in the comparison with simulation results. At higher current levels (figure 4.7), the pressure in the cylinder is subjected to significant pressure waves as a result of arcing. The pressure was measured on the

piston surface. The other pressure measurements at different locations inside the cylinder are similar and therefore will not be shown. The oscillation in cylinder pressure is possibly triggered by the sudden occurrence of the arc in a way assimilating explosion. It lasts well after the current passing through its final zero point, which suggests that the oscillation has a non-electric or magnetic nature. A two dimensional model is not able to catch the full characteristics of the pressure oscillation.

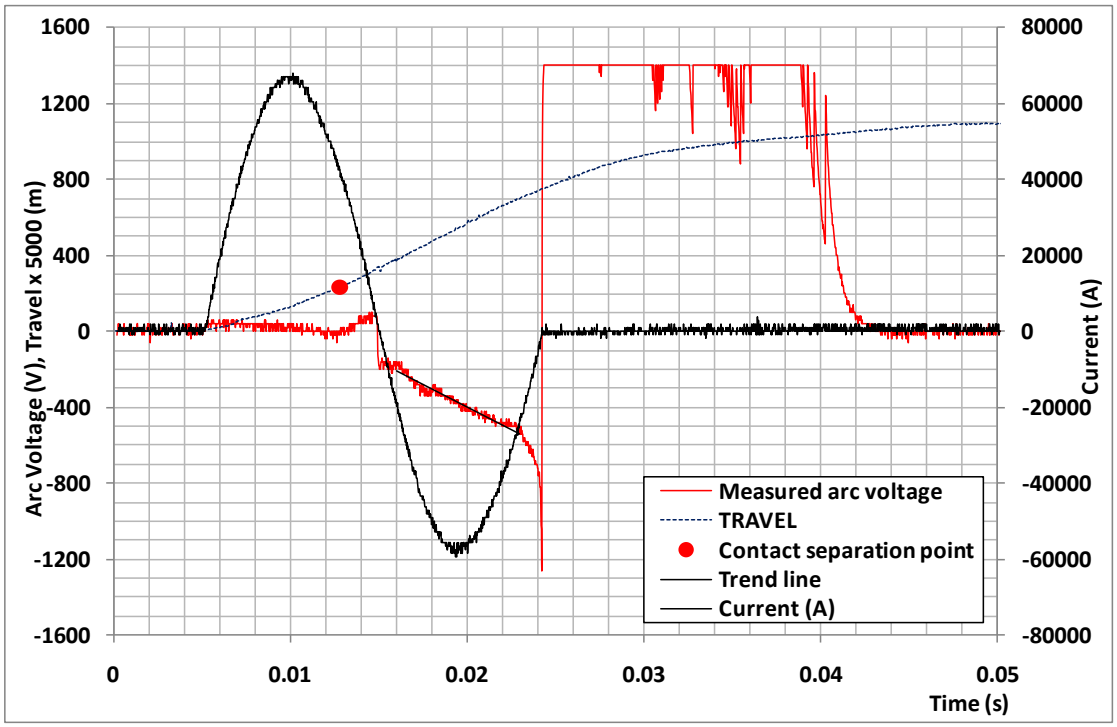

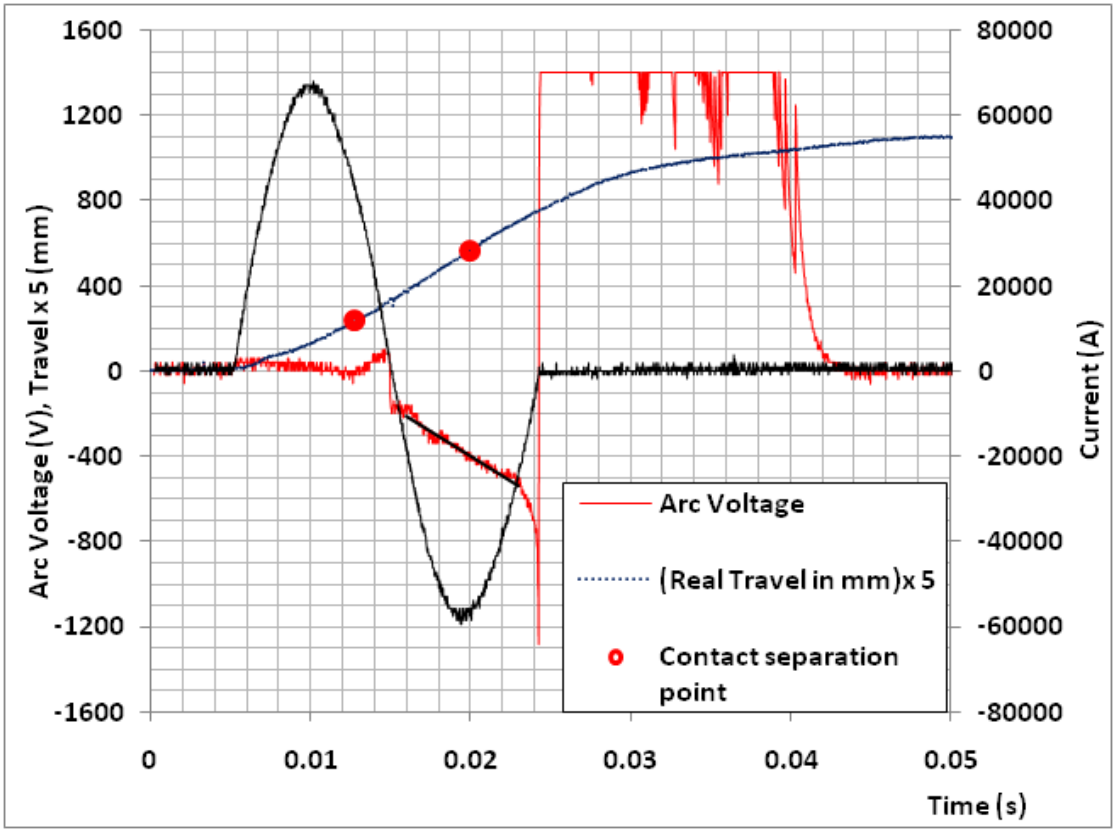
1600
1200
800
400
0
-400
-800
-1200
-1600
Arc Voltage (V), Travel x 5 (mm)
80000
60000
40000
20000
0
-20000
-40000
-60000
-80000
Current (A)
0
0.01
0.02
0.03
0.04
0.05
Time (s)
Arc Voltage
(Real Travel in mm)x 5
Contact separation point

(a)

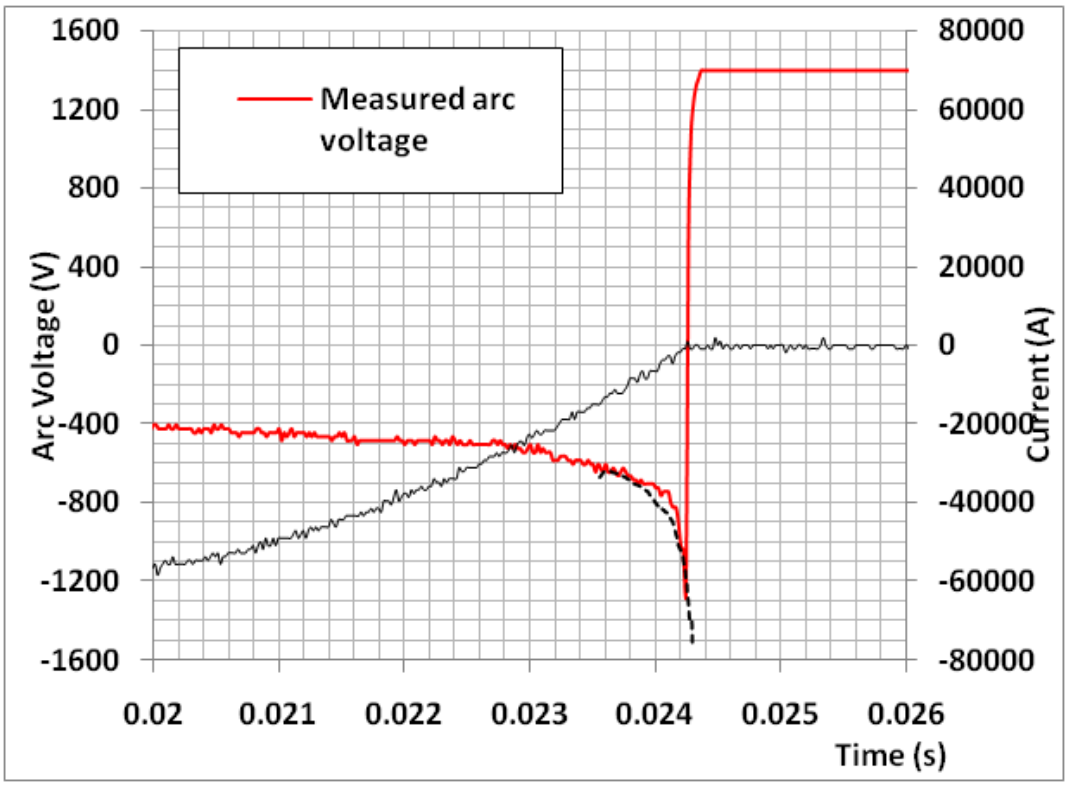

(b)

Figure.4. 4 Measurement for the 47 kA case. (a) Current, travel, arc voltage, and (b) the measued and predicted extinction peak.

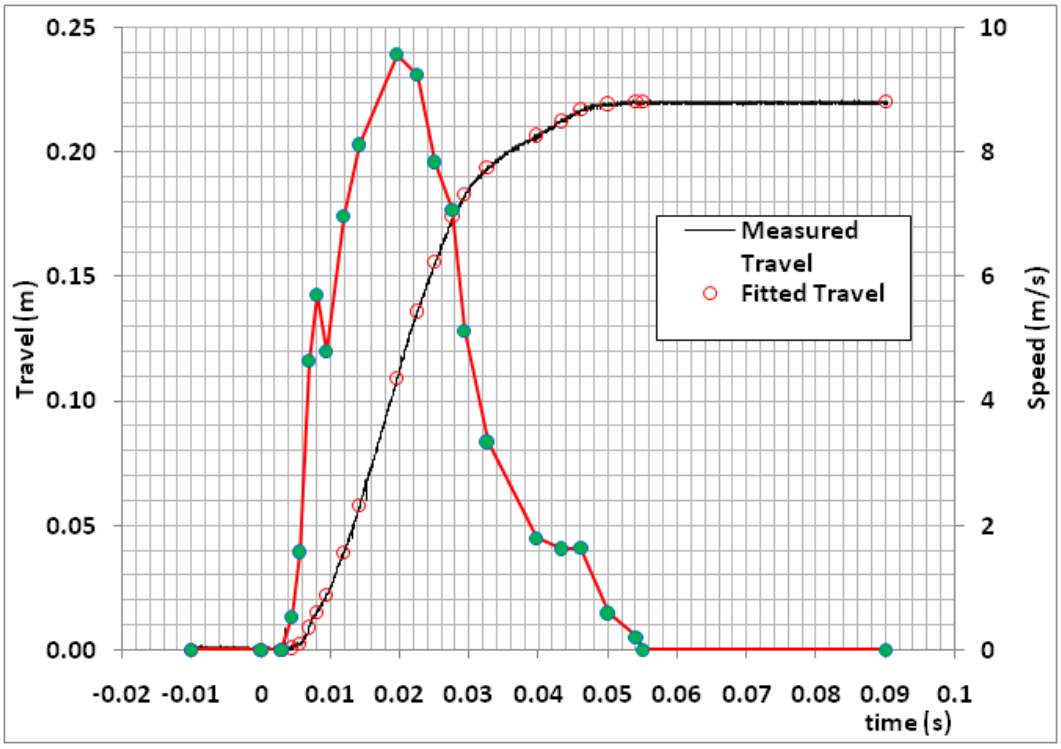

Figure.4. 5 Contact travel and speed derived from the original record and to be used in the simulation for the 47 kA case.

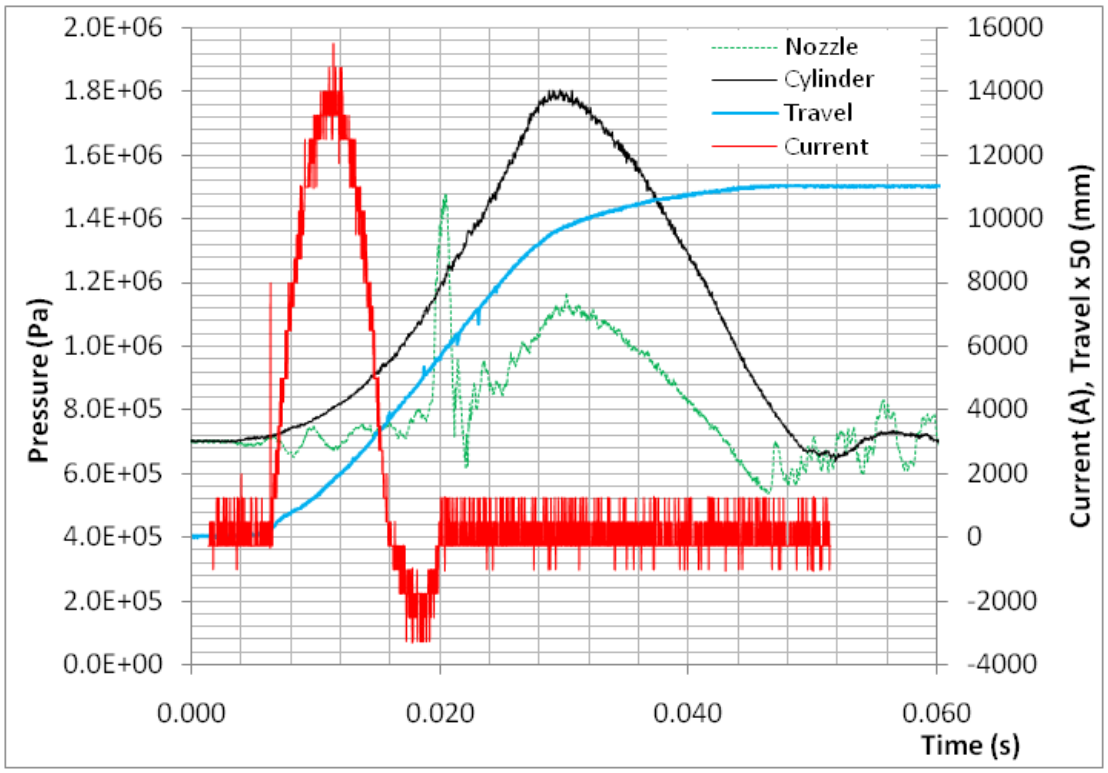

Figure.4. 6 Pressure measument at two locations for the 10 kA case.

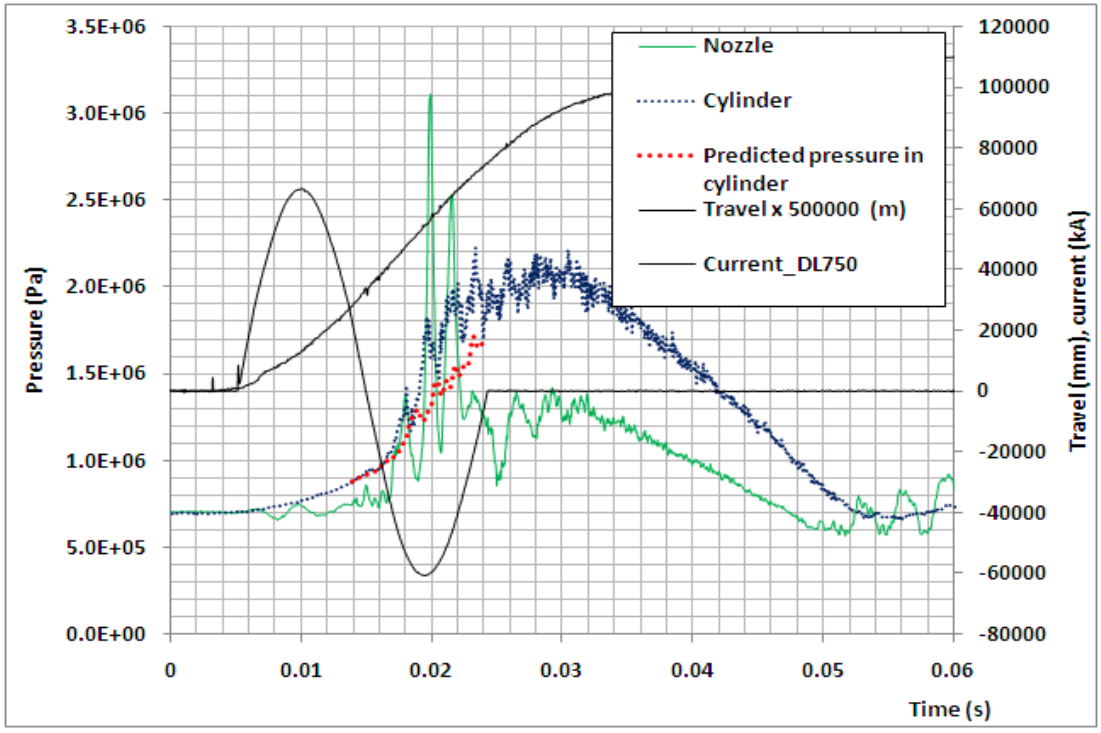

Figure.4. 7 Pressure measument at two locations for the 47 kA case.

4.3 Modelling of Arc Root near Hollow Contacts

Puffer circuit breakers with double hollow-contact arrangement, which is intended for maximum energy and metal vapour removal from the contact gap, creates additional complication for the simulation of the high current arcing phase. Firstly, it requires, with a two dimensional axisymmetric arc model, the use of transparent contacts to provide current collection from the arc column when the principle of current continuity is used to obtain the electric potential and electric field in the arcing chamber. The transient nature of the arcing process and the complex flow field, especially with the presence of strong Lorentz force which is directly coupled to the current density distribution, implies that unrealistic shapes of the arc column near the tips of the hollow contacts could be computationally produced if the arc roots are not properly dealt with. As discussed in Chapter 2, a short segment of unreasonably contracted arc column could take up to 30 % of the predicted arc voltage and result subsequently in a large increase in the latter. This sudden surge in arc voltage is however not observed in the measurement. Therefore the treatment of arc rooting in hollow contacts forms an important part of the present work. Several key issues associated with realistic computer simulation of arcs in puffer circuit breakers are discussed in light of the experimental results. Different test cases were simulated to assess the effectiveness of the proposed approach.

Arc rooting in circuit breakers with hollow contacts is an extremely complicated phenomenon. Apart from the physical mechanisms responsible for the non-LTE layer in front of an electrode surface [Ret96], there are further complications involved here. Firstly, in reality the arc column is attached to the surface of the hollow contacts and the position and size of the arc attachment is affected by the interaction between the current in the plasma column and the magnetic field produced by the current in the metallic contacts as well as in the external circuit to which the breaker is connected. Secondly, surface condition of the electrode affects the movement of the arc root. So far there has been no verified model that can successfully deal with 3D arc rooting in circuit breakers.

Since in reality the arc root is normally attached to the tip or inner surface of a hollow contact and at high current it is possible the arc column connects to the contact by one or more arc attachments (theoretically it is possible although for high pressure arcs multiple attachments of arc to electrode have not been observed.) as schematically indicated by the dotted line in figure 4.8. A contracted arc column sitting on the axis near the tip of the hollow contact is naturally the most unfavoured scenario. Computationally however, the results conform to the governing equations when a transparent contact fills the hole of the hollow contact. The arc root in front of the transparent contact is free to adjust its size under the influence of strong pinching Lorentz force. However, this is sensitive to the current density assumed at the transparent cathode.

Detailed analysis of the results shown in figure 4.9 suggest that contraction of the arc column in this case is triggered at 15 *ms* when the arc column blocks the hole of the moving hollow contact and the gas originally flowing into the moving hollow contact is forced to change its direction towards the fixed hollow contact. This change leads to stronger cross (radially) flow based convective cooling of the arc column near the tip of the fixed hollow contact and the arc column starts to shrink. The current is high enough so the hole of the hollow contact is almost filled. Newly produced nozzle ablation when the arc column reaches the flat nozzle throat (location close to the pressure measurement point shown in figure 4.8) also contributes to arc column shrinkage by enhancing convective cooling through cross radial flow towards the arc axis. Associated with the contraction of the arc column, the arc voltage rises to 340 *V* at 17 *ms*, which is 120 *V* higher than the measurement of 220 *V* (figure 4.9). At 17.2 *ms*, the arc column broadens rapidly as a result of the formation of circulating hot flow that engulfs the contracted section of the arc column and provides additional electrically conducting path. The spreading of electric current over the enlarged conducting cross section leads to the collapse of strong magnetic pinch. This type of sudden change in arc voltage such as that around 17 *ms* has not been observed in measurement and should not be produced by a realistic arc model.

The discussion above leads to the proposal that, within a two dimensional axisymmetric arc model, the effect of the Lorentz force immediately in front of the tips of the hollow

and transparent contacts must be mitigated to avoid the development of an extreme situation such as that shown in figure 4.8. The following approach was proposed for this purpose:

Firstly, a transparent arc root in front of each hollow contact is used, as shown in figure 4.10 by the pink patches. The thickness of the transparent arc root is chosen as a small fraction of the typical arc length. The initial arc length following contact separation is about 5-8 *mm*. The thickness of the transparent arc root is around 4 *mm* for the high current phase. For current zero period and post arc simulation, there is no need for the use of transparent arc root since the current is low (<15 *kA*) and Ohm's law is used to calculate the axial electric field (slender arc model). Lorentz force plays a moderate role in shaping the arc column.

The radius of the transparent arc root at a particular time, *t*, is determined according to the following equation

$$R_0 = \sqrt{I/\pi J_0} \qquad (4\text{-}3)$$

where I is the instantaneous current at time t and J_0 is an average current density in the arc root whose value is in the range of $5\text{x}10^7$ A/m^2 to $2\text{x}10^8$ A/m^2. The value of $1.5\text{x}10^8$ A/m^2 is found to be a good choice for high voltage puffer circuit breakers under investigation. The electrical conductivity in the tranparent arc root is fixed to a uniform value of $\sigma_0 = 10000\ \Omega^1 m^{-1}$ corresponding to a temperature of 17,000 *K* at 10 *atm*. The axial electric field is thus around $1.5\text{x}10^4$ *V/m*. This value is nearly three times that derived from the 47 *kA* case, which is $4.97\text{x}10^3$ *V/m* (section 4.2.2). The Ohmic heating is thus $2.25\text{x}10^{12}$ *W/s* which is in a reasonable range. The transparent arc roots help maintain the size of the arc roots to be comparable with that observed in reality. It is partucularly effective in sustaining the arc when the flow in the hollow contact is reversed to a direction opposite the normal gas flow and the arc can be easily numerically extingushed.

No current outside the transparent arc root is allowed to flow into the hollow contact body or its transparent contact. It is to be noted that the transparent arc root is only applied in the high current arc phase. When the magnitude of the instantaneous current beofre the final current zero falls below 15 *kA*, i.e. in the simulation of the current zero phase, the trnasparent arc root will no longer be used because an slender arc model is used for the calculation of the electric field.

Secondly, the azimulthal magnetic flux density within 20 *mm* (or half of the contact gap if shorter) from the tip is calculated based on the radial current density in the transparent arc root to mitigate the effect of the Lorentz force.

This approch will enevitably lead to inconsistencies in the model as a result of the fixed curent density and Lorents force inside an in the vicinity of the transparent arc root. For example, the prescribed Ohmic heating of 2.25×10^{12} *W/s* may be diferent from the value based on solution of the continuity equation using real electrical conductivity of the gas. The effect is however expected to be insignificant since the thickness of the transparent arc root is small in comparison with the total arc length and the arc parameters well away from the transparent arc root is controlled by the local Ohmic heating, radiation and flow field. The second consistency issue is Lorentz force. This inconsistency is actually a reflection of the discrepancy between the true distribution of the current density in reality as a result of three dimensional arc rooting near the tip of the hollow contact and the axisymmetric arc model that forces a cylindrical arc root to sit on the axis. An estimation of the magnetic pinching effect for an arc column with uniform current density can be obtained by

$$\Delta P = \frac{\mu_0 I^2}{4\pi^2 R^2} \tag{4-4}$$

where ΔP is the pressure increase on the axis as a result of magnetic pinch with reference to the surrounding gas. At high current, the axial current density in the arc core is rather uniform, as shown in figure 4.11. Therefore the difference is mainly with the radius R. Near the transparent arc root, the arc diameter is close to that of the

transparent arc root and the uncertainty caused by the Lorentz force approximation is again insignificant.

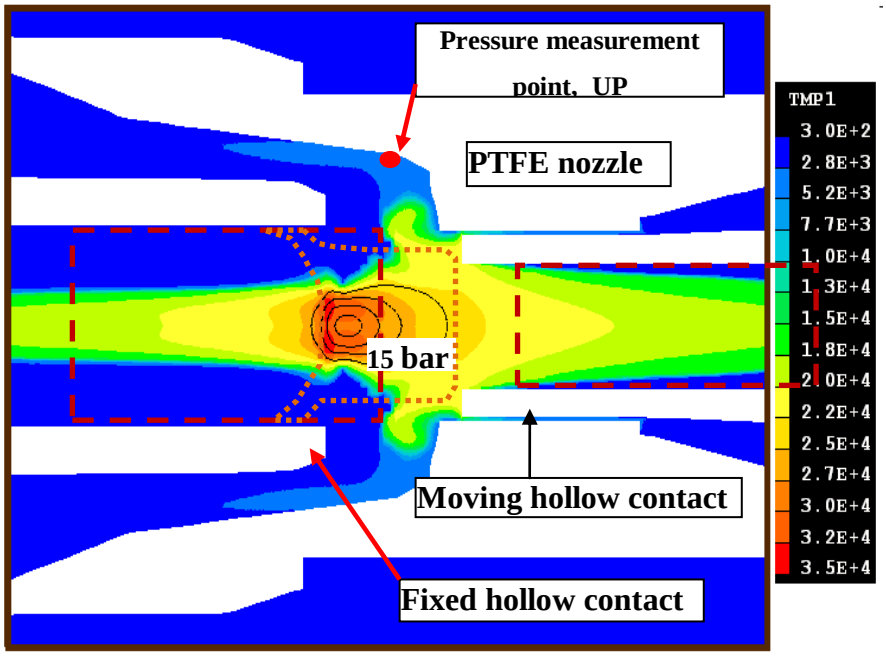

Figure. 4. 8 A typical case of unrealistic arc column contraction near the fixed hollow contact (and its filling transparent contact as marked by the broken square, acting as cathode in this case). The instantaneous current is 56 kA at 16.85 ms (see Figure 4.9). The isobars from the centre are 30, 25, 20 and 15 bars in sequence. The arc root is free to adjust its size in this case. The areas occupied by the transparent contacts are marked by the two broken rectangles inside the holes of the hollow contacts.

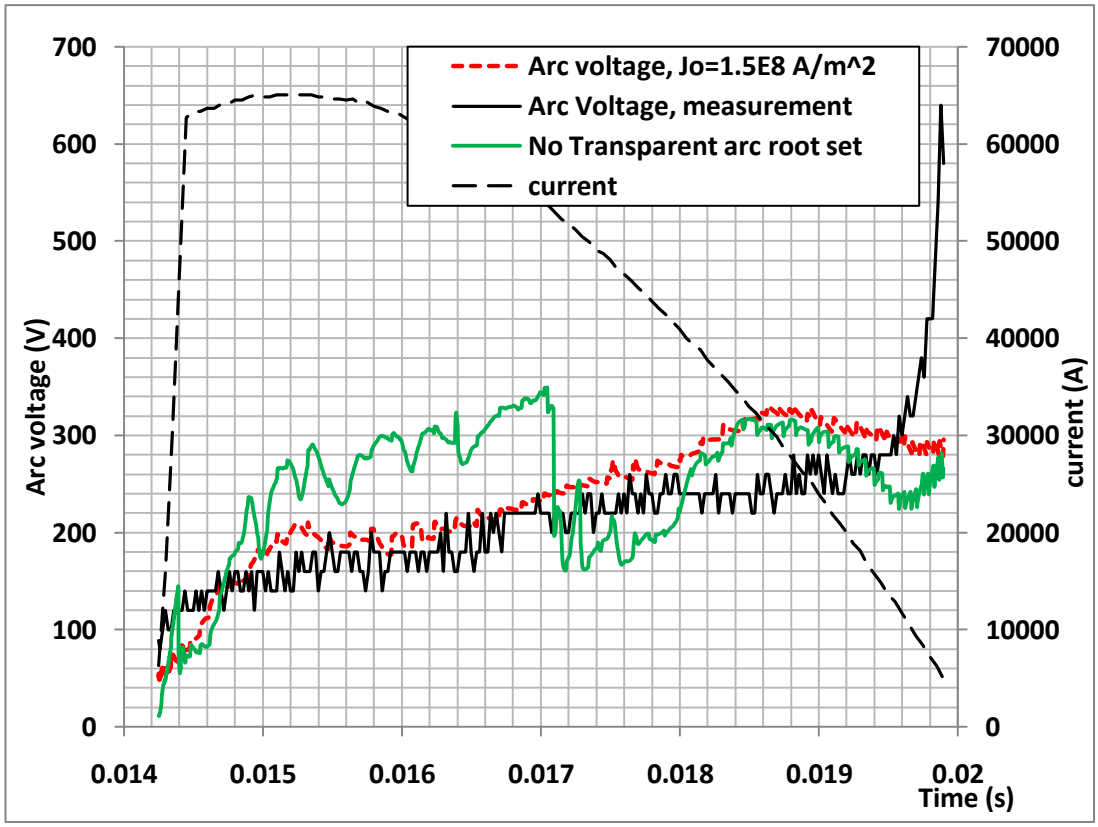

Figure.4. 9Predicted and measured arc voltage for the 46 kA (rms) case. J_0 is defined in equation (4.3)

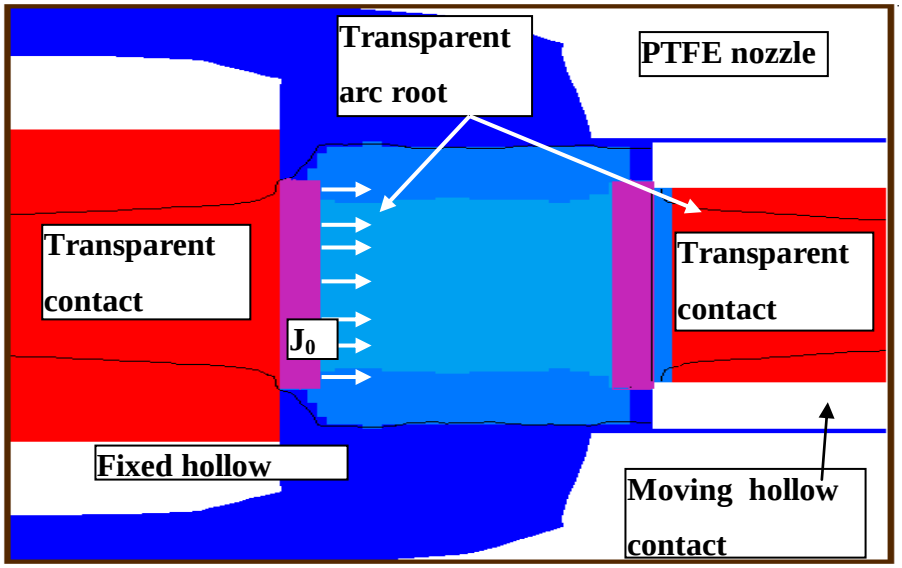

Figure.4.10 Schematic diagram of the transparent arc root implemented in front of the transparent contacts. The different colours represent regions with different range of electrical conductivity. The transparent contacts (red) have the highest value of 1.0×10^5 $\Omega^{-1}m^{-1}$, the arc roots (purple) have a typical value of 1.0×10^4 $\Omega^{-1}m^{-1}$, and this is

followed by the arc column, arc edge and the surrounding colder gas. The solid black line is the 10000 K isotherm.

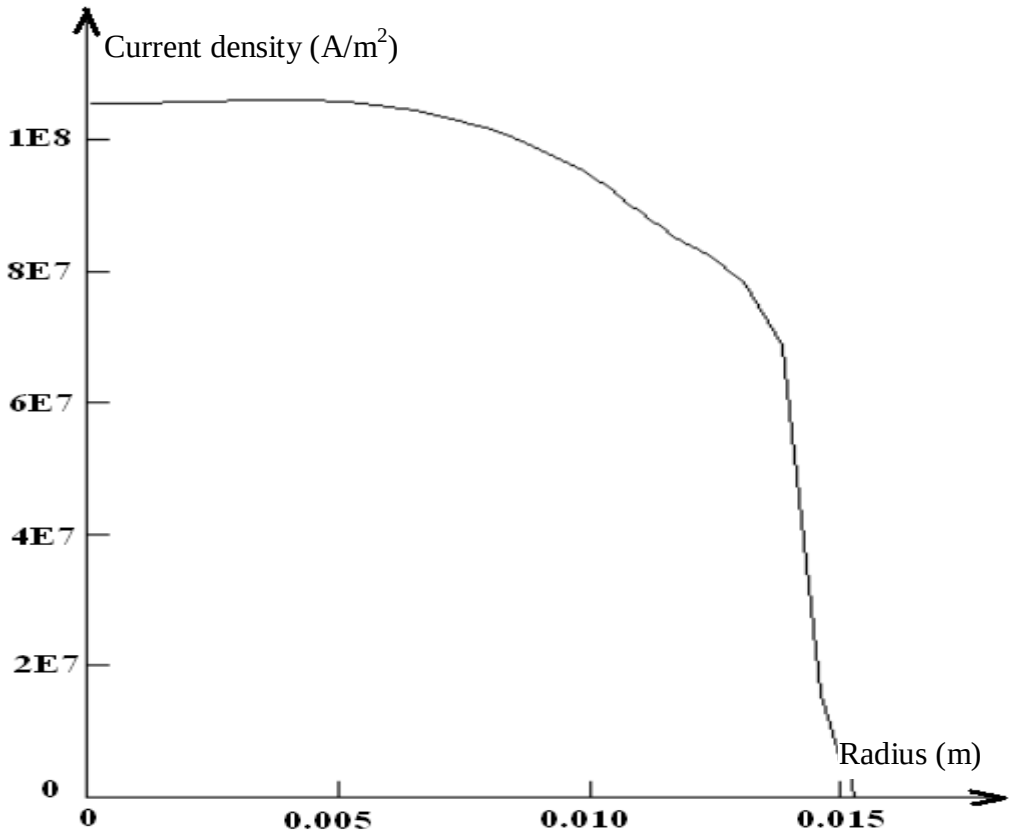

Figure 4.11 a typical radial profile of axial current density at the middle of the flat nozzle throat at an instantaneous current of 59.6 kA in the 47 kA case. The nozzle radius is 15.5 mm.

4.4 Grid system, Initial and Boundary Conditions

The circuit breaker used for testing the simulation model is a prototype 252 *kV* puffer circuit breaker. The computational domain is decided after discussing with Pinggao to make sure the boundary chosen for the domain does not significantly affect the solution so the computational results reflect the true situation in the arcing chamber. A schematic diagram of the domain is shown in figure 4.12 below. Gas is allowed to flow in and out at the boundary where there are no solid walls. The grid system in the contact space for high current phase simulation is given in figure 4.13 as an example. There are 95 cells in the radial direction and 265 cells in the axial direction.

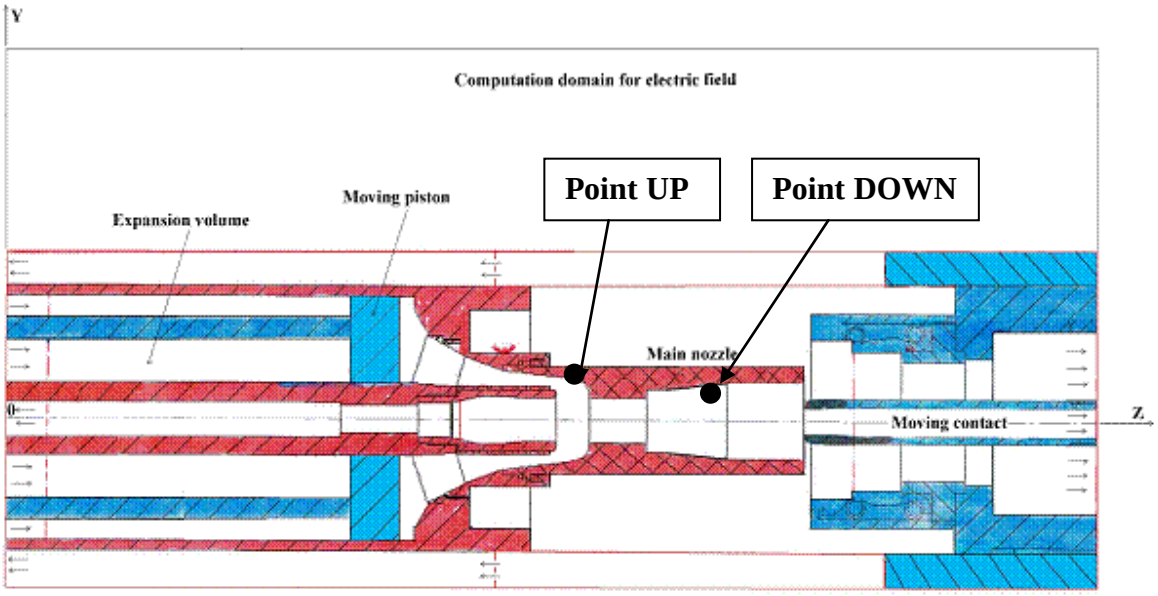

Figure 4.12 Schematic diagram of PingGao's 252 kV circuit breaker under investigation. The radius of the flat throat is 16 mm and its length is 40 mm.

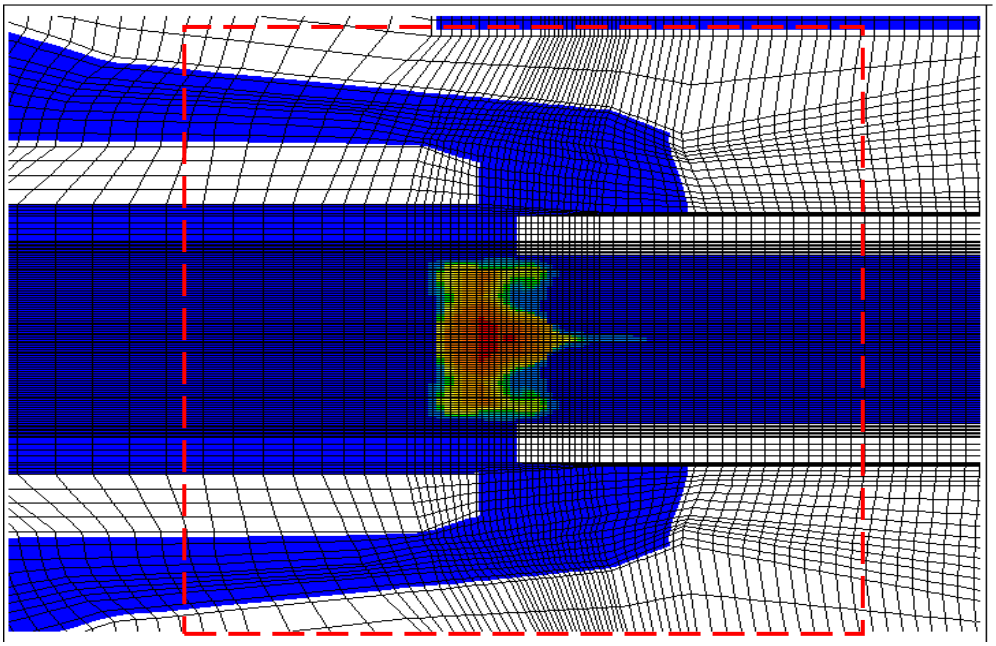

Figure 4.13 Example of grid distribution in the contact space for high current simulation. The visible lines do not truly reflect the number of cells in the nozzle hole. Sufficient spatial resolution is used for the simulation of cold flow and also arc.

When choosing the flow exits, care must be taken to consider how possibly the results will be sensitive to the location of theses exits. When it is not certain on their influence, test may have to be carried out to investigate this sensitivity.

The flow boundary conditions are the same for no-load and arc simulations. In reality the arcing chamber is placed inside an insulating cylinder (tank). For simulation efficiency, a smaller domain is used and flow exits have to be chosen. In the present case with two hollow contacts, the flow exit is chosen at the end of the hollow contacts and its pressure is set to the filling pressure. This implies that the pressure rise in the tank during an interruption operation is small and can be neglected. The detailed geometry of the simulation domain will be shown in next section when the results are discussed.

A cold flow simulation is needed to be performed first. Normally a simulation starts with a filling pressure, for example 7 bar in the present work. The gas is assumed to be stagnant and has a temperature of 300 *K*. The live hollow contact will gradually move out of the other hollow contact. This cold flow simulation runs up to a point when the live contact separates from the other contact by 5*mm*.

The high current phase then starts with this 5-8 *mm* contact separation by initiating an arc between the hollow contacts using a hot column, as shown in figure 4.14, the hot column has a linear radial enthalpy distribution, from a central value to the enthalpy of the filling gas. The value used at the centre is 1.5×10^{8} *J/kg*. The high current phase runs up to 15 *kA* just before the final current zero.

The current zero period deals with rapidly decreasing arc current and the arc column can become very thin. In order to maintain sufficient spatial resolution of the arc parameters, such as temperature and pressure, the radial grid density needs to be increased. The simulation model has such a function that it will automatically obtain the initial temperature, pressure, and contact position from a data file generated at the end of the high current phase. The simulation will use a small time step, typically less than 1 μs immediately before current zero, to run up to the exact time zero.

The post arc simulation starts from the end of the current zero simulation and run up to several to 15 μs to calculate the post arc current for the evaluation of the circuit breaker performance.

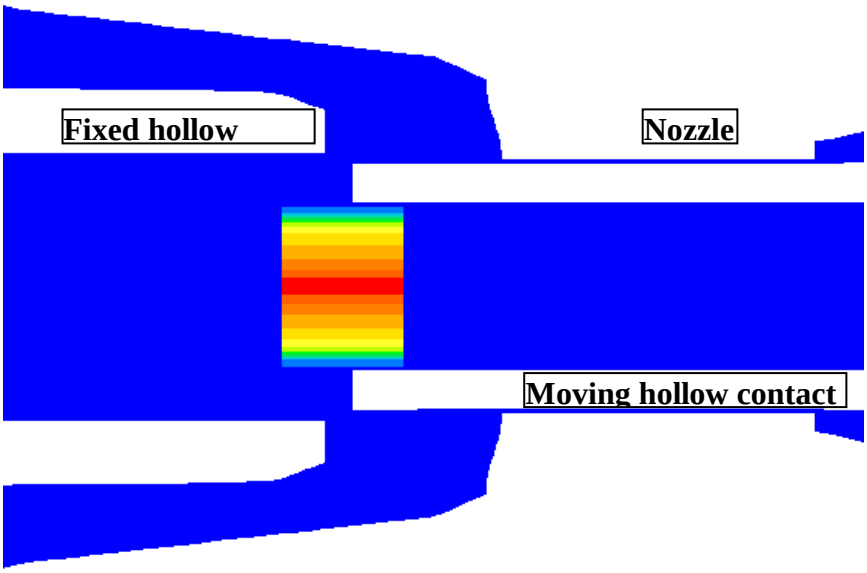

Figure 4.14 Diagram showing the use of a hot column to initiate the arc.

All solid surfaces apart from the ablating surface are assumed to have a fixed temperature of 300 *K* which therefore exerts cooling to the arc and hot gas in the hollow contacts. Pressure at the exit of the two hollow contacts is fixed to the filling gas pressure and mass momentum and energy fluxes are dominated by convective effect at the exit. The frictional forces exerted by solid surface to gas flow is taken into account by a wall function provided by the commercial Computational Fluid Dynamics (CFD) software PHOENICS [[Phoe]]. Because of the nature of the two dimensional axisymmetric arc model, the radial gradient of all solved quantities are set to zero on the axis.

4.5 Typical Results and Discussion

4.5.1 No-Load Simulation

Several cases have been simulated for the no-load case, both using nitrogen and SF_6 as the working gas. For no-load cases, the pressure measurement is relatively smooth and comparison can be conveniently made. The first case simulated is the cold flow for nitrogen. The filling pressure is 7bar. Since the contact travel and velocity substantially affect the pressure build-up and its variation in the cylinder, a comparison between the

actually measured travel and that specified by the manufacturer is made, which is shown in figure 4.15. The difference between the travels is mainly in the later stage of the movement at around 35 *ms*. The oscillation in contact speed is due to the fluctuation in the raw data of the travel. For comparison with simulation results, the measured travel is used in the simulation.

For the cold flow case, pressure measurement at different locations of the chamber is the main source of information for verification of the model. It can be seen that for the point in front of the piston, the difference between prediction and measurement is acceptable if the approximations that have been made to the geometry are considered, figure 4.16. The prediction is higher than the measurement mainly because in the simulation no energy loss to the solid walls is considered. Whereas in reality, there is always heat lost to the wall and the gas may not be ideal. The maximum pressure rise is only 4.6 *bar* which is much lower than that in the SF_6 case (later to be shown). The measured pressure at Point UP (See figure 4.16) suddenly collapsed at 21 *ms* while the prediction continues increase but with a lower rate as a result of the contact separation. Adjustment to the geometries included in the broken box in figure 4.13 has been made but the change in geometry does not significantly affect the prediction. The predicted pressure at the middle of the flat nozzle matches reasonably well with the measurement. The small shift in the peak is probably due to in reality the live contact tip is rounded and the fingers at the tip of the contact allow some gas to reach the measurement point earlier.

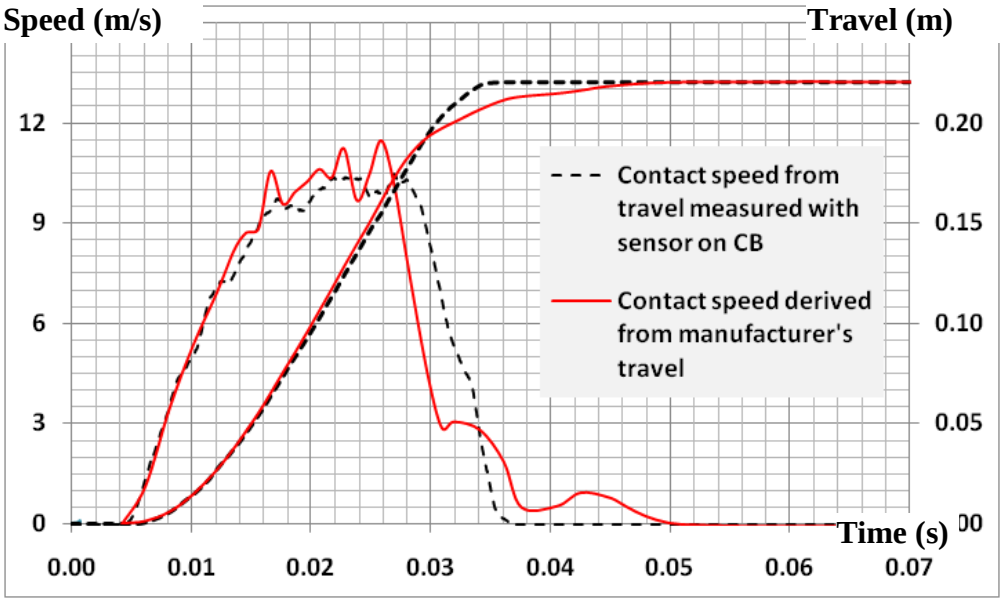

Figure 4.15 Diagram showing a comparison between the contact travel obtained using on board sensor and that provided by the manufacturer, for a noload test with nitrogen. Contact speed is derived from the travel curve.

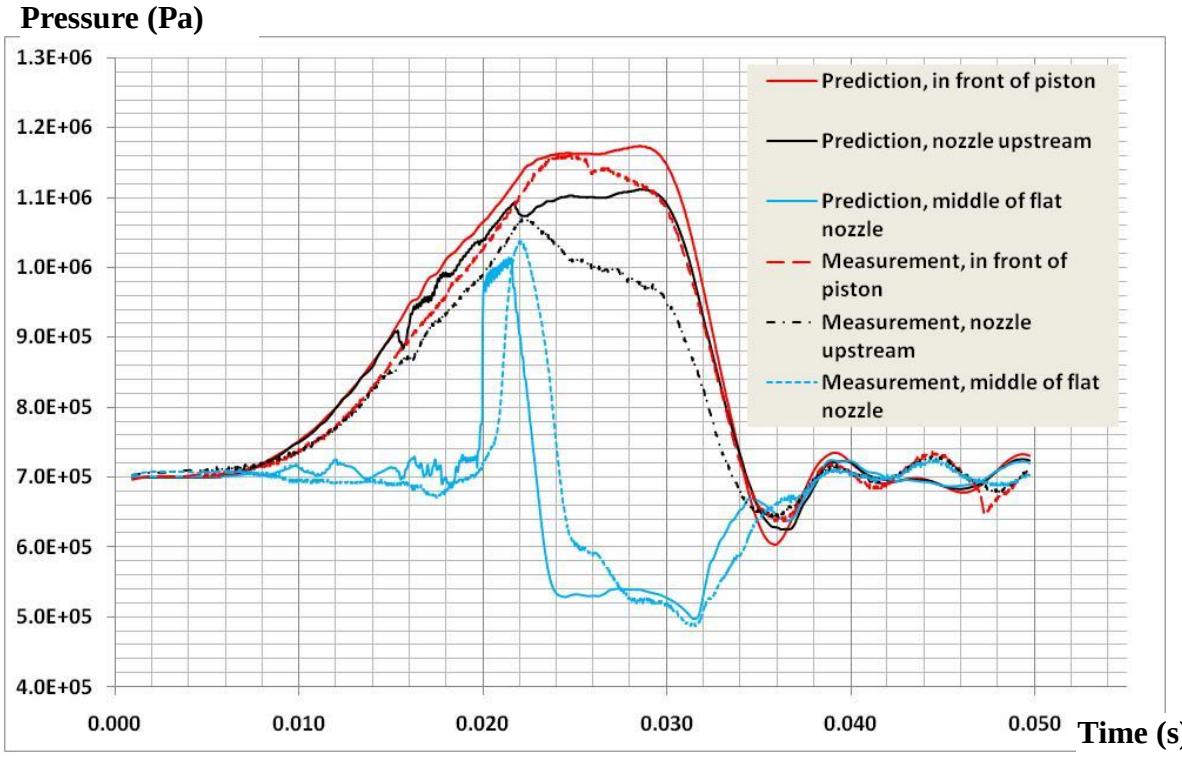

Figure 4.16 Comparison of predicted and measured pressure variation at three strategically chosen locations in the arcing chamber. Filling pressure of nitrogen is 7bar absolute. The measured contact travel (shown in Figure 4.15) is used to perform the simulation.

The other case is for SF_6. In this case the measured contact travel is close to the manufacturers data and the main difference is the contact speed (figure 4.17). The manufacturer gives a higher maximum contact speed. In order for us to gain confidence in the pressure measurement, the results from two shots have been compared. From figure 4.18 it can been seen that the scattering in pressure measurement can reach 1 bar easily. For the pressure at the nozzle, the difference reaches 2 bar. Therefore the maximum uncertainty in pressure measurement should be around 2 bar.

Figure 4.19 presents the results for SF6. In this case the difference between prediction and measurement is smaller than that in the case for nitrogen and is within 1bar. Considering the experimental uncertainties (at least 1 bar), the agreement is rather reasonable.

Another point that needs to be mentioned is that SF_6 behaves much differently from nitrogen according to the pressure measurement. For example, the pressure collapse observed with nitrogen at Point UP does not appear in the SF_6 case. This is due to the different thermal and aerodynamic properties between the two gases as shown in figure 4.20. For the same stagnation pressure and Mach number, nitrogen will have more pressure drop than SF_6 due to their difference in specific heats.

A sequence of the pressure distribution at different times is given in figure 4.21. A typical velocity field for nitrogen is given in figure 4.22. For SF_6, the velocity field is given in figure 4.23 and the sequence in figure 4.24.

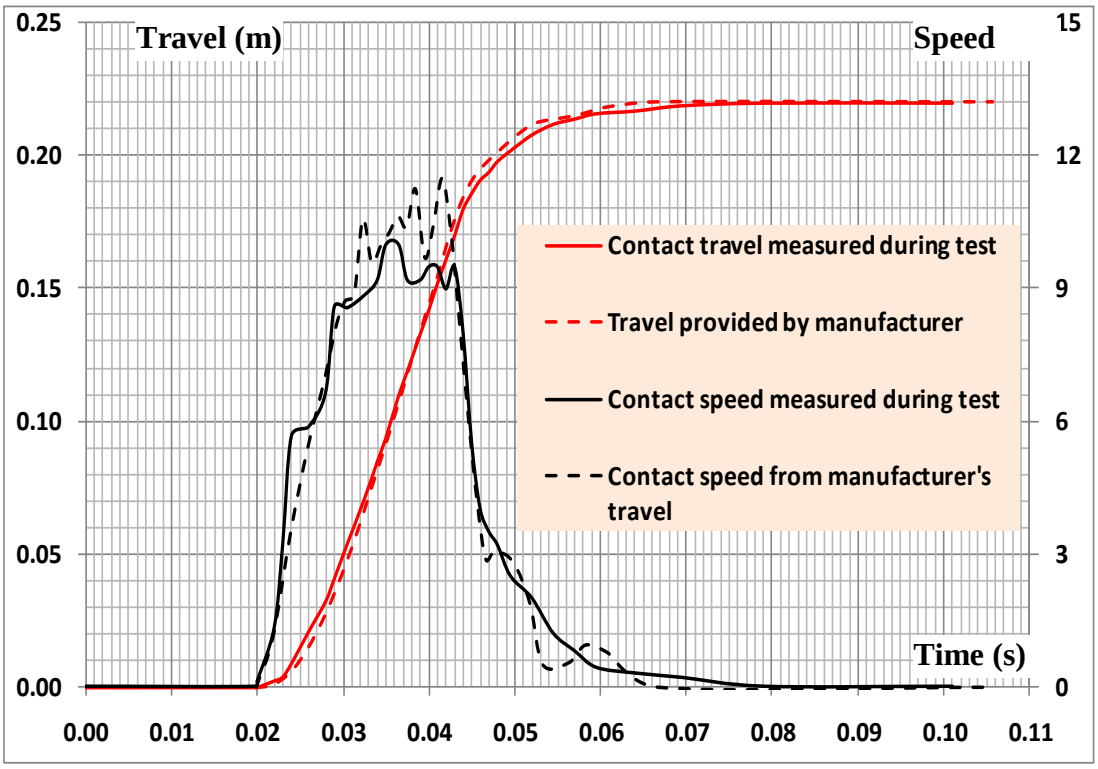

Figure 4.17 Diagram showing a comparison between the contact travel obtained using on board sensor and that provided by the manufacturer for noload test with SF_6. Contact speed is derived from the travel curve.

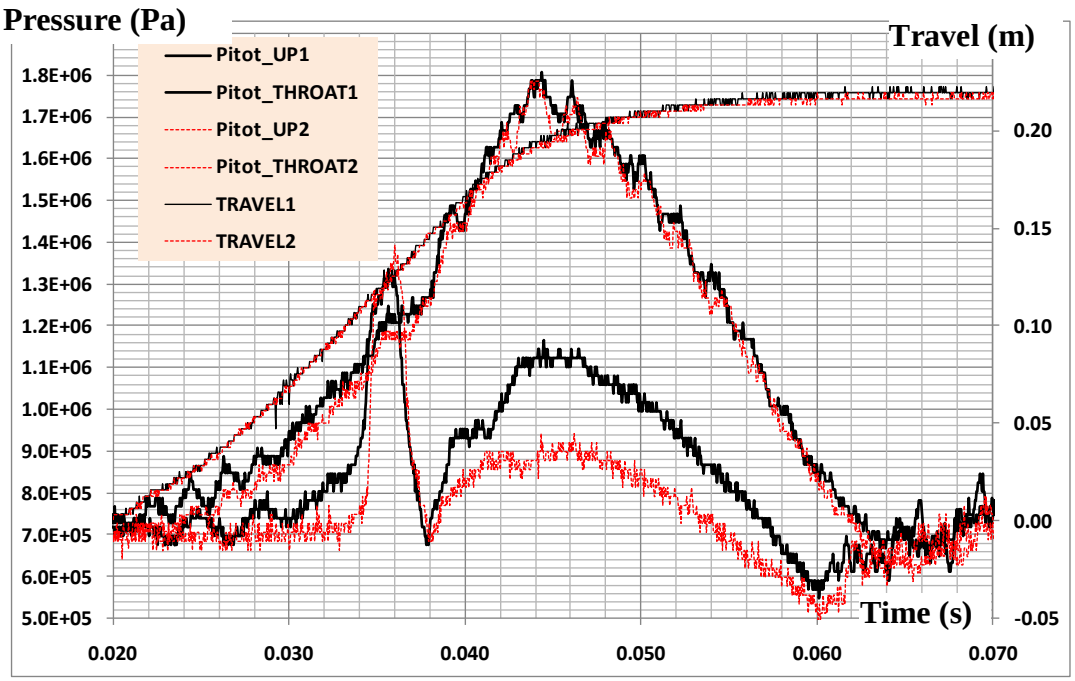

Figure 4.18 Comparison of two sets of pressure measurement results using Pitot tube for SF_6.

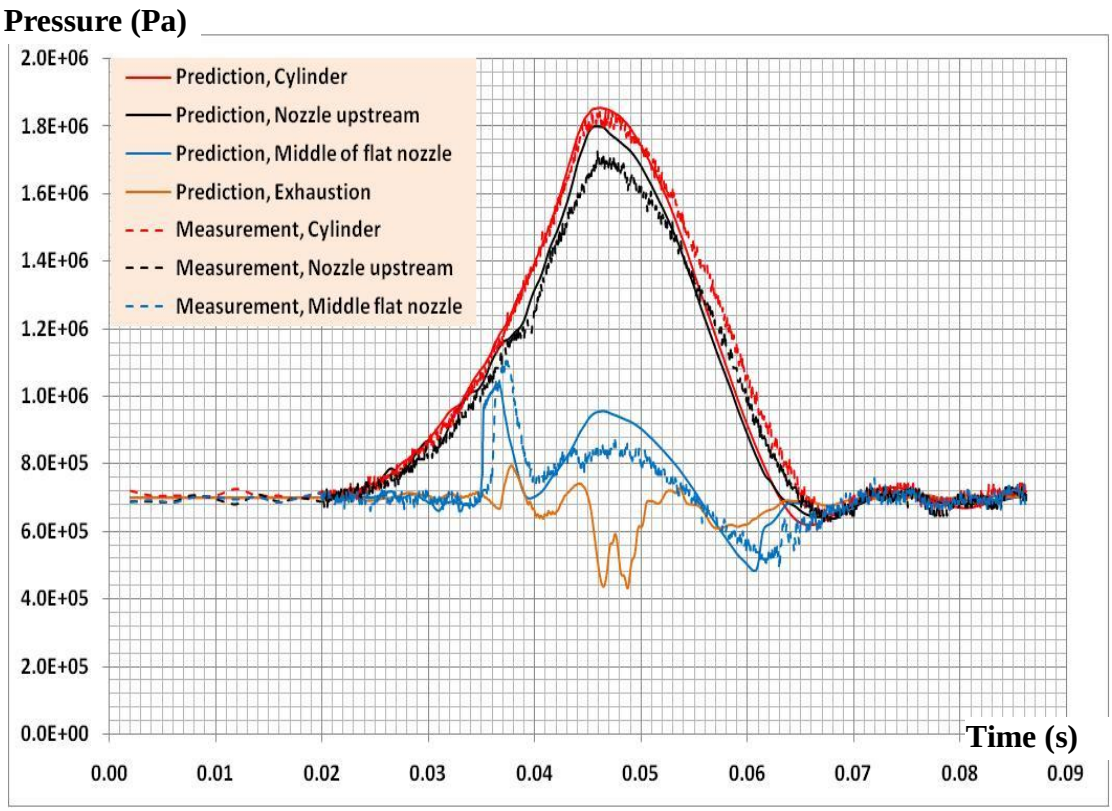

Figure 4.19 Comparison of predicted and measured pressure variation at three strategically chosen locations in the arcing chamber. Filling pressure of SF_6 is 7bar absolute. The measured contact travel (shown in Fig 7) is used to perform the simulation.

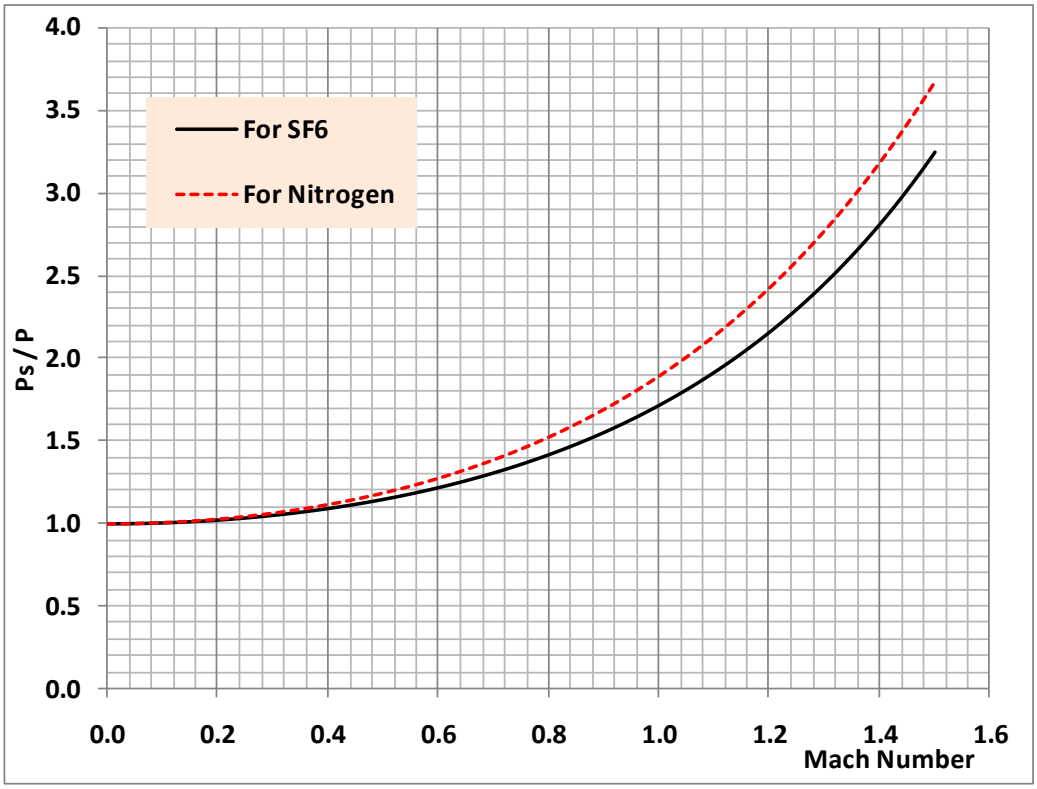

Figure 4.20 Relationship between pressure ratio (stagnant pressure to local pressure) and Mach number of gas flow. For Nitrogen gas $\gamma = 1.4$ and Cp = 1040 J/(Kg·K). For SF_6 gas $\gamma = 1.108$ and Cp = 575 J/(Kg·K).

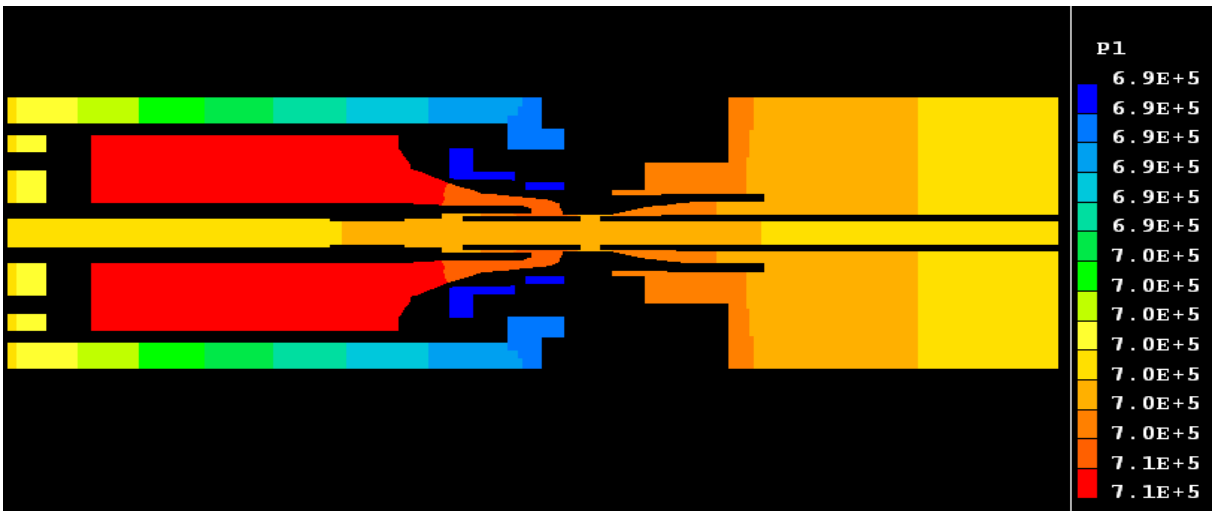

(a)

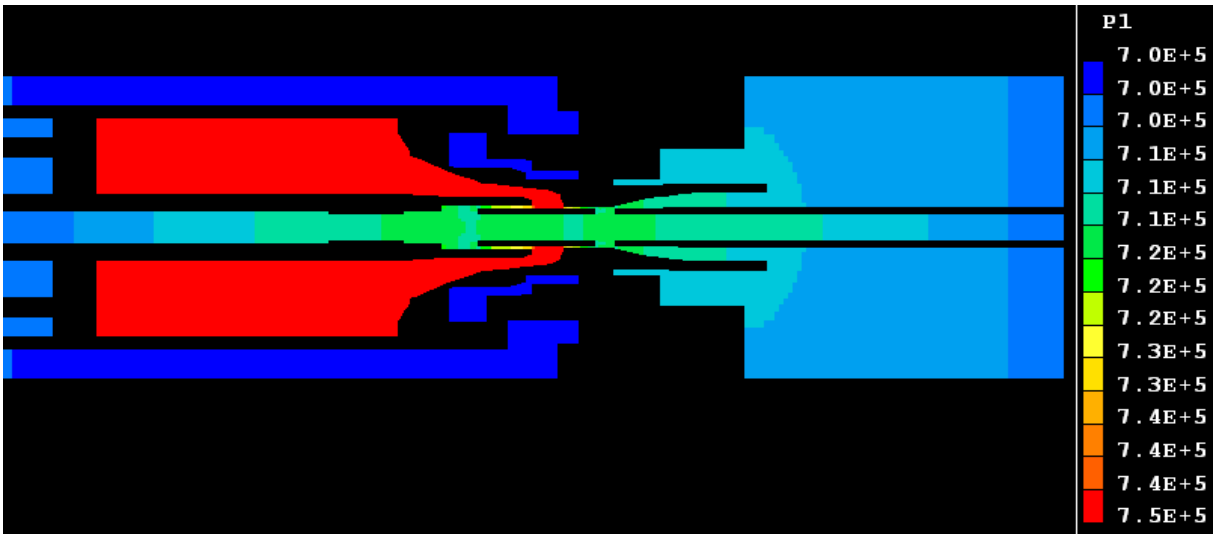
P1
7.0E+5
7.0E+5
7.0E+5
7.1E+5
7.1E+5
7.1E+5
7.2E+5
7.2E+5
7.2E+5
7.3E+5
7.3E+5
7.4E+5
7.4E+5
7.4E+5
7.5E+5

(b)

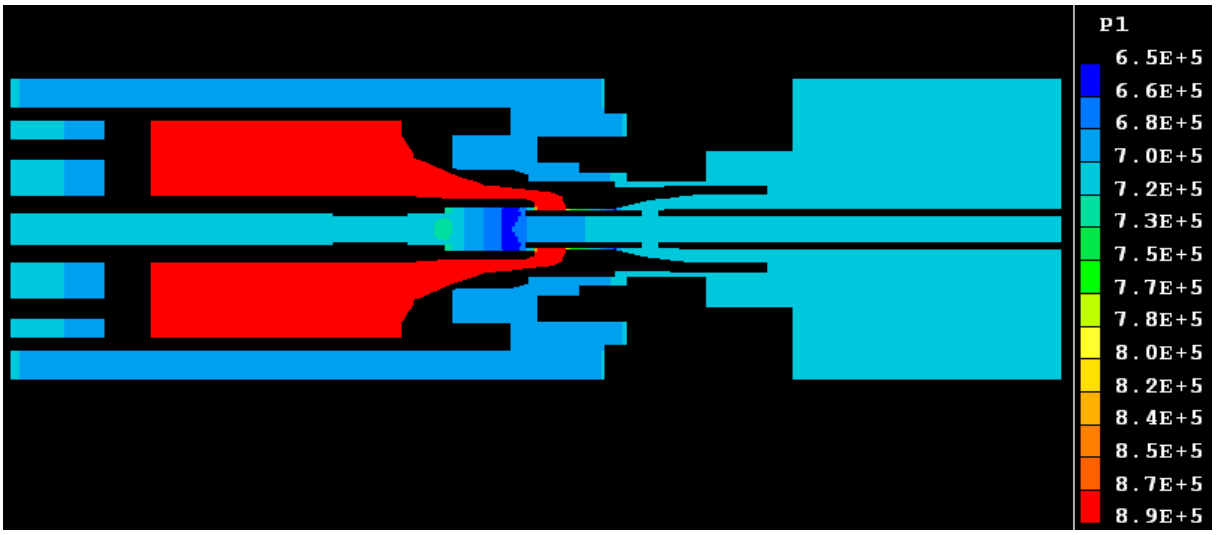
P1
6.5E+5
6.6E+5
6.8E+5
7.0E+5
7.2E+5
7.3E+5
7.5E+5
7.7E+5
7.8E+5
8.0E+5
8.2E+5
8.4E+5
8.5E+5
8.7E+5
8.9E+5

(c)

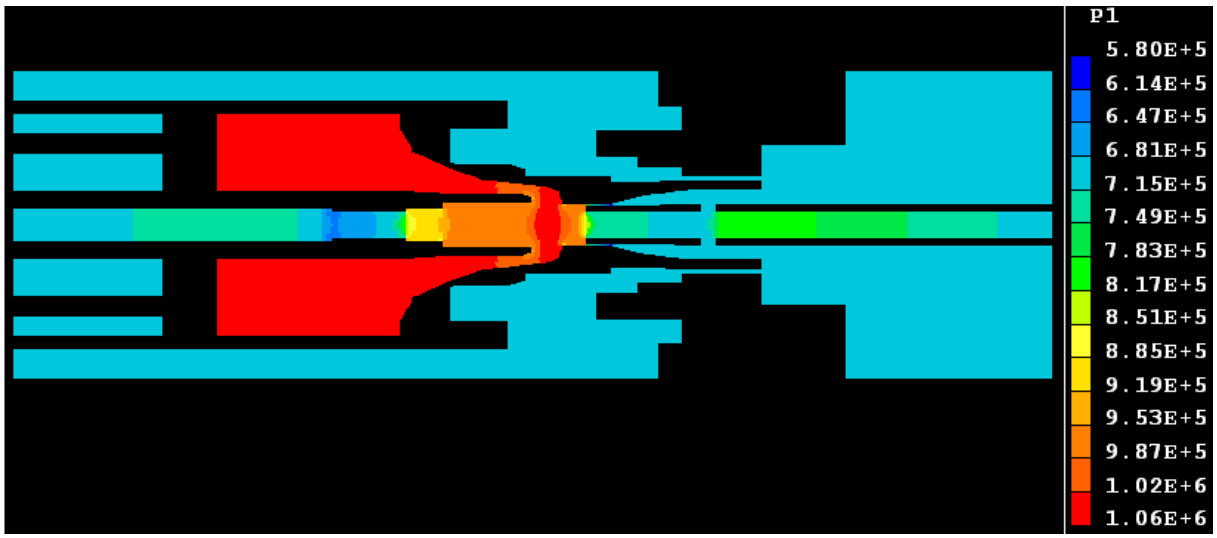
P1
5.80E+5
6.14E+5
6.47E+5
6.81E+5
7.15E+5
7.49E+5
7.83E+5
8.17E+5
8.51E+5
8.85E+5
9.19E+5
9.53E+5
9.87E+5
1.02E+6
1.06E+6

(d)

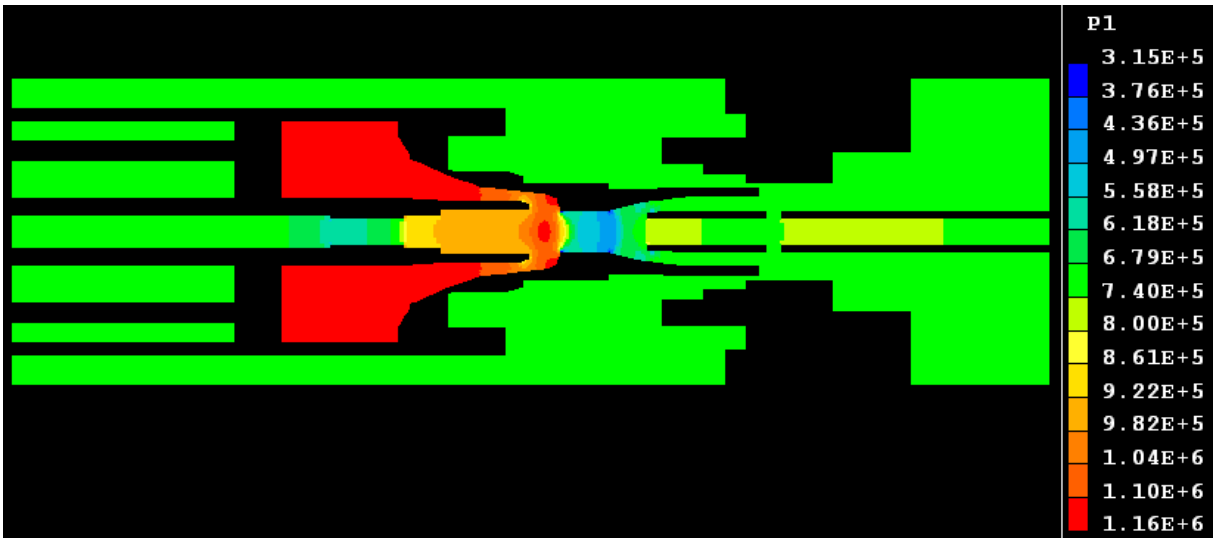

(e)

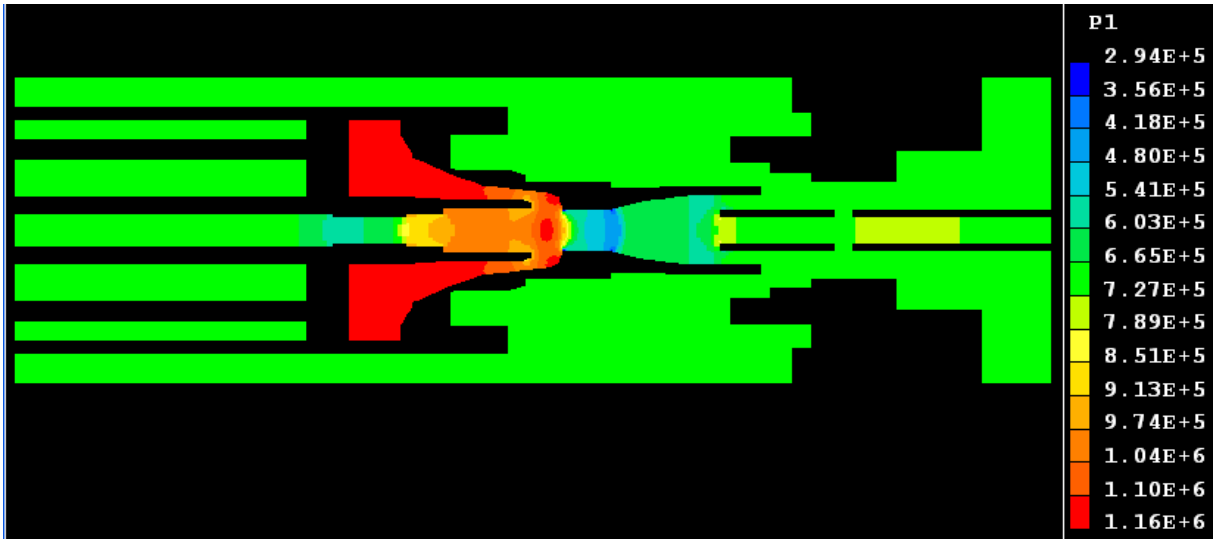

(f)

Figure 4.21 Changes of pressure field as a function of time with a contact moving away from the other. Nitrogen is used as working gas and filling pressure is 7bar at 300 K. The instants from (a) to (f) are in millisecond: 6.65, 9.65, 14.65, 19.65, 24.65, 29.65.

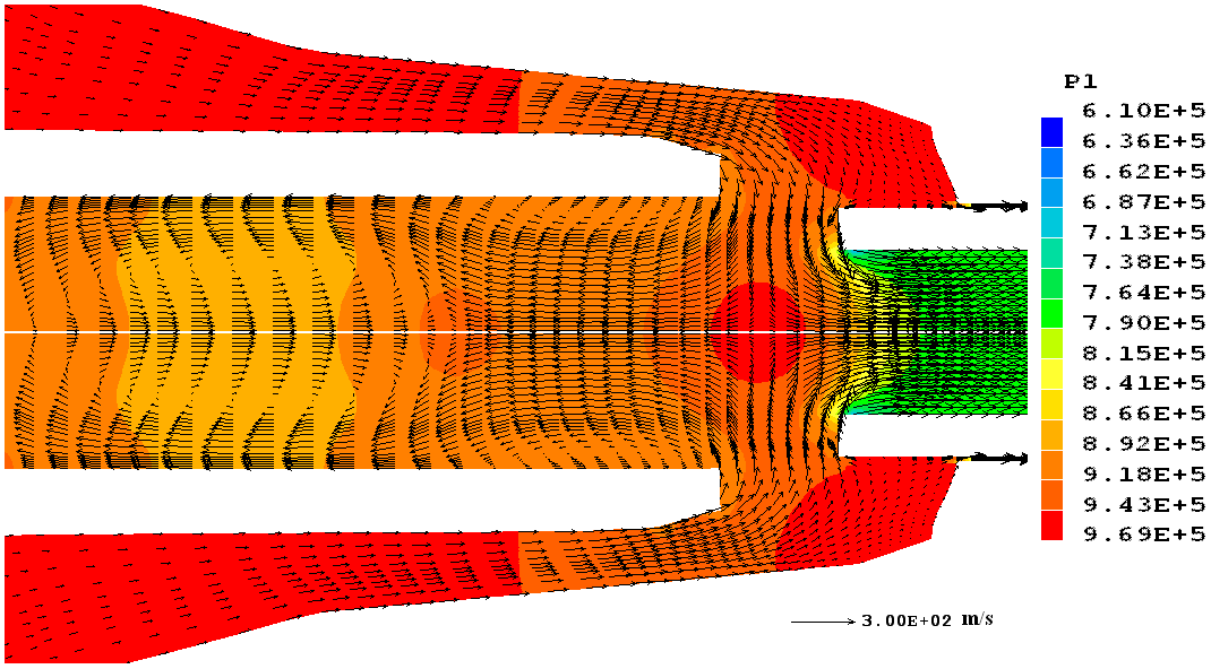

Figure 4.22 Flow field shortly after contact separation (14.65 ms) for nitrogen with the contact travel given in figure 11.

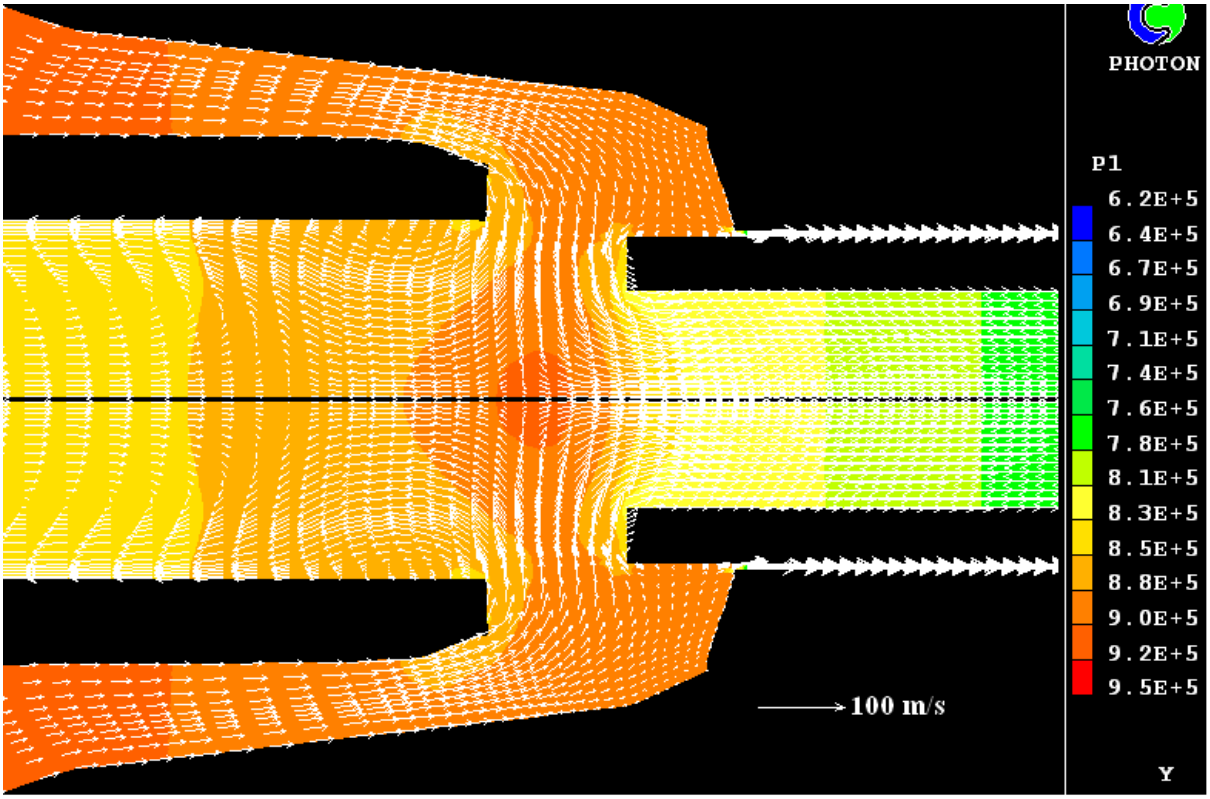

Figure 4.23 Flow field shortly after contact separation (31.69 ms) for SF_6 with the contact travel given in figure 4.15.

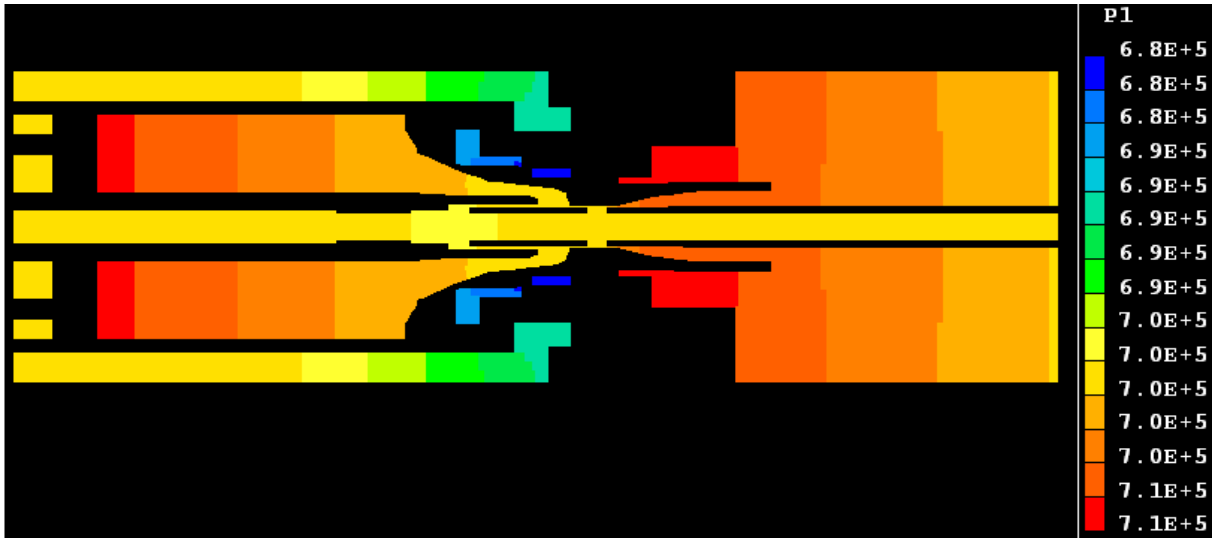
P1
6.8E+5
6.8E+5
6.8E+5
6.9E+5
6.9E+5
6.9E+5
6.9E+5
6.9E+5
7.0E+5
7.0E+5
7.0E+5
7.0E+5
7.0E+5
7.1E+5
7.1E+5

(a)

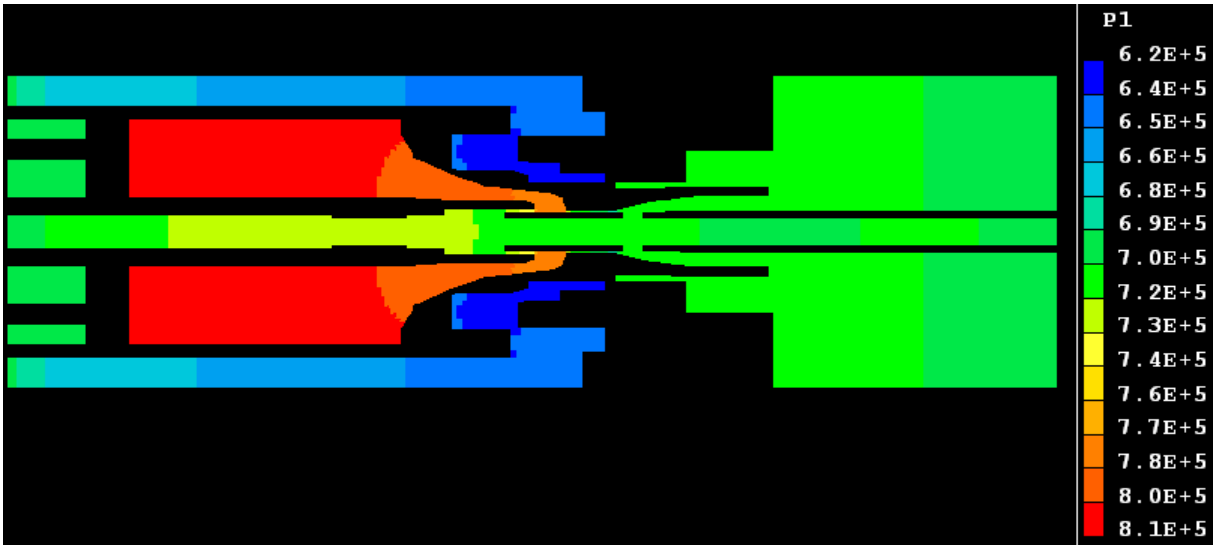
P1
6.2E+5
6.4E+5
6.5E+5
6.6E+5
6.8E+5
6.9E+5
7.0E+5
7.2E+5
7.3E+5
7.4E+5
7.6E+5
7.7E+5
7.8E+5
8.0E+5
8.1E+5

(b)

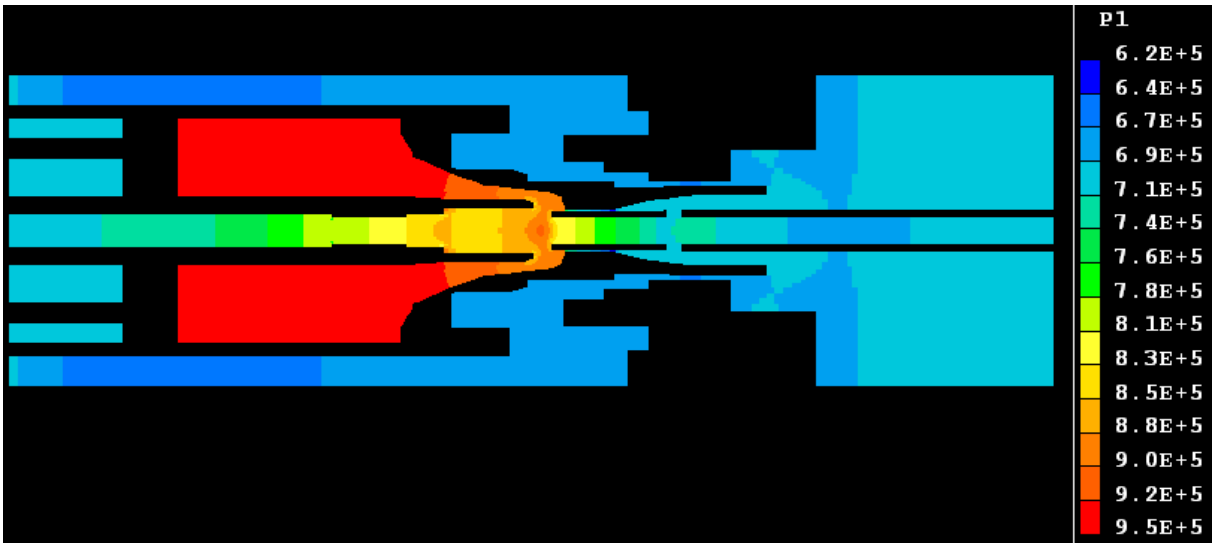
P1
6.2E+5
6.4E+5
6.7E+5
6.9E+5
7.1E+5
7.4E+5
7.6E+5
7.8E+5
8.1E+5
8.3E+5
8.5E+5
8.8E+5
9.0E+5
9.2E+5
9.5E+5

(c)

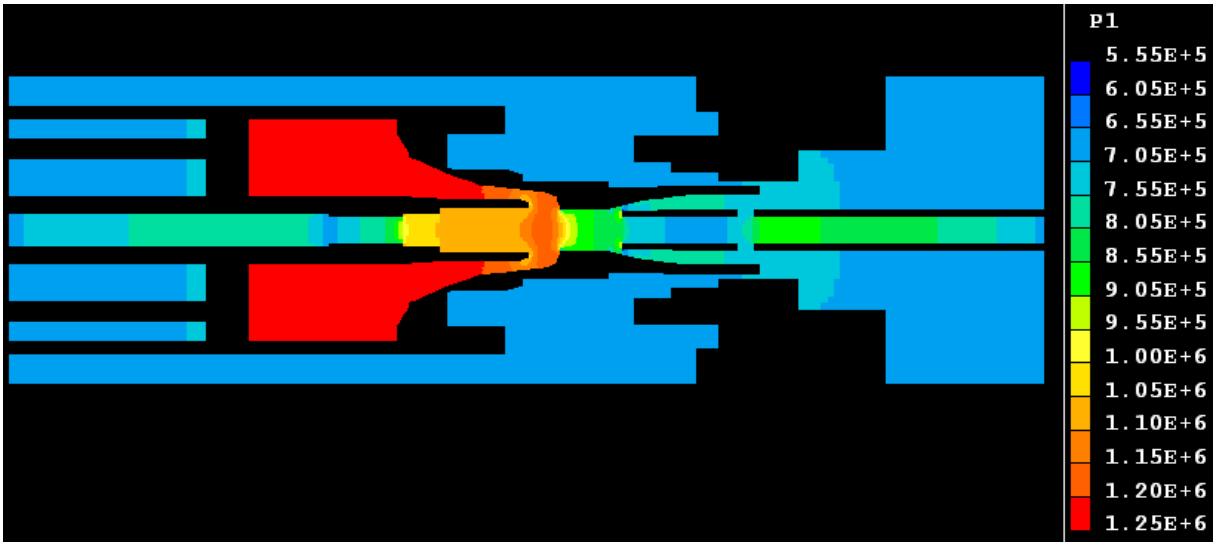
P1
5.55E+5
6.05E+5
6.55E+5
7.05E+5
7.55E+5
8.05E+5
8.55E+5
9.05E+5
9.55E+5
1.00E+6
1.05E+6
1.10E+6
1.15E+6
1.20E+6
1.25E+6

(d)

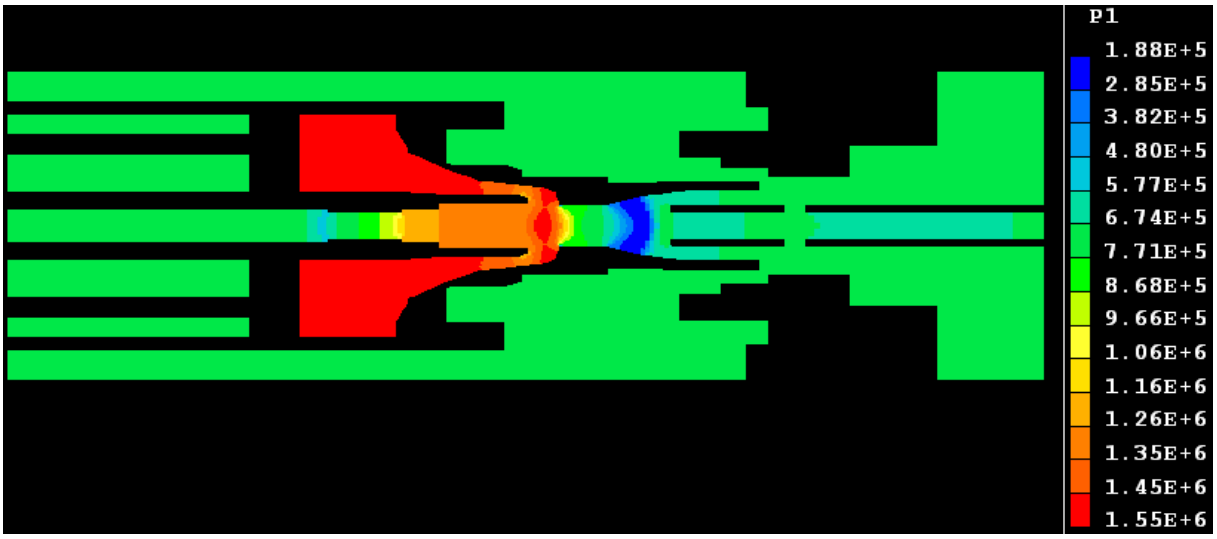
P1
1.88E+5
2.85E+5
3.82E+5
4.80E+5
5.77E+5
6.74E+5
7.71E+5
8.68E+5
9.66E+5
1.06E+6
1.16E+6
1.26E+6
1.35E+6
1.45E+6
1.55E+6

(e)

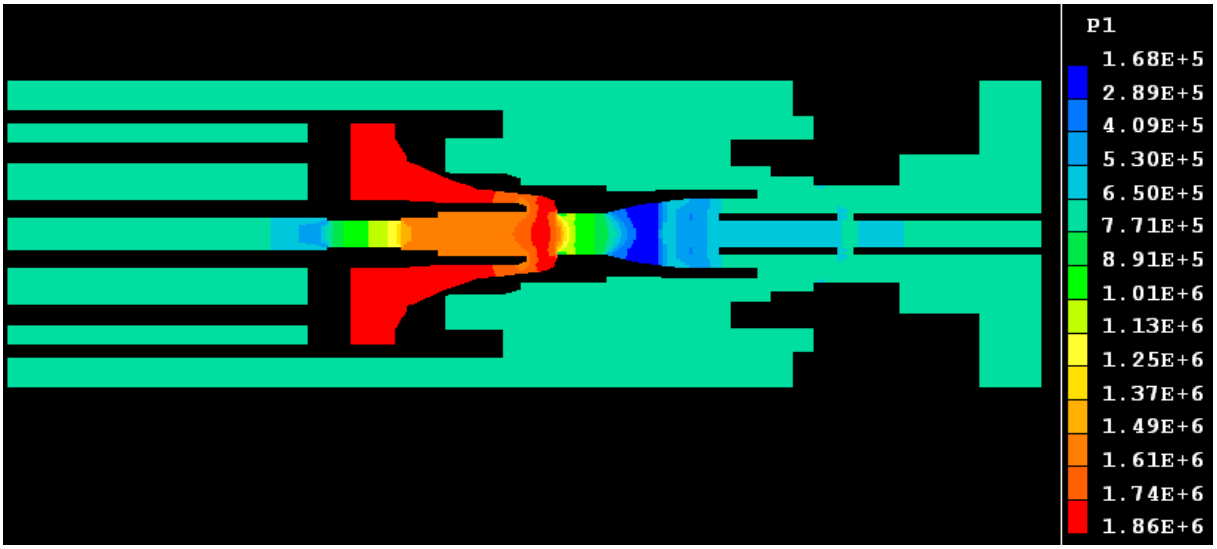
P1
1.68E+5
2.89E+5
4.09E+5
5.30E+5
6.50E+5
7.71E+5
8.91E+5
1.01E+6
1.13E+6
1.25E+6
1.37E+6
1.49E+6
1.61E+6
1.74E+6
1.86E+6

(f)

Figure 4.24 Changes of pressure field as a function of time with a contact moving away from the other. SF_6 is used as working gas and filling pressure is 7 bar at 300 K. The instants from (a) to (f) are in millisecond: 21.69, 27.69, 31.69, 37.69, 41.69, and 47.69.

4.5.2 High Current Phase

The high current phase is defined as the period from the initiation of the arc to the time when the instantaneous current is above 15 *kA* before the final current zero. Any intermediate current zeros will be considered as part of the high current phase because special treatment to these points will not add any additional information towards the interruption process. The choice of 15 *kA* is based on careful analysis of the arc voltage measurement for all four cases that Pinggao provided.

The case of 10 *kA* will be discussed in the current zero period simulation because the peak current in the second half-cycle is only 2.5 *kA*.

With the proposed use of two transparent arc roots and the special treatment of the magnetic pinch force near them, the predicted arc voltage agrees reasonably well with the measurement for the high current phase using a turbulence parameter of 0.1 for the arc region in equation (4.2). The comparison is given in figures 4.9, 4.29 and 4.30 for predicted and measured arc voltages. The discrepancy between 20 *ms* and 22 *ms* in the 24 *kA* case (figure 4.29) cannot be explained. Since good agreement is achieved for the 10 *kA* (next section), 46 *kA* and 47 *kA* cases, there is no reason to suggest that the model has large deficiency in predicting this case. Ideally, there should be at least two measurements of the arc voltage at the same current level to check the reproducibility of the measurement and to identify any particular reason associated with the operation of the breaker for the arc voltage discrepancy.

The temperature field, which reflect the arc column shape and size, is given at different times during the simulation in figure 4.31 to present a history of the arcing process of the 47 *kA* case. Figure 4.31d also displays the equo-potential lines with an interval of 20 *V* between adjacent lines. Soon after the arc is initiated, it quickly adjusts its

temperature field according to the distribution of Ohmic heating (4.31a). When the current passes its first zero at around 15 *ms*, the arc extends into the two hollow contacts under the axial pressure gradient generated by the Lorentz force (4.31b). After the first current zero, the arc current increases rapidly and by 17.66 *ms* at an instantaneous current of -49 *kA* the arc column fills the flat nozzle (4.31c) and a patch of hot gas is pumped towards the cylinder. The arc by this time roots on the tip of the moving contact where there is local high temperature. For most of the seocnd half loop, the arc near the fixed moving contact is always constrained by cold flow from the cylinder while the the hole of the moving contact is filled with hot gas (4.31d). At 16 *kA* before the final current zero, cooler SF6 has insulated the arc from the nozzle wall and the arc burns in a axially dominant flow regime (4.31f).

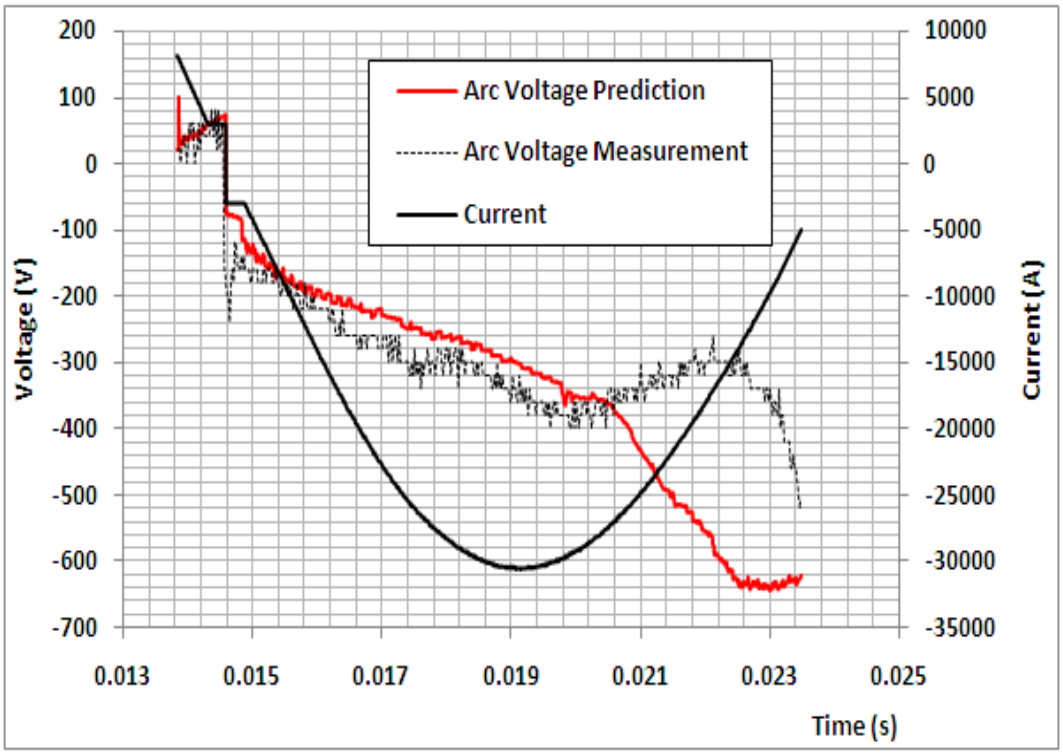

Figure 4.29 Predicted and measured arc voltage for the 24 kA case.

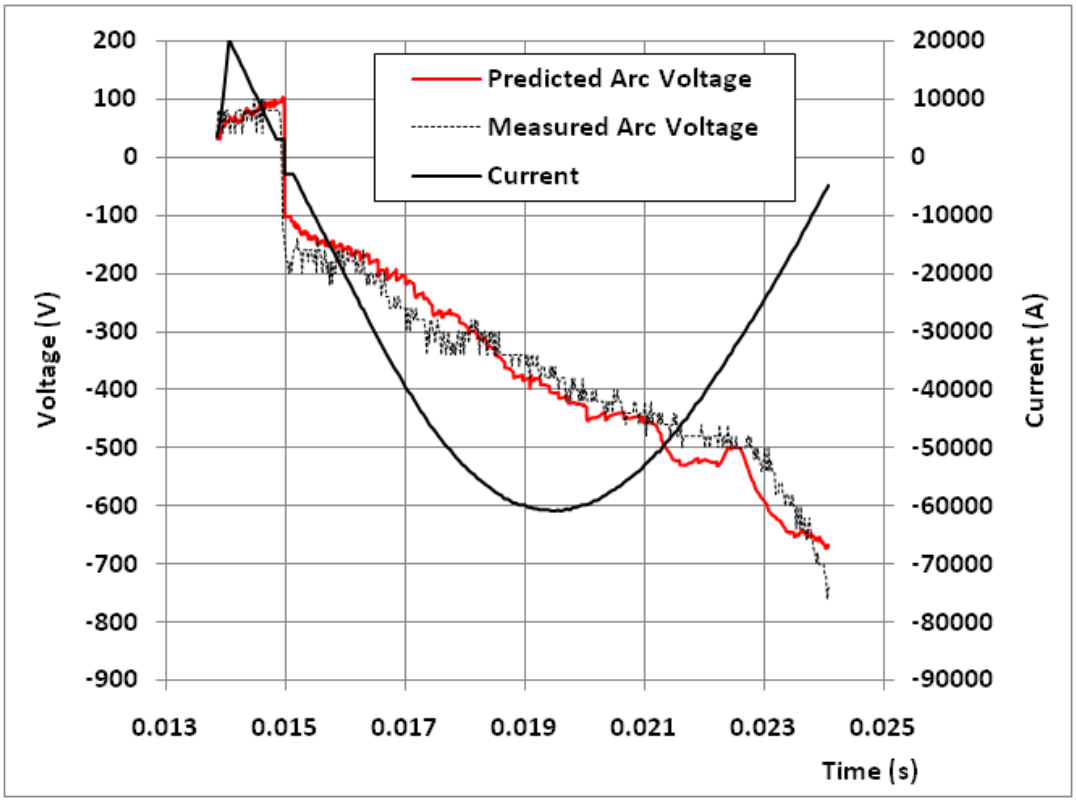

Figure 4.30 Predicted and measured arc voltage for the 47 kA case.

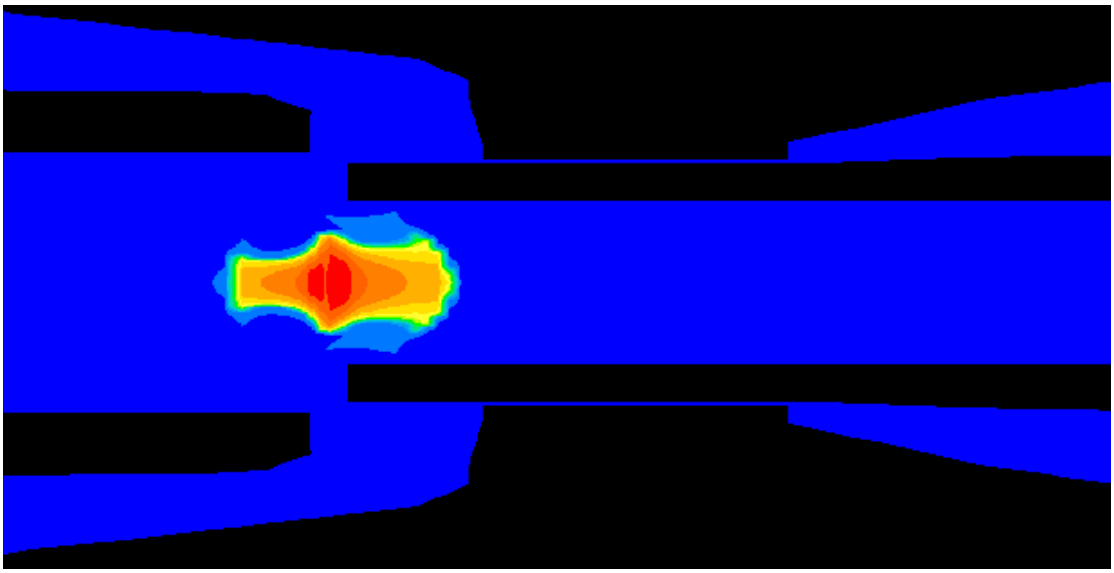

(a)

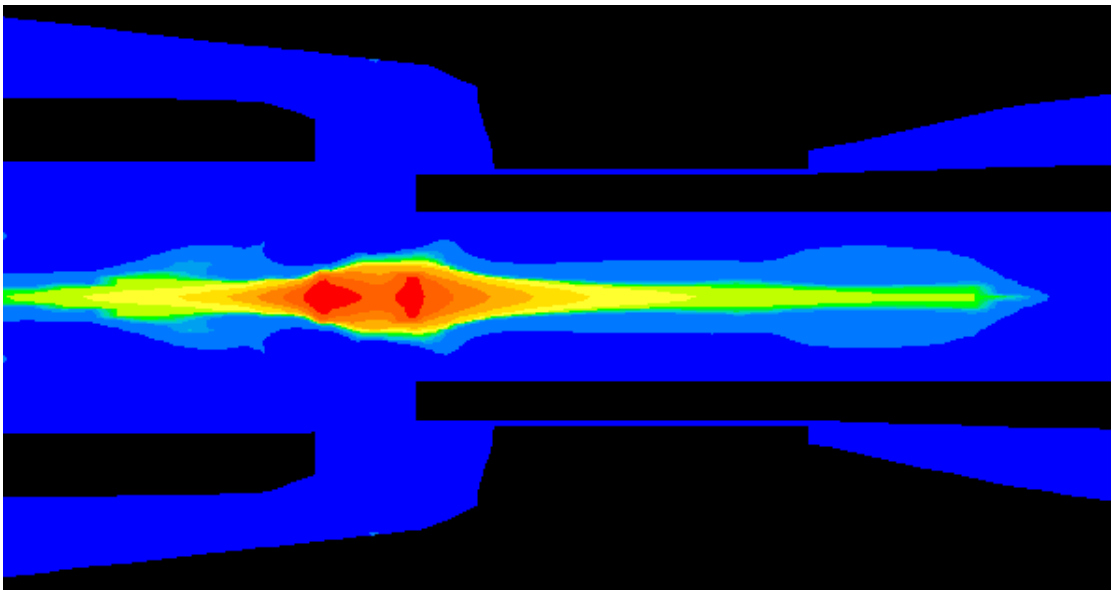

(b)

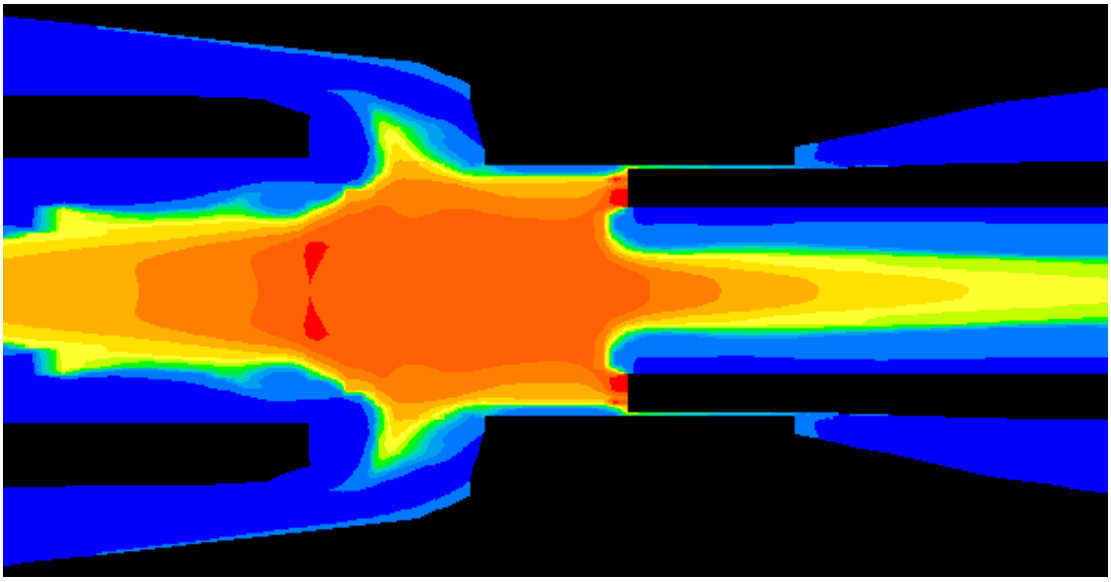

(c)

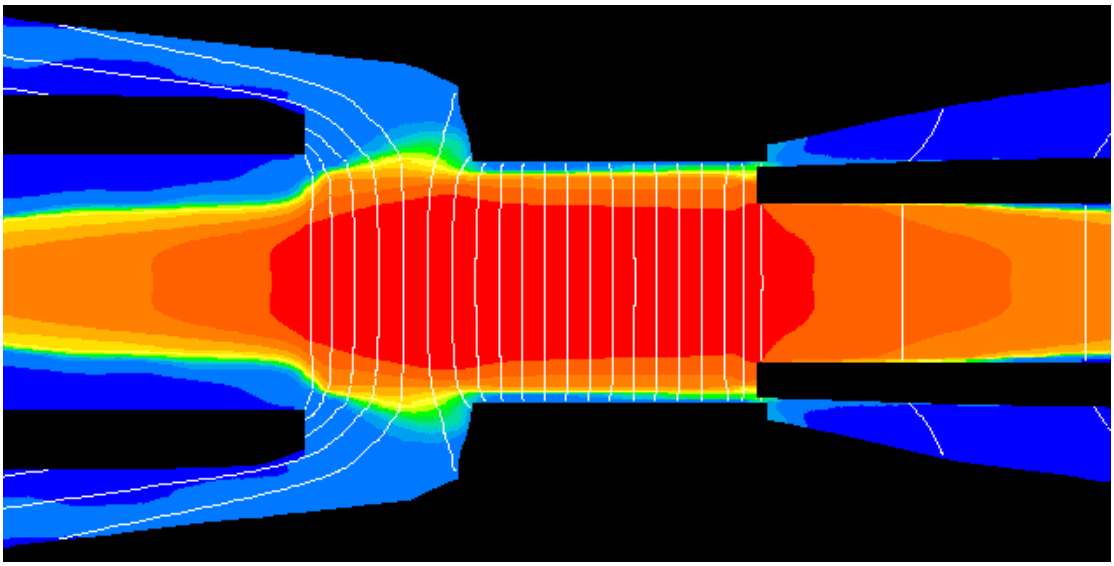

(d) arc voltage is 700V with equo-potential lines gapped at 20V.

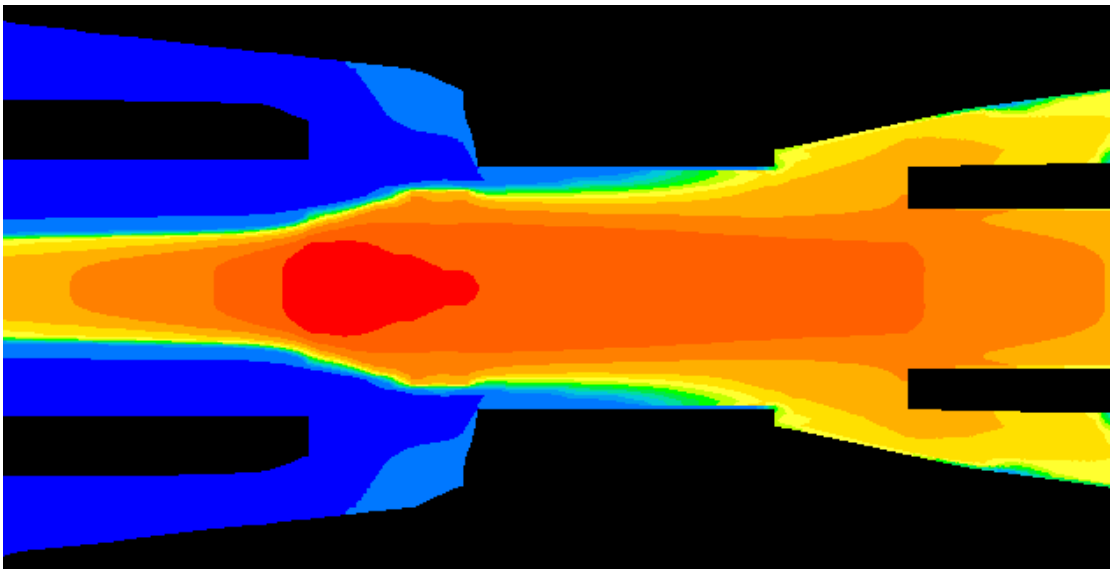

(e)

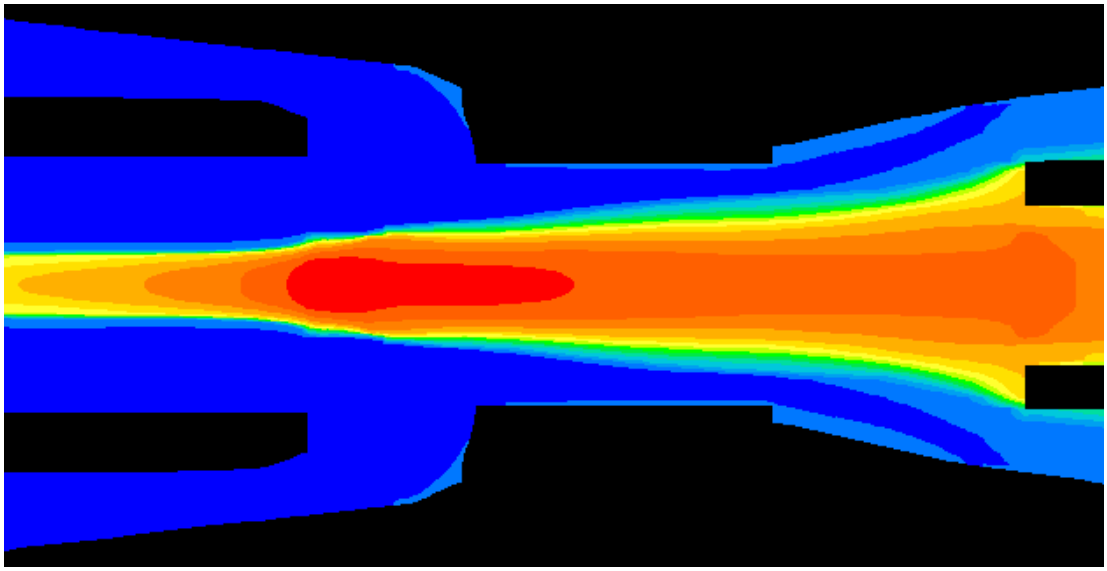

(f)

Figure 4.31Shape of arc column at different instants in the arcing process of the 47 kA case. The time, instantaneous current and maximum temperature in the arc are: (a) 14.06 ms,20 kA,25000 K; (b) 14.86 ms, <3 kA, 21000 K; (c) 17.66 ms, -49 kA, 24000 K; (d) 19.66 ms, -61 kA, 22000 K; (e) 21.66 ms, -45 kA, 23000 K; (f) 23.48 ms, -16 kA, 23000 K. The blue colour represents a temperature of 300 K.

The predicted pressure for the 47 *kA* case is shown in figure 4.32 by the dotted line segment for the arcing period. The prediction seems to be slightly lower than the average value of the measurement during the arcing process and slightly higher in the period 30 *ms* and 40 *ms*. Since pressure rise in the cylinder is mainly affected by nozzle

ablation, this implies that the nozzle ablaton is under –represented in the simulation model.

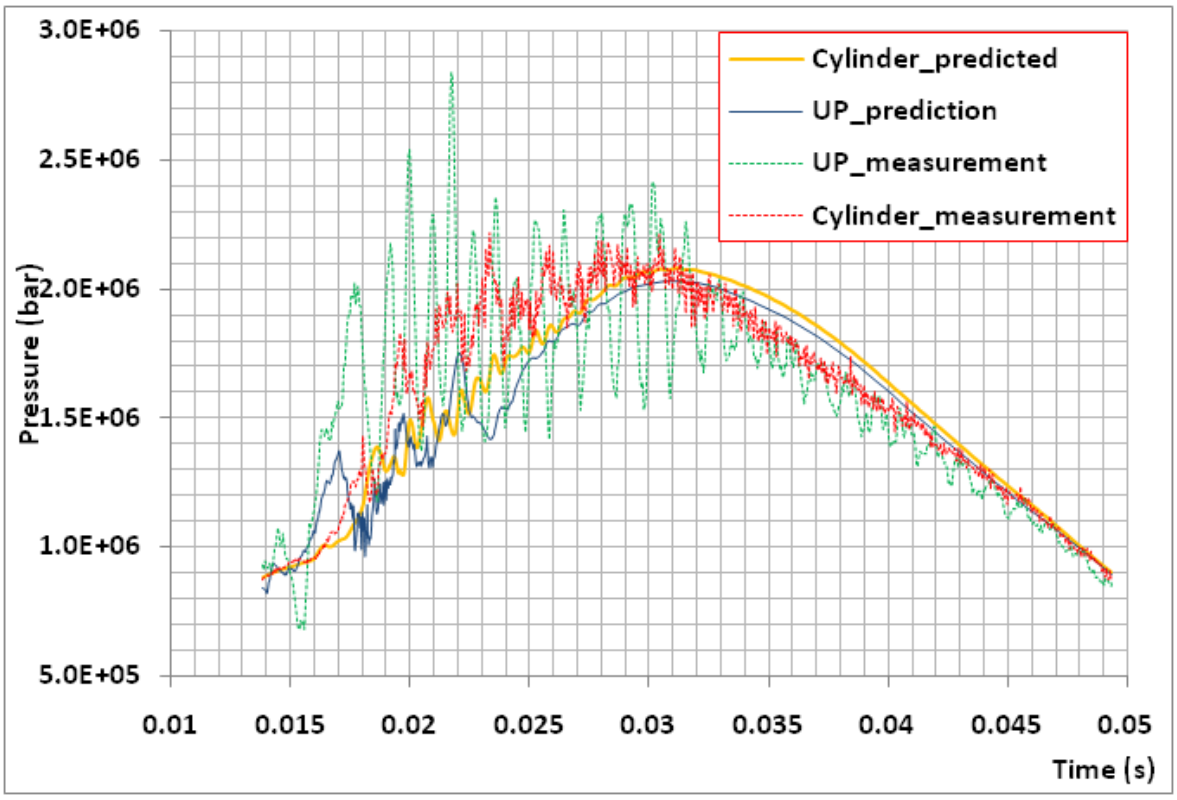

Figure 4.32 Predicted and measured pressure variation in front of the piston and at a point labelled as UP in figure 1 for the 47 kA case.

4.5.3 Current Zero Period

The current zero period simulation starts from 15 *kA* using the results from the high current phase as the initial conditions. The extinction peak in arc voltage reflects the change of arc resistance with a rapidly decreasing current. It is extremely important in studying the thermal interruption process.

As discussed in Chapter 2, the turbulence parameter in the Prandtl mixing length model is varied according to the instantaneous current, which is linked in general to the relative size of the arc column with respect to the confining nozzle. Based on the measurement, we have proposed that the parameter, c, in equation (4.2) is linearly changed from 0.1 starting from 15 *kA* to 0.3 at current zero. With this relationship, a

fairly good agreement is obtained not only for the arc voltage around the peak for the 10 *kA* case (4.12), but also around the extinction peak (figure 4.13). The linear setting performs much better than the fixed parameter settings for c. It is interesting to see that with a value of c=0.1 there is no extinction peak at all (4.12). The prediction for the 47 *kA* case characteristically matches the rapid voltage rise near current zero.

A comparison for the 24 *kA* and 46 *kA* cases cannot be made because the accuracy of the arc voltage measurement near the final current zero cannot be ascertained.

It must however be noted that the linear relationship for the turbulence parameter is only partially verified for the particular circuit breaker under investigation. Caution must be exercised to extrapolate the value to other breaker geometries.

The temperature field immediately before current zero and at exact current zero is shown in figure 4.33 and a typical diagram showing the velocity field is given in figure 4.34. It can be seen that the maximum arc temperature decreases rapidly from 29,000 *K* at 1*kA* to 12,000 *K* at current zero. In the majority of the column at current zero, the temperature is well below 10,000 *K*. Most of the temperature decrease takes place in the flat nozzle throat, indicating that turbulence cooling is most efficient in the nozzle throat. The temperature at the stagnation point between the main nozzle and the hollow contact also drops, but still remains the hottest in the whole arc column.

Results in figure 4.33 also show that the moving hollow contact, which is live in the real circuit breaker, is filled with hot gas for most of the time. This however may not reflect the real situation as a result of the axisymmetric arc model. In reality the arc is rooted on the surface of the hollow contact, instead of sitting on the axis. If the arc column is off axis, then the arc will produce fewer blockages for the hollow contact to clear itself. A three dimensional model will be required to study this aspect of the arcing process.

Shortly before current zero, the arc has a velocity of 2000 *m/s* on the axis (4.34). In the surrounding region, cold flow has fully developed and reaches a velocity of 150 *m/s*. Gas flow in the cold region is rather uniform radially in the nozzle section. The column

is surrounded by an axially dominant flow with uniform velocity profile in the radial direction.

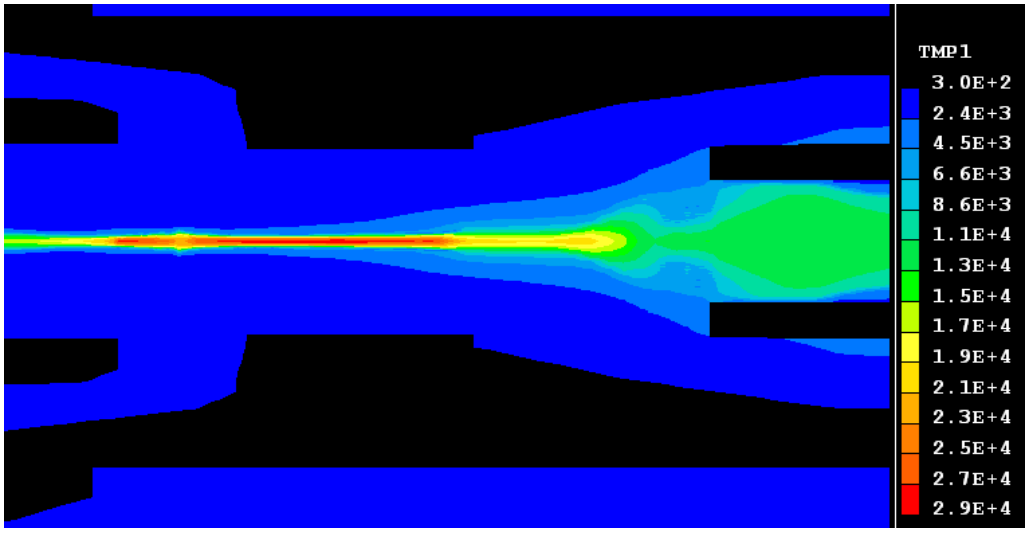

(a)

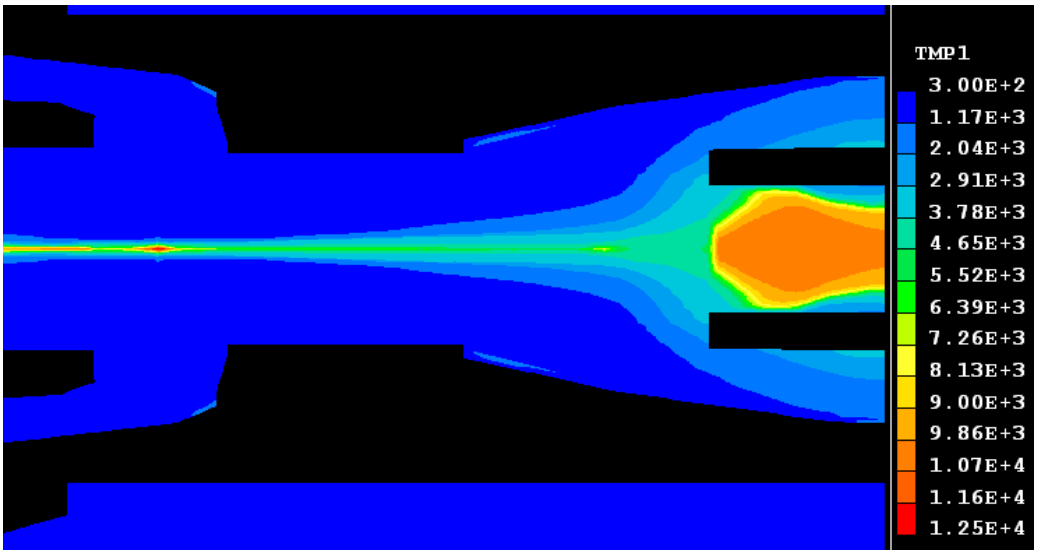

(b)

Figure 4.33 Temperature distribution at (a) 1kA and (b) exact curent zero for the 47 kA case.

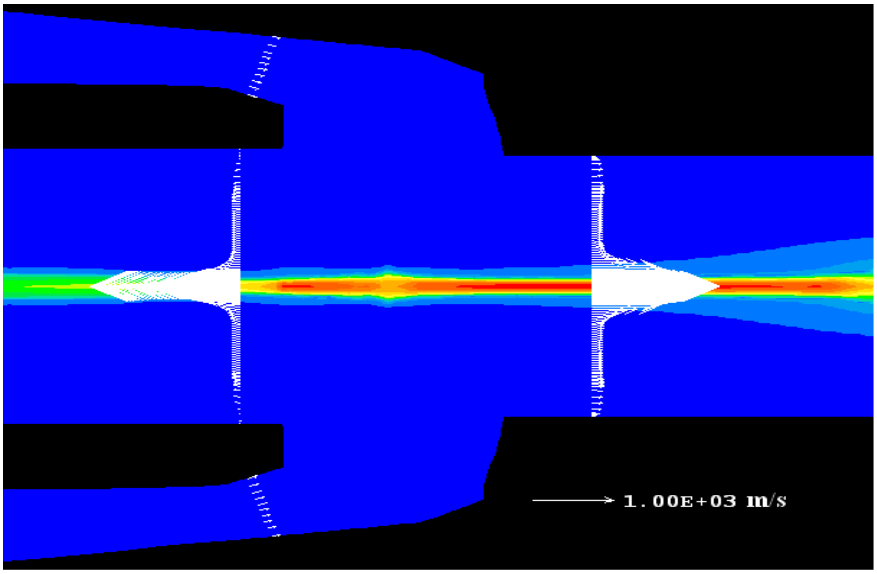

Figure 4.34 Velocity profile at 1kA before the final current zero for the 47 kA case.

4.5.4 Post Arc Period

The ultimate design purpose is to produce a circuit breaker with best possible interruption capability. In the interruption process a circuit breaker undergoes two interlinked processes, i.e. the thermal recovery and dieletric recovery processes. The thermal recovery process is concerned with energy removal from the arc column. A successful thermal recovery will lead to a decreasing arc temeprature. The didelectric recovery process is concerned with the removal of free charges (electrons) from the plasma so the gas in the region originally occpied by the arc can withstand high system recovery voltage without suffering a breakdown. For this project the main concern is on the thermal recovery process.

When the arc approaches its final current zero, the arc column shrinks rapidly due to convective and turbulent cooling. Previous studies have shown that turbulence enhanced energy transfer is the main cooling mechnism in the thermal recovery process.

Starting from the solution obtained at the end of the current zero period simulation, the behaviour of the plasma left between the two contacts can be assessed by applying different rates of rise of the recovery voltage (RRRV). The post arc current under

different RRRVs can be obtained by running a number of simulaitons. A particular value of RRRV can then be identified below which the post arc current will eventually decrease following an initial rise in a time scale of up to 10us. This RRRV is called the critical RRRV and is a direct measure of the thermal interruption capability of the circuit breaker under investigation.

However, it is generally accepted that so far there is no model that can accurately describe the turbulence phenomenon in plasmas and arcs without any adjustable parameters. Although it has been shown that improvement to the prediction of arc voltage in the current zero period can be made by using a variaiable turbulenc parameter, the validity of the model still needs further verification. The fact that the turbulence model optimised in this report leads to the prediction of an extinction peak builds further confidence in modelling the thermal recovery process of the puffer circuit breaker.

In spite of the uncertainties in the turbulence parameter, the simulation model can be used to study the trend of variation in the thermal interruption capability with different designs, such as the size and geometry of the arcing chamber and the use of different contact speeds.

To calculate the energy source under a certain recovery voltage, the following steps are used in the code to derive the electric field and Ohmic heating:

- Calculate the resistance of each slice of the arc column as divided by the grid system. This is done by using the following equation

$$Rsistance = \frac{\Delta z}{\int_0^{R3K} \sigma 2\pi r dr} \tag{4-5}$$

where R_{3K} is the radius of 3000 K.

- The resistance for each slice is added up to form the total resistance of the plasma column between the two contacts.

- Use Ohm's law to calculate the current that flows through the plasma column.

- Using the current to calculate the electric field and current density in each slice.

- Calculate Ohmic heating and radiation loss to obtain the total energy source term for each cell in the plasma column.

The temperature on the axis of the nozzle and hollow contacts after current zero is given in figure 4.35 for 7 instants after current zero for the case with a RRRV of 0.5 *kV/µs* in the 47 *kA* case. In this case the thermal recovery process is successful and the axis temperature in the middle section of the flat nozzle decreases steadily from 5000 *K* to less than 4000 *K* within 5 µs. Further increase in the applied RRRV will lead to a higher post arc current and if the RRRV is above the threshold value of 2.5 *kV/µs*, the current will rise violently after a period of stable discharge. This can be seen clearly in figure 4.36 where the post arc current is given for eight cases. An applied RRRV below 2 *kV/µs* will lead to a steady decrease in the post arc current and the contact gap will thermally recover. An applied value of higher than 3 *kV/µs* will eventually lead to a thermal re-ignition and result in a thermal failure of the interruption process.

This shows that the developed simulation model is able to perform the critical RRRV calculation based on solution from the current zero period simulation. It must be again noted that the accurate determination of the critical RRRV is still not possible due to uncertainties in the modelling of turbulence under plasma conditions and also the non-LTE nature of the residue plasma [Yan97].

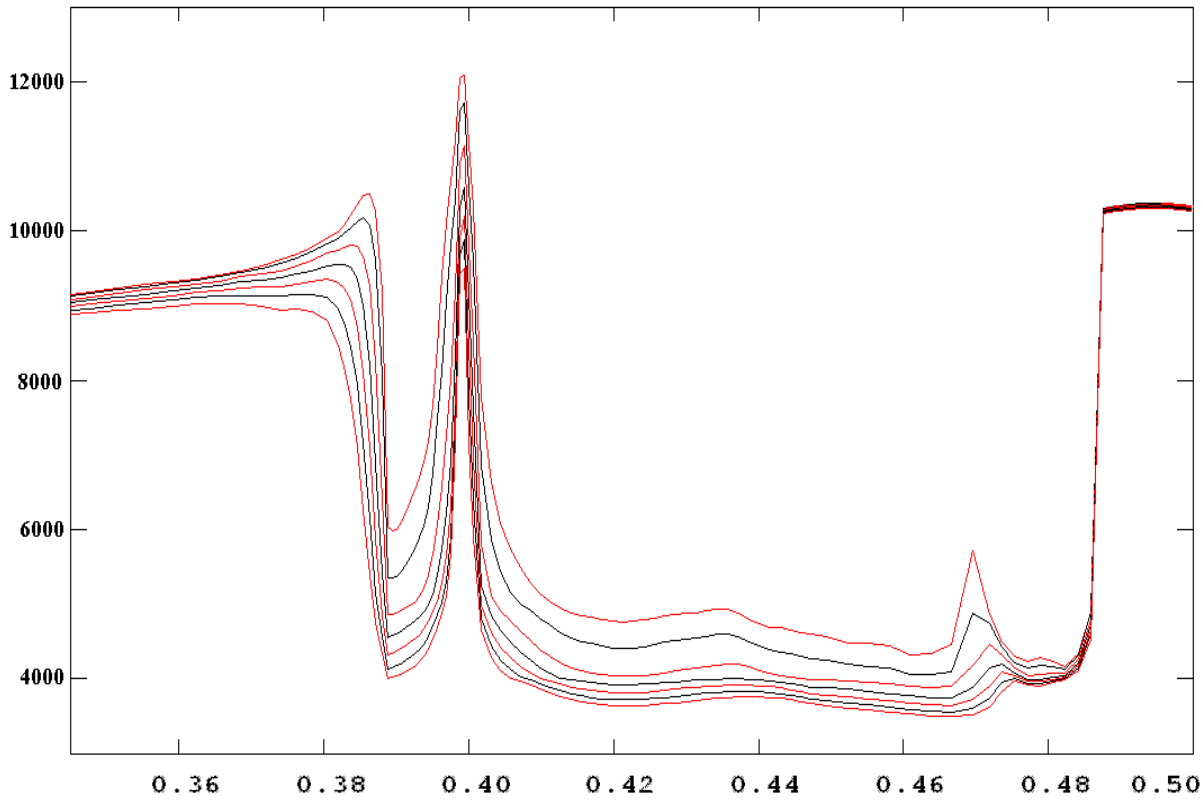

Figure 4.35 Temperature on the axis of the nozzle and hollow contact at different time after current zero for the case of 0.5 kV/μs RRRV. From top to bottom: 0.5 μs, 1 μs, 2 μs, 3 μs, 4 μs, 5 μs and 6 μs.

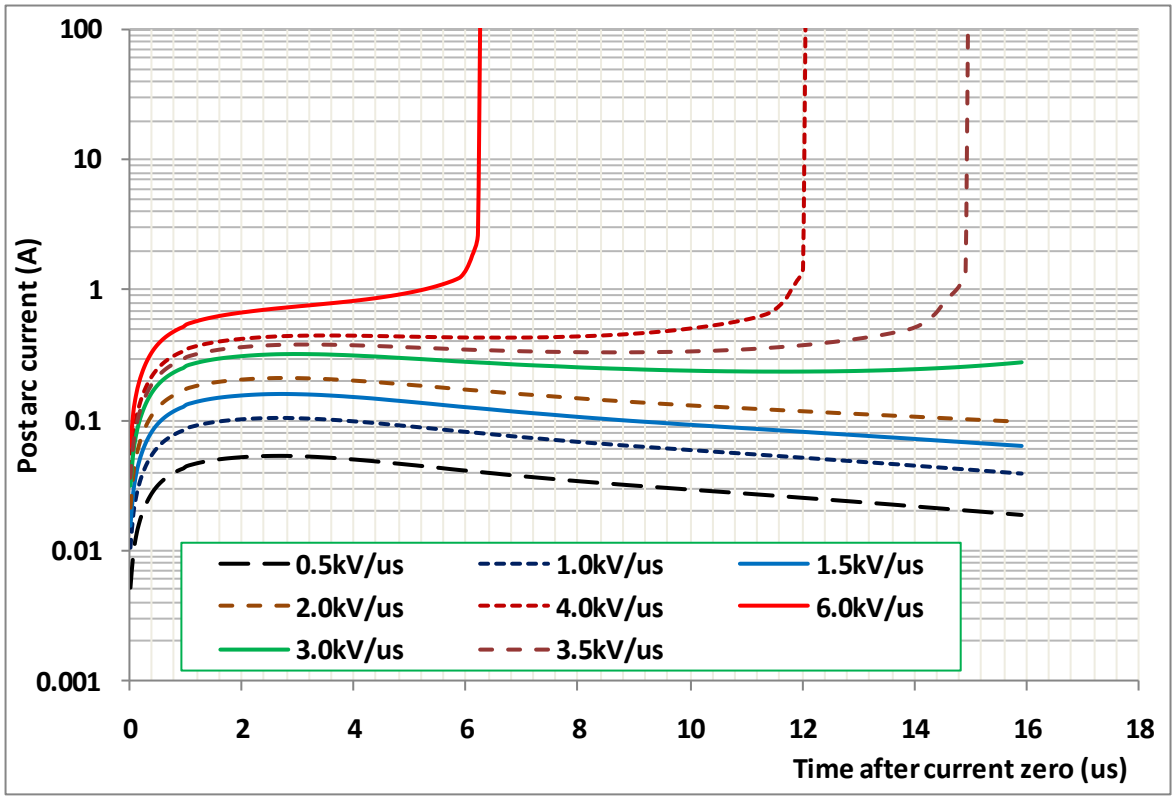

Figure 4.36 Post arc current as a function of time at different RRRV for the 47kA case. The critical RRRV is between 2.0kV to 3.0kV based on the proposed turbulence parameter.

4.6 Summary

The whole arcing process in a 252 *kV* puffer circuit breaker with duo-hollow contacts was simulated in this chapter. The basic features of the test results provided by the collaborating switchgear manufacturer was first analysed and necessary information for use in the simulation was extracted. The pressure measurement in the puffer cylinder is reliable but that in the nozzle and a point downstream of the main nozzle proves to be problematic because the accuracy cannot be verified.

The pressure prediction for the cold flow period, which represents the no-load case and also the initial stage of short circuit interruption, agrees reasonably well with measurement using nitrogen and SF_6.

For the high current phase, three cases were simulated with rms current of 24 *kA*, 46 *kA* and 47 *kA* with different arcing time. Results have shown that the predicted arc voltage agree well with the measurement as a result of the proposed approach to deal with the arc roots by the hollow contacts. This is a major achievement in comparison with the published data on arc voltage prediction in puffer circuit breakers. The pressure variation in the puffer cylinder was also recorded. The prediction is slightly lower than the measurement, indicating that the effect of ablation may be under-represented.

With the improved Prandtl turbulence model, the extinction peak immediately before the final current zero point can now be predicted although the absolute accuracy cannot be ascertained because the accuracy of the measurement is not know. Further research on the turbulence model is still needed, including the verification of the model when accurate measurement of the arc voltage near the current zero point is available. Results also show that most rapid temperature decrease in the contact gap takes place in the flat nozzle throat where strong axial flow is present and turbulent cooling to the arc is most

efficient. An important aspect of circuit breaker design is thus to guarantee a sufficient length of nozzle with strong axial flow providing turbulent cooling.

The post arc current calculation is based on LTE and the results are only indicative since the non-LTE nature of the residual plasma has not been considered. The results nevertheless demonstrated that the model is able to produce a threshold value of RRRV for the breaker. This is important for optimisation of circuit breaker design because the model can give qualitative indication of how the performance of the breaker changes when design parameters are changed. A lowered critical RRRV (i.e. the threshold value) indicate an adverse effect of a design parameter change.

4.7 References

[Ior08] A A Iordanidis and C M Franck, J. Phys. D: Appl. Phys. 41 (2008)

[Lia07] V.K. Liau, B. Y. Lee, Ki Dong Song, and Kyong Yop Park, “Computational investigation of arcing phenomena in 245 kv hybrid circuit breaker”, Jpn. J. Appl. Phys. 46 pp. 1674-1679, 2007

[San06] Sang Hun Park, Chae Yoon Bae, Hong Kyu Kim and Hyun Kyo Jung, “Computer simulation of interaction of arc-gas flow in SF_6 puffer circuit breaker considering effects of ablated nozzle vapour”, IEEE Transactions on Magnetics, vol. 42, pp. 1067-1070, 2006

[Ret96] B. Rethfeld, J. Wendelstor, T. Klein and G. Simon,”A self-consistent model for the cathode fall region of an electric arc”, J. Phys. D: Appl. Phys. 29 pp.121–128, 1996

[Phoe] PHOENICS is the name of a commercial CFD package supplied by CHAM which is based at Bakery House, 40 High Street, Wimbledon Village, London, SW19 5AU, UK.

[Yan97] Yan JD, Fang MTC and Liu QS, "Dielectric breakdown of a residual SF_6 plasma at 3,000K under diatomic equilibrium", IEEE Trans. on Dielectrics and Electrical Insulation, Vol. 4, pp. 114-119, 1997

Chapter 5 Summary and Future Work

The work in this thesis is concerned with the visual simulation of high pressure arc plasmas in two different applications. The first one is an arc maintained in water for the formation of nano-structures such as nanotubes and fullerenes. The second application is high puffer switching using puffer circuit breakers. The fundamental behaviour of both arc plasmas was computationally studied.

5.1 Arcs Maintained in Water

This is the first time that an arc model is applied to study the carbon arc confined in water. The arc is generated between two carbon electrodes which are immersed in water with a gap length of 1 *mm*. The anode has a conical shape with a rod diameter of 8.2 *mm* and a tip diameter of 2 *mm* with a full conical angle of 60^{o}. The anode has a cylindrical shape with a diameter of 12 *mm*. Because of the erosion of the anode and the evaporation of water due to arc energy, there is a gaseous environment immediately surrounding the arc column. The shape of this gaseous environment was approximated by a spherical bubble following experimental observation [Hsi01]. A local thermal equilibrium arc model was used to tackle the problem based without considering the sheath layer in front of the electrodes.

The present work focuses on the formation of the gaseous environment and the basic characteristics of the arc. The loss of carbon vapour due to formation of solid carbon structures is represented by a negative volumetric source near the cathode and at the edge of the arc column (4,500 *K*) where gas temperature experiences rapid change. The volumetric loss source near the cathode is set to 15% of the axial convection flux of carbon vapour and 15% of radial convection flux near at the arc edge designated by the 4,500 *K* point.

A uniform mass rate of carbon vapour injection at the anode tip surface is set to 2×10^{-6} *kg/s* which corresponding to the measurement of 117 *mg/min* [San02]. The arc was initiated with a hot column of 1 *mm* radius in water vapour. Results show that the strong influx of carbon vapour displaced the original water vapour in a few microseconds, typically 5 μs, in half of the electrode gap and by 4 *ms* the arc burns in a carbon dominated environment with about 25% of water vapour near the cathode. In the computation, the material properties of the arcing gas are obtained by interpolation from those of pure carbon vapour and pure water vapour. The uncertainties in the material property calculation for the gas in the arcing column can thus be considered as reasonable because of the dominant presence of the carbon vapour. To produce a useable amount of carbon nanostructures, in practice the arc runs for about 3 to 10 minutes in each round. Our results thus suggest that for most of the time the arc can be regarded as burning in a carbon vapour dominated environment.

Following suggestions in [San02], chemical reaction between carbon vapour and water vapour has been included in the model. Since the reaction rate between C and H_2O at elevated temperatures is not available, the reaction rate coefficient was derived from that at low temperature (300 *K*) using the well known Arrhenius expression. The value of this coefficient, *A* in equation (3-1), is $1.054\times10^{6}\frac{m^3}{mol\cdot s}$. Based on this value, it has been found that the mass concentration of H_2 and CO is negligible in the arc column and peaks in a layer surrounding the arc column. The maximum concentration is only 0.2% and 2.8% respectively, in a region near the cathode surface. Although 30% of the carbon vapour is consumed by chemical reaction, this rate (6×10^{-7} *kg/s*) is still much lower than the water evaporation rate (6×10^{-5} *kg/s*), thus in the region surrounding the arc, water vapour is still dominant. The validity of the chemical reaction and its rate coefficient cannot be verified because a lack of experimental result of the gaseous composition generated by the arc. This will be part of research in the future.

The predicted arc voltage at 30 *A* is 7 *V* while the measurement is 17 – 20 *V*. The difference is attributed mainly to the exclusion of the electrode sheath model in the present work. Theoretically, the voltage drop in the cathode sheath is comparable to the first ionisation energy of carbon vapour at ground state which is 11.26 *eV*. Considering this the predicted voltage of the arc column is well placed in the expected range.

A numerical scheme has been established in the present work to simulate the growth of gas bubble confined in water. The position change of the interface of the bubble-water is controlled by the pressure difference between that inside the bubble and the atmospheric pressure. The inertia of the water surrounding the bubble is taken into account in the construction of the dynamic response. Our results show that the growth of the bubble is dominated in the first half millisecond by the retreat of the water surface as a result of evaporation. Further on in the arcing process, the pressure difference makes a dominant contribution in the growth of the bubble.

5.2 Arcs in Puffer Circuit Breakers

The arcing process for four test duties of a 252 *kV* puffer circuit breaker has been simulated. In view of the large discrepancies between predicted and measured arc voltage in existing arc models used by different research groups worldwide, a novel method was proposed to improve the arc voltage prediction. The improvement is related to the mitigation of the effect of Lorentz force near the tips of hollow contacts and their filling transparent contacts used to collect the current in two dimensional axisymmetric arc model. Instead of allowing the size of the arc root to be determined by interaction of arc and flow field, a prescribed transparent arc root is used in front of each transparent (including the hollow) contact. The proposal of this method is based on consideration of the most probable practical scenario in reality. Results present in the thesis show that this method is effective and gives satisfactory arc voltage prediction for all four test cases at different current levels and arc durations.

Turbulence is important in the interruption process of high voltage SF_6 circuit breakers. It has been found that Prandtl mixing length model with a constant turbulence parameter, *c* defined in equation (2-12), is not able to predict the important extinction peak in the puffer circuit breaker. In the present work this turbulence parameter is made variable, as a function of instantaneous current that is an indirect measure of the presence of cold SF_6 flow around the arc column. The relationship is expressed by equation (2-16). The choice of a threshold value of 5,000 *K* in the high current phase and 3,000 *K* in the current zero period was explained and the implication of choosing a lower value such as 2,000 *K* for the current zero phase was studied. It was shown that

3,000 *K* is a preferred choice. The modified turbulence model was then applied to simulated the current zero period (from 15 *kA* before final current zero onwards to the current zero point) of a 47 *kA* case and a 10 *kA* case. The predicted arc voltage using the modified turbulence model starts to increase rapidly shortly before the final current zero point, qualitatively agree with the measurement. A detailed comparison is not sensible since the accuracy of the measurement is not known.

The present work covers the simulation of the cold flow period, the high current, current zero and the post arc periods. The predicted pressure variation in the puffer cylinder and another three points including the middle of the flat nozzle surface all agrees reasonably well with the corresponding measurement.

There is indication that the pressure prediction in the puffer cylinder is slightly lower than the measurement for the high current phase of the 47 *kA* case. The most probable reason is the use of 80% of the arc radiation from the arc core re-absorbed at the arc edge. This value may need to be lowered.

The thermal interruption capability of a circuit breaker is represented by the critical RRRV, a value of the rate of rise of recovery voltage that the circuit breaker can with stands. Procedures were set up and some example results reported in the thesis. It must however be recognised that the plasma after current zero may not be in LTE state and the accurate prediction of the critical RRRV is not yet possible. Nevertheless, the established procedure for the calculation of the post arc current under the influence of system recovery voltage can be of help in studying the behaviour response of a circuit breaker when a design parameter is changed. The shift of the critical RRRV in response to a design parameter change gives an indication of the effectiveness of the change in design.

5.3 Visual Simulation of High Pressure Arcs

Computer simulation of electric arcs for industrial devices proves a difficult job in the sense that much coding and setting is required to implement the arc in a chosen software package. An approach has proposed to use Object oriented programming to change the model setup from manually to automatic. The platform is named as integrated

simulation and evaluation environment, ISEE. This is to be realised by using a core concept called object in OOP. The use of object and its class in Windows based programme allows the definition of a component of a circuit breaker in a virtual environment. The components are then virtually assembled into a product. The geometric relationship of the components and the behaviour characteristics, such as arc radiation and nozzle ablation, can be automatically configured by the Virtual Model Builder. The virtual product is then translated into information required by the CFD package before the simulation is performed. The feasibility of the approach has been demonstrated in the present work by a component builder and a Visual Analyser and Monitor (VCM). Information exchange between ISEE and the CFD solver is through memory sharing. Typical results for visual simulation are given in Chapter 2, demonstrating a range of useful functionalities it provides and the benefits for arc modellers.

5.4 Future Work

5.4.1 Arc in Water

The present work on arc confined in water is only the first step in our attempt to understand the process of formation of nanostructures using electric arcs. A number of approximations and assumptions have been made to simplify the situation. There are three aspects that need to be improved based on the present work.

The first is the inclusion of electrode sheath layer in the model and the calculation of erosion rate based on arc–electrode interaction. The latter requires knowledge of the energy flux into the anode. Without a proper sheath model it is not possible to determine the energy flux into both electrodes. Much work has been published on the arc-electrode interaction but a review of the applicable models is out of the present work. It is hoped that with the inclusion of the sheath models, a direct comparison of the predicted and measured arc voltage becomes possible.

The second improvement needs to be on the chemical reactions and transport properties of the gas mixture. Water vapour at high temperature will be dissociated into H, O and

OH and the possible reaction paths become much more complicated. The present model is cruel and substantial work is needed to improve its accuracy. Experimental results on the composition and concentration of the gases produced by the arc in water system are essential to validate the models relating to chemical reactions. Using a suitably designed rig, the gas can be collected into a container and a mass spectrometer used to analyse its composition. With this the overall correctness of the chemical model can be checked.
In the present work only simulation was performed only at one current (30 *A*) for which some measurement is available. Simulation of more cases at different currents should be performed in future when experimental results become available.

5.4.2 Circuit Breaker arc

Although the proposed method of dealing with arc rooting at the tips of hollow contacts proves effective in improving arc voltage prediction at different current levels, the model should be tested against different circuit breakers. Because of limit of available time this has not been done. Validity should be carried out for auto-expansion circuit breakers as well if arc voltage measurement is available.

Improvement to the Prandtl mixing length model produced promising results but quantitative verification is not possible due to a lack of arc voltage measurement around the current zero point. Attempt has been made to account for density gradient at the arc edge in the two equation k-epsilon model by modifying the turbulence generation term. Its effectiveness is mixed. On one hand a rapid increase in arc voltage immediately before current zero was produced, however the predicted arc voltage around the current peak in the 10 *kA* case is much lower than the measurement. Thus the present modification to the k-epsilon model does not provide advantages over the simple Prandtl mixing length model apart from that no turbulence parameter has to be adjusted. Much work will be needed to further study the potential of the k-epsilon model in switching arc applications.

The accurate prediction of thermal interruption capability of circuit breaker requires an accurate turbulence model, consideration of the possible non LTE effect after current zero, and the three dimensional nature of the arcs. Any improvement to the simulation

of the current zero and post arc period will need to be adequately verified and the most effective way is to compare the predicted voltage (before current zero) and current (after current zero) with measurement.

5.5 References

[Hsi01] Hsin Y. L., Hwang K. C., Chen F. R. and Kai J. J., "Production and in-situ Metal Filling of Carbon Nanotubes in Water", Adv. Mater. Vol. 13, No. 11, 2001

[San02] Sano N., Wang H., Alexandrou I., Chhowalla M., Teo K. B. K. and Amaratunga G. A. J., "Properties of carbon onions produced by an arc discharge in water", Journal of Applied Physics, Vol. 92, No. 5, pp. 2783-2788, 2002